INVESTIGATIONS IN X-RAY ASTRONOMY

BY

ASHOK KUMAR JAIN
PHYSICAL RESEARCH LABORATORY
AHMEDABAD-380 009
INDIA

A THESIS
SUBMITTED TO THE GUJARAT UNIVERSITY
FOR THE DEGREE OF

B10000
043 JAI

DOCTOR OF PHILOSOPHY

1979

THE LIBRARY
PHYSICAL RESEARCH LABORATORY
AHMEDABAD-380009

TO

MY MOTHER

There is something fascinating about science. One gets such wholesale returns of conjecture out of such a trifling investment of fact.

Mark Twain, "Life on the Mississippi"

CERTIFICATE

I hereby declare that the work presented in this thesis is original and has not formed the basis for the award of any degree or diploma by any University or Institution.

Author

A.K. JAIN
Physical Research Laboratory
Ahmedabad 380 009, India

Certified by
Professor-in-charge.

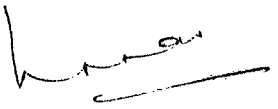

Prof.U.R.Rao
Director
ISRO Satellite Centre
Bangalore 560 058, India

and

Professor
Physical Research Laboratory
Ahmedabad 380 009, India

STATEMENT

Realising the advantage of conducting X-ray astronomy experiments near the geomagnetic equator, where the charged particle background is low, the X-ray astronomy group at the Physical Research Laboratory, Ahmedabad, India, under the leadership of Prof. U.R. Rao, planned a comprehensive programme in the field of balloon-borne X-ray astronomy. The author, as a member of this group, working under the guidance of Prof. U.R. Rao, has been actively involved in the planning, fabrication and execution of all the balloon borne experiments using oriented platforms, and in the analysis and interpretation of data on point X-ray sources, beginning with the first successful flight on the X-ray source Sco X-1 in November 1971. The present thesis incorporates the results of studies on the X-ray source Cyg X-1 obtained from a number of balloon flights conducted from Hyderabad, India.

Among discrete galactic X-ray sources Cyg X-1 has been noted for its peculiar features in several respects. It is remarkable for its irregular time variability over a wide range of time scales, ranging from millisecond bursts to abrupt intensity transitions with durations of weeks and months. Further, it is one of the brightest X-ray objects at high energies, with the spectrum extending upwards to a few hundred keV. Optical identification of this source with

OB supergiant star HD 226868 - a spectroscopic binary, associated radial velocity measurements and the short term (millisecond) fluctuations in X-ray intensity strongly indicate that this X-ray emitting compact object is a black hole.

Paucity of observations at high energies and the possibility that a study of the long and short term variations in intensity and energy spectrum of X-ray emission can shed light on the emission mechanism and the nature of source itself, led the author to embark on a comprehensive programme to study Cyg X-1 at energies >20 keV. A series of balloon flights spread over a period of four years were conducted from Hyderabad, situated close to the geomagnetic equator ($\lambda_m \approx 8^{\circ}N$), to study the source characteristics in the 20-160 keV energy range. Employing sensitive oriented X-ray telescopes onboard a balloon, long exposures ($\sim$1-3 hours) of Cyg X-1 with $\sim$85% efficiency were obtained during these flights, the results of which are presented in this thesis.

The thesis has been divided into seven chapters. The first chapter gives a brief introduction to X-ray astronomy, followed by a review of the present status of observational information available on Cyg X-1. The X-ray telescopes used in different flights are described in the second chapter. In Chapter III, the data acquisition system, telescope controls, aspect determination and other instrumentation details are briefly summarised. This is followed

by a brief account of mathematical and computational techniques used to retrieve the relevant information in Chapter IV.

Chapter V describes the observational programme of different flights and results obtained from these experiments in detail. In Chapter VI, these results have been discussed in conjunction with other low and high energy observations made on the source in an attempt to understand the behaviour of the source at high energies. For the sake of completeness of discussion on Cyg X-1 source, an overview of various models proposed to explain its X-ray emission has been included at the end of this chapter. It will be noted that although considerable strides have been made in recent years on theoretical side, the models have not advanced to the extent that they can explain all the results reported herein. The thesis concludes with a discussion of the effect of celestial X-ray sources, both steady and transient, on the night time D-region of the ionosphere.

Some of the important results that have emerged from the present study are listed below :

1. Observations indicate that at energies >20 keV, during low state as defined by low energy measurements and quiet condition, the spectrum of Cyg X-1 upto ~ 150 keV can be best fitted to a power law with an index of ~ 1.8. The high energy spectrum steepens when the source switches to high state at low energies.

2. Cyg X-1 occasionally exhibits flare like enhancements with intensity increasing by a factor of ~ 2 to 3. Such flare enhancements seem to be independent of the phase of the binary system.

3. In the particular event observed by us, the intensity enhancement in higher energy range of 87.5-160.0 keV was by almost a factor of 5 as compared to the observed two fold increase at the lower energy range of 29.0-76.0 keV. A peculiar feature of this event is the time delay of about 5 min in the enhancement of intensity in the lower energy channel compared to that in the higher energy channel. The energetics and spectral behaviour of the source during this flare event, when the power law index was around 1.0, closely resemble typical γ-ray bursts.

4. Our observation provides the first evidence for intensity fluctuations by a factor of ~ 3 to 4 at high energies on a minute to minute basis. In addition, our observation also indicates periods of high and low intensity for durations of $\sim$25 min. All such fluctuations in intensity seem to be mainly confined to energies $\lesssim$ 76.0 keV.

5. The intensity fluctuations over $\sim$ 25 min are also accompanied by complex variability in the spectral characteristics. The spectral index of the best fit power law spectrum varies over a wide range from 1.90 to 3.80, the time averaged spectrum showing a value of ~ 2.37, quite different from the normal spectrum.

6. The evidence presented in the thesis shows for the first time that the source has two distinct levels of hard X-ray emission differing in intensity by a factor of ~ 2. In addition, we show that the source exhibits a linear variability in intensity with the 5.6 day binary period, the variability being similar for both the states. The source apparently spends almost equal time in the two states.

7. From our observation, we suggest that the characteristic fundamental property of this source is the two state emission at high energies which are emitted from the inner disk, the two states having equal probability of occurrence. The normal state at low energies emitted from the outer disk is the one corresponding to the low state in intensity for about 90% of the time. On rare occasions when the low energy intensity emission flips to high state, the high energy X-ray emission seems to show a further decrease which could be interpreted as the third state of emission at high energies.

8. Investigations of effect of X-ray sources on night time D-region of ionosphere present quite a strong evidence for the detection of strong celestial X-ray sources like Sco X-1 through their ionospheric effect, especially at low latitudes. In other words, the ionosphere acts as a wide angle telescope for observing celestial X-ray sources.

A.K. JAIN
Author

U.R. RAO

LIST OF PUBLICATIONS

1. Possibility of Continuous Monitoring of Celestial X-ray Sources through their Ionization Effects in the Nocturnal D-region Ionosphere

   D.P. Sharma, A.K. Jain, S.C. Chakravarty, K. Kasturirangan, K.R. Ramanathan and U.R. Rao, Astrophysics and Space Science, 17, 409-425, 1972.

2. Balloon Observations of Sco X-1 in the Energy Interval 17-106 keV

   A.K. Jain, U.B. Jayanthi, K. Kasturirangan and U.R. Rao, Astrophysics and Space Science, 21, 107-116, 1973.

3. On the Detection of X-rays from Celestial Sources through their Ionization of the Terrestrial Atmosphere.

   U.R. Rao, D.P. Sharma, A.K. Jain, S.C. Chakravarty, K. Kasturirangan and K.R. Ramanathan, Space Research XIII, 861-866, 1973.

4. Balloon Observations of Celestial X-rays Part I: X-ray Emission from Cyg X-1 at Energies Greater than 20 keV.

   A.K. Jain, U.B. Jayanthi, D.P. Sharma, K. Kasturirangan and U.R. Rao, Proceedings of 13th International Cosmic Ray Conference, Denver, U.S.A., 17-30 Aug. 1973, Vol.1, pp 61-66.

5. Balloon Observations of Celestial X-rays Part II: Hard X-ray Emission from Her X-1.

   D.P. Sharma, A.K. Jain, K. Kasturirangan, U.B. Jayanthi and U.R. Rao, Proceedings of 13th International Cosmic Ray Conference, Denver, U.S.A., 17-30 Aug. 1973, Vol.1, pp 67-71.

6. Hard X-ray Emission from Her X-1.

   D.P. Sharma, A.K. Jain, K. Kasturirangan, U.B. Jayanthi and U.R. Rao, Nature Physical Science, 246, 107-108, 1973.

7. Intensity and Spectrum of Hard X-rays from Her X-1.

   U.R. Rao, D.P. Sharma, U.B. Jayanthi, A.K. Jain and K. Kasturirangan, presented at COSPAR/STP Symposium, Brazil, 1974.

8. X-ray Observations of Cyg X-1 at Energies Greater than 20 keV.

U.R. Rao, A.K. Jain, D.P. Sharma, U.B. Jayanthi and K. Kasturirangan, presented at COSPAR/STP Symposium, Brazil, 1974.

9. Soft X-ray Astronomy Payload for Use with Satellites.

K. Kasturirangan, U.R. Rao and A.K. Jain, Indian Journal of Radio and Space Physics, 4, 144-145, 1975.

10. Balloon Observations of X-rays from Celestial Sources.

U.R. Rao, K. Kasturirangan, D.P. Sharma, A.K. Jain and U.B. Jayanthi, Indian Journal of Radio and Space Physics, 4, 199-202, 1975.

11. Balloon Observations of Fast Intensity Fluctuations and Flare-Like Enhancements of X-ray Emission from Cyg X-1.

U.R. Rao, K. Kasturirangan, D.P. Sharma, A.K. Jain and U.B. Jayanthi, Astrophysics and Space Science, 42, 193-199, 1976.

12. Evidence for Short Term Changes in the Intensity and Spectrum of Hard X-rays from Cyg X-1.

A.K. Jain, U.B. Jayanthi, K. Kasturirangan and U.R. Rao, Astrophysics and Space Science, 45, 433-438, 1976.

13. Evidence for a New Variability in Hard X-ray Emission of Cyg X-1.

A.K. Jain, U.R. Rao and K. Kasturirangan, submitted for publication.

ACKNOWLEDGEMENTS

The work presented in this thesis was carried out under the kind supervision of Prof.U.R. Rao. I would like to express with deep sense of gratitude my indebtedness to Prof. Rao for introducing me to the exciting and fascinating subject of High Energy Astrophysics and for his inspiring guidance, constant encouragement and unwavering support throughout the course of the present work. His zeal and persistence were the driving forces behind the completion of the work presented herein. His optimistic and cheerful approach to Physics, profound knowledge and critical insight have left a deep impression on me and I consider it a privilege to have worked with him.

Dr.K. Kasturirangan has been closely associated with most of the work presented here and I would like to thank him for his constant encouragement and his keen interest in my research career so far. Many fruitful and stimulating discussions with him and his invaluable suggestions and kind advice throughout the course of this work are gratefully acknowledged.

It gives me great pleasure to acknowledge the fruitful collaboration of my colleagues Drs.U.B. Jayanthi and D.P. Sharma at various stages of the present work. They have been friendly critics and sources of information for many years and I extend my heartfelt thanks to them for their cooperation and encouragement at various times during the course of this work.

I am grateful to Drs.A.S. Prakasarao, V.S. Iyengar, T.M.K. Marar and R.K. Manchanda for several useful and lively discussions I had with them during final stages of preparation of this thesis.

It is a pleasant duty to thank Messrs K.S.V. Seshadri, N.J.N. Sarma and B.L. Agrawal for invaluable help they rendered in the design and development of electronic systems, and Messrs D.P. Devgan, K.S.B. Manian, R. Madhavan, J.S. Sidhu and K.A. Panchal for the excellent technical help in the fabrication and testing of various payloads and maintenance of ground support systems during the flights.

I wish to thank Mr.K.J. Shah and Mr.V.R. Chokshi for their sincere and able assistance in data processing. I also appreciate the help rendered by Mr.K.J. Shah in the production of the thesis.

The balloons were launched from TIFR Balloon Facility, Hyderabad, India and Mr.R.T. Redkar and his colleagues at Balloon Facility deserve my special thanks for their zealous cooperation and help during various balloon flights.

I am thankful to the personnel at various supporting facilities, in particular the library staff, for their assistance and kind cooperation on all occasions.

I also take this opportunity to thank Messrs R. Mahadevan, D. Prithviraj, N.R. Subramaniam, Srivatsa and Munnidev of ISRO Satellite Centre, Bangalore for providing

excellent typing and other assistance to me during the finalization of this thesis at ISAC, Bangalore. I very much appreciate their enthusiastic cooperation and helping and pleasing attitude throughout my stay at Bangalore.

The painstaking job of elegantly typing the final manuscript was most enthusiastically done by Mr. Manmadhan Nair N.P. I wish to record my special thanks and appreciation to him. I also thank Mr. Ghanshyam P. Patel for his careful and neat cyclostyling of the thesis.

I am grateful to Professors D. Lal, S.P. Pandya, R.V. Bhonsle, R. Raghavarao, B.H. Subbaraya, and Drs. G. Subramaniam, V. Kumar and Dinesh Patel for their enthusiastic concern in the progress of my work and for their timely encouragement and general helpful attitude, specially during the final stages of this work.

During those agonizing moments of anxiety and despair, at a critical period during the course of this work, the much needed encouragement and inspiration of Prof. Satya Prakash and family, Prof.B. Buti, S.K. Mattoo, H.S.S. Sinha and Aruna, Harish and Kamla, and Subhash and Sadhana always came to my rescue, infusing renewed hope and enthusiasm in me. With them it was a home away from home. I owe immensely to them for their affection and help and the memory of little time I spent with them will always remain fresh in my mind for years to come.

The task of bringing the work presented here to its conclusion was substantially lightened by the unfailing cheerfulness and patience with which a number of friends have helped me, directly or indirectly, whenever the occasion demanded. It is almost impossible to thank them all individually. Nevertheless, I wish to record with delight my explicit thanks to Harish Bhatt, who helped me in the strenuous task of proof-reading, and to Ashok Ambastha, C.M. Nautiyal, N.M. Ashok, N. Venkatramani and B.G. Anandarao, who helped me in various odd jobs during the preparation of the thesis.

It will be an important omission if I fail to record my indebtedness to my uncle, Shri Tarachand Jain, for his encouragement, support and inspiration during the preparation of this dissertation.

Finally, I express my deep gratitude to my parents for their understanding and cooperation throughout the course of this study.

A.K. JAIN

C O N T E N T S

		Page
STATEMENT	...	v
LIST OF PUBLICATIONS	...	x
ACKNOWLEDGEMENTS	...	xii
CONTENTS	...	xvi
CHAPTER I	X-RAY ASTRONOMY AND CYG X-1: AN INTRODUCTION	1
CHAPTER II	X-RAY TELESCOPES AND THEIR CHARACTERISTICS	51
CHAPTER III	DATA ACQUISITION AND TELESCOPE CONTROLS	68
CHAPTER IV	DATA REDUCTION AND ANALYSIS	85
CHAPTER V	OBSERVATIONAL PROGRAMME AND RESULTS	102
CHAPTER VI	X-RAY EMISSION CHARACTERISTICS AND MODELS OF CYG X-1: DISCUSSION AND CONCLUSIONS	130
CHAPTER VII	IONIZATION EFFECTS OF CELESTIAL X-RAY SOURCES IN THE LOWER ATMOSPHERE	187
APPENDIX I	ENERGY RESOLUTION IN A SCINTILLATION SPECTROMETER	214
REFERENCES	...	223

CHAPTER I: X-RAY ASTRONOMY AND CYG X-1 : AN INTRODUCTION

1.1 X-ray Astronomy : Its Impact 1

1.2 Early History of X-ray Astronomy and X-ray Sky 4

1.3 Galactic X-ray Sources 9

1.4 Cyg X-1 and Irregularly Varying Binary X-ray Sources 15

1.5 Historical Development of Our Knowledge of Cyg X-1 : Presence of a Black Hole 16

1.6 Characteristics of Low Energy X-ray Emission of Cyg X-1 20

1.6:1 Transitions 20

1.6:2 Absorption Dips and 5.6 Day Modulation 22

1.6:3 Short Term Variability 24

1.6:3.1 Characteristics of Short Term Variability 24

1.6:3.2 Shot Noise Model 26

1.6:3.3 Periodicity 27

1.6:3.4 Millisecond Bursts 29

1.7 Characteristics of High Energy X-ray Emission of Cyg X-1 31

1.7:1 Short Term Variability 32

1.7:2 Transitions 34

1.7:3 Periodicity 35

1.7:4 Gamma Ray Burst Candidate 35

1.8 Energy Spectrum of Cyg X-1 36

1.8:1 Low Energy (2-20 keV) Spectrum 37

1.8:2 High Energy (>20 keV) Spectrum 38

1.8:3 Soft X-ray (< 2 keV) Spectrum 39

1.9 Optical Observations : Star HDE 226868 39

1.9:1 Spectroscopy 39

1.9:2 Orbital Elements 41

1.9:3 Distance 41

1.9:4 Light Variations 42

1.9:5 Polarization 43

1.10 Radio Observations 45

1.11 Aims and Objectives of Present Investigations 47

CHAPTER II: X-RAY TELESCOPES AND THEIR CHARACTERISTICS

2.1 Introduction : Basic Requirements of a Balloon Borne X-ray Astronomy Experiment 51

2.2 Interaction of Photons with Matter 53

2.3 Choice of the Detector 55

2.4 Energy Resolution in a Scintillation Spectrometer 56

2.5 General Criteria in the Choice of Detector Dimensions and Design of Anticoincidence Shield and Collimator 56

2.6 X-ray Telescopes for Different Experiments 59

2.6:1 X-ray Telescope for March 29, 1972 Flight 59

2.6:2 X-ray Telescope for January 18, 1973 Flight 60

2.6:3 X-ray Telescope for February 11, 1975 Flight 61

2.7 Physical Properties of the Detector 61

2.7:1 Efficiency 61

2.7:2 Fluorescent X-ray Escape Effect 63

2.8 Experimentally Measured Response of Crystals to X-rays : Linearity and Resolution 66

CHAPTER III: DATA ACQUISITION AND TELESCOPE CONTROLS

3.1 Introduction 68

3.2 Pulse Processing Circuitry and Pulse Height Analyser 69

3.3 Orientation, Tracking and Aspect Systems 71

3.3:1 Construction of the Orientor 71

3.3:2 Servo System 73

3.3:2.1 Motor Control and Drive Circuits 74

3.3:3 Source Tracking 78

3.3:3.1 Azimuth Tracking System 78

3.3:3.2 Elevation Tracking System 79

3.4 Other Auxiliary Electronic Systems 81

3.4:1 Power Supplies 81

3.4:2 Telemetry and Data Recording 81

3.4:3 Altitude and Temperature Measurements 82

3.4:4 Inflight Calibration 82

3.5 Preflight Calibrations 83

3.5:1 Pulse Height Analyser Calibration 83

3.5:2 Aspect Calibration 84

3.6 Preparation of Payload for Flight 84

CHAPTER IV: DATA REDUCTION AND ANALYSIS

4.1 Introduction 85

4.2 Data Processing and Separation of X-ray Source Contribution from Background 85

4.2:1 Data Processing 85

4.2:2 Separation of X-ray Source Contribution from Background : Statistical Considerations 86

4.3 Response Function of X-ray Telescope to a Point Source 88

4.3:1 Response of a Cylindrical Telescope Collimator 89

4.3:2 Calculation of Position of Star in Sky 91

4.3:3 Calculation of Exposure Efficiency of Star as a Function of Time 92

4.3:4 Scan Path of Telescope in Sky 93

4.4 Spectral Analysis : Unfolding the Measured Spectrum 94

4.4:1 Introduction 94

4.4:2 Spectrum Transformations 96

4.4:3 Comparison of Experimental and Predicted Data 99

4.4:4 Spectrum Unfolding 100

CHAPTER V: OBSERVATIONAL PROGRAMME AND RESULTS

5.1 Balloon Flight Details : Observational Programme and Flight Performance 102

5.1:1 Summary of Different Flights 102

5.1:2 Observational Programme and Flight Performance 105

5.1:3 Count Rate Profile During the Flight 109

5.2 Contribution of Cyg X-3 in Three Flights 110

5.3 Results : March 29, 1972 Flight 113

5.3:1 Time Profile of Data : Observation of a Flare 113

5.3:2 Source Emission Spectrum During Quiet, Preflare and Flare Conditions 115

5.3:3 Characteristics of the Flare 116

5.4 Results : January 18, 1973 Observation 120

5.5 Results : February 11, 1975 Observation 121

5.5:1 Intensity Variations over One Minute Time Intervals 121

5.5:2 Spectral Variations over 20-25 Minute Time Intervals 125

5.5:3 Average Time Integrated Spectrum 129

CHAPTER VI: X-RAY EMISSION CHARACTERISTICS AND MODELS OF CYG X-1 : DISCUSSION AND CONCLUSIONS

6.1 Intensity and Energy Spectrum of Cyg X-1 130

6.2 Short Period Time Variations in Cyg X-1 136

6.2:1 Flare Phenomenon 136

6.2:2 Short Term Fluctuations in Intensity 144

6.2:3 Short Period Variations in Spectrum 148

6.3 Long Term Variations of Flux from Cyg X-1: Search for Systematic Variabilities 151

6.4 Models for Cyg X-1 165

6.4:1 Mode of Mass Transfer and Formation of a Disk 169

6.4:2 Accretion Disk Models 172

6.4:3 Modified Accretion Disk Models 177

6.5 Summary 182

CHAPTER VII: IONIZATION EFFECTS OF CELESTIAL X-RAY SOURCES IN THE LOWER ATMOSPHERE

7.1 Introduction 187

7.2 Response of Ionosphere to X-rays 190

7.3 Ambient Sources of Ionization in the Night-Time D-Region 193

7.4 Ionization due to Cosmic X-ray Sources 197

7.4:1 Ionization Effects of Sco X-1, Tau X-1 and Galactic Centre 197

7.4:2 Ionization Effects of Transient X-ray Sources 200

7.4:3 Integrated Effect of Cosmic X-ray Sources 205

7.5 Summary 211

APPENDIX I: ENERGY RESOLUTION IN A SCINTILLATION SPECTROMETER 214

REFERENCES 223

INVESTIGATIONS OF HIGH ENERGY X-RAY EMISSION CHARACTERISTICS OF CYG X-1

CHAPTER I

X-RAY ASTRONOMY AND CYG X-1 : AN INTRODUCTION

1.1 X-RAY ASTRONOMY : ITS IMPACT

X-ray astronomy, though only 17 years old, has already made a significant impact on physics in general and astrophysics in particular. X-ray observations have revealed new fascinating objects and phenomena, where the inferred energies, densities, and magnetic and gravitational field strengths are so extreme that we are not even confident that we know the relevant physics. On the theoretical front these observations have opened up new lines of investigation such as the study of the evolution of highly condensed stellar objects and the properties of high density matter under the influence of intense magnetic and gravitational fields. A typical example is the discovery of possible existence of a black hole in Cyg X-1 binary system, which has already given an impetus to the development of physics, because of the realisation that astronomical observations may provide the testing ground for rival gravitational theories. Black holes signify a region of space where matter density approaches infinity and radius tends to zero. Perhaps the paradoxes associated with such a singularity within a black

hole are as fundamental and as far reaching in their implications as the puzzles connected with black body radiation and stability of bound electron orbits in atoms, which confronted physicists at the beginning of this century and triggered the development of quantum theory.

Possible existence of black hole has profound implications on the development of ideas in astrophysics. Once one such object is shown to exist, it raises the possibility that many more such objects may be present in the universe. For example, Lynden-Bell has suggested that supermassive black holes may exist at the centre of active galaxies, and may explain very large energy emission from objects such as quasars. Hawking, using quantum theory of gravitation, has suggested that mini black holes of mass $\ll M_\odot$ might have been formed due to irregularities at the instant of primeval explosion and may be slowly disappearing giving rise to bursts of gamma rays.

On the astrophysical front, a new class of stellar objects have been discovered, where the dominant mode of energy loss is through the emission of X-ray photons. Sco X-1, for example, radiates 2×10^{36} ergs sec^{-1} in the 1-10 keV energy range which is $\sim 10^3$ times the energy radiated by it in the optical band. Moreover, X-ray objects are among the most luminous stellar objects in our galaxy. X-ray luminosity of Sco X-1 is 2×10^3 times the optical

luminosity and 10^{10} times X-ray luminosity of the sun.

Detection of X-ray emission from a large number of binary systems, where a large flux of X-ray photons is emitted when mass flow from a primary star accretes on to a compact companion, has led to the realisation that such an X-ray emitting phase is a rule rather than an exception in the evolution of close binary systems. It is clear that such systems form nature's unique astrophysical observatory for studying high density collapsed objects. For example, these systems make it possible for us to determine, for the first time, the mass of a neutron star, as in the case of Cen X-3, Her X-1, and Vela X-1 systems. We can determine the orbital elements of these systems with great precision and thus can get the mass function of the system. Knowing the mass of the primary star from a study of its visual spectrum, we can estimate the mass of the compact companion, which is of great significance in neutron star astrophysics. It immediately permits us to differentiate between different equations of state in density regions of 10^{15} g cm^{-3}.

Another remarkable advancement on the astrophysical front is the realisation of the fact that there exist a variety of stellar objects exhibiting regular and irregular variations in intensity having widely different frequency characteristics ranging from milliseconds (Cyg X-1), seconds

(Her X-1, Cen X-3 etc.), minutes (Vela X-1, A 1118-61, A 0535+26 etc.), and even to days and months (eclipsing binaries and transient sources). Whereas short period time variations such as milliseconds and seconds could be explained with black hole and neutron star hypothesis respectively, no unique model yet exists for transient sources as also for the sources exhibiting pulsations at larger time intervals.

Discovery of gamma ray and recently of X-ray bursters is yet another important milestone in the revelation of the hitherto unknown phenomena. The launching of more and more sophisticated instruments such as high resolution Bragg reflection spectrometers, and imaging devices (grazing angle telescope) onboard satellites, rockets and balloons capable of providing detailed features of X-ray emission will lead to a better understanding of these puzzling phenomena, and possibly to the discovery of still more puzzling processes taking place in the universe.

1.2 EARLY HISTORY AND X-RAY SKY

Table 1.1 summarises the early history of X-ray astronomy listing various important events starting from discovery of first X-ray source to the launch of Uhuru, the first satellite devoted entirely to the study of non-solar X-ray sources, on December 12, 1970. The launch of Uhuru revolutionized the subject of X-ray astronomy leading to many surprising discoveries and to a qualitative change in our understanding of X-ray sky, due mainly to the long

TABLE 1.1

X-RAY ASTRONOMY : EARLY HISTORY

Year	Event	References
1962	Discovery of Sco X-1, first extrasolar source of X-rays, and a diffuse X-ray background.	Giacconi et al. (1962)
1964	Development of modulation collimator leading to measurement of precise position of Sco X-1 and its optical identification with a 12.5 mag blue stellar object.	Oda et al. (1965) Gursky et al. (1966) Sandage et al. (1966)
1965	First detection of X-rays upto ~50 keV from Crab nebula using balloon borne detectors.	Clark (1965)
1966	Detection of X-ray emission from a source in Virgo constellation, coinciding with an extragalactic object M87.	Byram et al. (1966)
1969	First evidence for a periodically varying X-ray source, in Crab nebula, pulsating with a period of 33 milliseconds.	Fritz et al. (1969)
1969	Nearly 40 galactic sources discovered, but only three (Crab , Sco X-1 and Cyg X-2) identified with optical counterparts. Sources beginning to be catalogued according to their phenomenological characteristics.	Seward (1970) Matsuoka (1970)
Dec. 12, '70	Launch of Uhuru, first satellite devoted entirely to the study of non solar X-ray sources.	
After 1970	Launch of later satellite missions such as Copernicus, OSO-7, ANS, OSO-8, Ariel-V, SAS-3, HEAO-1, HEAO-2 etc.	

time available for observation coupled with high sensitivity and good temporal (96 milliseconds) and spatial ($\sim$1 arc min) resolution.

The fourth Uhuru catalogue of X-ray sources (Forman et al. 1978) lists 339 sources down to a limiting sensitivity of 3×10^{-11} ergs cm^{-2} sec^{-1} for a nearly complete sky survey, using the data accumulated over $\sim$2 years of operation of Uhuru. An additional $\sim$100 more sources have been discovered by rocket borne and balloon borne detectors and later satellite missions, namely Copernicus, OSO-7, ANS, Ariel-V, OSO-8 and SAS-3 (Markert et al. 1975, 1976, 1977; Seward et al. 1976a, 1976b; Villa et al. 1976; Pounds 1976; Gorenstein and Tucker 1976; Lewin 1977; Carpenter et al. 1977; Cooke et al. 1978). (This does not include the sources seen by HEAO-1). This includes about 20 transient sources and $\sim$25 X-ray bursters. Most of these sources have been observed in the 2-6 keV energy range. At lower energies, studies are limited by the absorption of X-rays in circumstellar and interstellar matter, whereas the steep spectrum of most of the sources does not permit their study at higher energies with presently available sensitivity.

A map of X-ray sky in galactic co-ordinates based on the fourth Uhuru catalogue (Forman et al. 1978) is shown

in Fig. 1.1. It is clear from the figure that most of the sources naturally divide themselves into two broad groups, those that are clustered at low latitudes, along the galactic plane, referred to as low galactic latitude sources ($|b| < 20^{\circ}$) and those that spread more uniformly about the sky, called high galactic latitude sources ($|b| > 20^{\circ}$). Majority of sources at low galactic latitudes are among the brightest and are believed to be stellar systems within our galaxy. Most of the high galactic latitude sources are faint and appear to be connected with extragalactic objects.

A large number of X-ray sources have now been studied in sufficient detail to enable us to classify them into few broad groups, based on their phenomenological characteristics. This has become possible because of the precise knowledge of their temporal and spectral behaviour coupled with their identification with known optical objects. A classification scheme based on above criterion is shown on page 8 . This classification scheme is tentative and not very rigid, as there is considerable overlap in observational features of different classes of objects. There are roughly 200 sources lying at high galactic latitudes. Among these, X-ray emission has been observed from normal galaxies like M 31, where X-ray emission is by

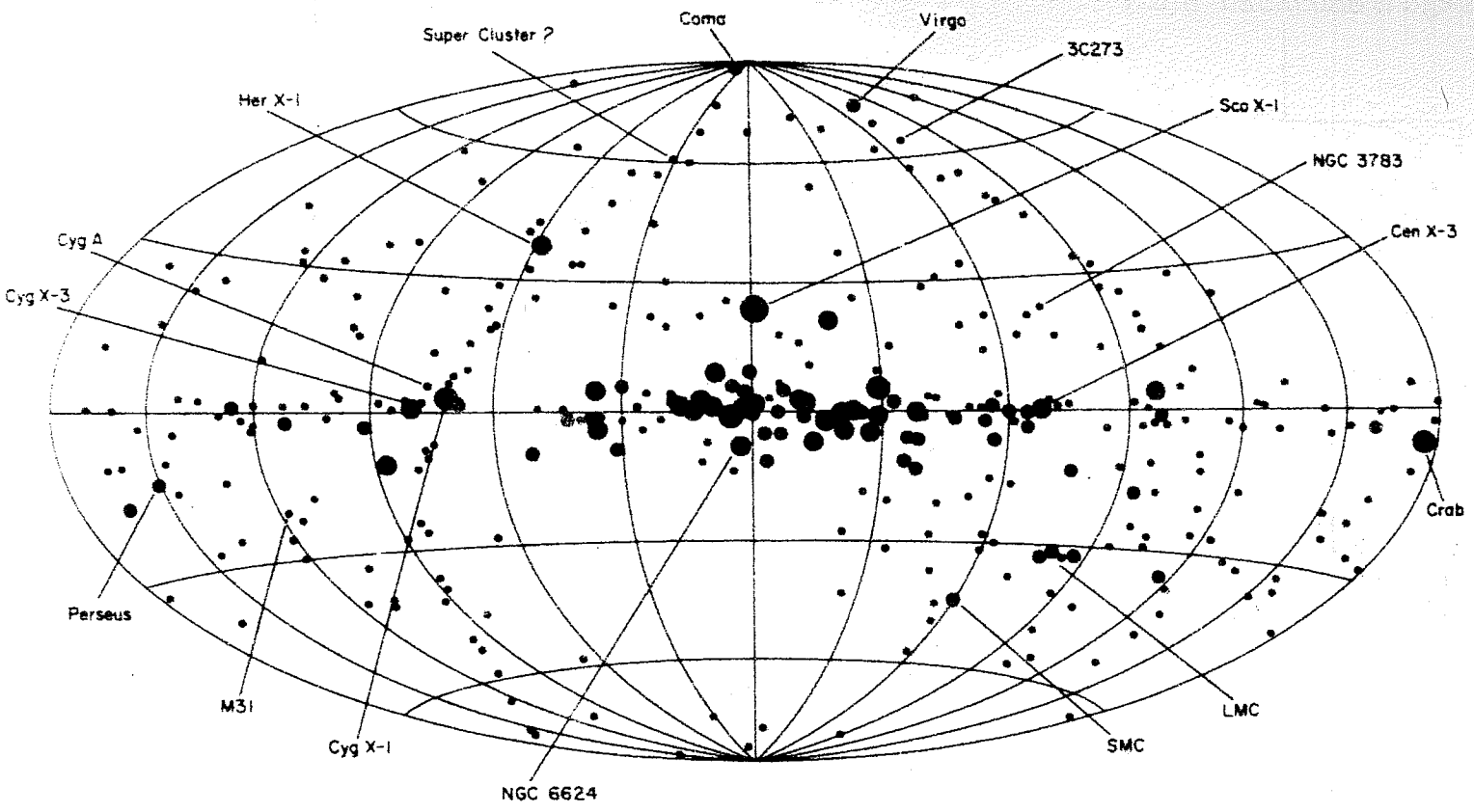

Fig. 1.1 : Distribution of X-ray sources in galactic coordinates based on fourth Uhuru catalog.

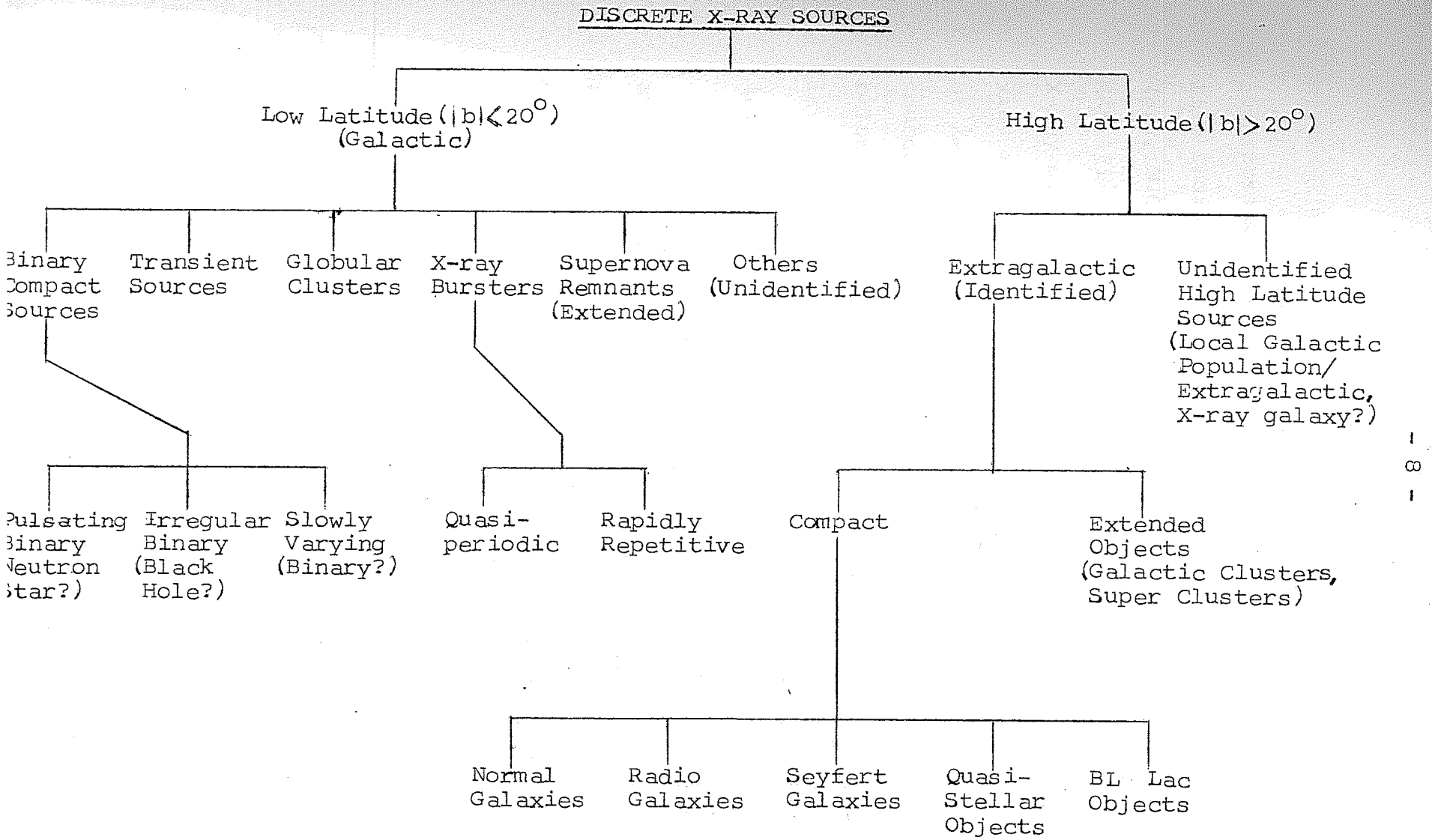
DISCRETE X-RAY SOURCES
Low Latitude (|b|<20°) (Galactic)
High Latitude (|b|>20°)
Binary Compact Sources
Transient Sources
Globular Clusters
X-ray Bursters
Supernova Remnants (Extended)
Others (Unidentified)
Extragalactic (Identified)
Unidentified High Latitude Sources (Local Galactic Population/ Extragalactic, X-ray galaxy?)
Pulsating Binary Neutron Star?)
Irregular Binary (Black Hole?)
Slowly Varying (Binary?)
Quasi-periodic
Rapidly Repetitive
Compact
Extended Objects (Galactic Clusters, Super Clusters)
Normal Galaxies
Radio Galaxies
Seyfert Galaxies
Quasi-Stellar Objects
BL Lac Objects

superposition of individual stars, and from active galaxies like radio galaxies (e.g. Cen A and M 87), Seyfert galaxies (e.g. NGC 4151), QSO's (e.g. 3C273) and BL lac objects (e.g. MKN 421). Clusters of galaxies also appear as extended X-ray sources, while in certain cases the most active galaxies in the cluster are also identified as a single source of X-rays. But more than half of high galactic latitude sources are as yet to be identified, some of which may belong to a new class of objects where principal emission is in X-ray region.

1.3. GALACTIC X-RAY SOURCES

There are about 250 X-ray sources which are lying at low latitudes and are believed to be galactic. The luminosity of these sources is in the range of 10^{35} - 10^{38} ergs sec^{-1}. Therefore, the energy released per gram of stellar material in these sources is much greater than that from normal stars. Quite a good number of these are members of one of the following six classes: binary compact sources, transient sources, globular clusters, X-ray bursters, soft X-ray sources and supernova remnants. Rest of the unidentified sources have been put in the category of others for want of more precise information. Many of these have shown remarkable variability in intensity (Villa et al. 1976; Forman, Jones & Tananbaum, 1976) and

it is quite probable that they are compact binary systems, even though such a confirmation is not possible at present due to their low intensity and poor statistics.

One of the most exciting discoveries in X-ray astronomy is the association of X-ray sources with short period binary systems, made possible by a study of their temporal characteristics (by observation of X-ray eclipses and Doppler modulation of pulse period) and identification with an optical star showing evidence of the binary nature. This class of X-ray sources can be further divided into three subclasses, based on their temporal characteristics.

i) Pulsating sources - depicting well-defined pulsations with periods ranging from fraction of a second to several minutes. Typical examples are Cen X-3, Her X-1 and Vela X-1.

ii) Irregular variables - depict irregular variability over milliseconds. Typical example is Cyg X-1.

iii) Slowly varying sources - depict slow variability (~ minutes to hours). Examples are Sco X-1, Cyg X-2 and Cyg X-3.

The typical X-ray source in our galaxy, with the exception of supernova remnants, is broadly interpreted as a compact object (white dwarf, neutron star or black

hole) orbiting about a stellar companion, and drawing gas supplied by either a stellar wind or critical lobe overflow from the companion star (see Fig. 1.2) (Pringle and Rees 1972; Davidson and Ostriker 1973; Lamb, Pethick and Pines 1973). The matter accreting onto the secondary, in general, has angular momentum with respect to the secondary and, hence, cannot radially fall onto the secondary. Instead it forms a disc and spirals inward as the angular momentum is transported outward by viscosity of the matter in the disc. As it falls through enormously strong gravitational field of the compact object, it is accelerated to almost the speed of light and gets heated to temperatures of $\sim 10^{10}$ ^{o}K thereby radiating X-rays. The maximum temperature achieved and the efficiency of gas accretion process primarily depend on the ratio of the mass of the compact object to its radius. The total X-ray luminosity depends upon the rate at which gas is accreted onto the compact star.

For a compact object of mass M_c and radius R, the gravitational energy released per gram would be of the order of $\frac{GM_c}{R}$. If the mass accretion rate is $\dot{M}$, the total gravitational potential energy released per second is

$$L \sim \frac{GM_c \dot{M}}{R}$$

$$\sim 10^{33} \text{ erg sec} \left(\frac{M_c}{M_\odot}\right)\left(\frac{R_\odot}{R}\right)\left(\frac{\dot{M}}{10^{-8} M_\odot \text{ per yr}}\right) \qquad (1.1)$$

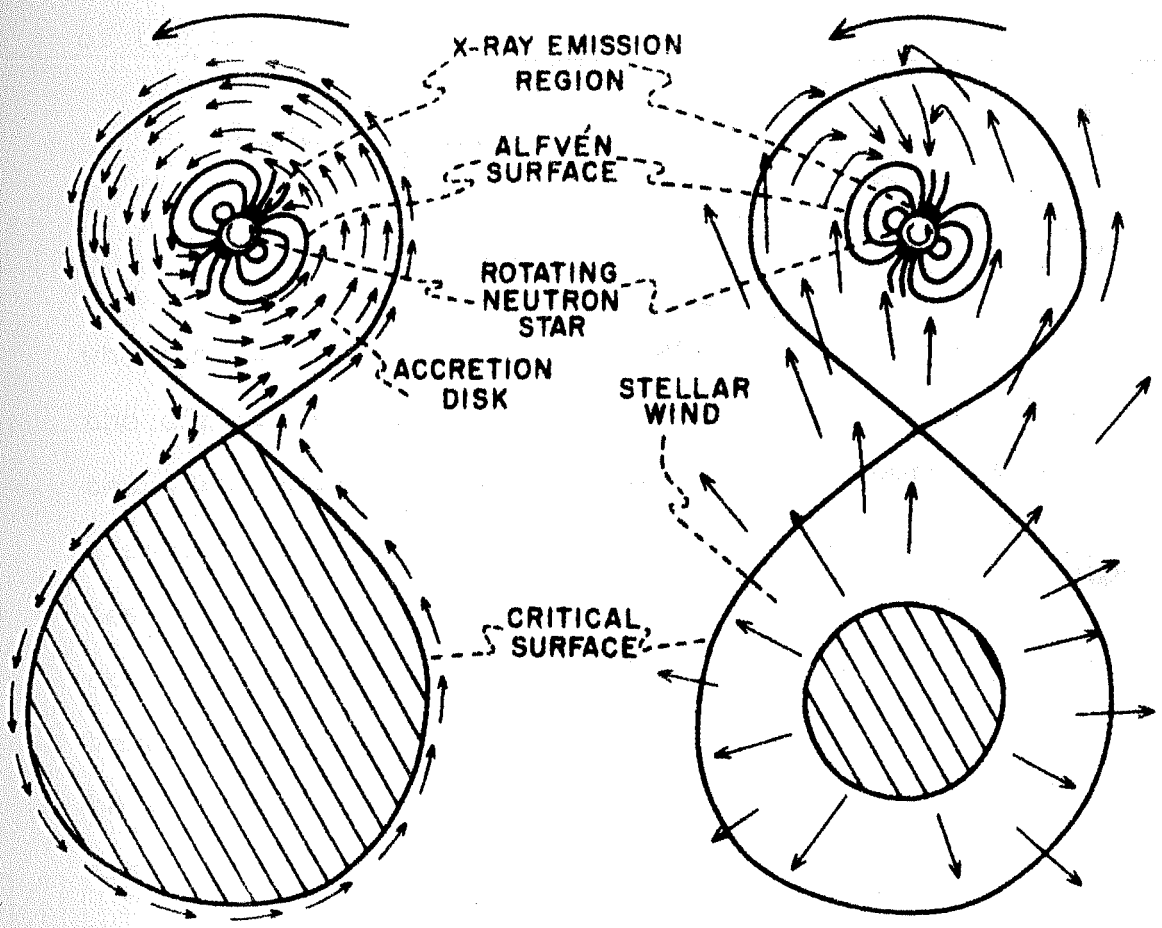

Fig. 1.2 : Schematic representation of the rotating neutron star model for pulsating X-ray stars for accretion disk and stellar wind cases.

Temperatures produced by thermalisation of this flow are of the order of

$$T \sim \alpha \frac{m_p}{k} \frac{GM_c}{R}$$

$$\sim 10^7 \alpha \left(\frac{M_c}{M_\odot}\right) \left(\frac{R_\odot}{R}\right) \ ^\circ K \qquad (1.2)$$

where m_p is proton mass, k is Boltzman's constant and α is the efficiency factor that depends on how the gas is heated. For adiabatic heating in a strong shock wave $\alpha \sim 0.1$ (Landau and Lifshitz 1959). For slower heating processes such as viscous heating in a disc, radiation losses are important and temperature is determined by a balance between radiation losses and heating. In this case α can be as small as 10^{-5} - 10^{-6} (Pringle and Rees 1972; Shakura and Sunyaev 1973).

If the accretion process is to produce temperature of the order of 10^8 $^\circ K$, the ratio of mass to radius must satisfy the relation

$$\left(\frac{M_c}{M_\odot}\right)\left(\frac{R_\odot}{R}\right) \sim \frac{10}{\alpha} \geqslant 100 \qquad \alpha \sim 0.1$$

For main sequence stars, mass-radius ratio is never greater than 3 in solar units. For degenerate white dwarfs it is about 100 and therefore temperatures

of the order of 10^8 ^oK can be produced by shock wave heating but not by viscous heating. For neutron stars and black holes it is 10^5, which means high temperatures can be produced even by viscous heating and temperatures of the order of 10^{12} ^oK can be achieved by shock heating.

From eqn. 1.1 we see that for degenerate dwarfs, mass accretion rates of the order of 10^{-7} $M_\odot$ yr^{-1} can produce luminosities of the order of 10^{36} erg sec^{-1}. For neutron stars and black holes, mass accretion rates of even 10^{-8} $M_\odot yr^{-1}$ will produce luminosities of the order of 10^{38} erg sec^{-1}.

The conditions at the inner boundary of the accretion disc depend upon the nature of the compact object. If the compact object is a slowly spinning neutron star with a dipole-like magnetic field, then the accretion disc may not be the dominant source of radiation. The infalling matter follows the magnetic field lines beyond the Alfven surface of the neutron star and thus must co-rotate and flow towards the magnetic poles. In this case both the star and its immediate vicinity may contribute to X-ray emission, and in the case of an oblique rotator the emitted radiation appears pulsed with a period equal to the rotation period of the neutron star. But for a black hole as the central body of the X-ray source the accretion disc must play an essential role in X-ray emission. Unlike in the case of neutron star the energy cannot be radiated at or near the "surface" of the

object, and it is only the characteristic observational features of X-ray emission which can give a clue to the understanding of the physical nature and structure of the accretion disc.

Many variations of the above fundamental picture can explain the diversity of galactic X-ray sources observed, and a fairly convincing case can be made on the basis of combined radio, optical and X-ray observations that all compact galactic X-ray sources, not associated with supernova remnants, are mass transfer binaries containing a collapsed object. For example, the transient sources can be explained by highly variable gas deposition onto the compact object. This can happen in two ways. There can be either a binary system with a highly eccentric orbit so that only for a small fraction of orbital time the two stars are close enough for gas transfer to occur or a binary with a cataclysmically variable primary star can exist, so that sporadic eruption of the surface layers of primary would cause a long-term variability in gas transfer. Evidently the transient source will be periodic in the former case and non-periodic in the latter.

Accretion can also take place on a massive black hole in the centre of a large collection of stars. In

fact, such a mechanism has already been given for X-ray emission from globular clusters (Bahcall and Ostriker 1975; Silk and Arons 1975). Basic model for production of X-rays in different types of galactic X-ray sources, however, is similar and it is quite probable that these X-ray sources form a continuous chain of sequence, rather than discrete classes of astrophysical phenomena.

1.4 CYG X-1 AND IRREGULARLY VARYING BINARY X-RAY SOURCES

The binary X-ray source Cyg X-1 is one of the most exciting X-ray sources in the sky and is a typical example of the type of X-ray sources described above. It is a binary system containing a collapsed object, which is a good candidate for black hole. The main characteristics of this class of X-ray sources is their short time period (0.1 to 1 sec) chaotic irregular variability, as well as the presence of millisecond bursts in their low energy X-ray emission, which requires that emission region should be very compact.

In what follows, irregularly variable binary X-ray source Cyg X-1 is reviewed since it is of direct relevance to the investigations described in this thesis.

1.5 HISTORICAL DEVELOPMENT OF OUR KNOWLEDGE ON CYG X-1: PRESENCE OF A BLACK HOLE

Cyg X-1 was one of the earliest X-ray sources to be discovered by Bowyer et al. (1965) during a rocket flight and has been extensively studied. Starting with the early observations of Byram et al. (1966), extensive measurements carried out since then using balloon platforms have firmly established the intensity variability of the source (see e.g. Overbeck and Tananbaum 1968a), at least in the region above 20 keV. From a careful analysis of all the data available till 1970, Dolan (1970) was able to demonstrate that not only the flux but also the spectral characteristics of this source exhibited time variability, the flux essentially varying between two levels.

In addition, earlier studies were also able to establish that the source had a hard power law spectrum extending upto few hundred keV, resembling the spectrum of supernova remnants like Crab nebula. The accurate location of Cyg X-1 was, however, fixed only in early 1971 by Uhuru (Tananbaum et al. 1971) and modulation collimator onboard an MIT rocket flight (Rappaport et al. 1971a) and a Japanese balloon flight (Miyamoto et al. 1971). The discovery of a weak variable radio source by Braes and

Miley (1971) and Hjellming and Wade (1971) within the error circle of the X-ray source location suggested that the radio source was also a part of Cyg X-1 system, even though the large error in position determination could not make the identification absolute. Observations prior to March 1971 at 2695 MHz and 1415 MHz could only indicate an upper limit of .005 flux units (Hjellming and Wade 1971; Wade and Hjellming 1972; Braes and Miley 1971) for the radio source. However, during March 1971 the intensity of this radio source increased three fold to .015 flux units, coinciding with a sharp reduction in the X-ray emission from Cyg X-1 in 2-6 keV by almost a fact of 4 (Tananbaum et al. 1972) and an enhancement of flux in the range 10-20 keV by more than a factor of two (Fig.1.3), thus confirming the X-ray/radio association of the source and subsequently leading to its optical identification.

The error box determined for the radio source ($\sim$1") included the 5.6 d spectroscopic binary star HDE 226868 (Webster and Murdin 1972; Bolton 1972a) of 9th magnitude which is at a distance of about 2 kpc (Margon et al. 1973). Based on the assumption that the star is a normal B0 Ib supergiant, the mass of primary star was estimated as greater than 20 $M_\odot$. Observations of Hydrogen and He II 4686 emission lines from the system indicate that

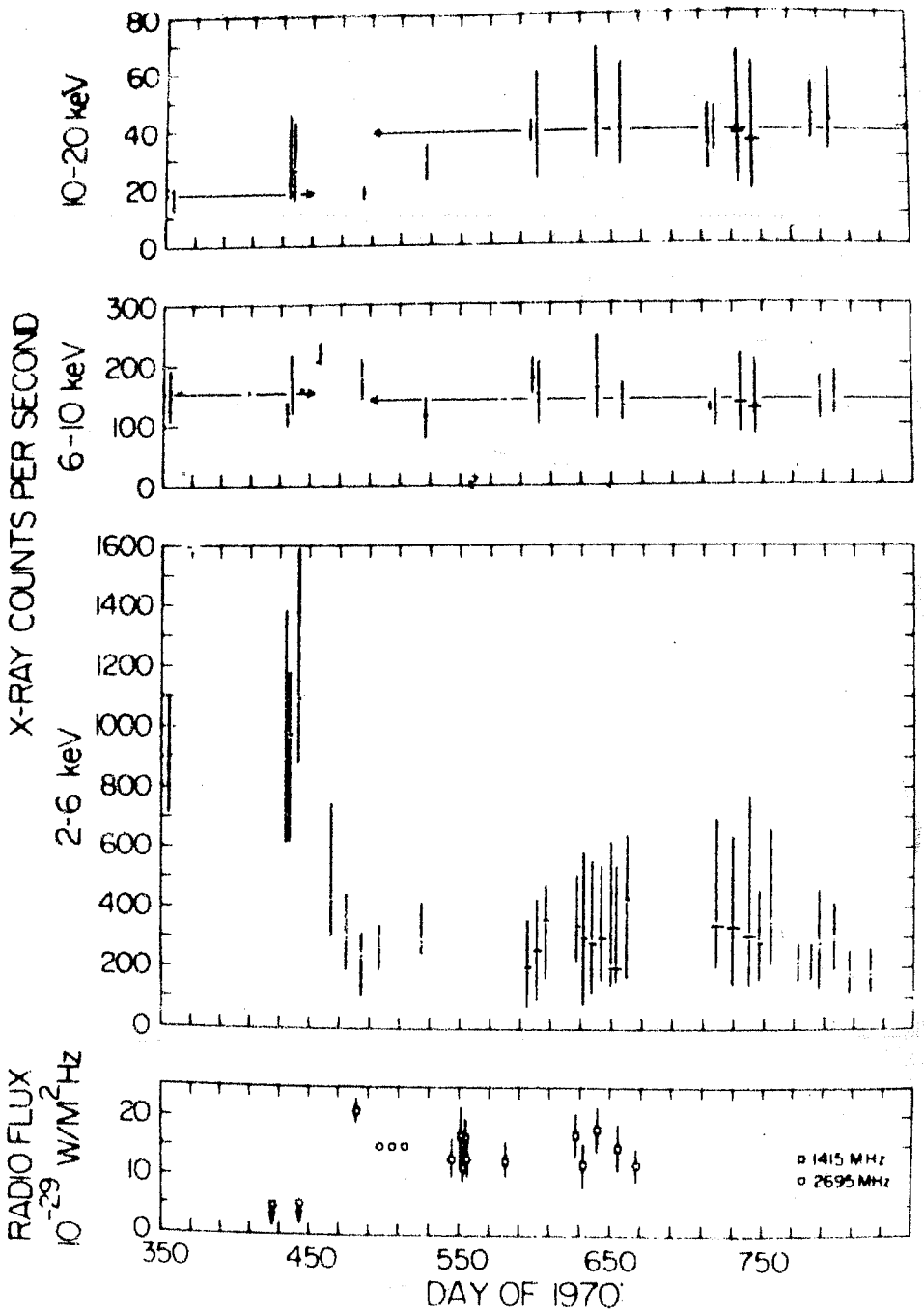

Fig. 1.3 : Simultaneous X-ray and radio observations of Cyg X-1 in 1971. The transition of X-ray intensity and spectrum occured during March 1971 (Tananbaum et al. 1972). The radio data exhibits an anticorrelated transition during the same period.

the emitter of the lines is on a stream at 60^{o} to the line joining the centres of two stars, providing evidence for the existence of streaming matter in the system. The orbital elements of the system determined from observation of HDE 226868 led to the mass of X-ray companion as $> 8\ M_{\odot}$. Recent data from Copernicus and OSO-7(Mason et al. 1974; Li and Clark 1974) have revealed small dips in the X-ray light curves near the superior conjunction (near the phase of closest approach of optical star to us) and the data from All Sky Camera onboard Ariel V showed a 5.6 d modulation of 3-6 keV intensity (Holt et al. 1976a,b). Thus the present evidence strongly supports the hypothesis that Cyg X-1 X-ray source forms a close binary system with HDE 226868, having a 5.6 d period.

The X-ray intensity from Cyg X-1 has been observed to vary significantly at time intervals down to one millisecond. Rocket observations carried out with high time resolution showed the presence of several bursts of $\sim$1 millisec duration (Rothschild et al. 1974, 1977; Oda et al. 1974). This X-ray variability and presence of millisecond bursts in its emission further confirm the compactness of the X-ray emitting region, with a size $\lesssim 10^{7}$ cm, assuming the X-ray emission is coherent over the size of the secondary star. Thus, it is very likely that X-ray companion is a compact object with a mass significantly

greater than 3 $M_\odot$. A mass of 2 to 3 $M_\odot$ is considered to be the limit that a compact star can resist against gravitational collapse and such objects inevitably become black holes (Rhoades and Ruffini 1974).

Numerous alternate hypotheses have been considered by various workers. Brecher and Caporaso (1976), for example, have proposed that the mass limit for a neutron star could be raised upto 4.8 $M_\odot$. Trimble et al. (1973) have pointed out an alternative interpretation of the system which does not require a highly massive primary, if the source is located at a distance of less than 1 kpc, even though this possibility is now ruled out because of the strong evidence confirming the distance of HDE 226868 as more than 2 kpc (Margon et al. 1973; Bregman et al. 1973). Attempts have been made to invoke small spots of size less than 0.1 light second (3×10^9 cm) on a normal star instead of a coherent compact star as a source (Kellogg 1975). In such a case, however, one finds that the Eddington limit is of the order of 10^{34} erg sec^{-1} which is far below the X-ray luminosity of this source ($\sim 10^{37}$ erg sec^{-1}). Models have been proposed (Bahcall et al. 1974; Fabian et al. 1974) in which the companion star of HDE 226868 is not the X-ray source, by invoking a separate low mass third body e.g. a neutron star as the X-ray source. Even though two such models 'distant triple' and 'close triple' have

been proposed, a fairly comprehensive search carried out for the third low mass star by Abt et al. (1977) has yielded no positive results. Phasing of observed X-ray absorption dips (Mason et al. 1974) also appears to present difficulties for three body models. In spite of a number of alternative models that have been proposed, in view of difficulties in explaining all the observational facts presently known, the conclusion that Cyg X-1 is a black hole seems to be almost inescapable.

1.6 CHARACTERISTICS OF LOW ENERGY X-RAY EMISSION

X-ray emission of Cyg X-1 at lower energies, $\sim$2-20 keV, is characterized by its irregular variability over all time scales from years, months and days to seconds and milliseconds. The main characteristics of its X-ray emission at energies $<$ 20 keV are the following.

1.6.1 Transitions

The slowest intensity change in X-ray emission of Cyg X-1 are transitions between low and high luminosity states on a long term (month and year) basis indicating two physically distinct states of Cyg X-1. First discovery of such a transition was made when Uhuru observed a major decrease of X-ray emission in the 2-6 keV range, by almost a factor of 5, which was associated with the sudden appearance of a faint radio source between March 22

and 31, 1971 (Tananbaum et al. 1972), as shown in Fig. 1.3. The reverse upward transition to the high level state occurred during May 1 to May 8, 1975 (Heise et al. 1975). The flux level in the 1-30 keV energy range during this time increased by a factor of about 8 compared to the low level flux established by Uhuru in April 1971, the bulk of the increase, almost tenfold, occurring between 1 and 2 keV. Close examination of the data from ASM onboard Ariel V (Holt et al. 1975) established April 22, nine days before initial observation from ANS, as the date of transition (Fig. 1.4). Close monitoring of the source by Ariel V (Sanford et al. 1975) showed that the source remained in the high state till around May 9-10, and then began to gradually return to the low state as shown in Fig. 1.5, the high state lasting for nearly 20 days. Rao et al. (1976) made X-ray observations on Cyg X-1 in 2.5 - 18.75 keV energy range from Aryabhata, India's first satellite, on April 19, 1975 and provided, for the first time, spectral information just prior to a transition from low state to high state. The spectrum observed by them was much harder ($\alpha \sim 0.7$) than the typically observed spectrum ($\alpha \sim 1.6$) for the source in low state. It is not clear whether the spectral hardening observed by them forms a prelude to transition of the source or is a property of its short term fluctuations, not necessarily related to the transition.

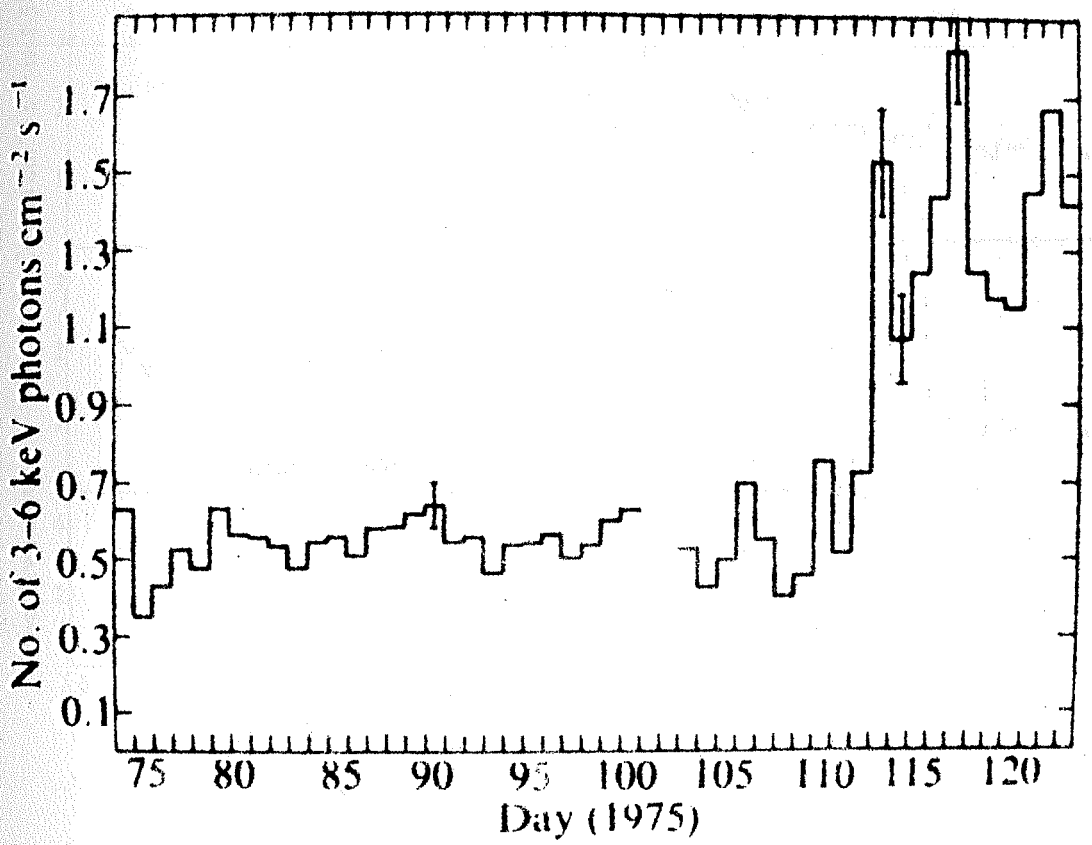

Fig. 1.4 : Transition of Cyg X-1 from low to high state in April 1975 observed by Ariel V All-Sky Monitor (Holt et al. 1975).

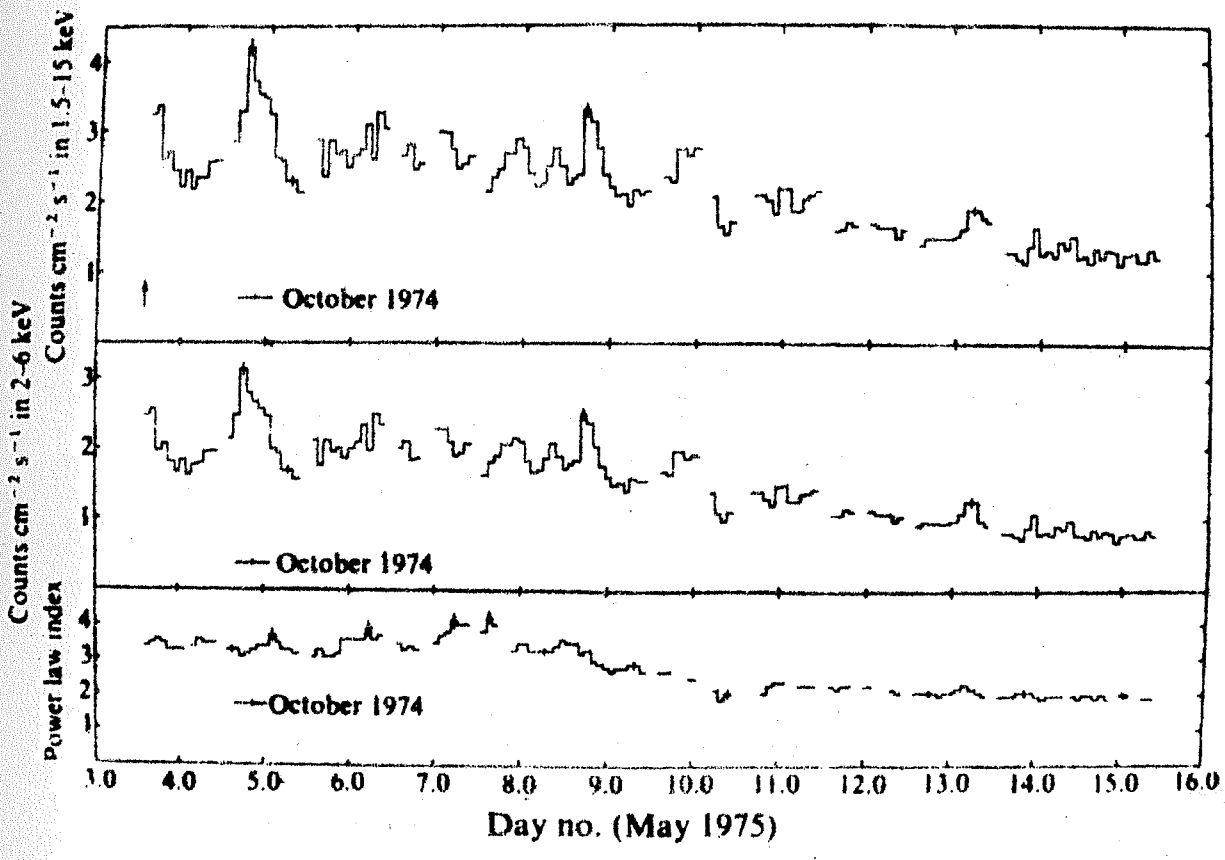

Fig. 1.5 : The X-ray intensity and spectral index of Cyg X-1 for high state and its decay phase in May 1975 observed with Ariel V (Sanford et al. 1975). The corresponding values observed with Ariel V during a brief look in October 1974 are also indicated.

Observations by ASM which has monitored Cyg X-1 quasi-continuously since its launch in October 1974 showed that Cyg X-1 again reverted to the high state in November 1975 (Holt et al. 1976b). A smaller increase with an e-folding decay time of order of a week was also reported in September 1975. The third increase in November was to the level of April event. It did not, however, decay over the same time scale and lasted for nearly three months. The high states appear to be characterised by considerably large variability on time scales of several hours (Holt et al. 1976a).

1.6:2 Absorption Dips and 5.6 d Modulation

X-ray detectors on OSO-7 (Li and Clark 1974), Copernicus (Mason et al. 1974) and ANS satellites (Parsignault et al. 1976) have detected dips in soft X-ray intensity light curves near the orbital phase 0.0 with respect to superior conjunction. The Copernicus satellite found five dips in seven observations, each of which occured just prior to the phase of superior conjunction of HDE 226868, and hence presumably were neither caused by absorption in the stellar atmosphere nor due to an eclipse phenomenon. These dips have been interpreted as due to the absorption caused by matter streaming from primary onto the X-ray star, which occasionally

intercepts the line of sight of Cyg X-1. The observed counter-correlation of X-ray intensity and spectral hardness appears to support this interpretation. Li and Clark (1974) detected one absorption event on January 2, 1973, out of three independent observations made near phase 0.0, which lasted at least 37 minutes and have estimated the columnar density of absorber to be of the order of 10^{22} H atoms cm^{-2}. The Copernicus data have demonstrated that the duration, column density, and also the phases of these dips are variable, all of which suggest that the absorber is not rigidly fixed to the system.

The ANS satellite observed Cyg X-1 from November 3 to 9, 1974 and detected three dips, at superior conjunction and half day and one day after the superior conjunction of HDE 226868. A typical dip is shown in Fig. 1.6, indicating rather short time scales of 10-15 min. During these events the X-ray spectrum was observed to be harder and dips may therefore be interpreted in terms of absorption in gas as suggested by previous observations. However, their observation suggested that the phenomenon of absorption dip may be a rather permanent aspect of Cyg X-1 emission possibly occurring during every binary cycle during some epochs, with a variable complex profile, implying that structure of absorber is rather complex.

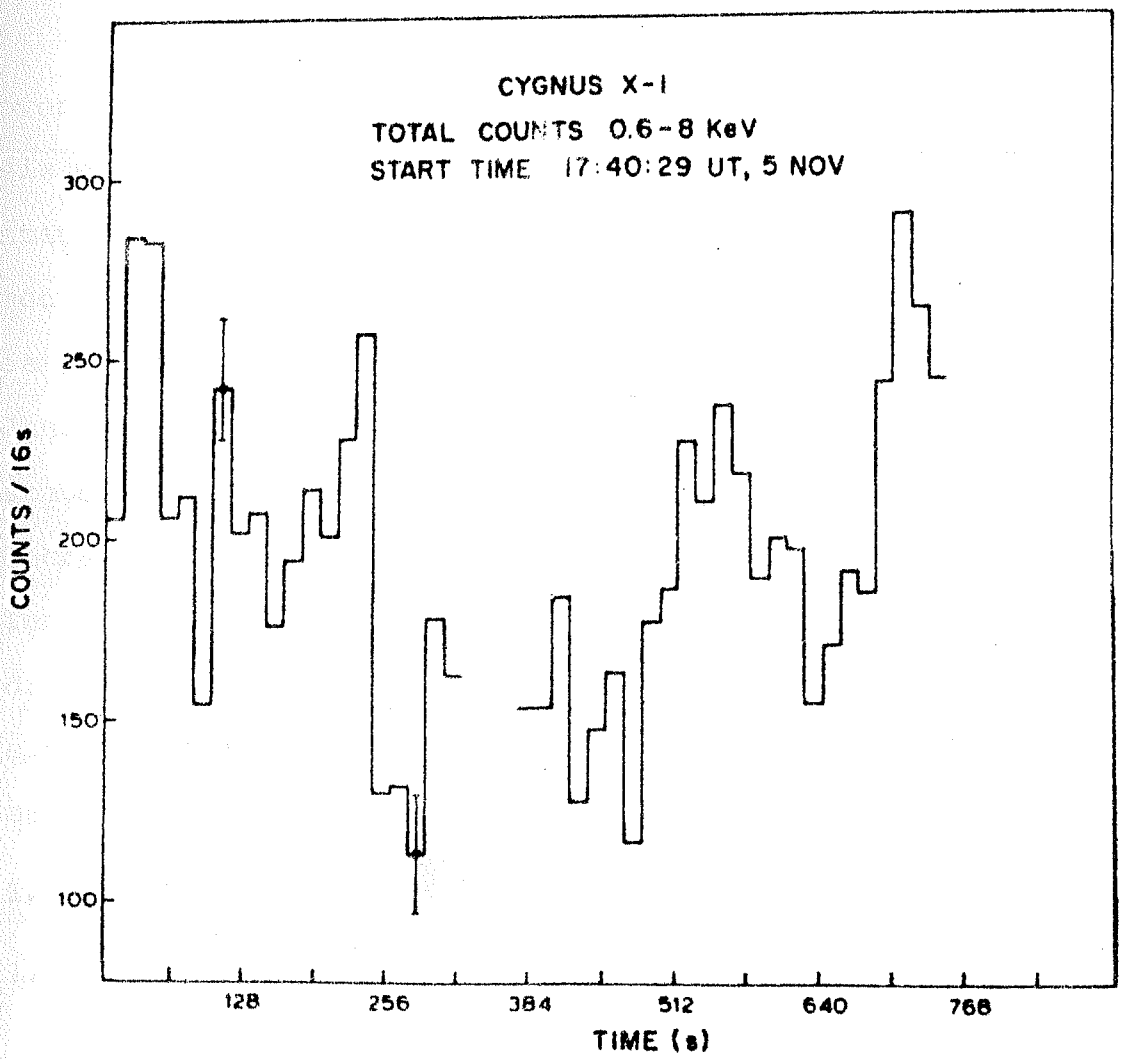

Fig. 1.6 : The counting rate profile of a typical absorption dip in Cyg X-1 low energy intensity observed by ANS (Parsignault et al. 1976).

The Ariel V ASM experiment found a 5.6 d modulation over 3-6 keV energy range, synchronised with HDE 226868, in six months of data prior to April 1975 transition from low state to high state (Holt et al. 1976a). A similar 5.6 d modulation with a smaller amplitude was detected by the same experiment over three months, November 1975 - January 1976, when the source was again in its high state. The results are displayed in Fig. 1.7 showing the decrement at phase 0.0. The amplitude of modulation is largely in excess of what is expected from the size of dips observed by Copernicus, OSO-7, and ANS and it is not clear how these two classes of superior conjunction decrements are related (Holt et al. 1976b).

1.6:3 Short Term Variability

1.6:3.1 Characteristics

On short time scales Cyg X-1 exhibits large fluctuations in intensity at seconds level, including bursts of seconds to millisecond duration. However, in spite of a number of observational studies, systematic understanding of the nature of the variability has not yet been reached because of its complex feature. The results on short term variability of Cyg X-1 are mainly from data by extensive observations of Uhuru and high time resolution rocket observation of MIT (Rappaport et al. 1971b), GSFC (Rothschild et al. 1974, 1977) and ISAS (Ogawara et al.1977).

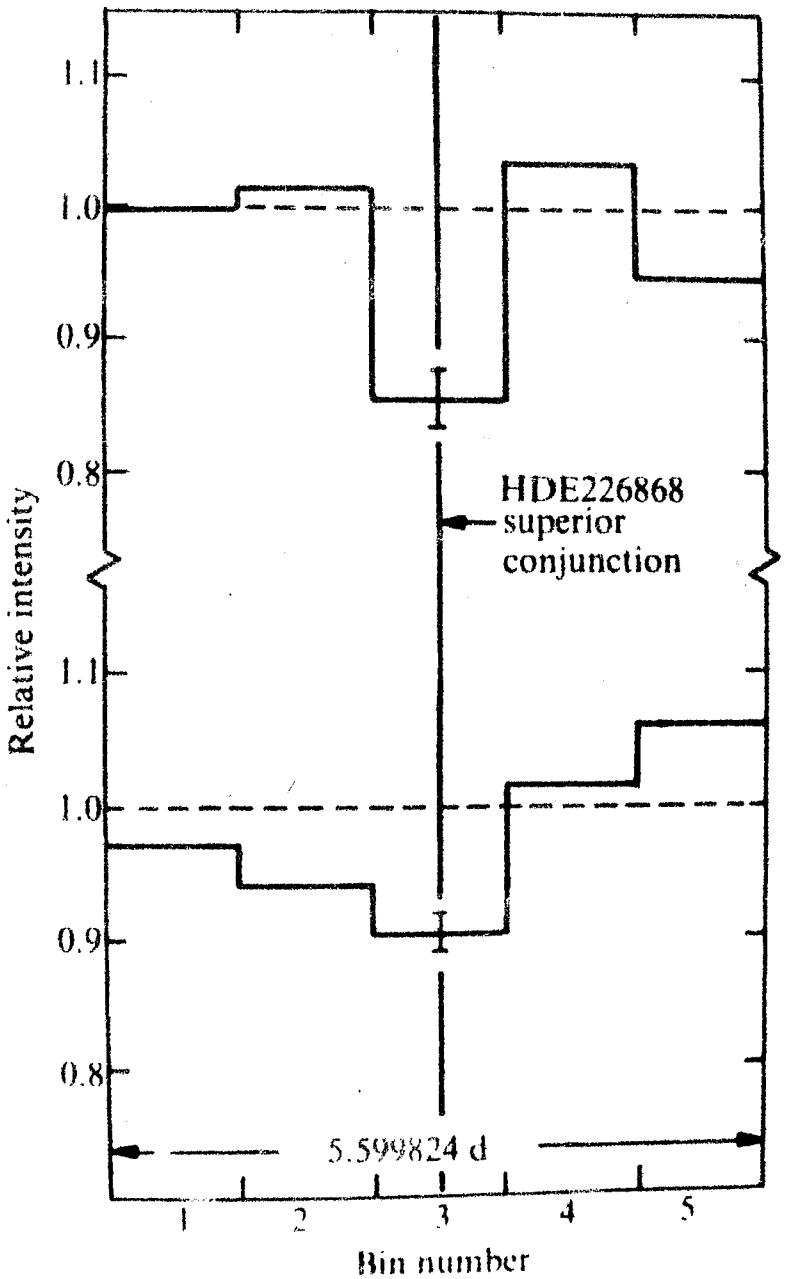

Fig. 1.7 : The 5.6 day modulation of 3-6 keV X-ray intensity of Cyg X-1, showing a decrease in intensity near phase 0.0, found by the Ariel V All-Sky Monitor (Holt et al.1976b). Data taken prior to April 1975 increase (upper trace) and after the start of November 1975 increase (lower trace) have been folded modulo 5.599824 d.

Most of these studies have been made when source was in its 'low state, except some Uhuru scans before March 1971 when source was in the high state. On the basis of these observations, the time profile of source counting rate appears as almost continuum over which are superimposed spikes of different sizes, ranging upto a few times the average intensity, with time scales of a fraction of a second. However, there has been one observation by SAS-3 (Canizares and Oda 1977) in October 1976 when Cyg X-1 exhibited an unusually high degree of variability in its X-ray emission compared to earlier observations, though the average intensity of source was similar to that observed during the low state. This observation showed the source to be in a highly active state exhibiting rapid, continual flaring on time scales of 1-10 sec. Power spectral analysis of the data (Brinkman et al. 1974; Boldt et al. 1975; Weisskopf et al. 1975) indicates that an appreciable portion of the power in Cyg X-1 is contained in the frequency below 1 Hz. Auto-correlation and variance analysis of the rocket data (Ogawara et al. 1977) also support this observation, though these data, in addition to the variations over .1$\sim$1 sec, also show additional characteristic time scale of $\sim$10 milliseconds in the 10-25 keV energy band.

1.6:3.2 Shot noise model

Successful attempts have been made to simulate the time profile of short term variability of Cyg X-1 by superposing random, overlapping and exponentially shaped shot noise pulses of constant height which are essentially characterised by the rate of occurrence (λ) and decay time constant τ which is typically $\sim$ 0.5 sec (Terrell 1972; Boldt et al. 1975). Such a model may physically suggest, for example, the formation of local "hot" spots in an accretion disc. Alternatively (Canizares 1976), $\sim$ 0.5 sec time shots might be the result of reverberation of millisecond pulses produced in the disc on the circumsource configuration of material. Such an interpretation severely imposes a lower limit to the number of photons per millisecond burst (see discussion on millisecond burst). Yet another view is that the shots are produced by turbulence or the twisting of magnetic field lines within the inner portion of accretion disc, in which case $\frac{1}{\lambda}$ may be the characteristic time for build up by differential rotation in an accretion disc of large magnetic stresses to the point of triggering an instability (see, e.g. Shields and Wheeler 1976; Wheeler 1977). The quantity τ could be associated with thermal relaxation time, a magnetic field reconnection time or the time for radial infall of flaring matter into the black hole.

The bulk of the present observations indicate that whereas the decay time τ of the shots is remarkably constant at a few tenths of a second (Boldt et al. 1975), the pulse rate λ scatters over a large factor depending on the intensity of the source, thus supporting the shot noise model. Few exceptions such as the SAS-3 observation by Canizares and Oda (1977) and studies by Ogawara et al. (1977) have yielded different times for τ, suggesting that probably the proposed model is too simple and the variability, in reality, may be more complex than what can be simulated by a simple shot noise model. The first attempt to examine the fraction of shot noise flux as a function of the state of Cyg X-1 by Sutherland et al. (1978) utilising Uhuru data taken in both high and low states indicates that the typical correlation time ($\sim$ 0.5 sec) and the fraction of flux in shots ($\sim$ 30%) are constant, independent of the state. Further, the rate of occurrence of shots also seems to be constant at nearly one shot per second, which, if confirmed, would imply that principal difference in time variability in two states is the amplitude of shots.

1.6:3.3 Periodicity

Several investigations have been carried out on short time-scale pulsations in Cyg X-1 beginning with the early studies by Oda et al. (1971) using Uhuru data. These studies have, however, yielded conflicting results

(Holt et al. 1971; Rappaport et al. 1971b; Shulman et al. 1971), several periods being reported by different workers. The suggestion from these observations was that Cyg X-1 shows sporadic and variable periodicities, which was further confirmed by Schreier et al. (1971) who found periodic pulse trains with periods in the range 0.3 sec to over 10 sec, with fractional power between 10 and 25%, each pulse train persisting for several seconds to several tens of seconds. This was also confirmed by Oda et al. (1972) who produced a dynamic spectrum for the time profile of rocket observation of Rappaport et al. (1971b), which showed that power is concentrated below a few Hz and also showed how various frequency components for the range of 0.1 $\sim$ 5 Hz appear and disappear. Terrell (1972) showed bycomputer simulation that the apparent quasi-periodicity of Cyg X-1 may be simulated by the super-position of shot-noise-like pulsation of a fraction of second duration and that this can reproduce the qualitative appearance of the observed power spectrum. However, Oda et al. (1976) summarising the power spectrum analysis on a number of observed data have suggested that the power in the dynamic spectrum analysis tends to concentrate in discrete bands such as 0.2 - 0.3, 0.4 - 0.5, $\sim$ 0.8 and 1.2 - 1.5 Hz. The probability of this clustering of pulses being produced by means of superimposed random shots simulating the average power spectrum is less than 0.3%, even though the

statistical significance of the result itself is questionable. Rothschild et al. (1977) have also found evidence for periodicities with frequency below 10 Hz. But, because of the marginal nature of results presently available, it is hard to distinguish whether the quasi-periodic behaviour corresponding to large peaks in the power spectrum is genuine (i.e. the period has some physical meaning) or it is merely a statistical and spurious effect with no connection to any oscillatory processes.

1.6:3.4 Millisecond bursts

In addition to the general variability over time scales of 0.1 - 1 sec, Cyg X-1 also exhibits millisecond bursts carrying peak count rates which are often several times the average intensity. These bursts were first discovered in GSFC rocket experiment of October 4, 1973 by Rothschild et al. (1974). They found eight significant bursts of $\sim$1 millisecond duration during 50 seconds of exposure on the source. Three of these occurred within an interval of enhanced emission lasting 20 milliseconds. Recently, GSFC group has confirmed (Rothschild et al. 1977) this finding by a second rocket observation on October 3, 1974. The existence of $\sim$10 milliseconds variability was also indicated by variance analysis of Ogawara et al. (1977).

The second rocket experiment of GSFC of October 3, 1974 identified five millisecond bursts in a 180 sec exposure. Duty cycle for bursting, based on these two flights, is $\sim 6 \times 10^{-5}$. During the combined 230 sec of exposure of two flights there are no other significant bursts over 0.16 - 5 milliseconds, suggesting a specific physical meaning for the "millisecond" bursts. Superimposed analysis conducted after aligning the centroids of a number of bursts showed no evident internal structure within the burst, even though the most intense of the 13 bursts observed in 1974 showed bunching of counts indicating the existence of substructure within the burst.

Canizares (1976) has suggested that the shot-noise pulse and one-second flares can be the result of reverberation of embedded millisecond bursts with the circumsource cloud. The observed millisecond bursts may then have some relation to these millisecond bursts, though the total energy contained in the observed millisecond burst is far too low to supply the energy of the shot-noise burst, and it is very difficult to attribute the shots to typical millisecond bursts observed todate.

The millisecond bursts are generally considered to reflect the nature of innermost part of the accretion disk around the black hole and may be associated with turbulence in disk accretion at the innermost orbit for a black hole.

However, recently Weisskopf and Sutherland (1978) have cast doubts on the physical reality of these observed millisecond bursts because of the statistical uncertainties due to small number of counts associated with these bursts. They have shown that many of the properties of the observed millisecond bursts, including their frequency and their profile, can be accounted for by suitably chosen shot-noise models whose parameters are consistent with Uhuru observations on longer time scales. It is obvious that further extensive observations are needed for establishing the physical nature of the millisecond bursts.

1.7 CHARACTERISTICS OF HIGH-ENERGY X-RAY EMISSION

Due to the steep spectrum and poor statistics, available information on the characteristics of Cyg X-1 X-ray emission at energies $\gtrsim$ 20 keV is scanty. The earlier observations of Cyg X-1 at these energies which have been summarised by Dolan (1970), were mainly confined to the study of its energy spectrum and long term variability over months and years. A variation of intensity by a factor of two in the hard X-ray range was found by Haymes and Harnden (1970) over a time-scale of 5 years. Since 1970, however, a few observational results indicating the time variability on shorter time scales have been reported (Agrawal et al. 1971, 1972a; Matteson et al. 1976;

Fuligni and Frontera 1973; Frontera and Fuligni 1975a; Nakagawa et al. 1973).

1.7:1 Short Term Variability

The first observation of short term variability, the intensity varying by almost a factor of two over time scales of a few minutes in the 22.5-88.0 keV energy range, was reported by Agrawal et al. (1971). In particular, they observed a sudden drop of intensity in 22.5-88.0 keV range by a factor of 2 compared to average intensity towards the end of the flight, without any associated change in the intensity in the 88.0-154.0 keV range. Matteson et al. (1975) carried out a series of five balloon observations of Cyg X-1 on June 10, 1969; July 17, 1969; September 9, 1970; June 11, 1972 and June 23, 1972. Among these the flux was found to be stable within a few ten per cent for an integration time of over a few minutes, except during the flight on June 23, 1972 during which the source intensity changed by a factor of nearly two on a time scale of the order of 10 minutes. Further, on long term time scale, they found that intensity on July 17, 1969 and September 9, 1970 in 20-200 keV range was factor of six below the intensity measured on other occasions, the lowest reported intensity to-date for Cyg X-1 at these energies. Fuligni and Frontera (1973) in a balloon observation of Cyg X-1 on July 1, 1972 detected a state of low flux at energies

between 100-200 keV. This low state was present at the beginning of the observation and lasted for about 20 minutes. After that the flux recovered to its normal state. However, no such large scale variation was observed below 100 keV. A flare like event, which will be discussed later, during the low flux state at higher energies was observed at energies $\lesssim$ 100 keV.

Apart from the existence of fluctuations in intensity of Cyg X-1 at energies $\gtrsim$ 20 keV, pronounced flare-like events of a few minutes duration, with a factor of 2 to 3 increase in intensity, have also been reported during three balloon observations (Agrawal et al. 1972a; Fuligni and Frontera 1973; Frontera and Fuligni 1975a; Nakagawa et al. 1973). Agrawal et al. (1972a) found on April 6, 1971 that Cyg X-1 X-ray emission in the 20-154 keV range increased by a factor of 2.3 in 2 minutes and remained at that level for next 3 minutes, the flare event lasting about 9 minutes. No change of spectrum was found during the flare. Likewise, Fuligni and Frontera (1973) observed a flare for 3 minutes on July 1, 1972 in 20-200 keV energy range, with the intensity of 20-100 keV X-ray increasing by a factor of two. However, unlike the earlier observation, these authors have reported a softening of the spectrum during the flare (power law spectral index changing from 1.84 to 2.7; Frontera and Fuligni, 1975a). The result is similar to

that of Nakagawa et al. (1973) who in a balloon flight on October 7, 1972 in 30-70 keV energy range observed a "flare-up" increase by a factor of 4 with $\alpha \sim 2.94$ and which lasted for a total of $\sim$25 minutes. The flare event, thus, seems to be very complex, and the presently available observational evidence is not good enough to clearly establish the exact nature of flare emission.

1.7:2 Transitions

First evidence for an (anticorrelated) intensity transition at energies $>$ 20 keV simultaneous with low energy transition from high state to low state in May 1975 was provided by Coe et al. (1976) from Ariel V observations, comparing the data taken on May 4-10 (high state) with that on May 11-15 (low state). They found that while below $\sim$ 7 keV the high state corresponds to a higher intensity, at higher energies extending to at least 150 keV, the change is in the opposite sense. Thus, the source shows anti-correlated spectral variability at a pivot point around 7 keV so that flux enhancement at low energy ($E < 10$ keV) is accompanied by a reduction at higher energies and vice versa, which is consistent with the observations of Sommer et al. (1976) and Dolan et al. (1977a). Comparison of OSO-8 observations on November 16, 1975, when the 23-153 keV X-ray flux showed a decrease by almost 40%, with the Ariel V observation (Holt et al. 1976b)

and OSO-8 observation (Fig. 1.8 - Dolan et al. 1977b) of X-ray flux in 3-6 keV range, which showed a corresponding increase, supports the above conclusion. Theoretical models in which X-ray emission is produced in a two temperature accretion disk surrounding the secondary component of binary system (Shapiro et al. 1976; Eardley and Lightman 1976) , predict such a pivoting behaviour. Further extensive observations, however, are needed to understand this important behaviour of Cyg X-1 source.

1.7:3 Periodicity

Even though Manchanda et al. (1971) reported no evidence for pulsation in their data obtained on April 6, 1971, the analysis of balloon data by Bologna group (Frontera and Fuligni 1975b) supports a possible presence of pulsation with 17 sec period in the 30-200 keV energy range. The power contained in the peak showed that 10% of intensity in 1971 and 5% in 1972 and 1973 were pulsed. Their data also indicate that this may be due to a periodic phenomenon, possibly powered ON and OFF on time scales of about one hour (Frontera and Fuligni 1976).

1.7:4 Gamma Ray Burst Candidate

At least two of the gamma ray bursts detected by Vela satellites (on March 15, 1971 and April 12, 1972) seem to have occurred at a location consistent with

B 10000

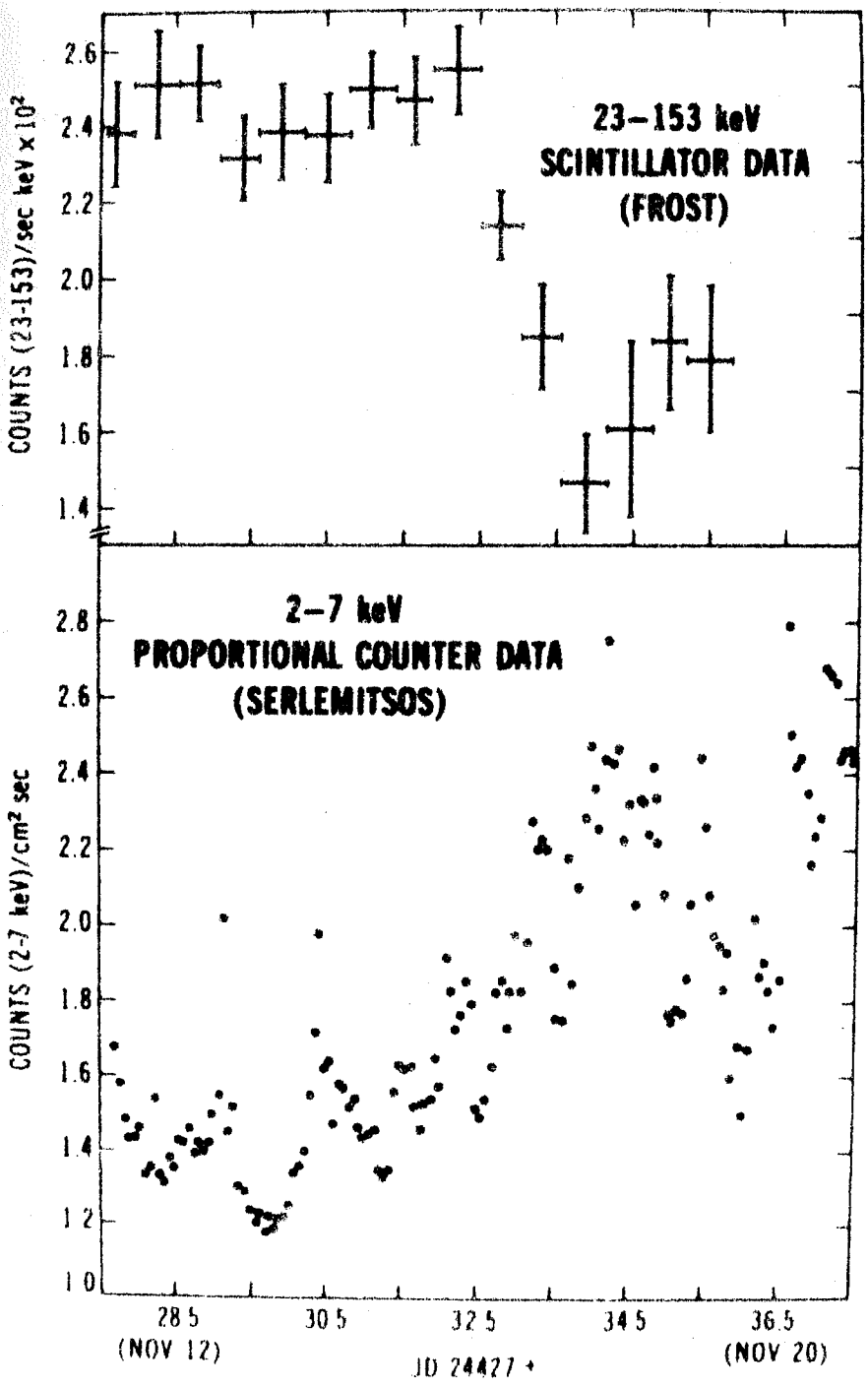

Fig. 1.8 : Counting rates from Cyg X-1 in 23-153 keV and 2-7 keV energy ranges in November 1975 showing the anticorrelated behaviour of the source (Dolan et al. 1977b).

Cyg X-1 (see Strong 1975; Strong et al. 1975; Strong and Klebesadel 1976). One of these occurred when Cyg X-1 was in transition from 'high state to 'low state, indicating the possibility of Cyg X-1 being a source of gamma ray bursts. Recent balloon observations by Ogawara et al. (1976) and Nishimura et al. (1978), which included a modulation collimator onboard, also detected few γ -ray bursts when Cyg X-1 was in the field of view. Even though the data from modulation collimator onboard the balloon indicated that none of the bursts could originate from Cyg X-1, the large statistical uncertainties involved introduce ambiguity. Hence this question should be considered as a still open question.

1.8 ENERGY SPECTRUM OF CYG X-1

Since the energy coverage of the instruments for each observation is limited, few single spectrum observations simultaneously covering a wide energy range are available at present, and hence one has to essentially reconstruct the composite spectra from different observations over limited energy bands. Fig. 1.9 (Oda 1977 and references therein) summarizes the available results on the spectra. It is clear from this figure that Cyg X-1 energy spectrum, like the intensity, shows considerable variability over all energy ranges. Major characteristics of the source spectrum can, however, be summarized as follows:

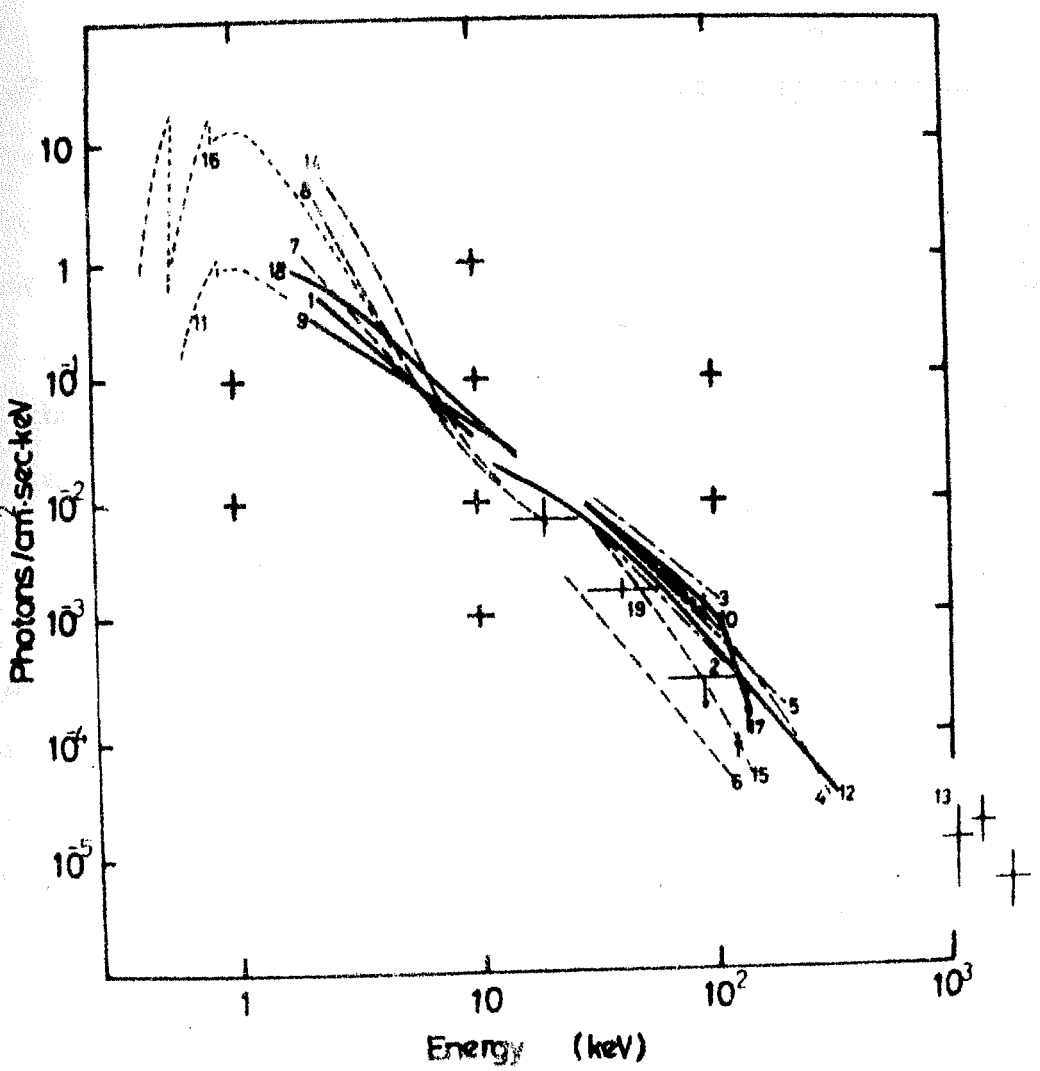

Fig. 1.9 : Summary of observed X-ray spectra of Cyg X-1 (Oda 1977). For details see Oda (1977).

1.8:1 Low Energy (2-20 keV) Spectrum

a) The observations over the low energy band $\sim$(2-20 keV) indicate that there are two distinctly different time-averaged spectra corresponding to the low and high states. In the low state the spectrum over 2-20 keV range is flatter and may be represented by a single power law $\frac{dN}{dE} \sim E^{-\alpha}$ where α is in range of 1.4 $\sim$ 1.8 (Tananbaum et al. 1972; Rothschild et al. 1977; Canizares and Oda 1977; Sanford et al. 1975 and references therein).

b) In the high state, however, the low energy ($<$ 10 keV) flux increases substantially with higher spectral index of $\sim$ 4.0 (Schreier et al. 1971; Heise et al. 1975; Sanford et al. 1975) while the high energy part ($\geq$10 keV) shows very little change with an indication of slightly lower luminosity compared to that of low state, indicating a counter correlation.

c) The shape of the composite spectrum for the high state appears to indicate that the spectrum consists of two physically distinct components, the high energy component and the low energy component, represented by two different power law spectra typically $\sim 1.5\ E^{-1.6}$ and $\sim 300\ E^{-5.0}$ photons $cm^{-2}\ sec^{-1}\ keV^{-1}$. At low energies, the spectrum shows great variability in high state over short time scales (Schreier et al. 1971), spectral index varying between 2.0 to over 5.0, whereas it is virtually stable in

the low state, α being ~ 1.6. Whereas the above mentioned features are generally correct, exhibition of spectral variability from one observation to other, even during the same state, does occur in reality.

1.8:2 High Energy (>20 keV) Spectrum

Above 20 keV, most of the investigators find power law spectra to be the best fit to their data. Below 150 keV, whereas most of the measurements yield a value of 1.8 to 2.0 for the spectral index α, occasional departures from the normal behaviour (see references in Oda 1977) do exist. Likewise, primarily because of poor statistics (Bingham and Clark 1969; Reinert 1969; Riegler 1969; Haymes et al. 1968), an exponential spectrum like $\frac{dN}{dE} \sim \exp(-E/E_o)/E$ where $E_o \sim 94$ keV is also found to adequately describe the high energy behaviour of Cyg X-1.

With a single detector covering soft and hard X-ray range, Baity et al. (1973) have shown that the spectral index changes from 1.04 for $E < 32$ keV to 2.28 for $E > 32$ keV. Observations by Haymes et al. (1968) and Haymes and Harnden (1970) indicate a further steepening of the spectrum of Cyg X-1 in the region of 100-150 keV, the exponent changing to 3.1 above 150 keV. There is some indication for the spectrum to extend beyond 5 MeV (Baker et al. 1973), with a flattening ($\alpha \sim 1.5$) in the MeV range.

1.8:3 Soft X-ray (< 2 keV) Spectrum

Soft X-ray spectrum of Cyg X-1 has been investigated by Gursky et al. (1971), Stevens et al. (1972) and Heise et al. (1975). The soft X-ray spectrum (< 2 keV) can be fitted by $\frac{dN}{dE} = AE^{-\alpha} \exp(-\sigma N_H)$ photons cm^{-2} sec^{-1} keV^{-1}, representing a power law spectrum at the source with an interstellar absorption, where σ is the effective cross-section for a mixture of the interstellar gas derived by Brown and Gould (1970) and N_H is the columnar density of hydrogen equivalent to the interstellar gas mixture. The value of N_H that fits the spectrum is of the order of 10^{21}H atom cm^{-2} (Stevens et al. 1972; Gursky et al. 1971). Two representative soft X-ray spectra, one taken by Stevens et al. (1972) in low state (11) and the second by Heise et al. (1975) in high state (16), are shown in Fig. 1.9. Search for X-ray polarization in Cyg X-1 at 2.6 and 5.2 keV (Weisskopf et al. 1977) during the high state has yielded negative results.

1.9 OPTICAL OBSERVATIONS : STAR HDE 226868

1.9:1 Spectroscopy

Cyg X-1, identified with the 9th magnitude spectroscopic binary star HDE 226868, is an early-type supergiant. It has a normal absorption-line spectrum, which was classified originally as BO Ib and later as O9.7 Iab by

Walborn (1973). The spectral type of the star may vary with phase of binary from about O9.5 to B0. The apparent magnitude and colours of the star are V = 8.87, B-V = 0.81, and U-B = -0.30 (Hiltner 1956). Absorption line velocities have been observed in many investigations with different spectrographs (see Bahcall 1975; Bolton 1975 and references therein). Intermittent emission at H_β has been observed by Bolton (1972b), while emission at H_α was noted by Smith et al. (1973). The unusual and variable emission line at He II λ 4686 was discovered by Bolton (1972b) and it has been suggested (Brucato and Kristian 1973; Hutchings et al. 1973; Bolton 1972b) that the velocities of this emission line are in antiphase with the absorption line velocities (Fig. 1.10 from Bolton 1975). Observations indicate that the emitter of the line is on a stream at 60° to the line of centre of two stars. As seen in Fig. 1.10 there is large scatter in the measured λ 4686 line velocities. Several authors have suggested that the emission lines may be gravitationally bound with the secondary and originate in a broad stream or region of matter flowing from primary HDE 226868 onto the secondary (see e.g. Bolton 1975). A part of large scatter of measured λ 4686 line velocities as seen in Fig. 1.10 may be due to variable velocity and location of emitting region on the mass stream.

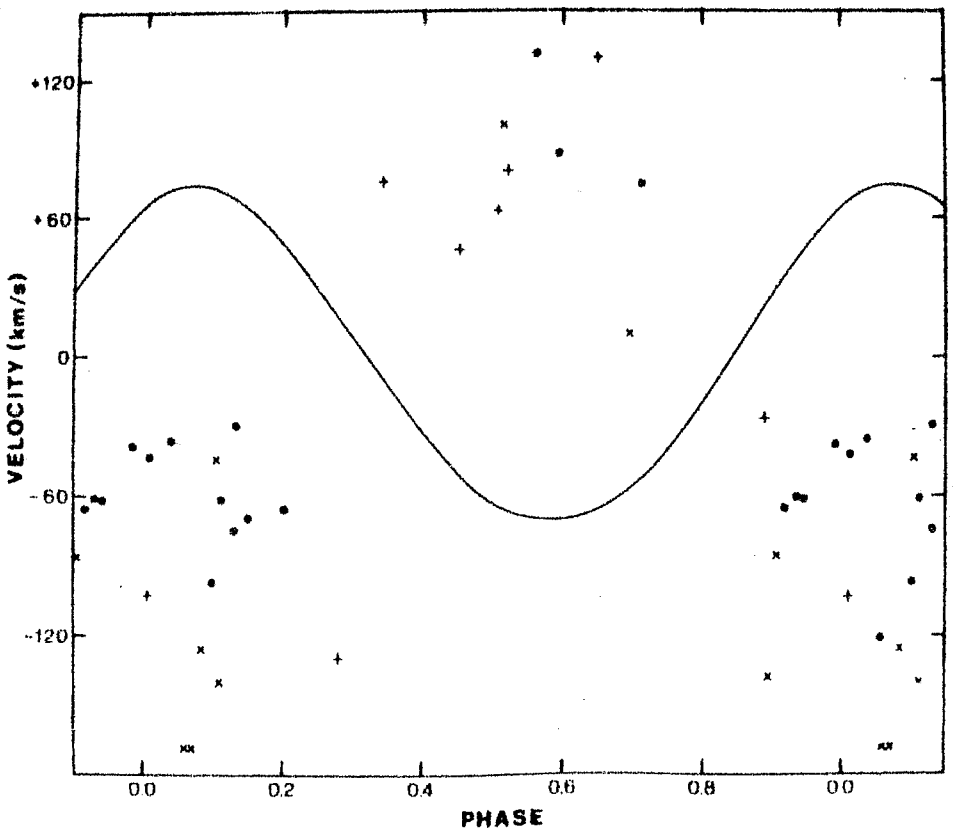

Fig. 1.10 : Radial-velocity phase curve and He II λ 4686 emission line velocities of HDE 226868 (Bolton 1975).

1.9:2 Orbital Elements

The orbital period of binary is well determined from spectroscopic observations of the optical star (see e.g. Bolton 1975) and is $\sim$ 5.60 days. Orbital elements of the system are as follows (see Bolton 1975):

Period (days)	5.599824 ± 0.000037
Epoch for phase 0 (JD 2,440,000+)	1556.46 ± 0.16
Superior conjunction (X-ray companion behind B star)	1561.22
Inferior conjunction	1558.24
Amplitude of velocity variation K(km sec^{-1})	72.2 ± 0.8
e	0.06 ± 0.01
ω	$330^{\circ} \pm 10^{\circ}$
a Sin i (10^6 m)	5.549 ± 0.061
Inclination i	27°
Mass function f(M)	$0.217 \pm 0.007\ M_{\odot}$

1.9:3 Distance

Various investigators (Walborn 1973; Margon et al. 1973; Bregman et al. 1973) have estimated that HDE 226868 is at a distance of $\sim$ 2.5 kpc, based on the absolute magnitude of primary derived from its spectral type, an estimate of interstellar reddening in the direction of star and consistency arguments involving other effects of interstellar medium.

1.9:4 Light Variations

Small amplitude light variations with the 5.6 day binary period were discovered in 1972 (Lyutyi et al. 1973; Walker 1972 and Lester et al. 1973). From various studies carried out so far (Hilditch and Hill 1974; Lanning 1975; Walker and Quantanilla 1974, 1978; Lester et al. 1976), the light curve is found to be double sinusoidal with two unequal maxima and minima per orbital period, generally attributed to changes in aspect of a distorted luminous primary.

Evseyev et al. (1974) have searched for super-rapid time variations in the range 10^{-4} to 3 sec and have put an upper limit of 0.03 on the amplitude of such variations. On the other hand, Auriemma et al. (1976) have reported modulated optical emission with an amplitude of a few per-cent and a period of $\sim$ 83 milliseconds as transient events, from two observations made with the 91 cm Catania Astro-physical Observatory. The observation on June 11, 1975 yielded a pulsation period of 83.531 $\pm$ 0.008 milliseconds which lasted for $\sim$10 minutes. On July 18, 1975 several events occured in span of $\sim$ 1 hour with periods ranging between 83.6 $\sim$ 83.7 milliseconds. It is argued that the modulated component superimposed on the bulk of luminosity from the supergiant may be generated by instabilities in "spots" in the accretion disk. However, Robinson et al.

(1978) have found no evidence of such pulsation in 90 hours of 10 minute long individual light curves, spaced over 65 nights in September to November 1976 and in May to October 1977. It is not clear whether the absence of pulsation by the latter authors is due to change in properties of Cyg X-1 between 1975 and 1976, or the periodicities detected by Auriemma et al. were spurious.

1.9:5 Polarization

A large average linear polarization ($\sim$5% at 5000 Å) of HDE 226868 has been reported (Hiltner 1956; Gehrels 1972; Coyne et al, 1974). This is primarily due to the interstellar dust and is consistent with the estimated distance of $\sim$ 2 kpc.

A search for 5.6 day period in the optical polarization of HDE 226868 (Nolt et al. 1975; and Kemp et al. 1978) has revealed a stable polarization variation in the V band which is synchronous with the 5.6 day orbital period, having a double sinusoidal curve with a dominant second harmonic (2.8d). The peak-to-peak amplitude of this variation is $\sim$ 0.25% and it is largely in the position-angle Stokes parameter and shows marked wavelength dependence; its amplitude in ultraviolet being at least a factor of $\sim$2 lower. This group has also found (Kemp et al. 1977) a new 39 day periodicity in the linear polarization of U band light for HDE 226868, which is about seven times the

5.6 day orbital period of binary system, Based on this result Milgrom and Shaham (1977) have produced a model for Cyg X-1 involving a three-body system in which the third component is in a 39 day orbit about the 5.6 day X-ray binary system. However, Walker et al. (1977) have failed to observe such a periodicity both in the 349 nights of B band optical data obtained during 1972 - 76, and in the X-ray data from Ariel V taken over 590 days which included both high and low states.

Observation of circular polarization of HDE 226868 in 1974 by Michalsky et al. (1975a,b) showed that it has both constant and variable components. The constant part is believed to be interstellar circular polarization whereas the time varying part of the circular polarization appeared to vary synchronously with the 5.6 day period, thus suggesting an intrinsic mechanism. This varying component had double sinusoidal curve similar to the blue intensity variation and the largest component of variation was at 2.8 day period. However, later observations (Michalsky and Swedlund 1977) in 1975 showed largest varying component at 5.6 day. The various results on periodic variation of polarization of HDE 226868 are thus still not consistent and hence require further observations.

1.10 RADIO OBSERVATIONS

Radio observations of Cyg X-1 from 1970 to 1975 have been made by Hjellming and Wade (1971), Hjellming (1973), Hjellming et al. (1976), Hjellming (1975) at 2695 MHz and 8085 MHz using NRAO radio interferometer, and by Braes and Miley (1971, 1972) at 1415 MHz using Westerbork synthesis radio telescope. The NRAO observations from 1971 to 1975 are summarized in Fig. 1.11 (Hjellming 1976).

Prior to March 1971, the radio emission from this source was below the upper limit of 0.005 flux units. Observations beyond April 1971 showed an unresolved radio source at the position of Cyg X-1. This sudden appearance of radio source was correlated with a drop in 2-6 keV intensity which led to the optical identification of Cyg X-1, as mentioned earlier. Since then Hjellming (1976) has monitored the source at 2695 and 8085 MHz upto October 1975, which is shown in Fig. 1.11. After the initial appearance of the radio source, the dominant characteristic of the source has been continuous presence of a flux at, on the average, 0.015 flux units level. Except for occasional fluctuations about the mean level, no major change in radio flux from this mean was reported until May 1975. No binary periodicity was evident in the fluctuations about the mean level. Coincident with the May 1975 increase of low energy X-ray intensity, however, the radio flux also

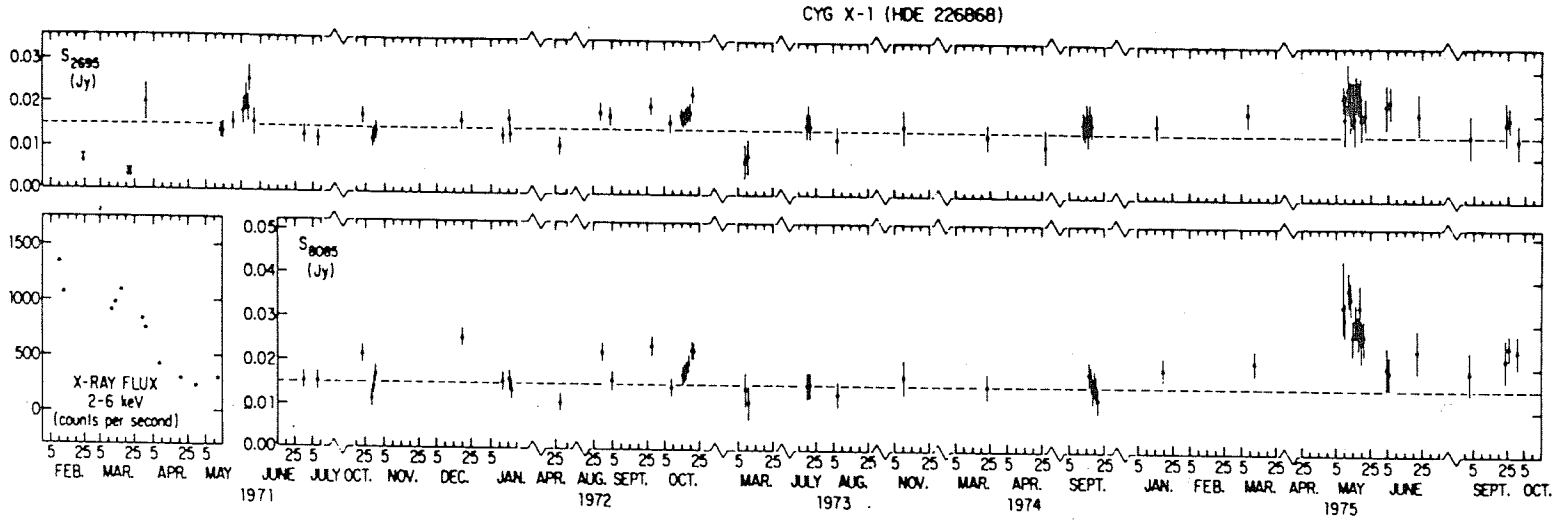

Fig. 1.11 : The radio flux densities of Cyg X-1 at 2695 and 8085 MHz for the period between February 1971 and October 1975 (Hjellming 1976), together with X-ray data in 2-6 keV range during March 1971 transition.

increased, which was in contrast to the apparent counter-correlation of the radio and X-ray intensity during the March 1971 transition. The mean level for the period of May 9 to May 20 was 0.031 flux units at 8085 MHz and 0.02 flux units at 2695 MHz, sometimes reaching value of 0.045 flux units at 8085 MHz. Further, the major characteristic of Cyg X-1 radio source between March 31, 1971 and April 1975 was a flat radio spectrum, that is, a spectral index of $\sim$ 0.0. However, during May 1975 increase the spectral index increased to $\sim$ 0.31 implying that if radio emission mechanism is thermal, the source has become optically thicker.

The May 1975 increase was followed by a rapid decay to only slightly above normal level at 8085 MHz and a slow decay at 2695 MHz, as shown in Fig. 1.11. The data during September-October show that radio source continued to be at normal or only slightly above normal flux level upto October 1975. The decay of Cyg X-1 radio source during May-June 1975 was qualitatively similar to decay seen at X-ray wavelength during this period. The general indication is that low state is the normal state and high state is a transient enhanced or unstable state. Attempts to observe a pulsed radio flux from Cyg X-1 have been made by Downes (1970), Mohanty et al. (1971) and Taylor et al. (1972) and have not yielded any positive results.

1.11 AIMS AND OBJECTIVES OF PRESENT INVESTIGATIONS

From the above discussion of presently available information regarding emission characteristics of Cyg X-1 at X-ray energies, it is clear that Cyg X-1 has peculiar features in its X-ray emission, in several respects, and a clear, coherent picture of its emission characteristics (specially at energies $>$ 20 keV) is yet to emerge because of complexity of source characteristics. The investigations of X-ray emission characteristics of Cyg X-1 assume greater importance because of the possibility of this emission coming from a region near a black hole, because such studies will give us clues to the understanding of the physical characteristics of accretion disks surrounding black holes and the behaviour of matter around black holes. Theoretical models of Cyg X-1 X-ray emission, based on accretion disk around black hole, possess certain characteristic time scales and predict various kinds of instabilities (Pringle et al. 1973; Lightman and Eardley 1974; Shibazaki and Hoshi 1975; Thorne and Price 1975; Shakura and Sunyaev 1976), which allow us to compare the observational results with various models and to discriminate between them, so as to arrive at an appropriate model describing the behaviour of matter around black holes. For example, the shortest time scales on which the source intensity is found to vary may be related to the physical nature (e.g. plasma

characteristics, nature of black hole and structure of binary system) of innermost domain of plasma disk surrounding the black hole, and the study of energy spectrum and variability is likely to give us clues to the structure of accretion disk and properties of plasma around the black hole and their temporal behaviour. Similarly, long term variation of flux and energy spectrum may be associated with instabilities in plasma disk surrounding the black hole.

While detailed information regarding variability of source intensity and energy spectrum is now available in 2-20 keV energy range through satellite observations, similar data at high energy are still very fragmentary and insufficient to attain a coherent picture of source emission. There are pieces of evidence for time variation of the hard component of X-ray flux but no concrete information is yet available regarding short term variability of energy spectrum at these energies. It is clearly very important to extend studies of source flux, energy spectrum and their temporal properties to higher energies to get an overall picture of the source variability at all energies, which can throw more light on nature of the source. Further, the shape of energy spectrum specially at energies > 40 keV, where not many statistically good measurements are available at present, is important for discriminating between various theoretical models (see for example, Thorne and

Price 1975). Similarly, no direct information is available regarding high and low transitions of source intensity at high energies, though there are pieces of evidence to suggest that source shows anti-correlated variability at energies $>$ 20 keV. Confirmation of the existence and nature of two states is very important for understanding the instabilities giving rise to such transitions.

The objectives of observations described in this dissertation were to improve the intensity and spectral measurements and their long and short term variability at energies $>$ 20 keV. This required significant improvements in X-ray telescope sensitivity (and less cosmic-ray produced background by making observations from a location near the geomagnetic equator) and long observations of the source with extremely good exposure efficiency. The observations presented here were obtained from balloon borne telescopes, using scintillation crystals as basic X-ray detectors, which are described in Chapter II. In Chapter III, the data acquisition system, telescope controls, aspect determination, and other aspects of instrumentation are briefly summarised. This is followed, in Chapter IV, by a brief account of mathematical and computational techniques used to retrieve necessary information from data collected.

Observational programme of different flights and results obtained from these experiments are described in Chapter V. The implications of these results in relation to X-ray emission characteristics and models of Cyg X-1 are discussed in Chapter VI. In this chapter we have compared the results obtained in our observations with both low and high energy observations obtained by other workers and have tried to give a description of X-ray emission to arrive at the total picture of X-ray emission characteristics of Cyg X-1. Various models proposed for explaining the emission of X-rays in Cyg X-1 are then described and discussed in the light of totality of the observations.

The thesis concludes with a discussion of effect of X-ray sources on night time D-region of ionosphere in Chapter VII.

CHAPTER II

X-RAY TELESCOPES AND THEIR CHARACTERISTICS

2.1 INTRODUCTION : BASIC REQUIREMENTS OF A BALLOON BORNE X-RAY ASTRONOMY EXPERIMENT

Two fundamental requirements thatgovern the basic design of all non-focussing X-ray astronomy telescopes are:

a) An efficient X-ray telescope, to detect the X-ray photons and convert them into electrical pulses and a collimator, to limit the field of view of the detector to a small region of the sky. The telescope should, in addition have a charged particle shield surrounding the detector to reduce the unwanted X-ray background produced by cosmic ray charged particles through their interaction in the material surrounding the detector.

b) A system to carry the detector to the top of the earth's atmosphere, to limit the absorption of X-ray photons in the atmosphere above the detector as much as possible. Any such platform (balloons, rockets or satellites) must incorporate attitude measurement devices and suitable orientation equipment to point the telescope in the desired direction.

The observations (in the energy range $\sim$20-200 keV) presented in this thesis were carried out using balloon-borne X-ray telescopes. Since the X-rays of energy $>$ 20 keV can penetrate 3-5 g cm^{-2} of residual atmospheric depth, stratospheric balloons can be conveniently used for investigations in this energy range. In addition to providing a large weight carrying capability, such balloons also provide a much larger observation time ($\sim$2-4 hours) compared to rockets ($\sim$ 10 minutes).

In addition to the above mentioned basic requirements of a X-ray astronomy experiment, the following considerations are of importance in designing a ballooon-borne X-ray astronomy instrument:

a) Periodic monitoring of the intensity of the X-ray background.

b) Periodic checking and calibration of the detector and its associated electronics.

c) Continuous measurement of the balloon altitude during flight, with an accuracy of at least 0.1 g cm^{-2}, to correct for attenuation of X-rays in overlying atmosphere.

d) Appropriate insulation of the instrument against low temperature environment in the troposphere.

2.2 INTERACTION OF PHOTONS WITH MATTER

The detection of X-ray photons is an indirect process which utilizes the property of their interaction with matter. In the X-ray energy range the photon wavelength being comparable to or less than the interatomic spacing of solid materials, the principal interaction is with individual atoms and their constituents rather than by processes such as reflection and refraction which involve large scale or coherent effects (Grazing-incidence reflection at low-energies, $\lambda \geqslant 3\text{Å}$., depends on the wavelength encompassing many lattice planes when projected tangentially onto a solid). Coherent photon scattering entails virtually no loss of photon energy nor does the process result in a fast secondary electron. The only processes of importance for the detection of the incoming photon are those in which the photons are absorbed or scattered in single events. Three principal interactions which the photons in the high energy radiation encounter are:

1. Photoelectric absorption by the entire atom
2. Compton scattering on the individual bound electrons of each atom
3. Positron-electron pair production in the Coulomb field of the nucleus.

Unlike charged particles, which lose energy continuously by ionisation and therefore have a definite range,

a well collimated beam of photons undergoes an exponential attenuation in passing through matter. This is because the photons are eliminated from the beam either due to a catastrophic loss in a single interaction, by photoelectric effect or pair production, or scattered due to Compton scattering. The absorption of X-rays is expressed by the relation :

$$I = I_o \; e^{-(\mu/\rho)x} \qquad (2.1)$$

where I_o is the incident flux, I is the flux remaining after traversing material of x g cm^{-2} thickness and μ/ρ (cm^2 g^{-1}) is the total mass attenuation coefficient of the medium.

The mass attenuation coefficient (μ/ρ) is made up of three different parts (μ_p/ρ), (μ_c/ρ) and (μ_{pp}/ρ), corresponding to each of the three processes of high energy photon interaction with matter listed earlier. For photons of energy $<$ 1.02 MeV, pair production is unimportant. The relative importance of photoelectric absorption and Compton scattering depends upon the energy of photons and the atomic number of the medium through which they propagate. Extensive literature (see e.g. Price 1964; Evans 1955) is available in this area. Fig. 2.1 summarises the results and shows photoelectric attenuation coefficient, Compton scattering coefficient, Compton absorption coefficient, total Compton coefficient, and total

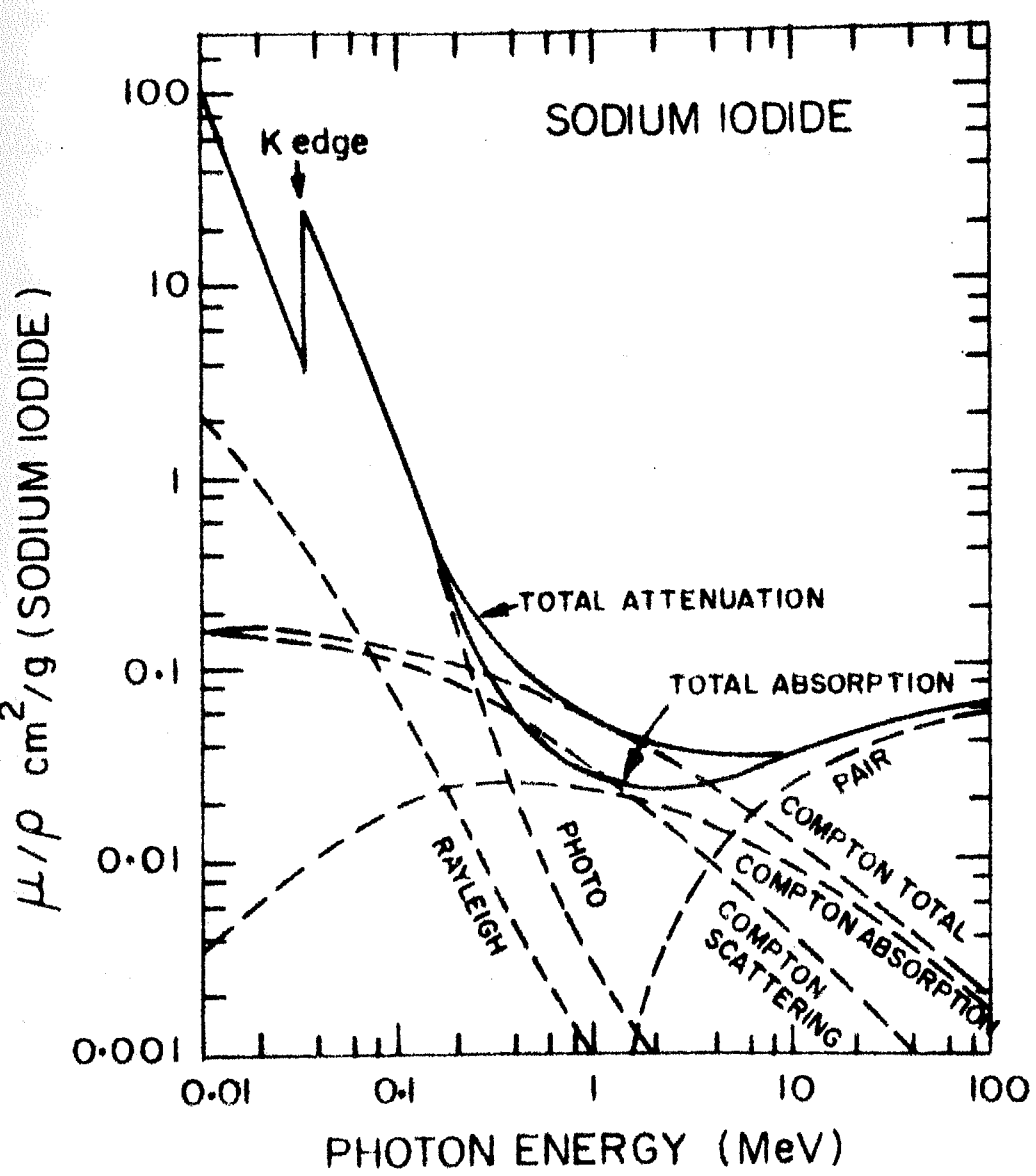

Fig. 2.1 : Photon interaction cross-sections for NaI(Tl) as a function of energy.

attenuation (sum of photo-electric, total Compton and pair production) and absorption coefficients (photoelectric + Compton absorption + pair production) for NaI, the detector used in the present experiments, in the energy range 0.01 to 100 MeV. It is seen that for NaI, in low energy range, below $\sim$300 keV, photoelectric absorption is the most important process and from 0.3 MeV to $\sim$ 3 MeV, Compton scattering is the dominant process of photon absorption.

2.3 CHOICE OF THE DETECTOR

Since, both from the point of view of scintillation efficiency and decay time, NaI is superior to CsI, NaI (Tl) crystal has been chosen as the detector element. The detector is coupled to a matching photomultiplier tube with S-11 response to get the maximum signal output. The light pulse output from the photomultiplier has a $\sim$ 60 n sec rise time and a decay time of $\sim$ 250 n sec. The pulse height is linear within 12% between 20 and 150 keV. Self-absorption in the crystal is negligible and scintillation efficiency is only weakly dependant on temperature, the light output dropping by about 20% when the temperature is lowered from + 50^{o}C to -50^{o}C. The mass attenuation coefficient for NaI (Tl) crystal for different energies is shown in Fig. 2.1.

2.4 ENERGY RESOLUTION IN A SCINTILLATION SPECTROMETER

It is well known that the processes occuring in a scintillation spectrometer, starting from energy loss in the crystal to the final pulse output at photo-multiplier anode, are subject to systematic and statistical variations. Consequently, the scintillation spectrometer renders an incident "monochromatic line" in the form of a broad pulse height distribution. It is necessary to have a clear understanding of the shape and width of the pulse height distribution of the system for a quantitative interpretation of the data. The shape and width of this distribution depend upon many factors such as detector geometry, uniformity of photocathode response, dynode structure etc. and hence have to be evaluated for each detector system. The FWHM of the detectors used in the present investigation were evaluated both theoretically and experimentally from the detector response to radioactive sources. Detailed analysis of the same is given in Appendix I.

2.5 GENERAL CRITERIA IN THE CHOICE OF DETECTOR DIMENSIONS AND DESIGN OF ANTICOINCIDENCE SHIELD AND COLLIMATOR

In order to improve the sensitivity of the telescope to a point source, it is essential that background counting rate of the telescope should be as low as possible to enhance the signal to noise ratio of the detection

system. Background counting rate of a X-ray telescope is determined largely by the radiation environment of detector during observation. At balloon altitudes, the background primarily consists of the following:

a) Diffuse cosmic X-rays

b) Atmospheric X-rays generated by cosmic rays through electron photon cascades in atmosphere

c) Primary and secondary cosmic ray charged particles

d) γ -rays and neutrons produced in the atmosphere, and

e) X-rays and γ -rays produced in the local material around the detector by cosmic ray charged particles.

Of the five sources mentioned above, charged particles passing through the detector pose no problem in being discriminated since they deposit $\sim$ 1.3 MeV of energy per g cm^{-2} of NaI, and therefore can be rejected by an upper level logic threshold. Neutrons mainly suffer inelastic collisions with iodine and sodium nuclei, causing their disintegration. Since a number of heavily ionizing particles are released in each such interaction, the neutron induced events can also be discriminated easily. Gamma-rays produced in the atmosphere and in the local material around the detector by cosmic ray charged particles contribute most to the background counting rate of

the telescope. Since the γ -ray produced background depends on the size and thickness, it can be minimised by choosing a low thickness for the detector, consistent with the requirement of high detection efficiency for X-rays under study. In the present investigations 4 mm thick NaI crystal was chosen which has efficiency close to 100% for X-rays of energy upto 80 keV and above 50% for X-rays in 100-150 keV range.

The background counting rate of the detector due to cosmic and atmospheric X-rays is proportional to the solid angle of the detector. Therefore, it is necessary that the opening angle of telescope should be kept as small as possible to minimise the contribution of the isotropic background. This is done by restricting the forward aperture of detector by a collimator, which absorbs X-rays outside the defined aperture. In addition, the detector assembly is surrounded by a passive shield to protect it against high energy X-rays and γ -rays leaking from the sides and rear of the detector. Shielding and collimation is provided by a combination of "graded" absorbers, tightly fitting one over the other, which have the property that valleys in the absorption just below K-edges of one are covered by the strong absorption above the K-edge of the adjacent material.

In addition, it is necessary to use active shielding to minimise the contribution from the cosmic ray charged

particles which produce X-rays when they interact in the local material around the detector. A plastic scintillator of thickness about 1.5 cm acting in anticoincidence with the main detector has been used as an active shield.

2.6 X-RAY TELESCOPES FOR DIFFERENT EXPERIMENTS

2.6:1 X-ray Telescope for March 29, 1972 Flight

Present observations were carried out in the energy range $\sim$ 20-150 keV. The lower energy limit is imposed by the absorption of X-rays in the atmosphere, the grammage at typical balloon height being 4-5 g cm^{-2}. Upper energy limit is essentially set by low X-ray flux due to the steep spectrum of X-ray sources in relation to the background counting rate.

Schematic diagram of the X-ray telescope used in the March 29, 1972 observation is shown in Fig. 2.2. The X-ray detector was a 10 cm diameter, 4 mm thick NaI (Tl) crystal with a .032" aluminium radiation window. The crystal was viewed by a 5" R.C.A. 8055 photomultiplier tube. The crystal was covered by a 9.5 mm thick quartz light pipe, to minimise the effect due to non-uniformity in the photocathode response and to protect the detector from beta and gamma radiation from K^{40}, contained as an impurity in the glass envelope of the photo-multiplier. The crystal assembly was coupled to the photomultiplier tube by means

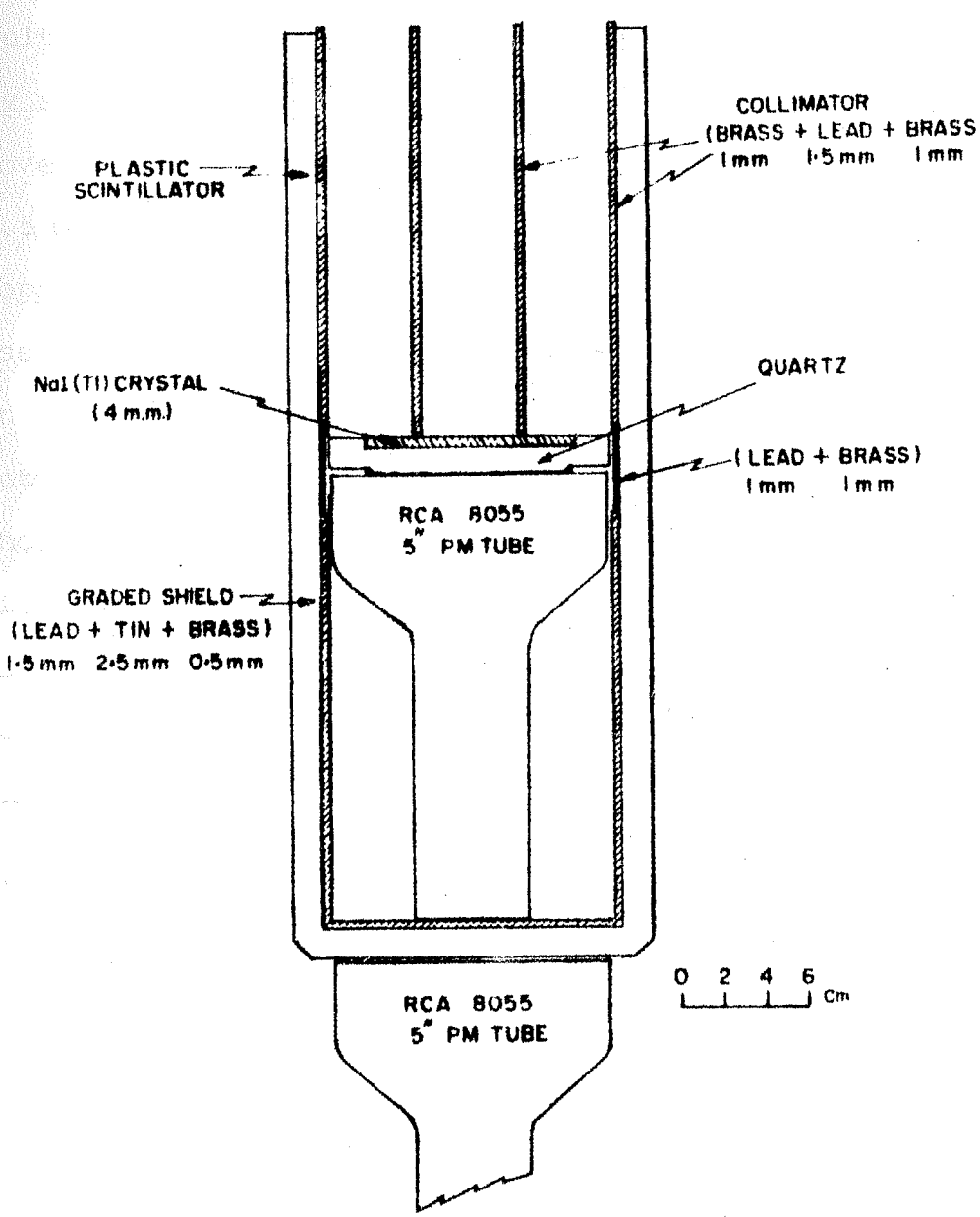

Fig. 2.3 : Schematic of X-ray telescope used in January 18, 1973 observation.

of silicone optical cement (Dow Corning 20-0057). The photomultiplier tube was shielded from external magnetic fields by a mu-metal shield. The entire detector assembly was covered on sides and bottom by a graded shield composed of 1.5 mm of lead, followed by 3 mm thick tin and 0.5 mm thick copper, to reduce the background contribution. The detector assembly with the passive graded shield was further enclosed in a 1.5 cm thick NE-102 plastic anticoincidence scintillator, viewed by a 5" R.C.A. 8055 photomultiplier tube, as shown in Fig. 2.2. The scintillator was wrapped on all sides with an aluminium foil of high reflectivity to increase the light collection efficiency. The forward aperture of the detector was defined by a collimator of brass and lead having a FWHM of 18.8° as shown in the figure.

2.6:2 X-ray Telescope of January 18, 1973 Flight

Schematic diagram of the X-ray telescope used in January 18, 1973 observation of Cyg X-1 is shown in Fig. 2.3. This telescope differed from that used in March 29, 1972 observation very slightly, namely the bottom of the NaI crystal was not covered by passive graded shield and plastic scintillator, as the contribution of particles and photons entering from rear of the detector was found to be negligible. Further, the passive shield extending above the detector was found to be adequate to provide appropriate collimation to X-rays with a FWHM of 13.5° and

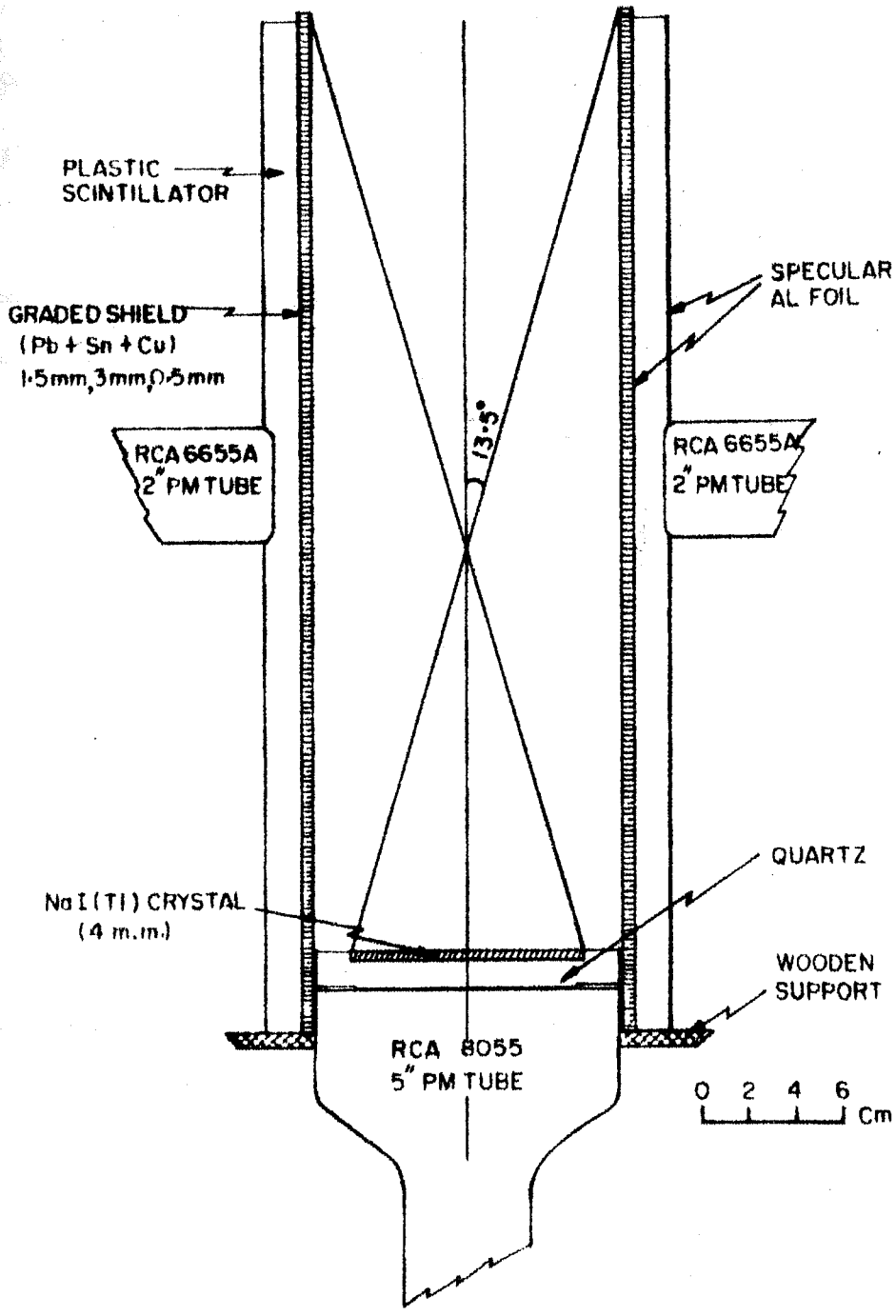

Fig. 2.2 : Schematic of X-ray telescope used in March 29, 1972 observation.

hence an additional collimator was dispensed with.

2.6:3 X-ray Telescope of February 11, 1975 Flight

The X-ray telescope for this flight consisted of three NaI (Tl) crystals to provide a large area. First two detectors were of 10 cm diameter and 4 mm thickness each, and the third detector was of 12.5 cm diameter and 1.25 cm thickness. All the three crystals had .032" aluminium radiation window. Each of the three detectors was viewed by a 5" R.C.A. 8055 photomultiplier tube and output of the three were monitored independently. No active anti-coincidence shield was used in this telescope as the large weight and the considerable complexity involved in encasing this large detector assembly in a plastic anti-coincidence well was not justified by the amount of background rejection obtainable by using it. A honeycomb collimator made out of hexagonal tubes of tin (4 mm) and copper (0.5 mm), having a length of 15.4 cm and area 41.5 cm^2, was used for defining the forward aperture of the telescope to 13.5^{o} FWHM. All the three detectors and the collimator were enclosed in passive graded shield of lead (2 mm), tin (3 mm) and copper (0.5 mm).

2.7 PHYSICAL PROPERTIES OF THE DETECTOR

2.7:1 Efficiency

The intrinsic efficiency of a counter i.e. the probability of the photon passing through the window and

getting fully absorbed in the crystal is given by

$$\varepsilon(E) = \exp\left[-\mu_w(E)\, d_w\right]\left[1 - \exp\left(-\mu_c(E) d_c\right)\right]$$

where μ_w and μ_c are the mass attenuation coefficients of the window and crystal material respectively in $cm^2\ g^{-1}$ and d_w and d_c are the thicknesses of window and crystal material respectively in $g\ cm^{-2}$. The computed values of the transmission factor of .032" thick aluminium window used presently and the detection efficiency of 1 mm, 4 mm and 1.25 cm thick NaI (Tl) crystals for various energies is plotted in Fig. 2.4. It is seen that at lower energies, the entrance window limits the transparency of photons for detection in the crystal. Also, for 4 mm crystal, detection efficiency given by continuous curve is almost 100% upto 70 keV and then starts dropping slowly with increasing photon energy. It falls to 90% at 100 keV, 50% at 150 keV and only 36% at 200 keV.

However, it should be noted here that the detection efficiency shown by continuous curve gives only the probability of detection of a photon of energy E, irrespective of what the energy of detected photon will be. Due to the escape peak effect (which will be discussed fully in next section), an X-ray photon of energy E keV may be detected as a lower energy X-ray of $(E - E_K)$ keV where E_K is the energy of iodine K-flourescent X-ray.

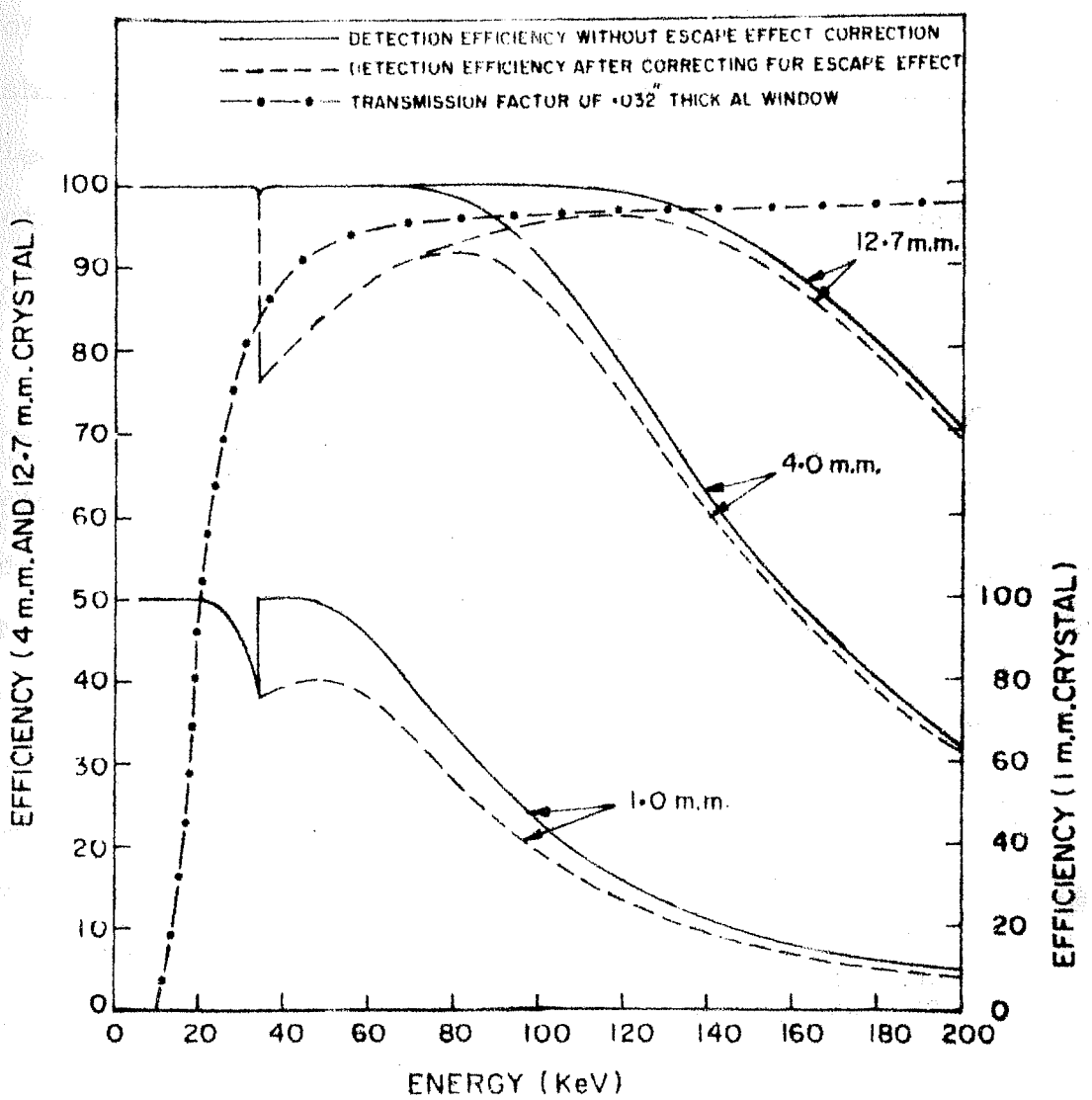

Fig. 2.4 : Detection efficiency of 1 mm, 4 mm and 1.25 cm thick NaI(Tl) crystals as a function of energy. Dashed line indicates transmission through 0.032" thick aluminium window.

In order to evaluate the probability $\varepsilon'(E)$ that a photon of energy E will be detected with its full energy, $\varepsilon(E)$ should be corrected for the escape probability (Stein and Lewin 1967) of iodine fluorescent X-ray. The corrected efficiency is shown by dashed lines in Fig. 2.4.

2.7:2 Fluorescent X-ray Escape Effect

Due to the escape effect, the incident photon spectrum is distorted. The necessity of correcting for this effect has been shown by Stein and Lewin (1967). In this section we will calculate the X-ray escape probability from NaI crystals used in present experiments. The escape probability depends upon the geometry and dimensions of the crystal used. Since the probability of ejecting photoelectrons from L shell in NaI is only 10%, L X-ray escape effect can be neglected in NaI and it is necessary to only consider K X-ray escape. Liden and Starfelt (1954) have given comprehensive treatment of calculation of escape probability for a crystal whose linear dimensions perpendicular to incoming X-rays are large compared with the mean free path of K X-ray iodine. In this case we can calculate the relative number of X-rays being photoelectrically absorbed at a given depth. Of these interactions δ_K take place in the K-shell and of that fraction the fluorescence yield ω_K is the probability that the atom relaxes by emitting a K-shell X-ray. Assuming isotropic emission

we can integrate the penetration probability of the K-shell X-ray over the variable path length to escape the detector. If P is the probability that an incident photon will give rise to a K X-ray photon which escapes from the detector with energy E_K, then P is given by the equation (Overbeck 1968)

$$P(E) = \int_0^{x_0} dx\, \mu\, e^{-\mu x}\, \frac{1}{2}\, \delta_k\, \omega_k \left[e^{-\mu_k x} + e^{-\mu_k (x_0 - x)} - \mu_k x\, E_1(\mu_k x) - \mu_k (x_0 - x)\, E_1\{\mu_k (x_0 - x)\} \right]$$

where x_0 = thickness of crystal in g cm^{-2}

μ = total absorption coefficient of crystal in cm^2 g^{-1}

and $E_1(X) = \int_x^{\infty} e^{-t}\, \frac{dt}{t}$

We have calculated P (E) for K_α and K_β fluorescent X-rays in NaI (Tl) crystal for values of E ranging from E_K to 200 keV. If f_{K_α} and f_{K_β} are fractions of K X-rays which are K_α and K_β X-rays respectively, then escape probability for K_α and K_β X-rays, P_α (E) and P_β (E), are given by

$$P_\alpha (E) = f_{K_\alpha}\, P_{K_\alpha} (E)$$

$$P_\beta (E) = f_{K_\beta}\, P_{K_\beta} (E)$$

and total K X-ray escape probability is

$$P_K (E) = f_{K_\alpha}\, P_{K_\alpha} (E) + f_{K_\beta}\, P_{K_\beta} (E)$$

Values of various physical parameters used in the calculations relevant to sodium iodide crystal are

ε_K = fraction of photoelectric processes taking place in K-shell = 0.875

ω_K = K-fluorescent yield of iodine = 0.84

E_{K_α} = 32.5 keV

E_{K_β} = 28.6 keV

$\mu_{K_\alpha} = \mu(E_{K_\alpha}) = 6.62 \text{ cm}^2 \text{ g}^{-1}$

$\mu_{K_\beta} = \mu(E_{K\beta}) = 4.66 \text{ cm}^2 \text{ g}^{-1}$

f_{K_α} = fraction of K X-rays which are K_α X-rays = 0.7937

f_{K_β} = fraction of K X-rays which are K_β X-rays = 0.2063

The results of the computations carried out are shown in Fig. 2.5. It is seen from this figure that total K X-ray escape probability for incident photons of energy 33 keV is $\sim$ 23% which is a significant fraction and hence should be considered in deriving the true spectrum of incident radiation. The computed escape factors have been used for correcting the observed spectrum of cosmic X-rays to get the true incident spectrum, as described in Section 4.4.

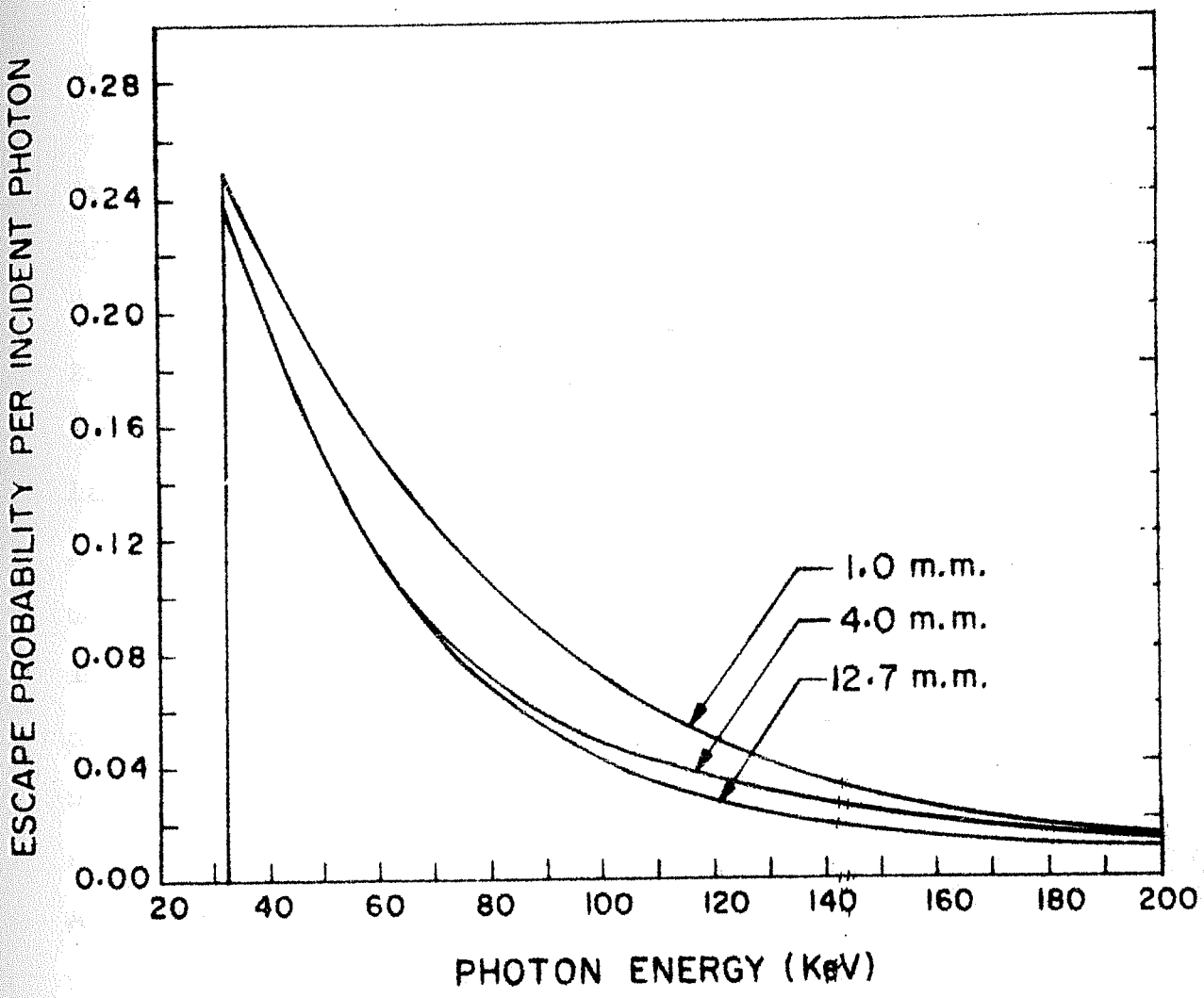

Fig. 2.5 : Total fluorescent K X-ray escape probability for NaI(Tl) crystals of different thicknesses as a function of energy.

2.8 RESPONSE OF CRYSTALS TO X-RAYS : LINEARITY AND RESOLUTION

Response of crystals to X-rays was experimentally determined by exposing them to radioactive sources Am^{241} and Cd^{109}. Both Am^{241} and Cd^{109} produce two prominent X-ray lines at effective energies of 16.8 and 59.6 keV and 22.5 keV respectively. In each case, detector response was determined by feeding the amplified detector pulses to a laboratory multichannel pulse height analyser. A typical pulse height distribution obtained by irradiating the first detector of February 11, 1975 observation by these sources is shown in Fig. 2.6. It is seen from the figure that the detector response is linear, within the experimental uncertainty, over the energy interval 17-90 keV. The resolution of the counter defined in terms of FWHM (see Appendix I) is 47.0% at 16.8 keV, 32% at 22.5 keV, 20.0% at 59.6 keV and 17.0% at 87.5 keV, for this detector. For other detectors resolution at 59.6 keV varied between (20.0-26.0)% and at 22 keV between (32.0-41.0)%. From the experimentally measured values of FWHM, we have deduced σ $\left(= \frac{\text{FWHM}}{2.35}\right)$ of photopeak for X-ray lines at various energies. Variation of σ as a function of photopeak energy E is shown in Fig. 2.7. It is seen that slope of the best fit straight line to data points is close to $E^{\frac{1}{2}}$ dependence pointed out in Appendix I. The standard

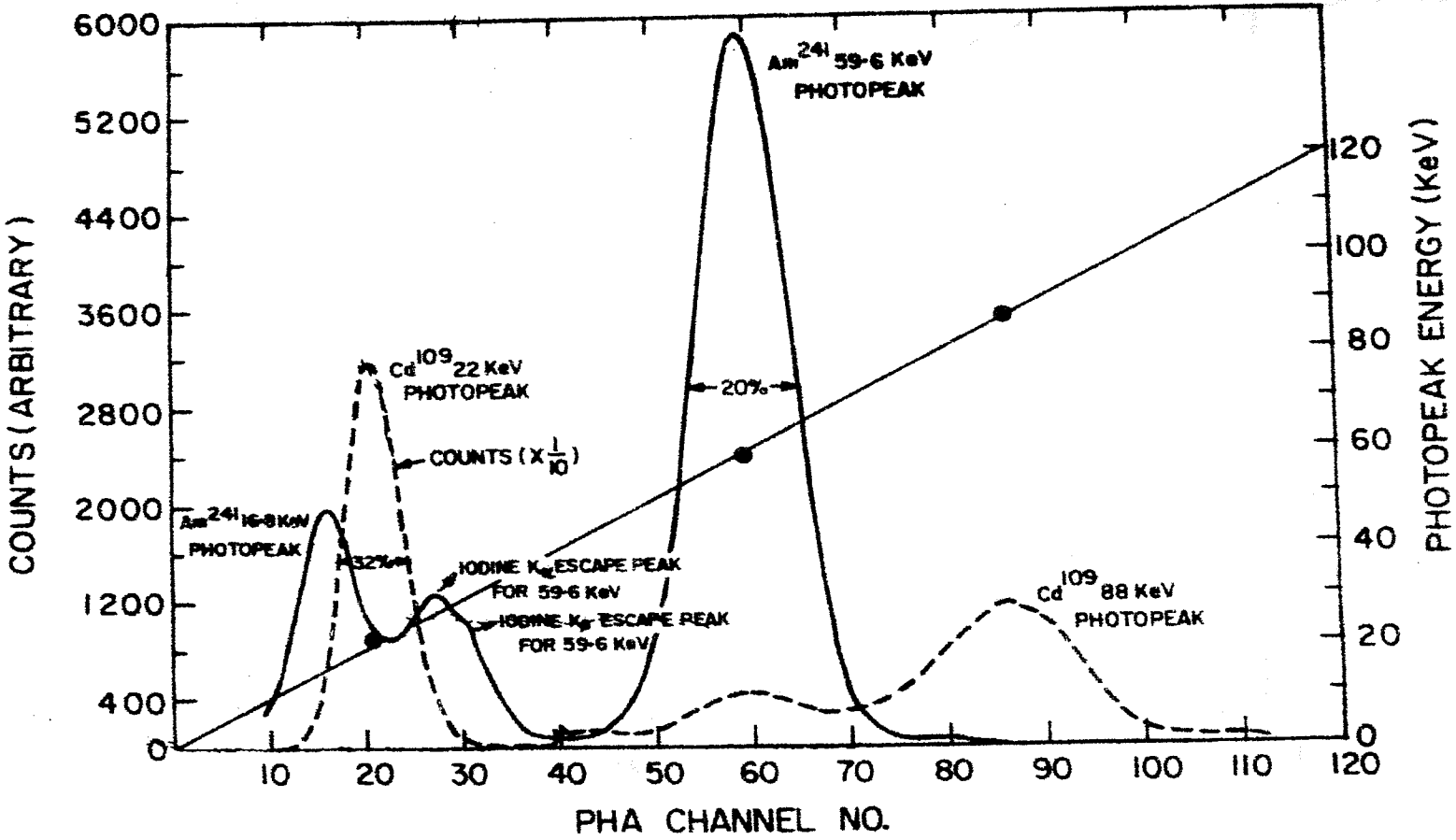

Fig. 2.6 : Typical pulse height distribution in the first detector of February 11, 1975 observation due to X-rays from Am^{241} and Cd^{109} radioactive sources. The linear response of the detector in terms of PHA channel No. vs photopeak energy is also shown.

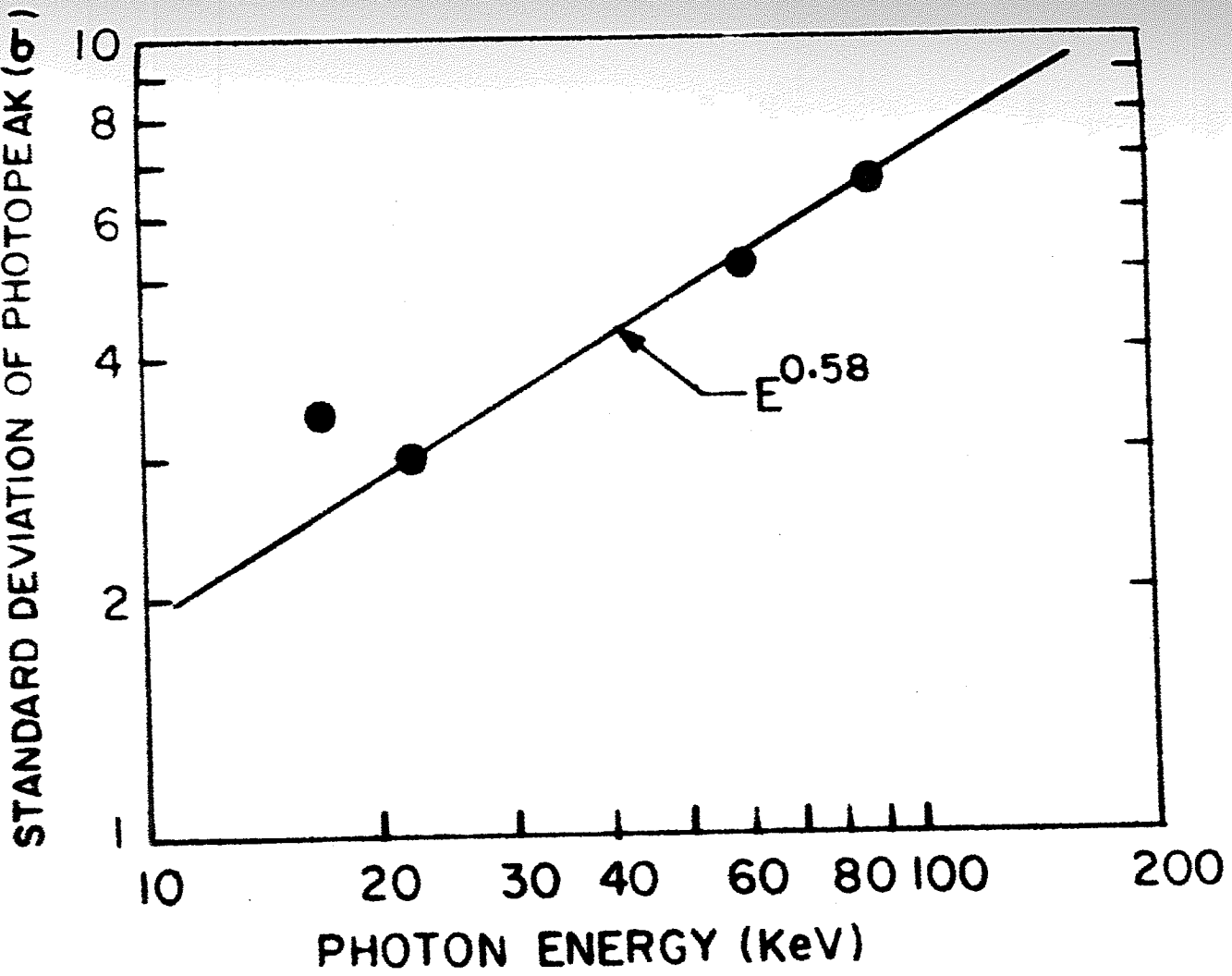

Fig. 2.7 : Variation of detector resolution (σ) with photon energy for first detector of February 11, 1975 observation.

deviation for 16.8 keV X-ray line of Am^{241} appears to be considerably more than that expected from the straight line fit to the data. This is due to the presence of multiple lines in the Am^{241} source at this energy, which considerably broadens this photopeak. Therefore in general we have

$$\sigma = KE^{\alpha}$$

These experimentally measured values of exponent of E and constant K were used for correcting the observed energy spectra of X-ray sources.

CHAPTER III

DATA ACQUISITION AND TELESCOPE CONTROLS

3.1 INTRODUCTION

In this chapter we briefly describe electronics and other associated instrumentation used in present experiments. Essentially, they consist of pulse processing circuits for carrying out pulse height analysis of genuine X-ray counts and orientation, control and attitude determination circuitry. The pulse processing circuitry consisted of amplifiers and pulse shapers, an anticoincidence switch to reject background counts and an onboard pulse height analyser to derive energy information.

The orientation system used to stabilise the telescope and to point the telescope in the desired direction was based on the principle of azimuth stabilisation using earth's magnetic field as a reference. The direction of the telescope was defined with respect to horizontal component of earth's magnetic field and any deviation from the required direction was sensed by a flux gate magnetometer and the corresponding error signal was fed to the servo motor which corrected the telescope direction by rotating the circular platform. The detector background was monitored by periodically orienting the telescope in a direction

where there are no known X-ray sources, using an onboard timer. The X-ray source under study was tracked for a long time by changing the zenith angle and azimuth angle of the telescope at a predetermined rate, using an onboard programmer. An independent magnetometer was used to check the working of the orientation and tracking system. The detector system, in addition, had provision for onboard calibration of the detector.

The pulse height analyser information as well as other house-keeping information were continuously transmitted to the ground using standard IRIG FM/FM telemetry system.

Extensive laboratory tests were performed on all the individual electronic systems and the X-ray telescope to test their ability to withstand the space environment. All the high voltage points were potted with silicone rubber compound to prevent corona discharge effects. In addition, the entire payload assembly was thermally insulated to protect it from outside low temperature during flight. The temperature inside the experiment housing was monitored by a suitable thermograph.

3.2 PULSE PROCESSING CIRCUITRY AND PULSE HEIGHT ANALYSER

A block diagram of pulse processing circuitry for the actively shielded X-ray telescope used in March 29, 1972 and January 18, 1973 observations is shown in Fig. 3.1. It

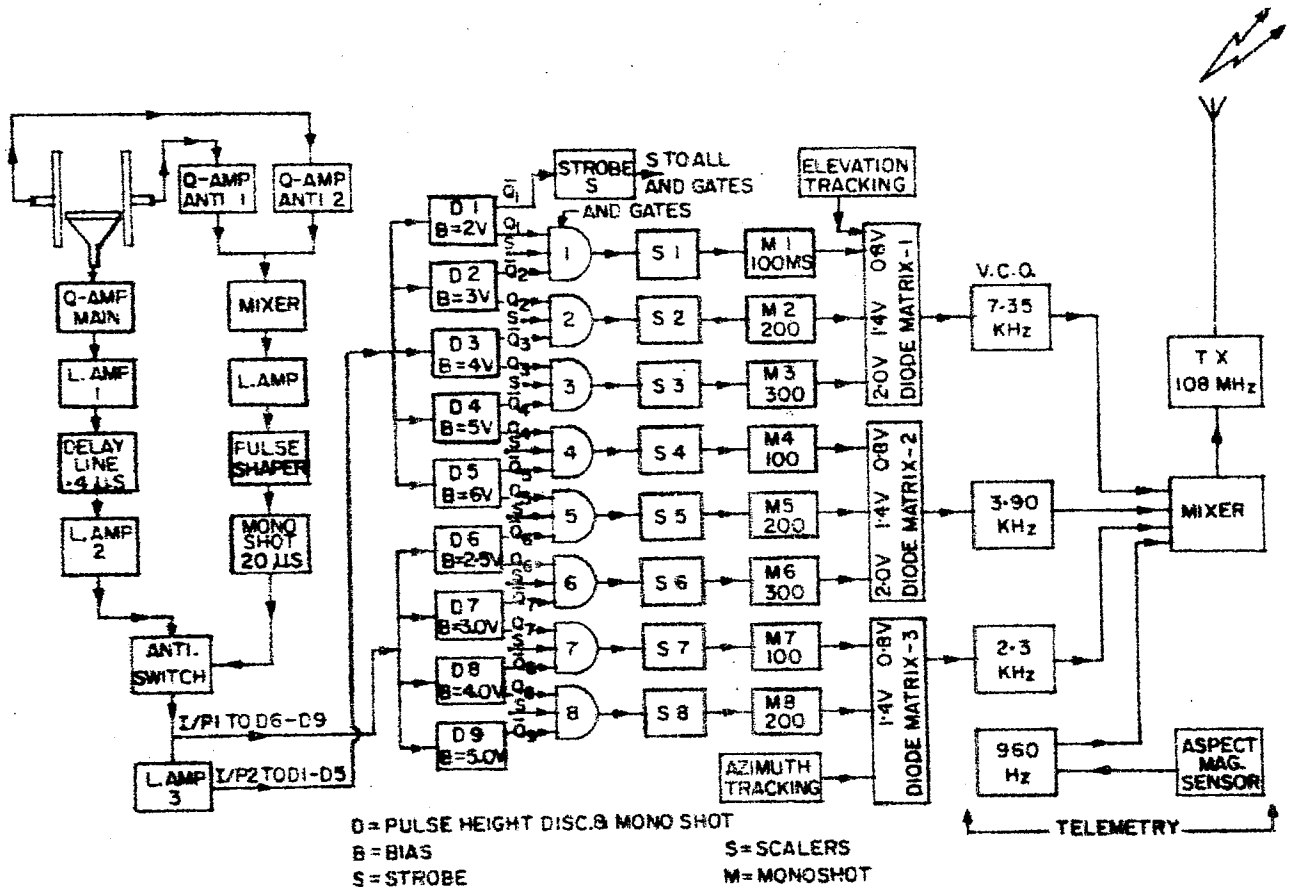

Fig. 3.1 : Block diagram of pulse processing-circuitry and telemetry for actively shielded telescopes.

consists of various amplifiers for amplifying the output of NaI crystal and plastic scintillator, an anticoincidence switch to reject those events in the main NaI crystal which are accompanied by an event in the plastic scintillator and a pulse height analyser for energy classification of the events.

The negative pulses from the anode of photomultiplier of the main detector (with a rise time of $\sim 1.2\,\mu$sec and $\sim 1\,\mu$ sec width) and the plastic scintillator are amplified and shaped in the charge-integrating preamplifiers, mounted close to the photomultiplier tubes to reduce pick up noise and to avoid charge division over cable capacitance. The positive pulses from the main detector pre-amplifiers with about $.4\,\mu$sec rise time and $\sim 7.0\,\mu$sec width are fed to a linear amplifier with high negative feedback, to achieve gain stability. These pulses from the main detector are then delayed by $\sim 0.4\,\mu$sec, using a lumped constant delay line, and further amplified before being applied to the anticoincidence switch. The pulses from different pre-amplifiers of anticoincidence plastic scintillator are mixed, amplified and shaped using a conventional Schmidt trigger before applying to the anticoincidence switch.

The output of the anticoincidence switch is fed to a eight channel pulse height analyser. Pulse height analysis was accomplished by using nine threshold discriminators

D_1 to D_9, which consist of high gain differential comparators whose reference voltages were adjusted by giving appropriate D.C. bias for different energy levels,viz. 20-30, 30-40, 40-50, 50-60, 60-75, 75-90, 90-120 and 120-150 keV for January 18, 1973 flight. In March 29, 1972 flight 60-75 and 75-90 keV channels were combined and an additional sum channel of 30-60 keV was provided for redundancy. The output of each energy channel was suitably scaled down and fed to long time monoshots. The outputs of these monoshots were used to modulate the subcarrier voltage controlled oscillators and transmitted to the ground.

In the February 11, 1975 experiment, which did not have anticoincidence, each of the three detectors was provided with completely independent amplifiers, pulse height analyser, EHT supply and independent data channels in the telemetry. The output pulses of the three detectors were separately amplified and pulse height analysed into 6 energy channels, viz. 30-45, 45-60, 60-75, 75-90, 90-105 and 105-120 keV.

3.3 ORIENTATION, TRACKING AND ASPECT SYSTEMS

3.3:1 Construction of the Orientor

The payload was constructed in two parts - an outer, non-oriented part attached to the load line and an inner orientation platform, on which the telescope along with aspect sensors was mounted and which could be rotated

with respect to the outer platform. The EHT for the photo-multiplier tubes and Q amplifiers were mounted near the base of the telescope housing. Rest of the systems like linear amplifiers, pulse height analyser, V.C.O.'s, transmitter batteries and servo controls etc. were mounted on the base of outer frame.

The telescope was gimbal mounted to enable the assembly to freely rotate about both azimuth and elevation, and servo controlled to pin-point in the pre-programmed azimuthal directions. The construction of the orientor and the full payload is shown schematically in Fig. 3.2. The telescope housing is supported by non-magnetic stainless steel shafts, passing through ball bearing B_1, in an inner rectangular frame IF made of aluminium channels. This frame is supported by stainless steel shafts, passing through ball bearing B_2, in a L shape support, which is fixed on two pillars P. The pillars, also made of aluminium channels, are fixed to a rectangular lower frame LF which is fixed to the outer frame OF and tied to the balloon through a rope. Lower end of the telescope housing carries a non-magnetic stainless steel rod R along its axis, which fits into a self aligning mounting with ball bearing B_3 in the 'U' shaped mount D on a circular oriented platform CP. The zenith angle of the telescope can be set to any desired value by moving the mount on a worm gear, along a radius of the circular platform. The circular platform is

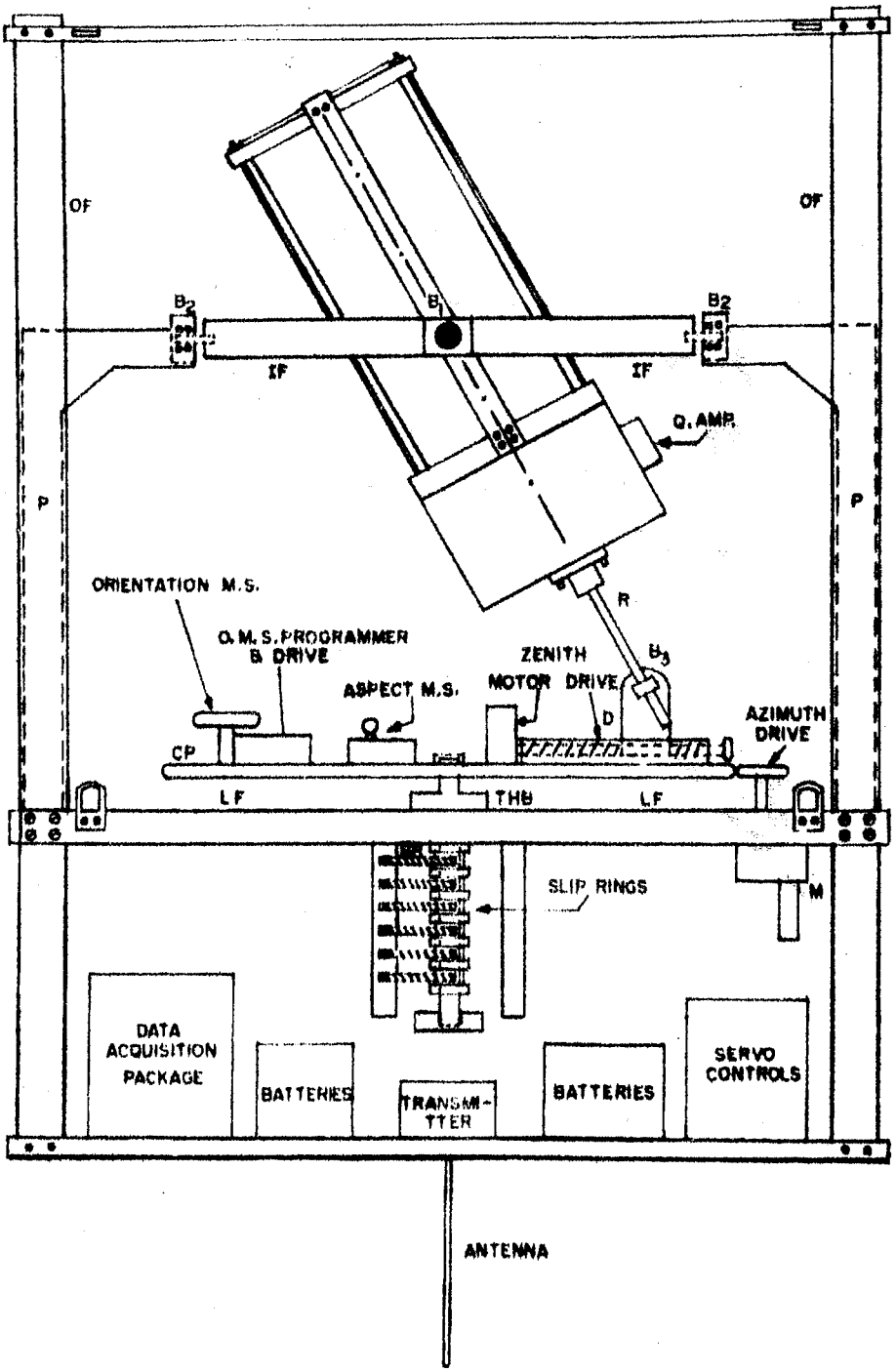

Fig. 3.2 : Construction of the orienter and complete balloon borne X-ray astronomy instrument.

mounted through thrust bearing THB, supported by cross bars, on to the square shaped outer frame. Orientation of the telescope in azimuth is achieved by servo control of the circular platform. As the circular platform goes through a complete rotation, the telescope scans all azimuths, but the inner frame supporting the telescope executes only an oscillatory motion. The absence of relative motion between the telescope and base allows power and signal cables to be taken directly from the detector to the circuits in the base. Signals to and power from the electronics on the circular platform are taken through wires which pass through a deep groove made in the circular platform shaft and soldered at the other end to phosphor-bronze slip rings, which are mounted on the shaft with proper insulation in between. The cylindrical carbon-bronze brushes BR are used for making contacts with the slip rings. Each slip ring is swept by two brushes, one on each side, connected in parallel to ensure reliable contact.

3.3:2 Servo System

The block diagram of the flux gate magnetometer controlled servo system is shown in Fig. 3.3. The circuit diagrams for the magnetic sensor, motor control circuit and motor drive circuit are shown in Fig. 3.4, 3.5 and 3.6 respectively. Servo system uses a null sensing reference flux gate magnetometer to maintain a given azimuthal angle.

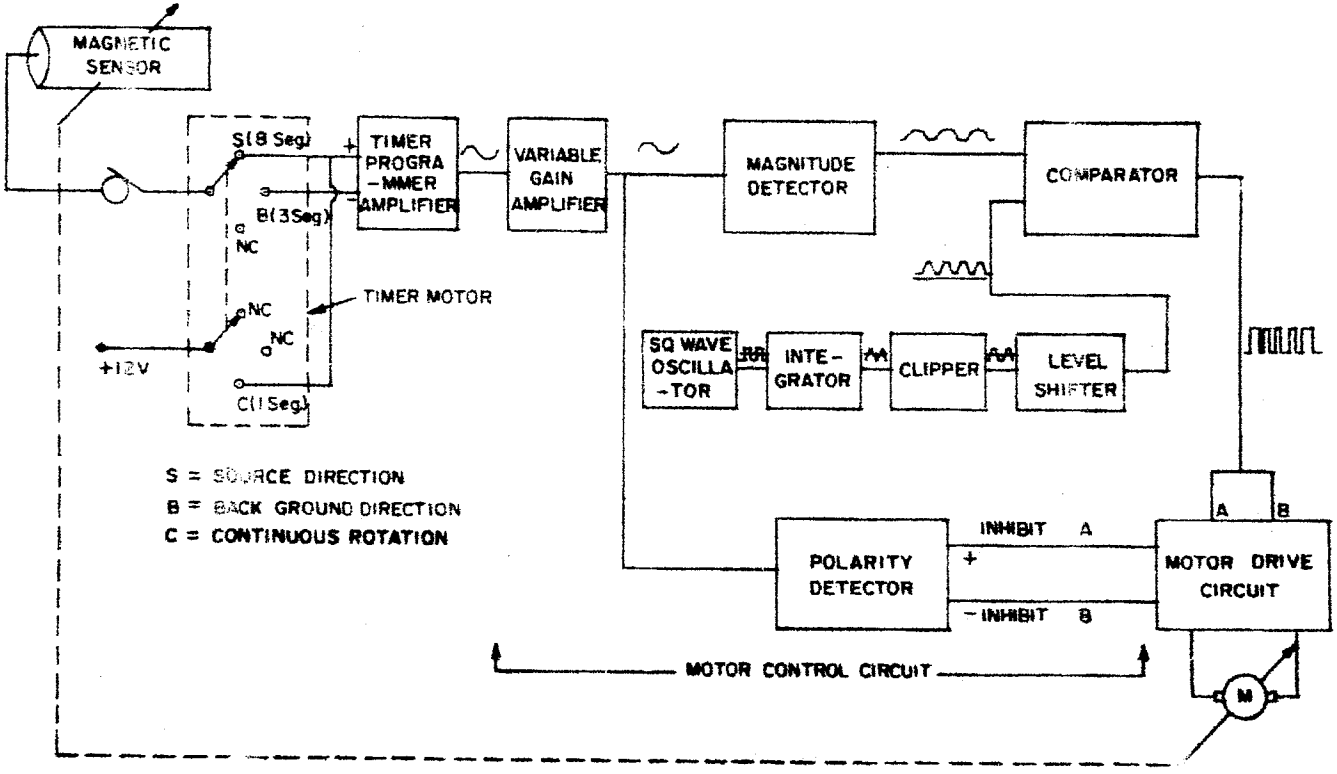

Fig. 3.3 : Block diagram of servo system.

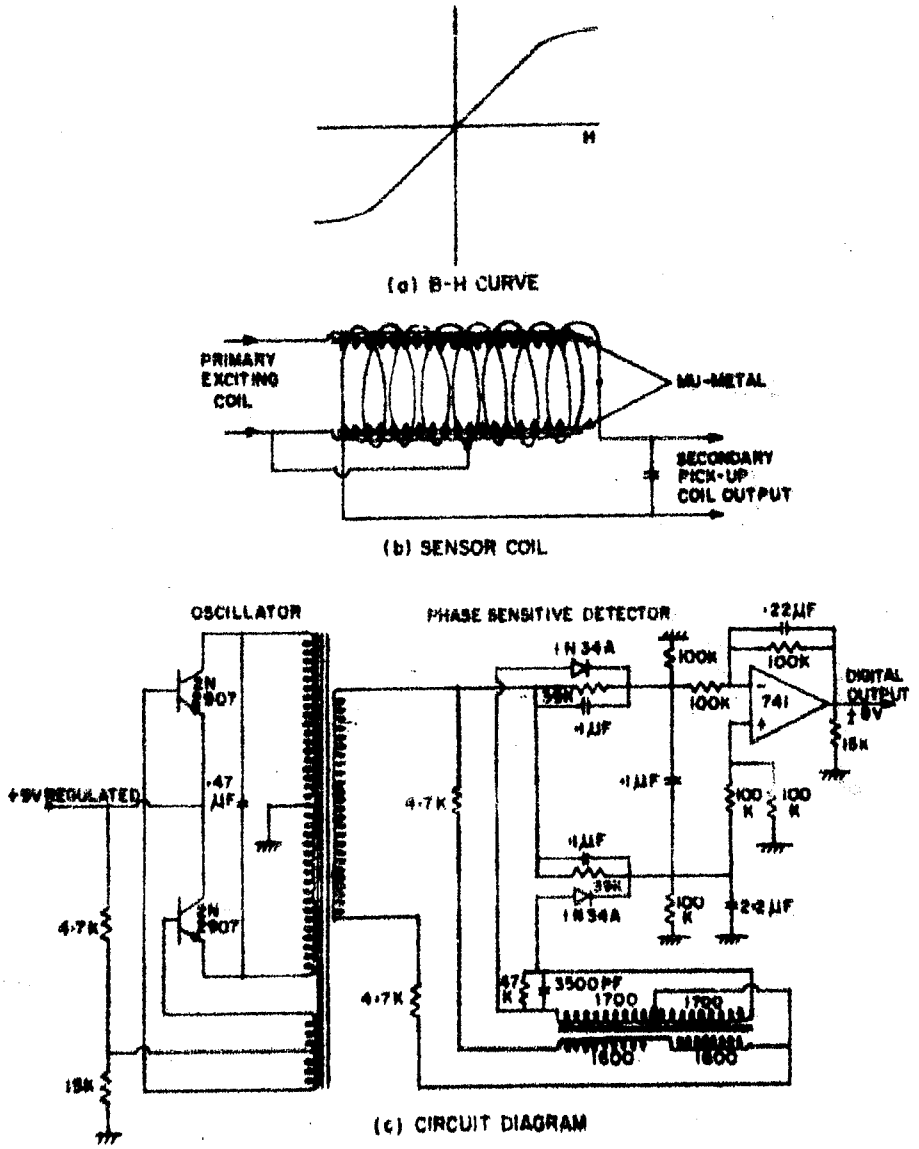

Fig. 3.4 : Flux gate magnetometer (a) B-H curve of mu-metal (b) construction of the sensor coil (c) circuit of the magnetometer.

The magnetic sensor output depends upon its orientation with respect to the horizontal component of the magnetic field. It gives a zero output voltage when its axis is parallel to the E-W line, but a D.C. signal (error signal) appears when it deviates from it. The magnitude of this D.C. voltage is proportional to the component of the magnetic field along the axis of the coil and is either positive or negative depending upon the sense of displacement (towards N or S).

3.3:2.1 Motor Control and Drive Circuit

The output of the magnetic sensor, which indicates the degree and direction of displacement of the circular platform and the telescope from the required azimuthal angle, acts as an error signal for the servo system. This signal, after amplification, is fed to the servo motor control circuit via a timer motor (Fig. 3.5), which controls the look direction of the telescope and acts as an onboard programmer. The sequence of observational programme involved a sequence of three different observations for fixed time durations. These were, observation of the source for 200 sec, measurement of background by locking the telescope in a direction 180^{o} away from source direction for the next 75 sec, followed by 25 sec inflight calibration of the detector system by continuously rotating the circular platform and simultaneously exposing the telescope to a radio-

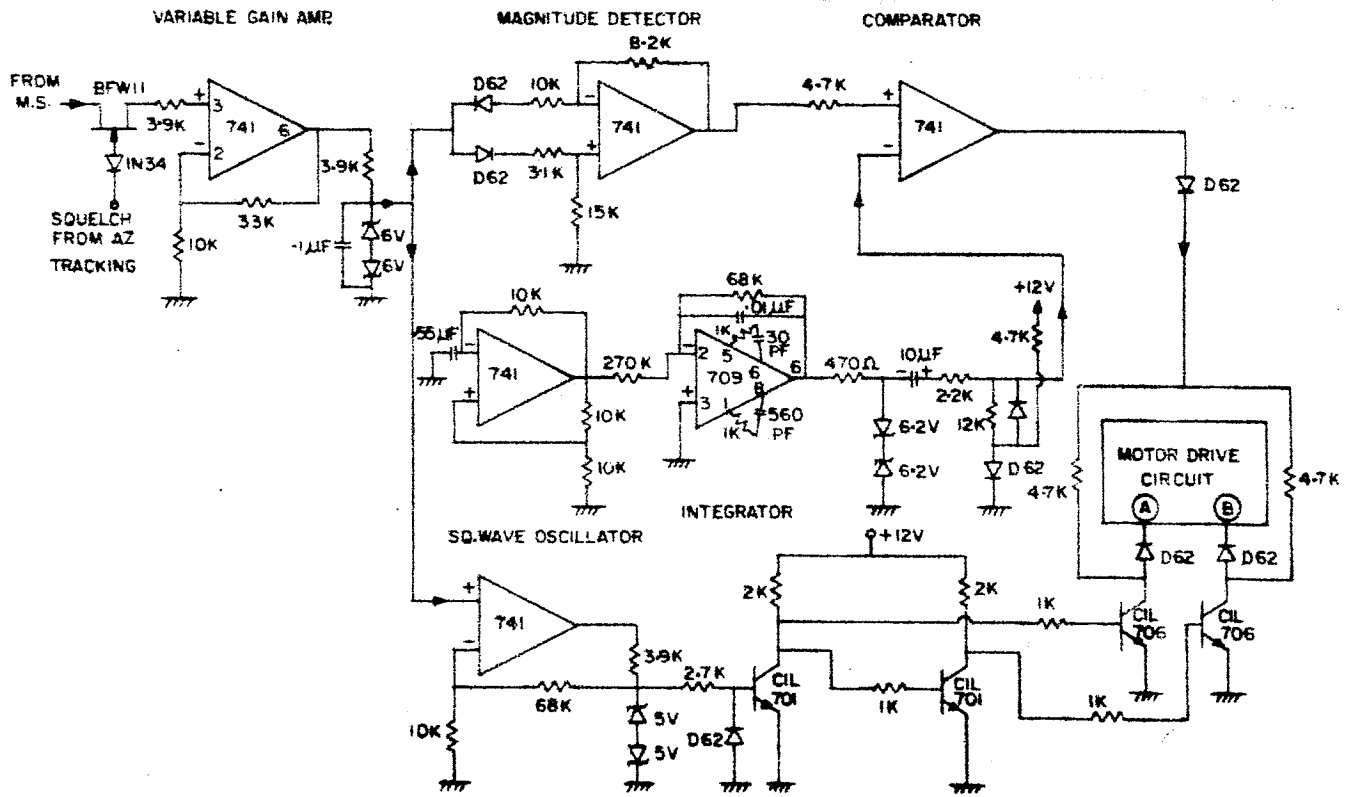

Fig. 3.5 : Circuit diagram of motor control system.

active source. The continuous rotary motion of the circular platform for calibration is achieved by applying a constant D.C. voltage of +12V to the motor control circuit.

For achieving smooth operation of the system with minimal hunting and to avoid unnecessary over-shooting, the speed control of the motor was made proportional to the amplitude of the error signal. This was achieved by feeding the error signal to a linear power amplifier (Motor drive circuit) whose output drives the D.C. motor, so that the motor driving voltage and thus its speed becomes proportional to the amplitude of the error signal. Excessive power dissipation in the motor drive circuit was avoided by converting the amplitude information of the error signal into time information and giving the signal to motor drive circuit in a pulsed form.

The motor control circuit (Fig. 3.5) controls the movement of the servo motor and ensures optimum performance and efficient functioning of the orientation system (e.g. to achieve maximum sensitivity with minimal hunting etc.) about the orientation point. The error signal for the motor control circuit is derived from the magnetic sensor, after suitable amplification in a variable gain D.C. amplifier. The magnitude and polarity of this amplified error signal are detected separately, as shown in Fig. 3.5. The output of the magnitude detector is compared with the reference

THE LIBRARY
PHYSICAL RESEARCH LABORATORY

signal, a clipped positive triangular wave, to derive a pulse width modulated output, whose width is proportional to the amplitude of the error signal. The reference signal for the comparator is generated from an oscillator which gives a 100 c/s square wave output, which is integrated to make it triangular. This triangular wave is clipped at both ends and its level is then shifted to make the voltage of the lower clipped portion slightly above zero.

The motor drive circuit (Fig. 3.6) is a pair of complementary symmetric power amplifiers whose outputs drive the reversible D.C. motor in either of the two directions. The motor responds only to the time integrated voltage of the fast pulsed output of the motor drive circuit and hence moves in either of two directions with an effective speed determined by the time average of this output. The polarity detector detects the polarity of the error signal and depending upon the polarity inhibits one of the two pulse width modulated inputs to the motor drive circuit by making the appropriate switching transistor conducting and providing a low resistance path for this input to pass through to ground. Thus, in the motor control circuit, the polarity detector determines and controls the direction of movement of the motor whereas the magnitude detector and comparator determine and control the speed of the movement.

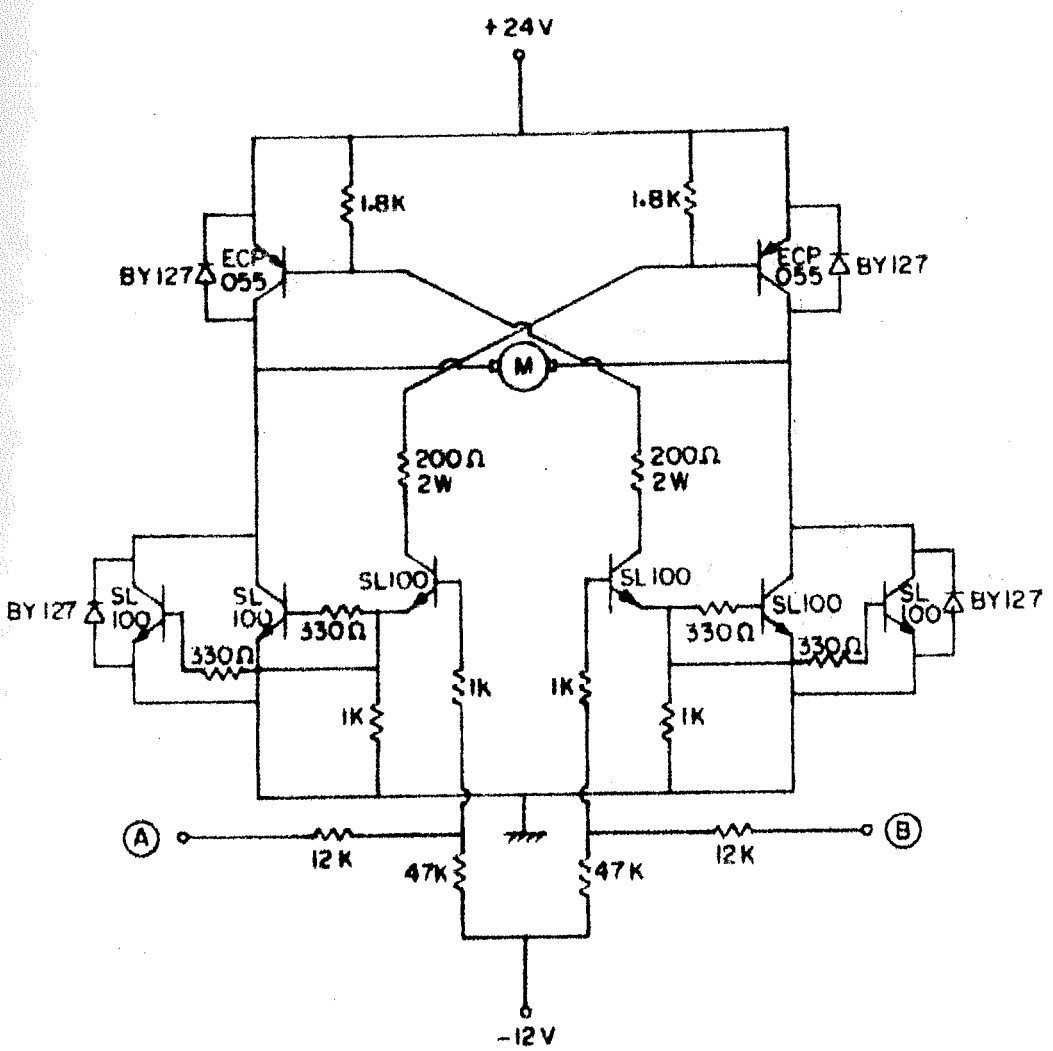

Fig. 3.6 : Circuit diagram of motor drive system.

Clipping of the reference triangular wave to the comparator is done to essentially inhibit the application of the driving voltage to the motor when the error signal is small, to reduce the noise voltage across the motor drive circuit during such periods. The level of the clipping is adjusted such that the time integration of output pulses of the motor drive circuit, corresponding to the lower clipped portion of the triangular reference wave, results in an effective average voltage which is sufficient to move the motor with its associated load and at the same time does not result in appreciable loss of sensitivity of the orientation system. Since speed variation of the motor is not necessary for large deviations of the platform, upper portion of the triangular wave is also clipped at a suitable level, beyond which speed control is not necessary ($\sim \pm 10^{o}$). This helps in avoiding very small OFF periods of comparator output, which will otherwise be present for large error signals and which also produce unnecessary magnetic noise in the system. Further, this uncontrolled full drive for larger deviations of platform makes transition of the telescope from one observational mode to other much faster.

In addition to the level clipping, it is also necessary to have the level shifting of the clipped triangular reference wave to make its lower clipped portion slightly above zero, so that the servo system is insensitive to very small values of error signal, thus avoiding unnecessary

hunting of the platform near the orientation point. The level of this voltage was adjusted to make it insensitive for deviations of magnetometer axis within $\pm 1^{o}$ of E-W, which essentially puts an upper limit on the sensitivity of the orientation system. From simulation tests carried out on ground the pointing accuracy limitation of $\pm 1^{o}$ was confirmed.

An independent aspect magnetometer, mounted perpendicular to the above one on the circular platform, was used to check the working of the orientation system and monitor the telescope azimuth.

3.3:3 Source Tracking

In order to achieve a maximum exposure time on the pre-selected X-ray source, it is necessary to track the given star both in elevation and in azimuth during the balloon float period. This versatility in the system also enables one to make observation on more than one star in a single flight. The azimuth and elevation tracking in the present experiments was achieved using onboard timer programmers.

3.3:3.1 Azimuth Control System

The block diagram and circuit diagram of azimuth control system are shown in Fig. 3.7a and b respectively. Azimuth tracking was accomplished by rotating the

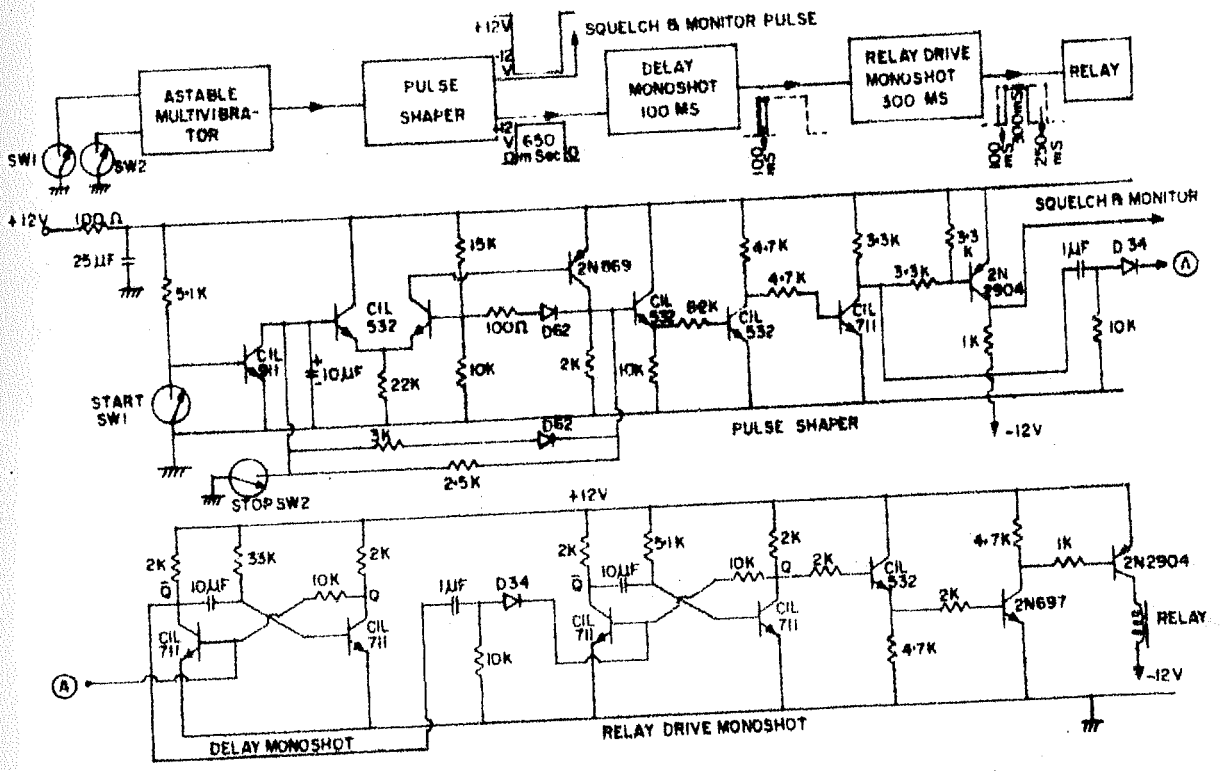

Fig. 3.7 : Block diagram and circuit diagram of azimuth control system.

orientation magnetic sensor with respect to the detector axis by commands given by a programmer which simulated projection of motion of source in local azimuthal plane. Since the servo system always aligns the magnetic sensor with the magnetic East-West axis, the displacement of the magnetic sensor is translated as an equal displacement of the telescope, thus providing an azimuthal control of the telescope. The rotation of magnetometer axis was accomplished by mounting it on a gear wheel, which was driven by a ratchet relay. The relay was activated periodically by the azimuth control circuit (Fig. 3.7a and b). However, since the operation of relay produces lot of magnetic noise in the system and to avoid sudden jerky motion of the platform, the orientation system was made inactive for a short time whenever the relay operated. The correction for the change in angular position of magnetic sensor was affected smoothly when the orientation system again became active and magnetic sensor position stabilized, after the completion of the relay operation. The operation of the azimuth control circuit was monitored through the telemetry system to obtain the position of the telescope at various times during the observation.

3.3:3.2 Elevation Control System

The elevation tracking was accomplished by moving the 'U' mount carrying the self aligning ball bearing B_3,

in which the telescope housing axial rod 'R' fits (see Fig. 3.2), along a radius of the circular platform. The 'U' mount was moved on worm gear with an appropriate speed by a D.C. motor. The speed of the D.C. motor was controlled by elevation control circuit, which consisted of an astable multivibrator whose ON and OFF times (pulse width and time between subsequent pulses) were fixed according to the desired change in the elevation of telescope. The output of astabler was fed to a motor drive circuit, similar to the one used in orientation system, which drives the motor and the 'U' mount in either of two directions. The effective speed of the motor and thus the rate of change of elevation angle of telescope was determined by the ratio of ON and OFF time of astabler output. The direction of the movement of 'U' mount was controlled by feeding the astabler output to appropriate power amplifier of motor drive circuit. The elevation changes, in flight, were affected by an onboard timer according to the preset plan. The movement of the 'U' mount was monitored through a Cam switch on the worm drive shaft which gave a monitor pulse to telemetry for every revolution of the shaft. Since the change in elevation angle of telescope is not a linear function of the straight line movement of 'U' mount on worm gear, the pitches of the gearing were calibrated with respect to elevation angle of telescope before the flight.

3.4 OTHER AUXILIARY ELECTRONIC SYSTEMS

3.4:1 Power Supplies

Power for all the systems of the payload was derived using 4V, 3 Amp-hour lead-acid cells, which work satisfactorily down to $-40^{\circ}C$, as the primary source of power. The different supply voltages needed for various circuits and for driving various mechanical systems were derived from series combinations of these cells. Sufficient current capacity was ensured for each system by connecting number of cells in parallel. All the voltages were regulated by electronic regulators to ensure proper functioning of the systems.

High voltage supplies for photomultiplier tubes viewing NaI (Tl) and plastic scintillators consisted of conventional corona stabilised D.C.-D.C. converters, which worked with a regulated 9V D.C. input and supplied regulated output voltage of $\sim$ 1500V. Fig. 3.8 shows the schematic of the D.C.-D.C. converter. The high voltage supply was potted with silicone rubber (RTV60) to avoid corona discharge problems at high altitudes.

3.4:2 Telemetry and Data Recording

The X-ray pulse height information from the pulse processing circuitry (Fig. 3.1) and the telescope attitude information (magnetometer output, azimuth and elevation tracking monitor pulses) were telemetered to ground, in

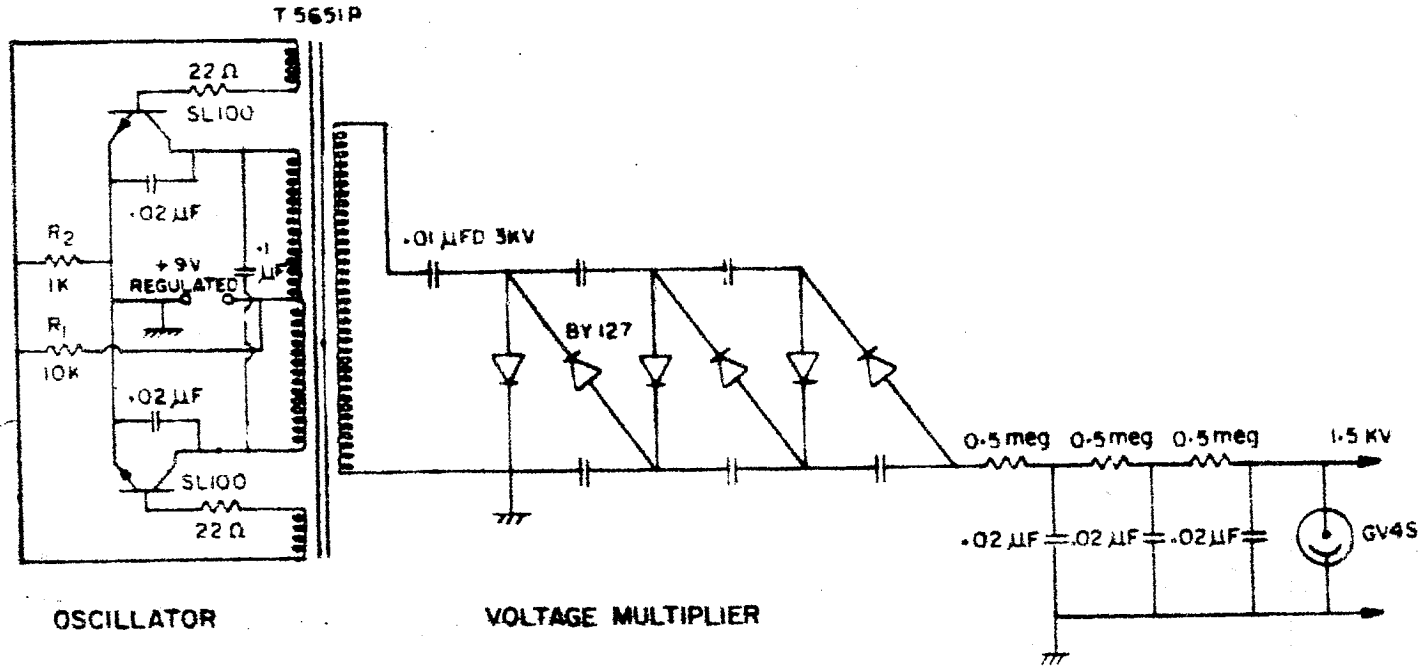

Fig. 3.8 : Circuit diagram of D.C. - D.C. converter.

real time, through standard FM/FM telemetry system at 108 MHz. The system consisted of subcarrier oscillators, operating at standard IRIG frequencies, compatible with the ground receiving station. The transmitter output was fed to a quarter wave antenna mounted underneath the bottom platform, for transmitting the data to the ground.

The ground antenna system was a conventional eight element yagi mounted on a steerable platform. The antenna output was fed to a suitable FM receiver and after demodulation was recorded on two fast four channel galvanometric strip chart recorders along with the timing information.

3.4:3 Altitude and Temperature Measurements

The balloon altitude was monitored continuously during the entire flight by radiosonde and radar. A clockwork thermograph provided the thermal history of the payload during the flight.

3.4:4 Inflight Calibration

The detector was exposed periodically during the flight to a collimated Am^{241} radioactive source to check the performance of detector and its associated electronics. Any drift in overall gain of the system can be determined by recording the shift in the position of 59.6 keV X-ray peak of Am^{241} by comparing the distribution of the number of pulses in each of discrete energy channels. The radio-

active source was mounted on the side of X-ray telescope. In the normal mode of operation the photons from the source were prevented from reaching the detector by a thick lead shutter. During the calibration cycle the D.C. motor was given a positive supply, through the orientation timer motor, which lifted the shutter, thereby exposing the detector to the radioactive source. During this time the telescope made continuous rotary motion in azimuth so that no particular region of sky was seen by the detector. This circular motion of the platform also helped in checking the calibration of the aspect magnetic sensor. The system was such that in case of any malfunction the shutter was restored to the DOWN position thus not affecting the normal mode of operation.

3.5 PRE-FLIGHT CALIBRATION

3.5:1 Pulse Height Analyser Calibration

The energy thresholds of various channels of PHA used in flight were calibrated before the flight using Cd^{109} and Am^{241} radioactive sources, a laboratory 128 channel analyser and a standard pulse generator. In practice, it was possible to calibrate the threshold levels of each discriminator to an accuracy of better than $\pm$ 0.5 keV. The absolute energy calibration used in data analysis was obtained from the analysis of inflight calibration data

for correcting for any variation in the preflight calibration during the course of flight.

3.5:2 Aspect Calibration

The aspect magnetometer was calibrated in terms of telescope azimuth aspect angle relative to geographic north pole in the local geomagnetic field at Hyderabad, at a place far from the local disturbing effects of buildings and other structures containing ferro-magnetic materials. Corrections due to drift of balloon to regions of different declination and inclination can be applied knowing balloon trajectory, though in practice it is rarely necessary as drifts in Hyderabad are mostly along geomagnetic latitude.

3.6 PREPARATION OF PAYLOAD FOR FLIGHT

By providing adequate thermal insulation over different subsystems and the total payload, it was ensured that the temperature within the payload was maintained above $0^{o}C$. In order to have adequate margin of safety, all subsystems, including electronic circuits, were tested for satisfactory operation down to $-20^{o}C$. The entire payload including its calibration was checked for its performance, both under high vacuum and low temperature conditions, prior to the flight.

The weight of the payload, including batteries, was 150 Kg. The balloon trajectory during the flight was obtained from radar and theodolite observations carried out by the TIFR Balloon Facility at Hyderabad.

CHAPTER IV

DATA REDUCTION AND ANALYSIS

4.1 INTRODUCTION

Since the X-rays detected by the balloon-borne detector have already undergone attenuation in the atmosphere and in the detector, in addition to their being transformed by the detector response characteristics, the observed data has to be processed to take into account all these factors, before being capable of related to the characteristics of the X-ray source itself. In this chapter, the methods of data reduction and analysis are described which enable us to obtain the true properties of the source such as its intensity, spectral characteristics and time variation from the observational data.

4.2 DATA PROCESSING AND SEPARATION OF X-RAY SOURCE CONTRIBUTION FROM BACKGROUND

4.2:1 Data Processing

As described in the last chapter, the data from the flight were recorded on a paper chart. X-ray data consist of events recorded as pulses of varying height and width on telemetry record, the height/width differentiation being

used to designate pulses representing different energy intervals. In addition, the azimuth and elevation tracking pulses, analog aspect magnetometer information and time marks were also recorded on the chart. The X-ray source was tracked continuously by the telescope by following its motion in azimuth and elevation. For data processing, the counting rates of various energy channels in all the three modes of observation viz. normal mode, background mode and calibration mode were read manually and expressed as counting rates for each time interval. The short periods of data recorded when detector was in motion or changing its observational mode from one to the other were neglected.

4.2:2 Separation of X-ray Source Contribution from Background : Statistical Considerations

In order to derive the intensity of X-ray source, it is necessary to estimate and then subtract the background counting rate in each energy channel from the total counting rate in that channel. Information about the background counting rate was obtained in the present investigations by periodically looking at directions 180^{o} away from the source, as stated in the earlier chapter. The average of background counting rate for each energy interval just prior to and following a source observation during each observation cycle was taken as background rate for that particular source observation.

Let N be the number of counts recorded by the detector in certain energy channel in a time interval t_1 when an X-ray source is being viewed and B the number of background counts accumulated during a time interval t_2.

The counting rate R_s due to the source is

$$R_s = R_N - R_B = \frac{N}{t_1} - \frac{B}{t_2} \qquad (4.1)$$

If the observed quantities are stationary during the period of measurement, the standard error due to statistical fluctuations is given by

$$\delta N = \sigma_N = \sqrt{N}$$

$$\text{and } \delta B = \sigma_B = \sqrt{B}$$

The fractional variance in source counting rate is given by

$$\frac{\delta R_s}{R_s} = \frac{\sqrt{N t_2^2 + B t_1^2}}{N t_2 - B t_1} \qquad (4.2)$$

From eqn. 4.2 it is clear that to keep the statistical uncertainty in measurement of source flux to a minimum, the precision in measurement of B should be as good as that of N. Since at typical balloon altitudes of $\sim$5g cm^{-2} excess counts due to a strong source like Cyg X-1 in 20-200 keV energy band is only about 15-20% of the total counting rate, it implies that in order to optimize it is necessary

to divide the total observing time roughly equally between the source and the background. In practice, to minimise the error due to instrumental defects and statistical uncertainties, the mean of the background measurement just prior and after the source observation is taken as the true background counting rate.

The assumption that in the background mode of observation there are no X-ray sources needs to be checked, particularly to ensure that the background count rate derived is not vitiated by the presence of weak sources in these directions. This was checked by taking average of all background measurements made during the total observational programme and comparing each individual measurement of background with this average. Any deviation of more than 3σ is a definite indication of significant contribution from a source to such a measurement and hence the particular measurement which shows significant deviation was discarded.

4.3 RESPONSE FUNCTION OF X-RAY TELESCOPE TO A POINT SOURCE

In order to reduce the observed excess counts S to normalised X-ray flux from the source, it is necessary to compute the exposure efficiency (fraction of detector area exposed to a point source) of the detector as a function of time for various sources under observation. The exposure efficiency of detector depends upon the collimation response of the telescope and the space angle θ between the source

and the telescope axis, which changes continuously as both the source and the telescope axis move with time. Calculation of exposure efficiency of a telescope to a point source as a function of time, therefore, involves a knowledge of response of the telescope to a point source, precise position of the source (i.e. its zenith and azimuth) and the telescope axis in the sky and then the space angle θ between them, as a function of time. In this section we briefly describe the calculation of each of the above parameters.

4.3:1 Response of a Cylindrical Telescope Collimator to a Point Source

The area of the detector exposed to a parallel beam of photons from a point source depends on angle θ, the angle between the source and telescope collimator axis. This area is maximum when the incident beam is parallel to the collimator axis, decreasing to zero as θ increases to θ_{max}. As shown in Fig. 4.1, the maximum acceptance angle θ_{max} is given by

$$\tan \theta_{max} = \frac{2r}{h}$$

where r and h are the radius and height respectively of the collimator.

The illuminated surface of the detector, shown by shaded line in Fig. 4.1a, for a parallel beam of photons

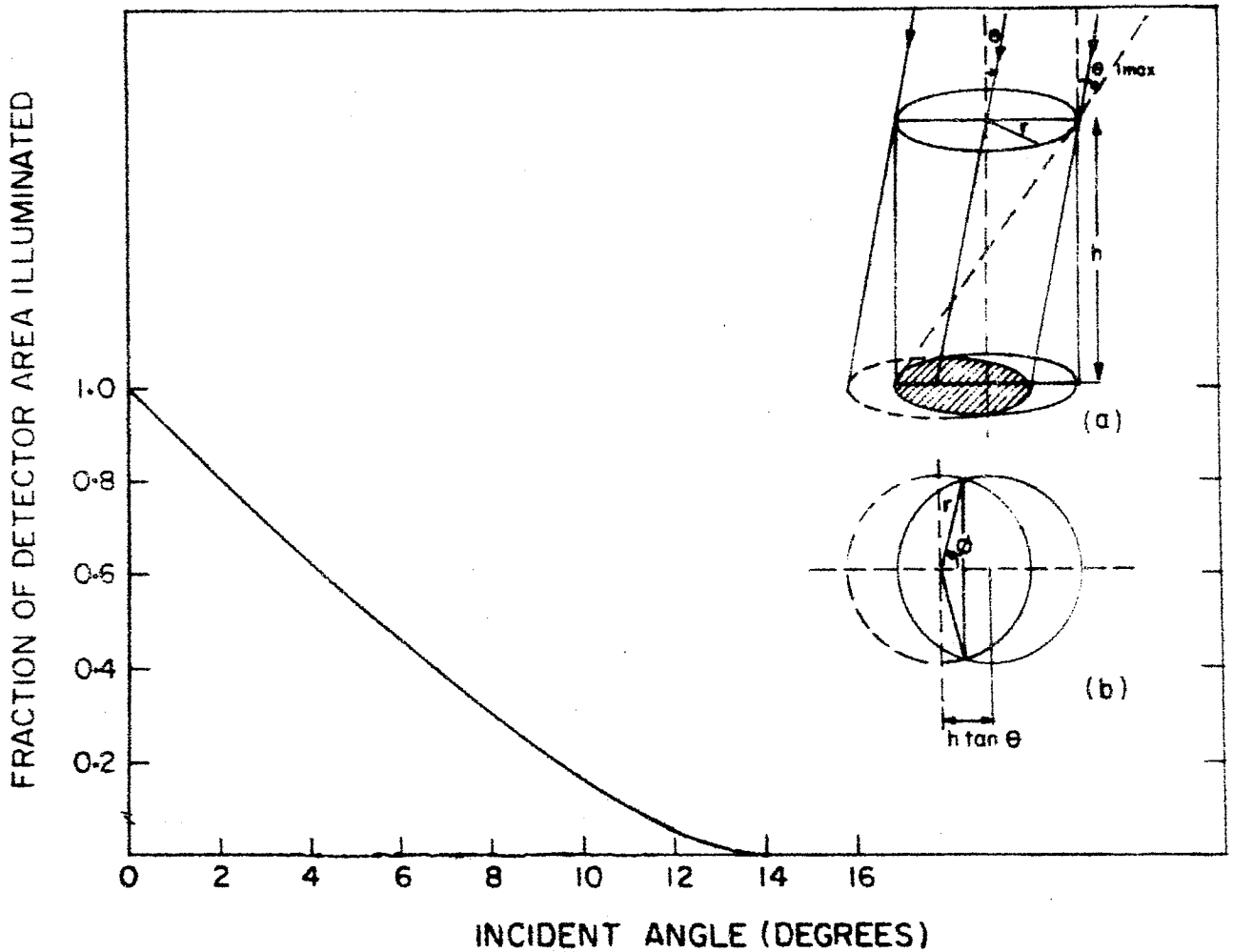

Fig. 4.1 : Exposure of a cylindrical collimator and angular response of X-ray telescope used in February 11, 1975 flight as a function of the angle between the source and the telescope axis.

from a distant point source, incident at an angle θ with the axis of the collimator, is that bounded by the two arcs of circles, as shown in Fig. 4.1b. The angle ϕ as shown in Fig. 4.1b is given by

$$\text{Cos } \phi = \frac{h/_2 \tan\theta}{r} = \frac{h \tan\theta}{2r}$$

Area of sector of circle with angle 2ϕ (Fig. 4.2b)

$$= \pi r^2 \cdot \frac{2\phi}{2\pi}$$

$$= r^2\phi$$

and area of triangle $= \frac{1}{2} \cdot 2r \text{ Sin } \phi . r \text{ Cos } \phi$

$$= \frac{r^2}{2} \text{ Sin } 2\phi$$

Therefore, the total exposed area for a beam incident at an angle θ is

$$S(\theta) = 2\left[r^2\phi - \frac{r^2}{2} \text{ Sin } 2\phi\right]$$

$$= 2\, r^2 \left[\phi - \frac{\text{Sin } 2\phi}{2}\right] \qquad (4.3)$$

The fraction of detector area exposed to a point source as a function of incident angle θ with respect to

telescope axis is

$$\mathcal{E}(\theta) = \frac{\text{Illuminated area normal to the beam}}{\text{Total detector area}}$$

$$= \frac{2r^2 \cos\theta \left[\phi - \frac{\sin 2\phi}{2}\right]}{\pi r^2}$$

$$\mathcal{E}(\theta) = \frac{2}{\pi} \cos\theta \left[\phi - \frac{\sin 2\phi}{2}\right] \qquad (4.4)$$

Fig. 4.1 shows calculated response of the X-ray telescope used in February 11, 1975 flight.

4.3:2 Calculation of Position of Source (Azimuth and Elevation) in Sky

Calculation of the angular separation θ between the source and the telescope axis as a function of time requires a knowledge of the precise position of the source (i.e. its zenith and azimuth) and the telescope axis during the course of observation. The azimuth angle (A_T) and zenith angle (Z_T) of the telescope during the flight are computed from the data obtained from the aspect magnetometer and azimuth and elevation tracking pulses recorded on the telemetry chart. The azimuth angle (A_S) and zenith angle (Z_S) of the source as a function of time are determined from its coordinates (right ascension α and declination δ) in the celestial sphere

using the well known relations

$$\text{Sin } Z_s \text{ Sin } A_s = -\text{Cos } \delta \text{ Sin } h \qquad (4.5)$$

$$\text{Cos } Z_s = \text{Sin } \delta \text{ Sin } \phi + \text{Cos } \delta \text{ Cos } h \text{ Cos } \phi \qquad (4.6)$$

$$\text{Sin } Z_s \text{ Cos } A_s = \text{Sin } \delta \text{ Cos } \phi - \text{Cos } \delta \text{ Cos } h \text{ Sin } \phi \qquad (4.7)$$

where ϕ is the latitude of the place of observation, and hour angle h of the source is related to right ascension by the relation

$$h = S.T. - \alpha \qquad (4.8)$$

where S.T. is the local sidereal time at which the observations are made. Azimuth of star at a certain time can be calculated from equations 4.5 and 4.7 , and its zenith angle from equation 4.6 . Any variation in latitude and longitude of the balloon during the course of the flight are also taken into account in calculating A_s and Z_s.

4.3:3 Calculation of Exposure Efficiency of Star as a Function of Time

Knowing azimuth and zenith angle of telescope, $A_T(t)$ and $Z_T(t)$, and azimuth and zenith angle of source, $A_s(t)$ and $Z_s(t)$, as a function of time, the space angle $\Theta(t)$ between source and the telescope axis as a function of time can be

calculated from

$$\text{Cos}\,\theta(t) = \text{Cos}\ Z_S(t)\ \text{Cos}\ Z_T(t) + \text{Sin}\ Z_S(t)\ \text{Sin}\ Z_T(t)\ \text{Cos}\left[A_S(t) - A_T(t)\right] \qquad (4.9)$$

Exposure efficiency of the telescope to a point source as a function of time, $\eta(t)$, can be derived by combining eqn. 4.4 and eqn. 4.9 . The exposure efficiency at a time t is given by

$$\eta(t) = \mathcal{E}\left[\theta(t)\right] \qquad (4.10)$$

where $\theta(t)$ is given by eqn. 4.9.

The excess counts due to a source at a time t, for each energy channel of the experiment, is to be divided by $\eta(t)$ to get normalized excess counts due to that source corresponding to normal incidence (full exposure).

4.3:4 Scan Path of Telescope in Sky

Scan path of telescope in sky (right ascension and declination of telescope axis as a function of time during the course of experiment) can be obtained knowing the zenith angle and azimuthal angle of telescope as a function of time. The right ascension α and declination δ for a particular value of telescope zenith angle Z_T and azimuth angle A_T can

be calculated using the relations

$$\cos\delta \sin h = -\sin Z_T \sin A_T \quad (4.11)$$

$$\sin\delta = \cos Z_T \sin\phi + \sin Z_T \cos A_T \cos\phi \quad (4.12)$$

$$\cos\delta \cos h = \cos Z_T \cos\phi - \sin Z_T \cos A_T \sin\phi \quad (4.13)$$

and $$\alpha = S.T. + h \quad (4.14)$$

The value of declination is given directly by eqn. 4.12 and hour angle h is obtained by dividing eqn. 4.11 by eqn. 4.13. From local sidereal time of observation (S.T.), the right ascension is obtained from eqn. 4.14. The scan path of the detector is then obtained by calculating right ascension α and declination δ of telescope axis in sky as a function of time for various values of telescope zenith angle Z_T and azimuth angle A_T during the course of experiment.

4.4 SPECTRAL ANALYSIS: UNFOLDING THE MEASURED SPECTRUM

4.4:1 Introduction

Characterization of the spectra of X-ray sources, for determining the physical parameters responsible for X-ray emission, has been one of the major goals in the present study. Simultaneous flux observations at a number of energies are used to determine the source spectrum. However, because of the complex properties of X-ray detectors the count rates observed from a given astronomical X-ray

source have no one-to-one relationship to the flux from that source incident at the top of the atmosphere. The transformations which an X-ray flux incident at the top of atmosphere undergoes before being detected as counts in the detector can be divided into those which merely attenuate the beam (including the residual atmospheric absorption above the detector, absorption in the detector window and quantum efficiency of the detecting medium), and those which redistribute it in detected energy (fluorescent photon escape phenomenon and the inherent energy resolution of the detector). In this section we briefly describe the computer simulation method used in the present investigations for deriving the energy spectral characteristics of the source from the observed count rates.

The general procedure adopted for analysis of spectral data consists of assuming a certain primary spectral form having some free parameters, based on a particular physical model of X-ray production, and convolute this model spectrum to include the attenuation properties of the atmosphere and the detector response to obtain counting rate histograms in the specified energy intervals. The measured pulse height distribution is then compared with the predicted model in each case to judge the correctness of the model based on the goodness of fit between the predicted and observed data. The process is repeated for

different types of model spectra, till a good fit is achieved.

4.4:2 Spectrum Transformations

Transformation of the model spectrum through the atmospheric and detector properties into counts in the detector was done using a procedure similar to that of Overbeck (1968). Let $\left(\frac{dN}{dE}\right)_o$ be the assumed differential number spectrum incident on the top of atmosphere, simplest model being exponential and power law representing thermal bremsstrahlung from a hot thin plasma and synchrotron emmission of high energy electrons respectively. The photon power law spectrum resulting from synchrotron mechanism is written as

$$\frac{dN(E)}{dE} = K\, E^{-\alpha} \text{ photons } cm^{-2}\ sec^{-1}\ keV^{-1}$$

and the exponential spectrum due to thermal bremsstrahlung is

$$\frac{dN(E)}{dE} = \frac{K}{E} \exp\left(-E/_{kT}\right) \text{ photons } cm^{-2} sec^{-1}\ keV^{-1}$$

where α and T represent the electron spectra responsible for the X-ray emission and K is a constant.

The spectrum at the detector after attenuation in the atmosphere and detector window (Al) will be

$$\left(\frac{dN(E)}{dE}\right)_1 = \left(\frac{dN(E)}{dE}\right)_0 e^{-\mu_a(E)\, X_a}\, e^{-\mu_{Al}(E)\, X_{Al}}$$

where $\mu_a(E)$ and $\mu_{Al}(E)$ are mass absorption coefficients in air and aluminium respectively for X-rays of energy E; and X_a and X_{Al} are thicknesses of residual atmosphere along the line of sight to the source and of detector window respectively in g cm^{-2}. Since Compton scattering is the most important mode of interaction for X-rays of energy > 30 keV, the absorption coefficients of air were calculated taking Compton absorption coefficients of nitrogen, oxygen and argon. In computing the amount of residual atmosphere along the line of sight, the variation of zenith angle of the source during the period of observation was also taken into account.

The spectrum of energy losses in the detector after correcting for efficiency of crystal and flourescent X-ray escape effects will be

$$\left(\frac{dN(E)}{dE}\right)_2 = \left(\frac{dN(E)}{dE}\right)_1 \left[\varepsilon(E) - P_\alpha(E) - P_\beta(E)\right]$$

$$+ \left(\frac{dN}{dE}^{(E+E_{K_\alpha})}\right)_1 P_\alpha(E + E_{K_\alpha})$$

$$+ \left(\frac{dN}{dE}^{(E+E_{K_\beta})}\right)_1 P_\beta(E + E_{K_\beta})$$

where $\mathcal{E}(E)$ is the efficiency of the detector given by

$$\mathcal{E}(E) = 1 - \exp\left[- \mu_c (E)\, d_c \right]$$

where μ_c (E) is the mass attenuation coefficient of crystal material in $cm^2\ g^{-1}$ and d_c is the thickness of crystal in $g\ cm^{-2}$. P_α and P_β are the probabilities that an incident photon gives rise to a K_α and K_β photon (of energy E_{K_α} and E_{K_β}) respectively which escapes from the detector. Efficiency of the crystal and escape probabilities P_α and P_β for the crystal used in present investigations have been computed as given in Sections 2.7:1 and 2.7:2 respectively.

The above spectrum is then smeared by a Gaussian energy dependent resolution function of the detector to obtain the final output spectrum recorded in the detector given by

$$\left(\frac{dN(E)}{dE}\right)_{final} = \int_0^\infty \left(\frac{dN(E')}{dE}\right)_2 \; e^{\frac{-(E'-E)^2}{2\sigma(E')^2}} \; \frac{dE'}{\sqrt{2\pi}\,\sigma(E')}$$

The standard deviation $\sigma(E')$ as a function of E' is related to experimentally measured full width at half maximum (FWHM) of a Gaussian line by the relation

$$\sigma = 0.424\ \text{FWHM}$$

and has been determined experimentally for each detector.

4.4:3 Comparison of Experimental and Predicted Data

The experimental data consists of counts in various energy channels having finite widths. For making a comparison between experimental and predicted data, the above differential spectrum is integrated between the lower and upper energy thresholds, E_l and E_u, for each channel to give the average count rate flux C_i in channel i as follows

$$C_i = \int_{E_{il}}^{E_{iu}} \left(\frac{dN(E)}{dE}\right)_{final} dE \text{ counts sec}^{-1} \text{ cm}^{-2}$$

A computer programme based on the above procedure was used to generate predicted counting rate histograms in the energy intervals into which the pulse heights were quantised by electronics, for different trial spectra having certain free parameters. Various probable values of the free parameters of the spectrum (e.g. A, α, KT) were fed into the programme. The predicted count rates C_i thus obtained were compared with observed count rates N_i using χ^2 analysis and the least square ($\min \chi^2$) criterion was then used to determine the best fit values of unknown parameters for each trial spectrum and to evaluate goodness of fit between observed spectrum and model spectrum. Here χ^2 is

defined as

$$\chi^2 = \sum_{i=1}^{n} \left[\frac{(N_i - C_i)}{\Delta N_i} \right]^2$$

where ΔN_i is error for observation in the i^{th} energy channel and n is the total number of independent energy bins. Alternate spectral models are accepted or rejected by comparing the observed χ^2_{min} values against a χ^2 probability table, which gives the probability P of obtaining a value of χ^2 greater than or equal to that observed for the specified number of degrees of freedom. If the above probability is less than 10% it is unlikely that the model with its best fit parameters describes the data, otherwise it is considered to be acceptable.

4.4:4 Spectrum Unfolding

The measured spectrum can now be unfolded through atmospheric and detector response characteristics to give the true incident spectrum. The ratio of counts per channel before and after folding of the acceptable best fit trial spectrum are used as correction factors for unfolding the measured results. For observed counting rate N_i counts cm^{-2} sec^{-1} in i^{th} energy channel, correction

factor R_i will be

$$R_i = \int_{E_{il}}^{E_{iu}} \left(\frac{dN(E)}{dE}\right) dE \Bigg/ \int_{E_{il}}^{E_{iu}} \left(\frac{dN(E)}{dE}\right)_{final} dE$$

In this way any features in the measured spectrum are retained in the unfolded result.

CHAPTER V

OBSERVATIONAL PROGRAMME AND RESULTS

This chapter describes the observational programme and other details of various balloon flights conducted to make observations on the X-ray star Cyg X-1 in the energy range 20-200 keV, followed by a presentation of the results obtained from these investigations.

5.1 BALLOON FLIGHT DETAILS : OBSERVATIONAL PROGRAMME AND FLIGHT PERFORMANCE

5.1:1 Summary of Different Flights

Table 5.1 furnishes the details of the balloon flights carrying X-ray payloads, in which the author has participated. These flights were conducted from Hyderabad (India) situated close to geomagnetic equator ($\lambda_m \approx 8^\circ N$) and important sources such as Sco X-1, Cyg X-1, Her X-1 etc. were investigated as a part of this programme.

Since the present thesis is exclusively concerned with studies on Cyg X-1, further discussion is carried out only in relation to flight numbers 2, 4, 5, 6 and 7. Among these flights, flight 5 was aborted owing to the accidental crashing of the payload on the ground during launch, thereby

TABLE 5.1

SUMMARY OF BALLOON FLIGHTS

Flight No.	Date & time of flight	Ceiling duration	Ceiling altitude g cm^{-2}	Detector and effective area	FWHM of collimator	Energy range of observation (keV)	Objectives	Remarks
1	2	3	4	5	6	7	8	9
1.	Nov.15, 1971 launch 0138 UT	0430 UT to 0825 UT	$\sim$5.6	One 5" dia NaI(Tl) crystal with plastic anticoincidence shield. Effective area $\sim$94 cm^2	11.6°	17-106	To observe Sco X-1	Sco X-1 observed for 25 min with exposure eff. > 60%
2.	Mar.29, 1972 launch 0116 UT	0430 UT to 0914 UT	$\sim$5.7	One 4" dia NaI(Tl) crystal with plastic anticoincidence shield. Effective area $\sim$76 cm^2	18.8°	20-160	To observe Cyg X-1	Cyg X-1 was tracked for 1 hr and 15 min with exposure eff. > 80%
3.	Dec.28, 1972 launch 0155 UT	0430 UT to 0852 UT	$\sim$5.1	One 4" dia NaI(Tl) crystal with plastic anticoincidence shield. Effective area $\sim$81 cm^2	13.5°	20-120	To observe Her X-1	Zenith drive malfunction. Her X-1 observed for $\sim$15 min.
4.	Jan.18, 1973 launch 0216 UT	0445 UT to 0732 UT	$\sim$ 4.6	-do-	13.5°	20-140	To observe Her X-1 and Cyg X-1	Her X-1 observed for $\sim$15 min. Cyg X-1 tracked for $\sim$1 hr with exposure eff. > 95%

TABLE 5.1 (contd.)

1	2	3	4	5	6	7	8	9
5.	Feb. 12, 1974	-	-	Two 4" dia NaI(Tl) crystals with plastic anticoincidence shield. Effective area $\sim$160 cm^2	13.5^o	30-120	To track Cyg X-1 for two hours	Payload crashed on the ground during launch
6.	Mar. 2, 1974	-	-	-do-	13.5^o	30-120	To track Cyg X-1 for two hours	Balloon bursted 1 hour 30 min after launch
7.	Feb. 11, 1975 launch 0146 UT	0415 UT to 0726 UT	$\sim$5.0	Two NaI(Tl) crystals of 4" dia each and one of 5" dia. Effective total area $\sim$225 cm^2. No anticoincidence shield.	13.5^o	30-120	To observe Cyg X-1 for three hours	Cyg X-1 observed for 3 hrs with exposure eff. > 80%

incapacitating the payload. Flight 6 proved unsuccessful due to the tropopause burst of the balloon. Useful observational data on Cyg X-1 was obtained during flights 2, 4 and 7 conducted on March 29, 1972, January 18, 1973 and February 11, 1975 respectively. The experimental objectives in conducting these flights were to study flux, energy spectrum, flaring activity and short and long term fluctuations of Cyg X-1 in the 20-160 keV energy range.

5.1:2 Observational Programme and Flight Performance

In all these flights long time observation of the source was planned by changing the zenith and azimuth angle of telescope, as described in chapter III, thereby enabling the tracking of the source in sky. The rate of change of zenith and azimuth angle was preprogrammed by calculating the zenith and azimuthal angle of the star for the day of observation. In this section, we briefly describe the observational programme of different flights and actual performance of each experiment.

The X-ray telescope used in March 29, 1972 observation has been described in Section 2.6:1 of Chapter II. The detector had an effective area of $\sim$76 cm^2 and FWHM field of view of 18.8^o. The balloon was launched at 0646 hrs Indian Standard Time (IST), reaching a ceiling altitude of $\sim$ 5.7 g cm^{-2} at 0945 hrs IST and floated at nearly constant altitude till 1444 hrs IST. Cyg X-1 was

tracked by changing the zenith angle of telescope, initially fixed at 30°, from 0940 IST onwards. The azimuthal angle of telescope was kept fixed at 305° (in NESW system). This way the source was tracked for 1 hour and 15 minutes, from 0950 IST to 1105 IST, with an exposure efficiency of $\sim$ 90%. The data was monitored in seven contiguous energy channels, viz. 20.0-29.0 keV, 29.0-38.2 keV, 38.2-48.5 keV, 48.5-60.0 keV, 60.0-87.5 keV, 87.5-119.5 keV, 119.5-160.5 keV and a sum channel of 29.0-60.0 keV. The flight was successful except for a malfunction in the 60-87.5 keV energy channel, the data from which therefore had to be rejected in further analysis.

The next observation on January 18, 1973 used the X-ray telescope described in Section 2.6.2 of Chapter II. The detector had an effective area of $\sim$ 81 cm^2 and FWHM field of view of 13.5°. The observations were made in 20-140 keV energy range. The balloon, which was launched at 0746 hrs IST, reached a ceiling altitude of $\sim$ 4.6 g cm^{-2} at 1015 hrs IST and floated at this height upto 1302 hrs IST. In this flight, it was planned to make observations on two X-ray stars Her X-1 and Cyg X-1 by changing both zenith and azimuthal angle of telescope during the flight at a pre-programmed rate. This way observations were made on Her X-1 for $\sim$ 15 minutes and on Cyg X-1 for $\sim$ 1 hour with exposure efficiencies $\sim$ 95%. The observations on Cyg X-1 were made

from 1140 hrs IST to 1245 hrs IST. Fig. 5.1 shows counting rate of the detector in the source direction after reaching the ceiling altitude and also indicates the time intervals when Her X-1 and Cyg X-1 were under observation. The average background counting rate $\bar{B}$ is shown by dotted line. It is seen that while Cyg X-1 has clearly contributed to the counting rate of the telescope, there is no statistically significant increase in counting rate during exposure to Her X-1. These observations on Her X-1 were made in middle of its OFF state (35 day), 5 days before the onset of 12 day ON state, and have been discussed elsewhere (Sharma et al. 1973). The observations on Cyg X-1 will be discussed in a later section.

The February 11, 1975 observations were carried out using the large area telescope described in Section 2.6:3 of Chapter II, having three NaI (Tl) crystals with a total effective area of ~ 225 cm^2 and a FWHM field of view of 13.5°. The balloon was launched at 0716 hrs IST and reached a floating altitude of ~ 5.0 g cm^{-2} at 0945 hrs IST, which it maintained till 1256 hrs IST when the payload had to be cut-off from balloon by command, because the balloon had drifted too far due to high winds prevailing at float altitude. Extensive calibrations were done immediately after the payload recovery by exposing the detector to X-ray calibration sources Cd^{109} and Am^{241} to check the drifts,

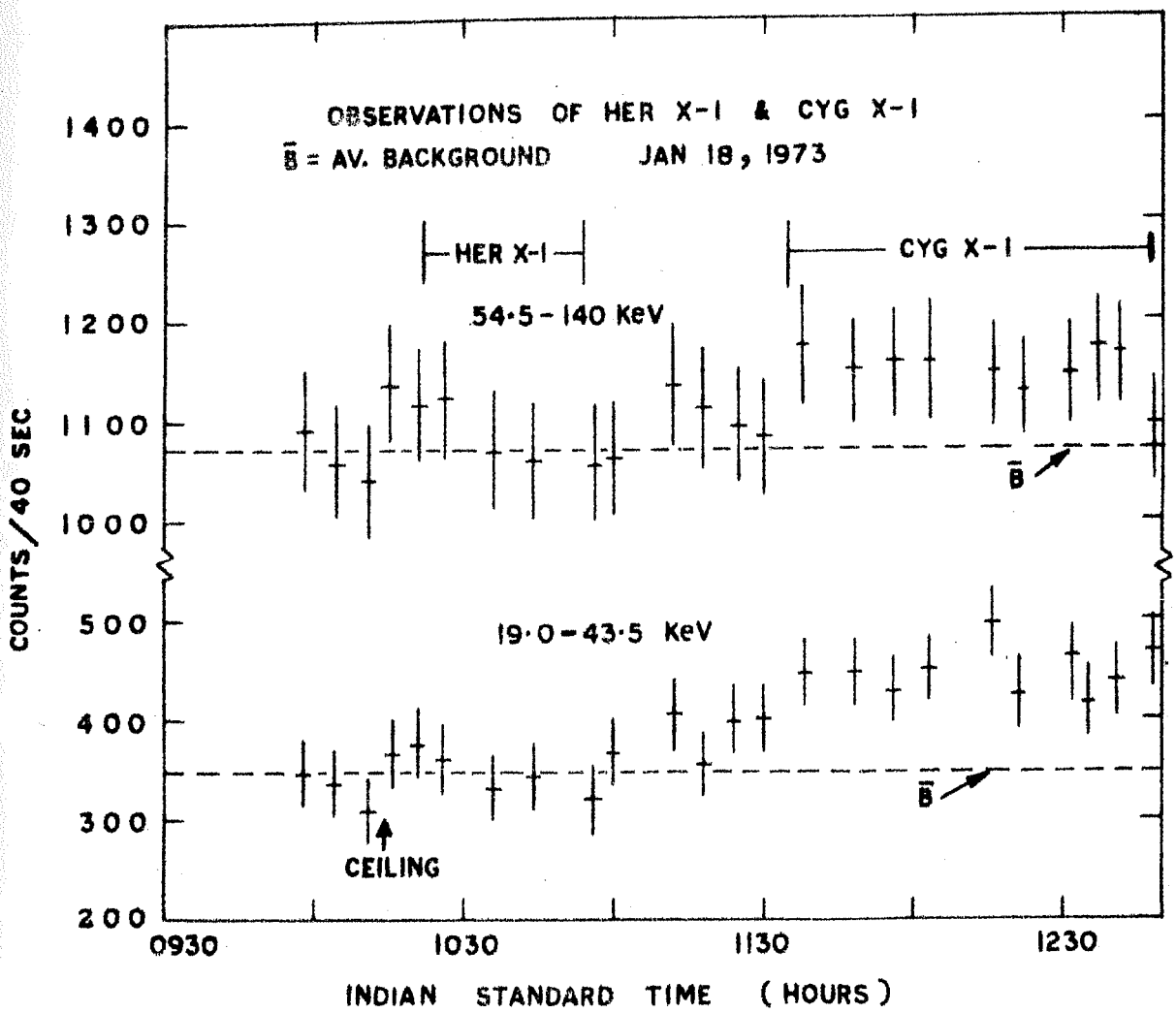

Fig. 5.1 : Counting rates in source direction for January 18, 1973 flight. The time intervals for which Her X-1 and Cyg X-1 were under observation are shown. The average counting rate is shown by dotted line.

if any, in performance parameters of the detector in flight. In this flight, with the large area telescope, it was planned to obtain longest possible exposure of the source Cyg X-1 by changing both zenith and azimuthal angles of telescope continuously by pre-programmed azimuth and elevation controls of the oriented platform. The azimuthal angle of telescope, which was initially fixed at $\sim 32^{\circ}$ in NESW system (32°E of north), was changed, starting from 1000 hrs IST, at a constant rate of 0.6° per minute till 1210 hrs IST, when the azimuthal angle reached $\sim 314^{\circ}$ (46°W of north). The zenith angle of the telescope was initially fixed at $\sim 19^{\circ}$ and was increased at a rate of $\sim 1^{\circ}$ per 6 minute from 1135 hrs IST to $\sim$ 1250 hrs IST, till zenith angle reached $\sim 32^{\circ}$. The tracking programmers and other control systems worked as planned throughout the flight and in this way Cyg X-1 was observed for the complete duration of balloon float time from 0945 hrs IST (0415 UT) to 1256 IST (0726 UT) with exposure efficiencies ranging between 80% to 99%. The data was monitored in six contiguous energy intervals, viz. 29.0-44.5 keV, 44.5-60.5 keV, 60.5-76.0 keV, 76.0-91.0 keV, 91.0-106.0 keV and 106.0-121.0 keV. Of the three detector systems, two performed satisfactorily throughout the flight, whereas the third one (4" dia detector) did not behave properly during the flight. However, since all the three detectors had completely

independent electronics and other pulse processing systems, the malfunction of this detector did not affect the satisfactory operation of the other two. The excess counts due to Cyg X-1 in the two detectors were, however, combined to provide a total effective area of $\sim$ 163 cm^2 for the observation of Cyg X-1, thus considerably improving the statistics.

5.1:3 Count Rate Profile During the Flight

A typical counting rate profile for the detectors used in the above flights is shown in Fig. 5.2 for the first detector of February 11, 1975 flight. In this figure we have plotted the observed counting rate in source and background directions in 29.0-76.0 keV energy range as a function of time and atmospheric depth. The major contribution to the detector counting rate on the ground comes from X-rays produced in natural radio active decays. Therefore, as the detector is released from the ground the counting rate first registers a sharp fall, upto a height of about 100 feet, and then starts increasing due to rise in the secondary cosmic ray effects in the atmosphere. As the detector rises higher and higher, the counting rate increases monotonically till it reaches a maximum at the Pfotzer maximum which is at a depth of $\sim$ 120 g cm^{-2}, at these latitudes. Above the Pfotzer maximum the detector counting rate again starts decreasing till it reaches a

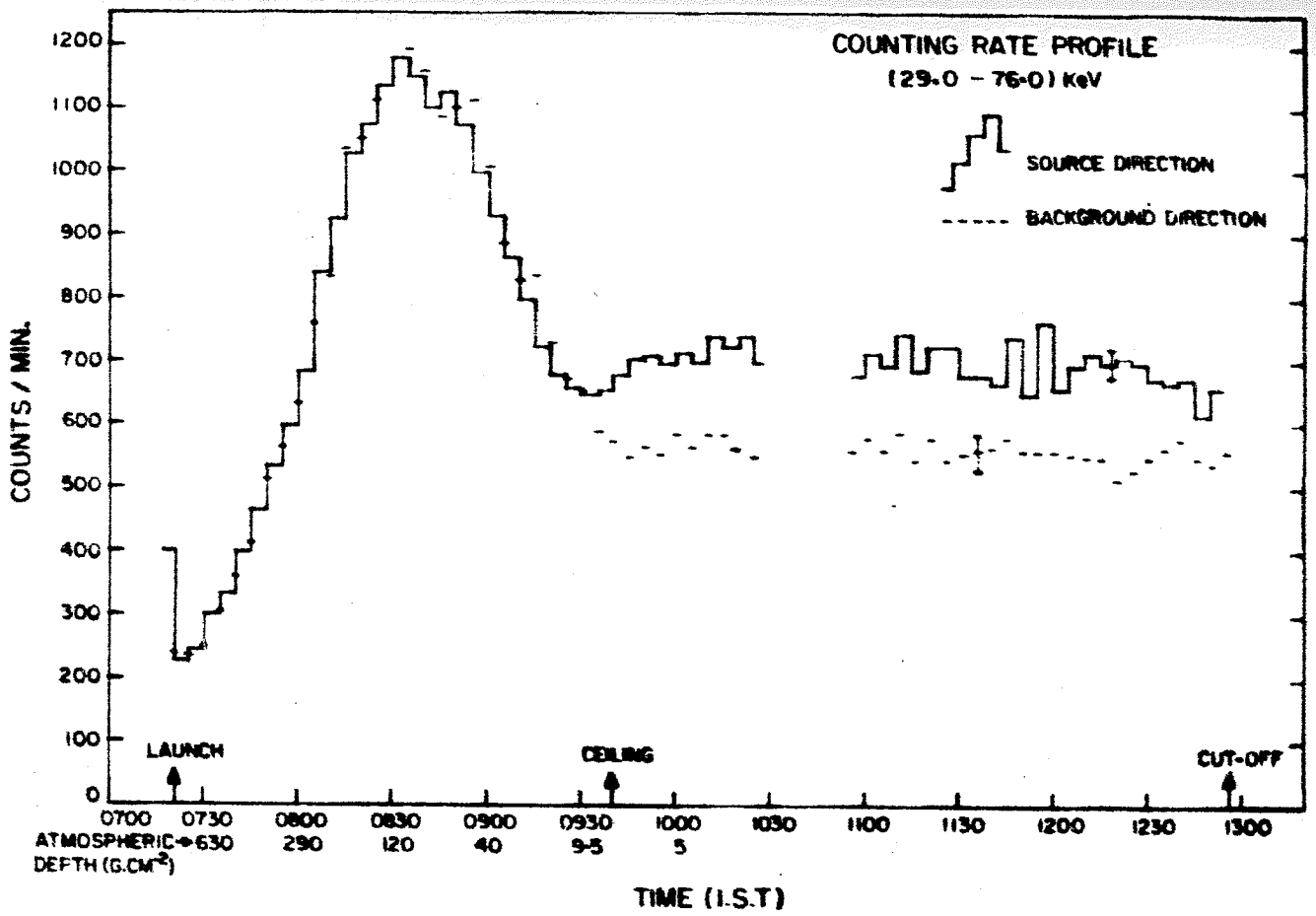

Fig. 5.2 : Counting rate profile in source and background directions for first detector of February 11, 1975 flight during ascent phase of balloon and at ceiling, plotted against time and pressure (pressure written for 0730, 0800, 0830, 0900 and 0930 hrs IST).

minimum at a depth of $\sim$15 g cm^{-2} of residual atmosphere, and in fact should continue to further decrease if there were no contribution from extraterrestrial sources. But, in spite of the atmospheric absorption the celestial X-rays can penetrate upto 10-15 g cm^{-2} depending on their energy, the degree of penetration being less at greater depths. This results in an upward turn in the counting rate and the count rate shows a steady increase with altitude. However, the counting rate in the source direction is higher than in the background direction because of the X-ray photons contributed by the X-ray source, in this case Cyg X-1. This can be very clearly seen in Fig. 5.2 at float altitude, where counting rate in the direction of Cyg X-1 is much higher than in the opposite direction devoid of sources. The fluctuations in counting rate in source direction are due to varying exposure efficiency of the source, time variations in the flux of Cyg X-1 and also due to minor fluctuations in float altitude, besides the statistics of the incoming photons themselves.

5.2 CONTRIBUTION OF CYG X-3 IN THREE FLIGHTS

To derive the number of observed counts from the source Cyg X-1, the background counting rate is subtracted from that observed in the source direction, as explained in Chapter IV. However, due to the large aperture of the telescopes used in the present investigation, the X-ray

source Cyg X-3 which is $\sim 7^{\circ}$ away from Cyg X-1 was also in field of view of the telescopes for most of the time. In this section, therefore, we will estimate the fraction of observed excess counts in the source direction which could come from Cyg X-3 and also examine whether the observed variations in Cyg X-1 could arise due to intensity variations of Cyg X-3.

The exposure efficiency for Cyg X-1 and Cyg X-3 sources for March 29, 1972 and February 11, 1975 flights, during which Cyg X-1 was tracked continuously and exhibited flare-type enhancement and large fluctuations in intensity (results to be presented in later sections), are shown in Fig. 5.3a and b respectively. It can be seen from this figure that in March 29, 1972 observation exposure efficiency for Cyg X-3 is $\sim$ 40% for most of the time and in February 11, 1975 flight it is only $\sim$10% in the beginning and gradually increases, but is less than $\sim$ 45% throughout most of the observation time. The intensity of Cyg X-3 at energies $\gtrsim$ 20 keV is normally reported to be nearly one tenth of Cyg X-1 intensity (Matteson 1971; Brisken 1973; Ulmer et al. 1974; Ulmer 1975 and Pietsch et al. 1976) but on two occasions its intensity has been reported to be as high as a third or a fifth of Cyg X-1 intensity (Rocchia et al. 1969; Peterson 1970). It is, therefore, necessary to take account of the possibility of a relatively high

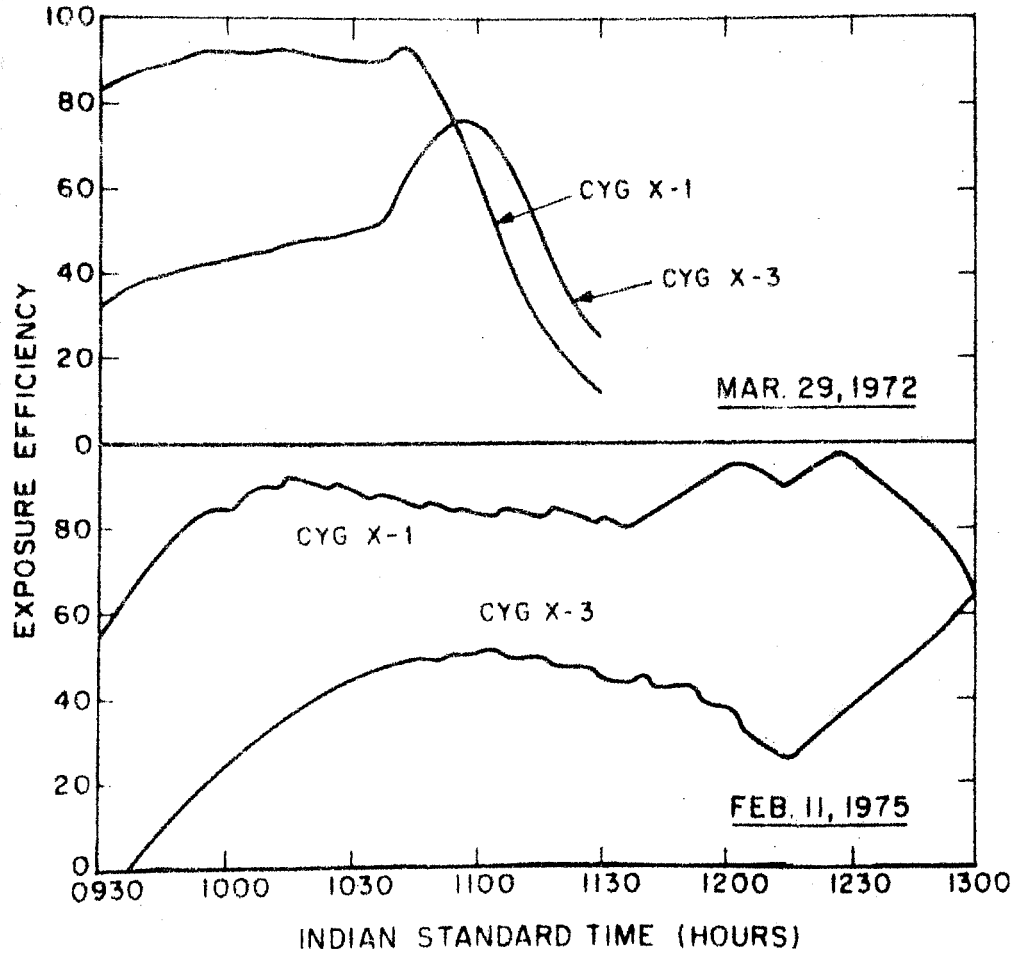

Fig. 5.3 : Exposure efficiency of the telescope for Cyg X-1 and Cyg X-3 sources during March 29, 1972 and February 11, 1975 observations.

intensity of Cyg X-3 (say one third) while discussing the time variation of Cyg X-1, observed in the present investigations. Since the percentage contribution of Cyg X-3 is less than 45% for most of the time in all the three flights, even if we assume, in the worst case, the intensity of Cyg X-3 to be one third of Cyg X-1 intensity, the estimated contribution from Cyg X-3 will be less than 15% in our observations i.e. approximately a factor of 7 below the Cyg X-1 contribution. Under normal conditions, Cyg X-3 contribution will be only $\sim$ 7%. Further, based on counting rate profile at different times, and by comparing counting rates for March 29, 1972 observation in 0957 - 1016 IST time period, when R, the ratio of exposure efficiency of Cyg X-3 to Cyg X-1, is $\sim$ 0.5 (and average counting rate in 29-60 keV is $\sim$ 47 $\pm$ 8); to the counting rate beyond 1100 hrs IST i.e. in 1100 - 1113.5 IST period, when R is $\sim$ 1.5 (and average counting rate in 29-60 keV $\sim$ 27 $\pm$ 9), we get counting rates of Cyg X-1 and Cyg X-3 to be $\sim$ 47 $\pm$ 11 and $\sim$ 9 $\pm$ 4 respectively. Therefore, during March 29, 1972 observation counting rate of Cyg X-3 is at least a factor of 4.5 smaller than that of Cyg X-1 and the contribution of Cyg X-3 to the observed excess counting rate is only 10% for this observation, which can be neglected. Similarly, for February 11, 1975 experiment an upper limit to the contribution of Cyg X-3 can be derived by comparing the data in

the initial observation period of 0940 - 1000 IST, when exposure efficiency of Cyg X-3 is very low, to counting rate in 1100 - 1130 IST period, when exposure efficiency of Cyg X-3 is large (see Fig. 5.3). Such a comparison, though difficult to make in view of large fluctuations in intensity of Cyg X-1, gives an upper limit of intensity of Cyg X-3 being one third of that of Cyg X-1. In view of this and the fact that long term monitoring of Cyg X-3 above 20 keV seems to indicate that this source does not show flare type fluctuations, we can conclude that presence of Cyg X-3 is not going to materially change our conclusions regarding the flare type behaviour and fluctuations in intensity of Cyg X-1 discussed later.

In the following three sections we will present the results obtained from the observation of X-rays from Cyg X-1 in $\sim$ 20-160 keV energy range in three experiments conducted on March 29, 1972; January 18, 1973 and February 11, 1975 respectively.

5.3 RESULTS : MARCH 29, 1972 FLIGHT

5.3:1 Time Profile of Data : Observation of a Flare

The excess counting rates for Cyg X-1, derived after subtraction of the background, normalizing for the off set angle of telescope with respect to the source, as well as correcting for atmospheric and crystal transmission

effects, are plotted as a function of Indian Standard Time in Fig. 5.4a, b for March 29, 1972 observation of Cyg X-1. Fig. 5.4a represents the counting rate averaged over 10 minutes and 5.4b represents same counting rate with better time resolution, as five minute averages, in two energy ranges: 29-60 keV and 87.5-160 keV. The statistical error at 1σ level in the counting rate is indicated by vertical bars.

From these figures, it is quite clear that Cyg X-1 has contributed statistically significant counts to the observed count rates from 1000 hrs IST to 1110 hrs IST. The observed counting rate from the source was constant within 1σ level from approx. 1000 hrs IST to 1020 hrs IST, but at 1038 hrs IST the counting rate showed a significant enhancement by a factor of two for nearly ten minutes, upto 1048 hrs IST. Following this enhancement the counting rate again dropped to its normal value which it maintained till 1110 hrs IST, beyond which source was not observed. Figures 5.4a and 5.4b show two distinct phases of X-ray emission of Cyg X-1, which were observed during this flight:

i) 'Quiet Condition' observed at the beginning of observation from 0958 hrs IST to 1018 hrs IST, and

ii) Short period (from 1038 hrs IST to 1048 hrs IST) 'Flaring Condition' in the emission of Cyg X-1,

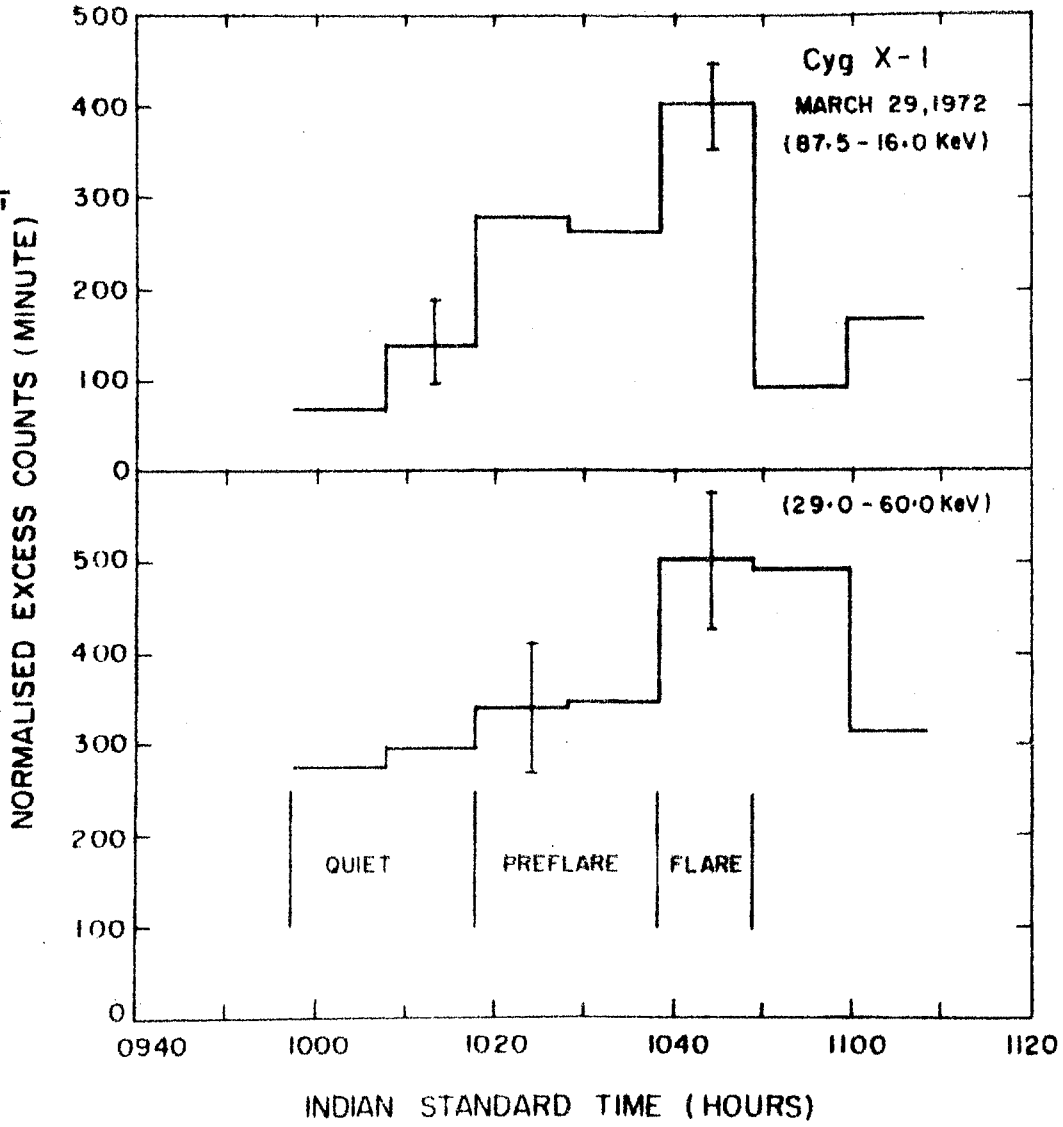

Fig. 5.4a : Normalized excess counting rates due to Cyg X-1 in 29-60 keV and 87.5-160 keV energy intervals as a function of time for March 29, 1972 observation, averaged over 10 min.

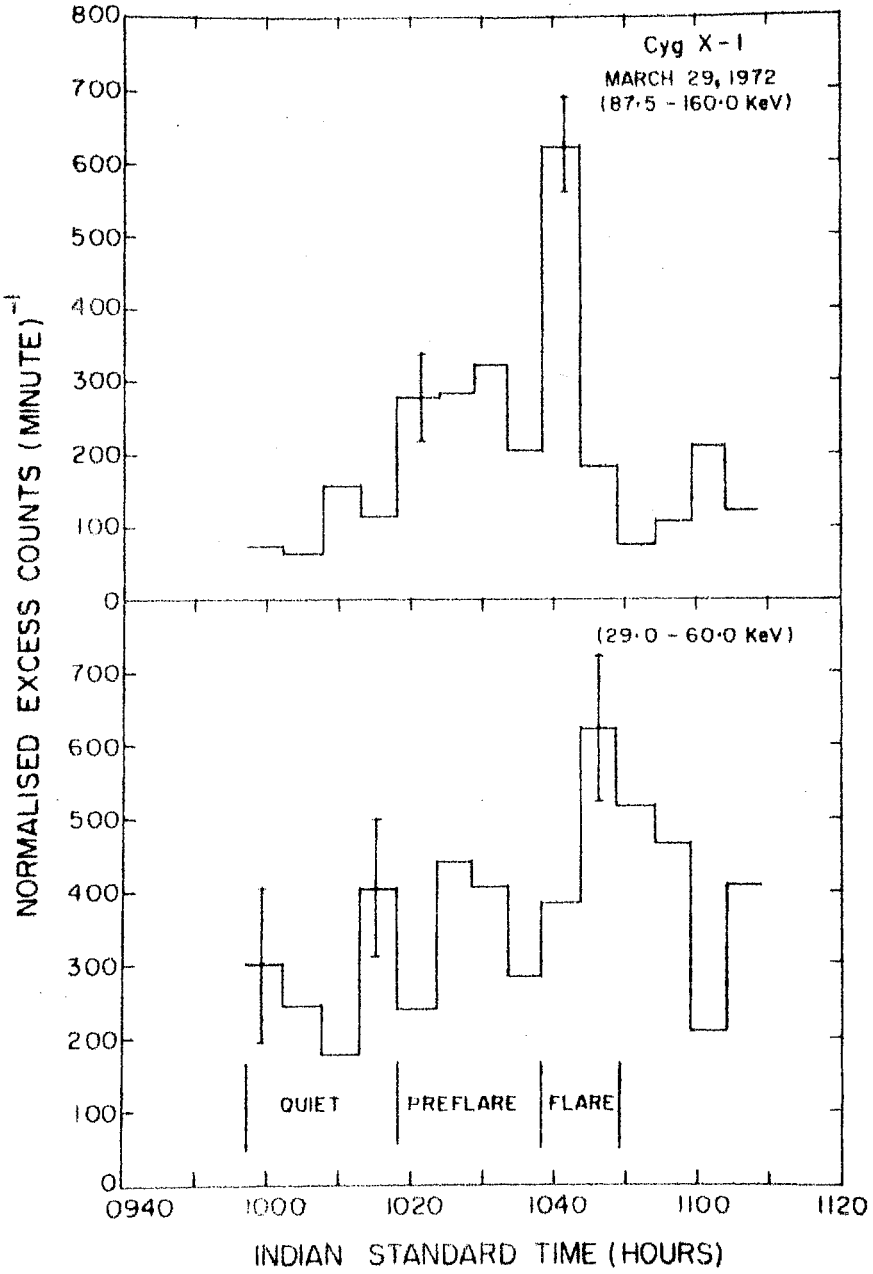

Fig. 5.4b : Same as in Fig. 5.4a but data averaged over 5 min time scale.

when the source emitted greatly enhanced intensity compared to that during 'quiet' condition.

The observation just prior to the flaring condition, from 1018 hrs IST to 1038 hrs IST, also shows some activity and has been termed as 'Preflare' condition.

5.3:2 Source Emission Spectrum During Various Phases

To know the emission characteristics of the source in these three states, we have calculated the photon spectrum of the source for these three phases of its emission. Fig. 5.5 shows the photon counting rate from Cyg X-1 during 'quiet', 'preflare' and 'flare' conditions of its emission as a function of energy, using the procedure described in Section 4.4. The best fit spectrum based on the observations is also shown in figure. The best fit spectrum for Cyg X-1 in the energy range 20-160 keV during the quiet condition is consistent with a power law which can be represented by the equation :

$$\frac{dN}{dE} = 3.621\ E^{-1.90 \pm 0.1}\ \text{photons cm}^{-2}\ \text{sec}^{-1}\ \text{keV}^{-1}$$

The average integrated intensity in the energy range 20-150 keV during this flight in the quiet condition is $\sim 1.74 \cdot 10^{-8}$ ergs cm^{-2} sec^{-1}.

The preflare spectrum, from 1018 hrs IST to 1038 hrs IST, is also consistent with a power law, but with

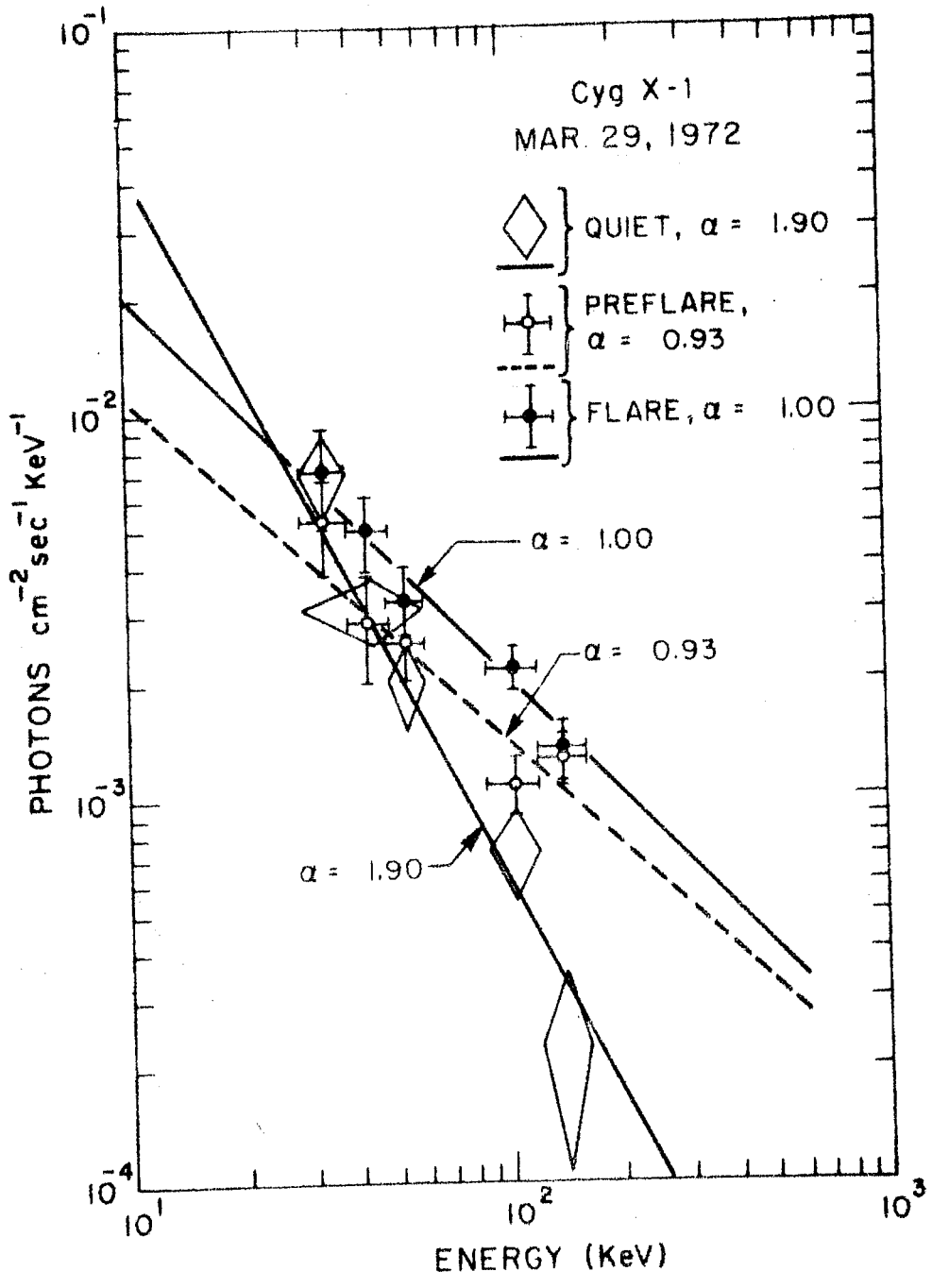

Fig. 5.5 : Photon spectrum for 'quiet', 'preflare' and 'flare' phases of X-ray emission of Cyg X-1 for March 29, 1972 observation.

a different spectral index ($\alpha = 0.93$)

$$\frac{dN}{dE} = 0.1\ E^{-0.93 \pm 0.10} \text{ photons cm}^{-2} \text{ sec}^{-1} \text{ keV}^{-1}$$

The average integrated intensity in the energy range 20-150 keV in Preflare condition has increased to $\sim 2.83 \cdot 10^{-8}$ ergs cm^{-2} sec^{-1}.

During the flare condition the spectral index remains nearly same as in the earlier preflare condition, but the average integrated intensity in 20-150 keV energy range increases to $\sim 4.64 \cdot 10^{-8}$ ergs cm^{-2} sec^{-1}, which is ~ 2.7 times the intensity in quiet condition. The best fit spectrum in this condition is represented by the equation :

$$\frac{dN}{dE} = 0.223\ E^{-1.00 \pm .05} \text{ photons cm}^{-2} \text{ sec}^{-1} \text{ keV}^{-1}$$

5.3:3 Flare Characteristics

As stated earlier, around 1038 hrs IST the X-ray flux from the source showed an abrupt increase in all the energy bands in the range 30-160 keV. This enhancement lasted for about 10 minutes during which period our detector registered approximately 2.7 times the flux (in 20-150 keV) from the same source as observed during the quiet condition. After the completion of the flare,

the source flux decreased abruptly and returned to the normal quiet condition.

Close examination of its characteristics reveals some distinct features of this flare :

i) Since the spectral index α of the source changed from 1.9 to 0.93 fifteen minutes prior to the onset of the flare (preflare condition) and remained almost same during the flare; it means that the activity giving rise to the enhanced emission from the source started in preflare condition and thus the rise time to reach peak intensity of the flare was very slow $\sim$15 min. On the other hand, the decay to normal condition is very abrupt. Though the statistical significance of the data is not sufficient to precisely quantify this characteristic, nevertheless, the observation strongly points to the difference in the rise and decay time of the flare.

ii) A close examination of Fig. 5.4b indicates that there is a distinct time delay between low and high energies when the source is in flare condition. The observations indicate that flaring at high energies (87.5-160.0 keV) starts about 5 minutes earlier to that at low energies (29-60.0 keV),

a behaviour which is quite contrary to the normal expectation. To check the validity of this result we have very carefully examined the behaviour of each energy channel in the calibration mode, when the entire detector is subjected to periodic calibration using a radioactive source. We conclude that the observed delay of approximately 5 minutes in the rise in intensity in lower energy channel compared to the rise at high energy is a phenomenon which must have its origin in the X-ray source itself.

iii) As mentioned earlier, best fit spectrum during flare hardens considerably compared to that during quiet condition; spectral index changing from $\alpha = 1.9$ during quiet condition to $\alpha = 1.0$ during the flare condition. The percentage enhancement at higher energies (87.5-160.0 keV) is much more than at lower energies (29-60.0 keV) and basically the flare is a hard X-ray flare.

iv) The average integrated intensity in 20-150 keV energy range during flare is $4.64 \cdot 10^{-8}$ ergs cm^{-2} sec^{-1}, which is 2.7 times that during quiet condition ($1.74 \cdot 10^{-8}$ ergs cm^{-2} sec^{-1}).

To know the characteristics of the flare in detail, we have carried out one minute time resolution study of

the normalised excess counting rate of the source. This is shown in Fig. 5.6a for 29.0-160.0 keV and 87.5-160.0 keV energy intervals. It can be seen from this figure that due to the poor statistics, no definite conclusions can be drawn regarding fluctuations in source intensity at one minute time interval in the energy range 29.0-60.0 keV. However, in the higher energy range (87.5-160.0 keV) the increase at 1039 hrs IST is very prominent. The enhancement in source intensity in this energy range is by a factor of nearly 4 to 5. The statistical significance of this increase is at 5 to 6 σ level, which means that this increase in intensity of the source is genuine and cannot be due to statistical fluctuations. This is also clear from Fig. 5.6b where we have plotted one minute counting rates for 87.5-119.5 keV and 119.5-160.0 keV energy intervals separately. It is seen from this figure that the increase in source intensity has taken place in both energy channels at the same time. An interesting feature of this event is that it is mainly confined to energies > 90 keV only and corresponding increase at lower energies at this time is relatively very small. This again points to the fact that this flare is basically a hard X-ray flare, unlike the flares reported by other observers. One feature of this hard X-ray flare is the presence of dips in source intensity just before and after the flare, at

THE LIBRARY
PHYSICAL RESEARCH LABORATORY

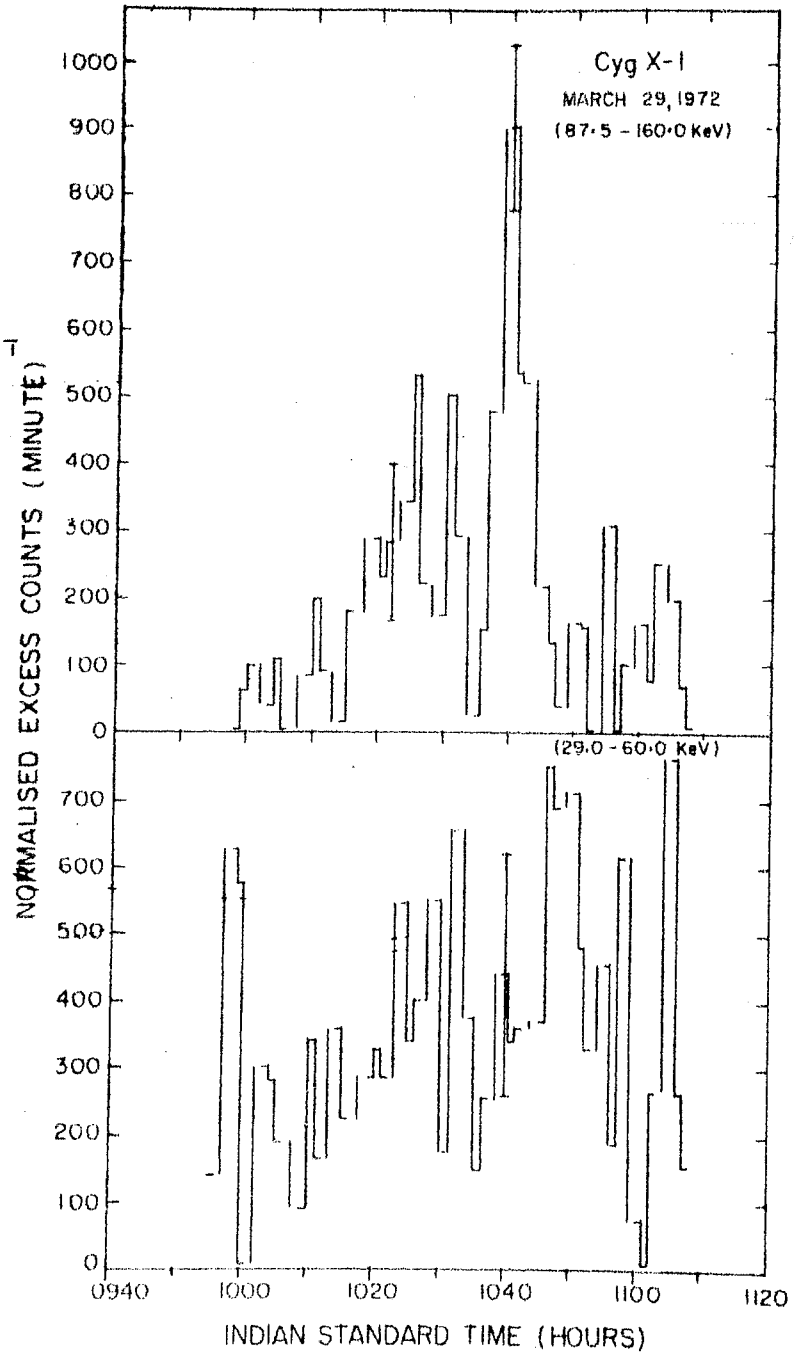

Fig. 5.6a : Normalized excess counting rates due to Cyg X-1 in 29-60 keV and 87.5-160 keV energy intervals as a function of time for March 29, 1972 observation, shown in 1 min bins.

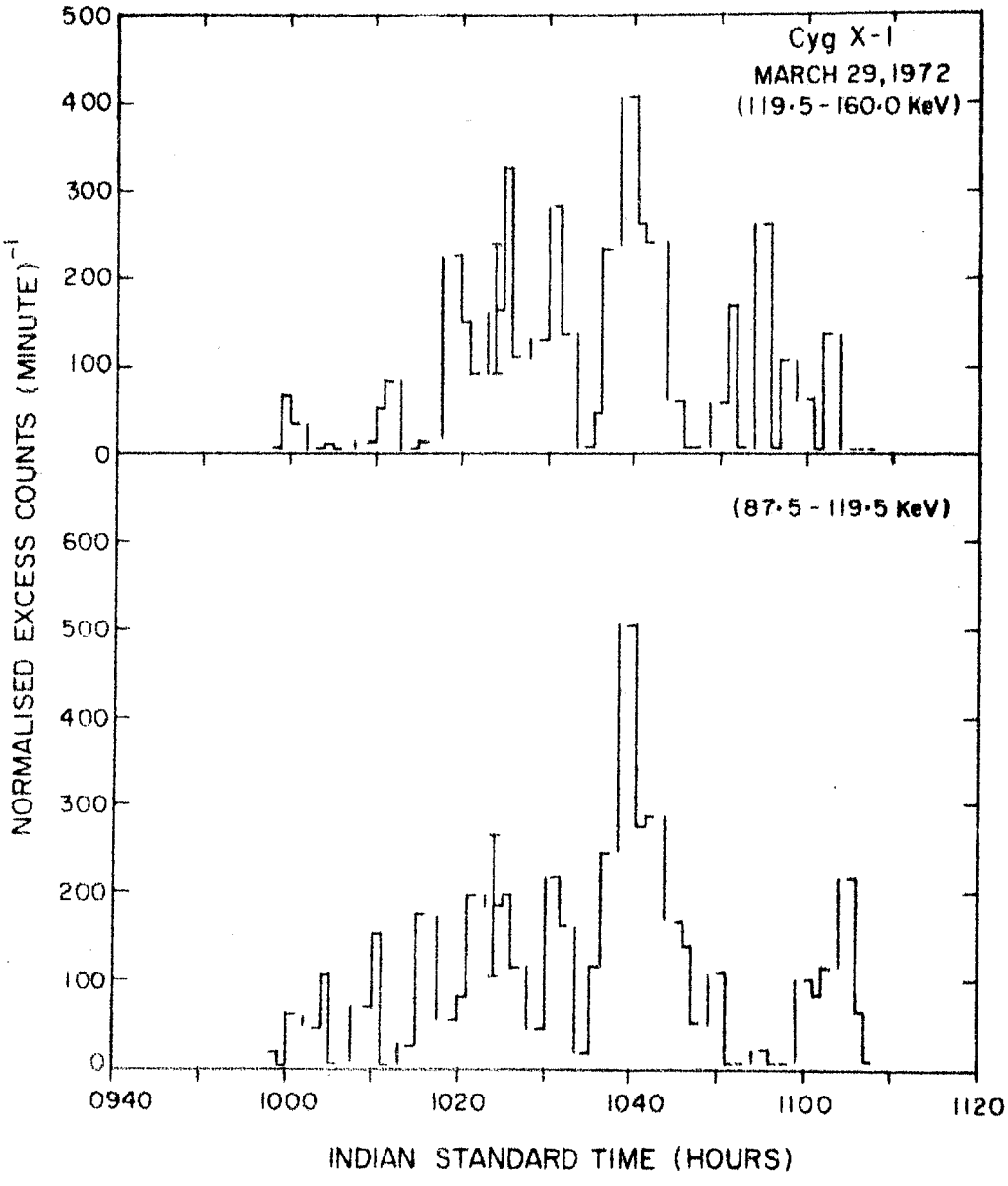

Fig. 5.6b : Counting rates in 87.5-160.0 keV energy interval of Fig. 5.6a shown in 87.5-119.5 keV and 119.5-160.0 keV energy intervals separately.

1035 hrs IST and 1048 hrs IST respectively. Also, if we take the increase in intensity at 1047 hrs IST in low energy channel as that corresponding to the hard X-ray flare (we should note here that counting statistics at low energy is not sufficient to draw any definite conclusions), then we see that the dip in source intensity in this energy range before the onset of flare is time coincident with that at higher energies i.e. at 1035 hrs IST, but the peak rise is six minutes later, at 1045 hrs IST. Further, the post-flare dip is also 6 to 7 minutes later, at 1055 hrs IST. Besides, at higher energies the source intensity has started increasing at around $\sim$1020 hrs IST itself, approximately 20 minutes before the peak of the flare, but the intensity drops down suddenly after the peak rise. This also supports the earlier conclusion that rise time of the flare is much slower than its decay time.

5.4 RESULTS : JANUARY 18, 1973 OBSERVATION

The observed counting rate from Cyg X-1 during this flight is shown in Fig. 5.1. The photon counting rate as a function of energy, after applying all the necessary corrections for transmission through air, collimator transmission efficiency and detector efficiency etc. to the excess counting rate as described earlier, is shown in Fig. 5.7. The observations during this flight, which lasted for about an hour of time, did not show any

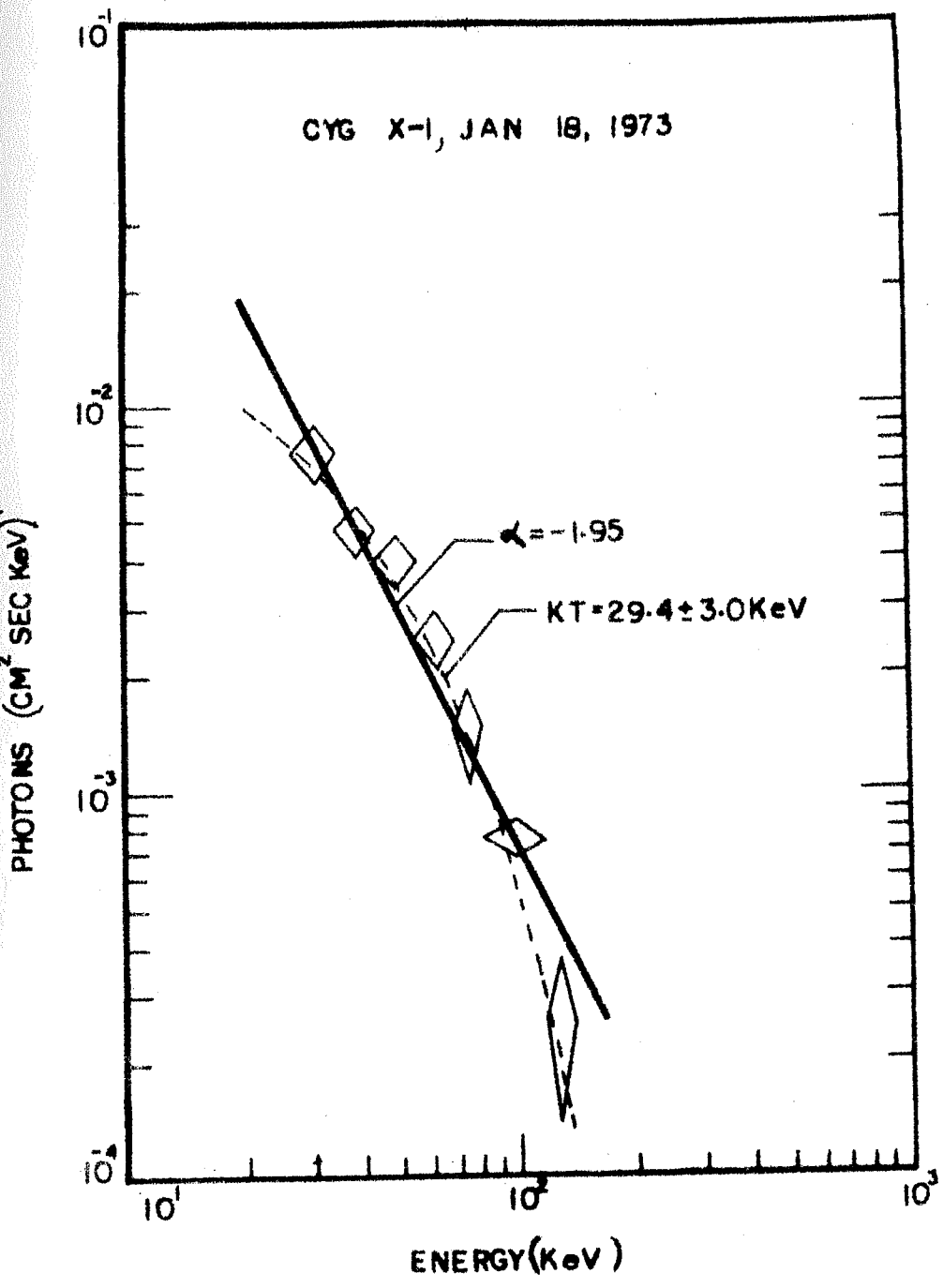

Fig. 5.7 : Photon spectrum for entire duration of January 18, 1973 observation of Cyg X-1. The best fit power law and exponential spectra have been shown by continuous and broken lines respectively.

indication of the presence of fluctuations in the source intensity. In other words, the source was essentially in the 'quiet' condition. The best fit spectrum consistent with the observations in 19-160 keV energy range is a power law, and can be represented by

$$\frac{dN}{dE} = 6.6\ E^{-1.95 \pm .11}\ \text{photons cm}^{-2}\ \text{sec}^{-1}\ \text{keV}^{-1}$$

This best fit spectrum fitted to the observations is shown in Fig. 5.7 by continuous line. It may be noted here that the power law index α is consistent with spectral behaviour observed during the 'quiet' condition of March 29, 1972 flight, within statistical errors.

The average integrated intensity in 20-150 keV energy range is observed to be $\sim 2.6 \cdot 10^{-8}$ ergs cm^{-2} sec^{-1}. Owing to the rather poor statistics of the data obtained for a short period of observation during this flight, the data could also be fitted equally well to an exponential spectrum of a hot thin plasma with temperature given by kT = 29.4 keV corresponding to a temperature of $\approx 8 \cdot 10^{8}$°K.

5.5 RESULTS : FEBRUARY 11, 1975 OBSERVATION

5.5:1 Intensity Variations over One Minute Intervals

In Fig. 5.8 the excess counting rates for Cyg X-1, derived after subtraction of the background, normalizing for the offset angle of the telescope with respect to the

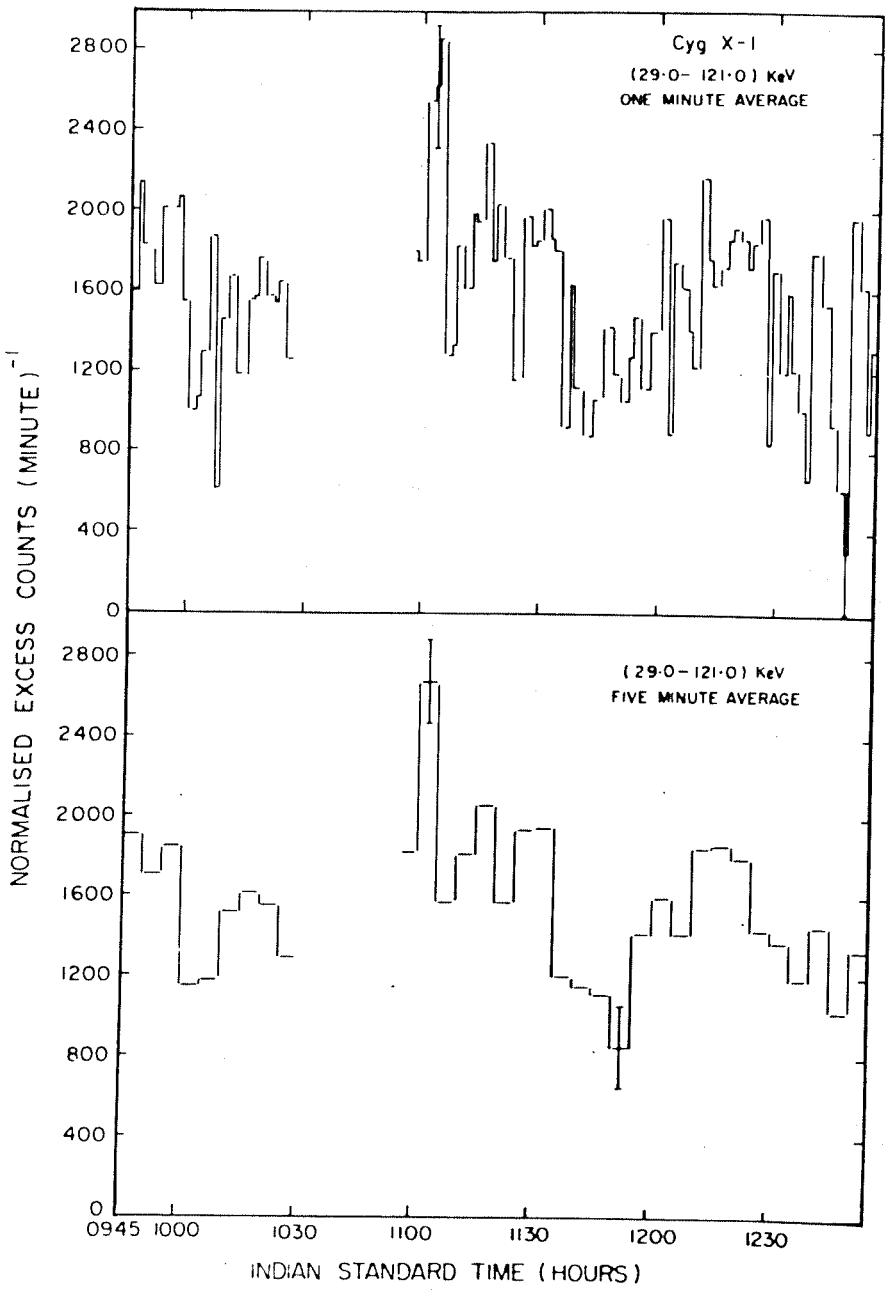

Fig. 5.8 : Time profile of the normalized excess counting rates due to Cyg X-1 for February 11, 1975 observation averaged over 1 and 5 min intervals in the 29.0-121.0 keV energy range.

source, as well as correcting for air and crystal window transmission effects, are plotted as a function of time as one and five minute averages in 29.0-121.0 keV energy range. It is clear from this figure that counting rate from the source has been fluctuating at one minute time interval during this observation of Cyg X-1. The time averaged counting rate in the 29.0-121.0 keV energy range for the entire duration of the observation is 1570 $\pm$ 30 counts/min. This average counting rate when compared with the counting rates in one minute bins shows that fluctuations in intensity at 2 to 3 σ level exist for almost the complete duration of observation. Further, at least on two occasions, around 1007 hrs IST and 1247 hrs IST, the data shows dips in intensity of the source where the deviations from the average are as high as 5 σ, which in no case can be due to statistical fluctuations. Similarly, on another occasion, around 1100 hrs IST, it shows flare like increase where again deviation from average is nearly 5 σ. It should be noted here that these variations in source intensity cannot be attributed to the background fluctuations, because the corrections applied are based on the background data immediately prior to and after the observation on the source during each observation cycle. To our knowledge, this observation provides first definitive indication of fluctuation in intensity of

Cyg X-1 at energies > 20 keV on a minute to minute basis, possibly because of better exposure efficiency on the source and lower background conditions.

For knowing the overall amount of fluctuation in source intensity from mean for the entire duration of observation period, we have analysed the normalised excess count rate data using χ^2 technique. The analysis was performed for each energy channel separately to determine the magnitude of fluctuations in source intensity at different energy intervals. For each energy channel we have computed χ^2 which is a measure of the source variability in that channel. Here χ^2 is defined as

$$\chi^2 = \sum_{i=1}^{n} \frac{(x_i - \bar{x})^2}{\sigma^2}$$

where x_i and $\bar{x}$ are counting rates in the i^{th} time interval and average of the total counting rate respectively, n is the total number of observations and σ is the statistical uncertainty associated with each observation. One striking result of this analysis was that for first three energy channels i.e. 29.0-44.5 keV, 44.5-60.5 keV and 60.5-76.0 keV, the probability that source intensity is fluctuating and intensity in each time interval is different from average intensity is more than 99%; whereas for the last three energy ranges i.e. 76.0-91.0 keV, 91.0-106.0 keV and

106.0-121.0 keV, this probability is less than 35%. This points to the fact that significant fluctuations in source intensity are present only upto $\sim$76.0 keV. This is also clear from Fig. 5.9 where we have plotted one-minute normalised excess counting rates for first three (29.0-76.0 keV) and last three (76.0-121.0 keV) energy channels separately. The time averaged counting rates for the entire duration of flight in 29-76.0 keV and 76.0-121.0 keV energy channels are 1290 ± 26 and 280 ± 16 respectively. These averages when compared with counting rates in individual one minute bins in two energy channels show that whereas fluctuations in intensity at 2 to 3 σ level exist for almost the entire duration of flight in 29.0-76.0 keV energy range, the fluctuations in source intensity in 76.0-121.0 keV energy range are almost within the statistical error for most of the observation period. We, therefore, conclude that this phenomenon has its origin in the X-ray source itself. This point is also supported by the discussion which follows.

The above data were classified into six time intervals of typically 20 - 30 minute duration. In Fig. 5.10, we have plotted intensity averages over these time intervals in all the energy bands separately. This figure shows that in first three channels i.e. upto 76.0 keV, the variations in source intensity seem to be well correlated. However, above 76.0 keV the corresponding fluctuations in

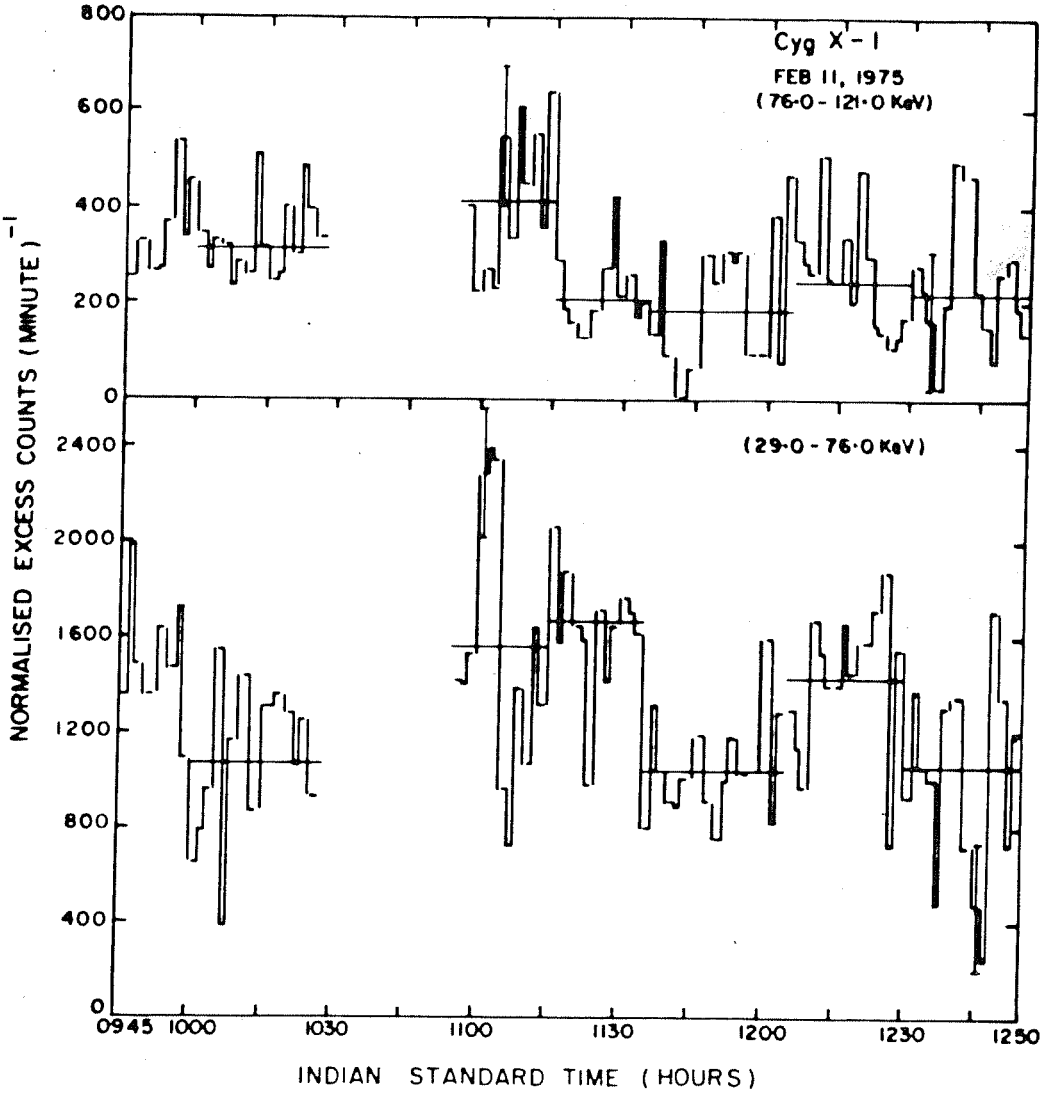

Fig. 5.9 : Time profile of normalized excess counting rates due to Cyg X-1 in 1 min bins in 29.0–76.0 keV and 76.0–121.0 keV energy intervals for February 11, 1975 observation. Also shown are counting rates for longer time intervals of ~20–25 min for the two energy channels.

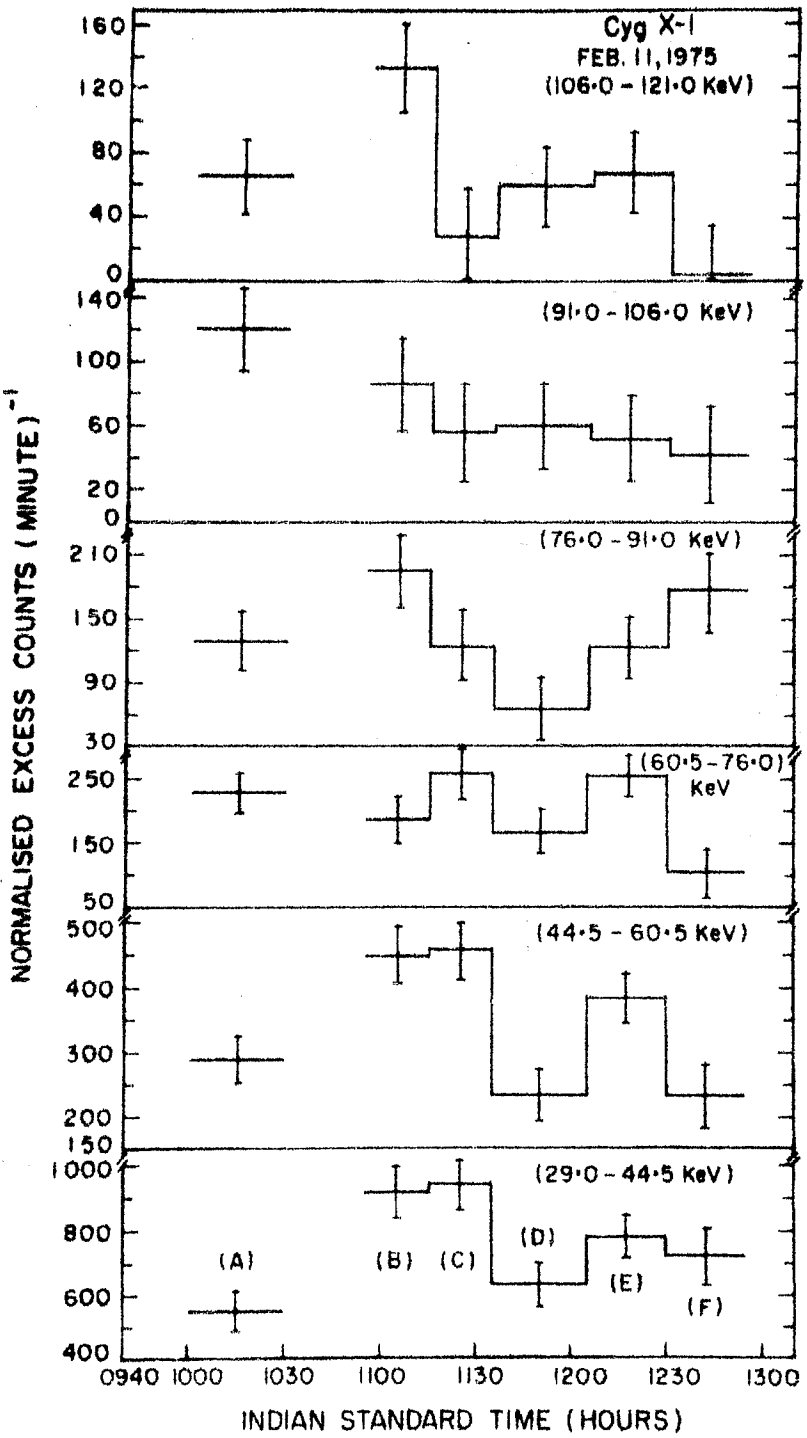

Fig. 5.10 : Normalized excess counting rates due to Cyg X-1 as a function of time, averaged over 20-25 min intervals, in six energy channels viz. 29.0-44.5, 44.5-60.5, 60.5-76.0, 76.0-91.0, 91.0-106.0 and 106.0-121.0 keV, for February 11, 1975 observation.

source intensity are less conspicuous.

This and the fact that fluctuations in the intensity of the source are present mainly upto 76.0 keV is perhaps indicative of the fact that same mechanism and region of the source is responsible for X-ray emissions upto $\sim$76.0 keV, and above $\sim$ 76.0 keV the X-ray emission originates from a different region of the source.

5.5:2 Spectral Variations over 20 - 25 Min. Intervals

For the purpose of detailed investigation of spectral variation in hard X-ray emission of Cyg X-1, we have calculated the photon spectrum of this emission for the time intervals shown in Fig. 5.10, when the source intensity was roughly constant. Fig. 5.11 shows the photon counting rate from Cyg X-1 during each of six time intervals as a function of energy, following the procedure described earlier. The best fit spectrum based on the observations during these time intervals is also shown in this figure. We have tried to fit both power law and exponential spectrum to the observed data and the results of this fitting procedure for various time intervals are as follows:

(A) In the time period (1000-1030) IST the measured flux values are best represented over the entire energy range by a single power law spectrum. The

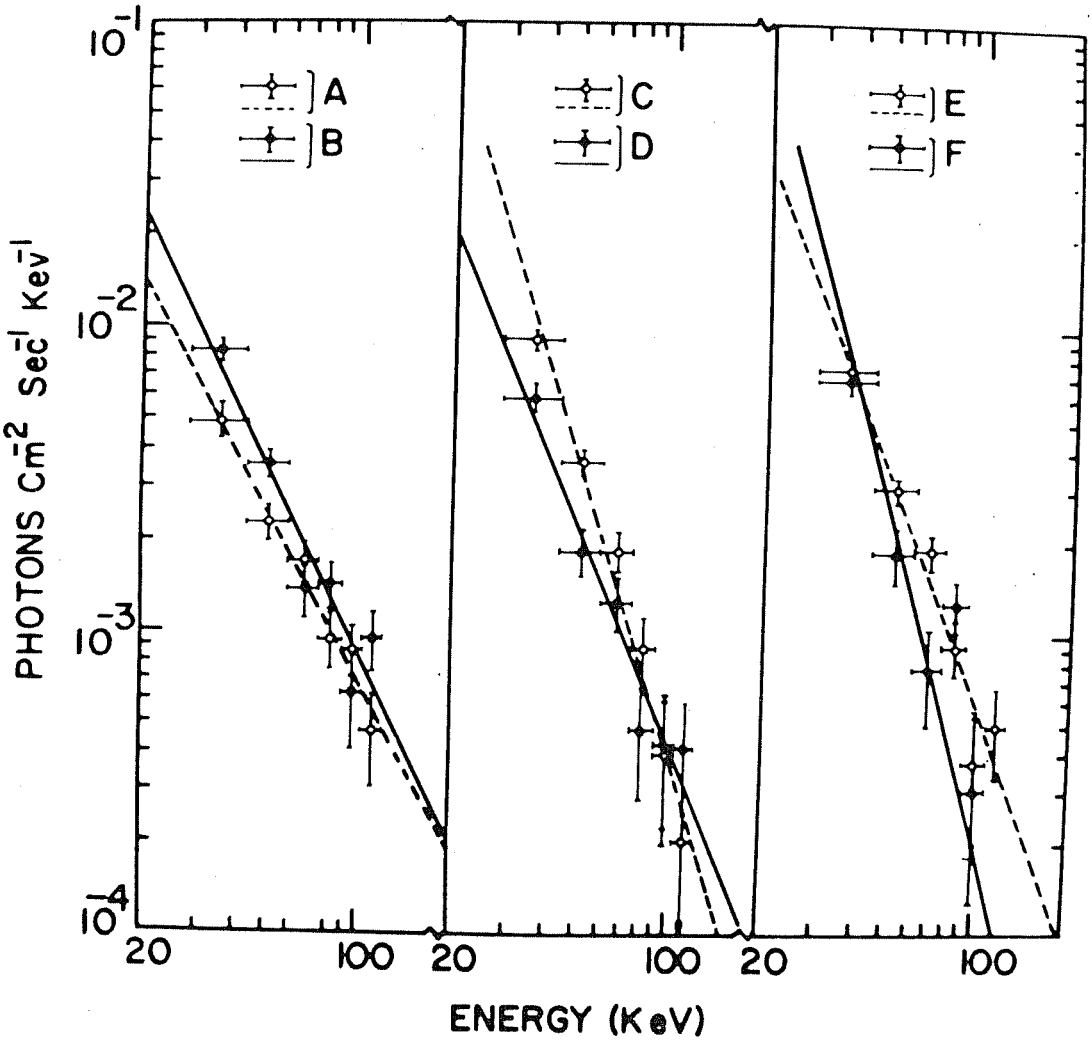

Fig. 5.11 : Photon spectra of Cyg X-1 during time intervals shown in Fig. 5.10 for February 11, 1975 observation (see text for details).

best fit spectrum for this time interval is given by

$$\frac{dN}{dE} = 4.2 \quad E^{-1.88 \pm .15} \text{ photons cm}^{-2} \text{ sec}^{-1} \text{ keV}^{-1}$$

The spectral index of 1.88 is the normal spectral index for the source in quiet condition and is consistent with the earlier two observations. The exponential spectrum provided a very poor fit to the data for any value of parameter kT in this time interval, as determined by χ^2 test.

(B) Between (1055 - 1115) IST again power law spectrum given by

$$\frac{dN}{dE} = 12.7 \quad E^{-2.09 \pm .33} \text{ photons cm}^{-2} \text{ sec}^{-1} \text{ keV}^{-1}$$

provides best fit to the observations, but the fit is not good as is obvious by the large error (0.33) in the value of spectral index. Exponential spectrum was also fitted to the data but it provided a worse fit compared to power law. In this time interval the spectral index has remained same, within statistics, as in previous time interval, but the total X-ray flux from source has increased, as is evident by the larger value (12.7) of constant K.

(C) However, during the next time interval, (1115-1135) IST, the spectrum softens considerably, spectral index α changing to 3.24. The best fit power law spectrum in this case is given by

$$\frac{dN}{dE} = 1207.1 \quad E^{-3.24 \pm .26} \text{ photons cm}^{-2} \text{ sec}^{-1} \text{ keV}^{-1}$$

However, for this time interval an exponential spectrum with $kT \approx 33$ keV fits the data equally well.

(D) During (1135 - 1205) IST period there is a tendency for spectral index to be restored to its normal value and its value becomes 2.40. The best fit power law spectrum is represented by

$$\frac{dN}{dE} = 27.3 \quad E^{-2.40 \pm .26} \text{ photons cm}^{-2} \text{ sec}^{-1} \text{ keV}^{-1}$$

This value of spectral index is different from all the previous three values of the index. In this case also exponential spectrum does not provide a good fit to the data.

(E) In the subsequent period of (1205 - 1230) IST the spectral index has remained almost same but there is an increase in the intensity of the source by a factor of two. The best fit power law spectrum

can be represented by

$$\frac{dN}{dE} = 84.3 \; E^{-2.59 \pm .28} \text{ photons cm}^{-2} \text{ sec}^{-1} \text{ keV}^{-1}$$

Here again exponential spectrum provides very poor fit to the data.

(F) In the last part of the observation, (1230 - 1255) IST, the spectrum again softens considerably, spectral index changing to 3.79 $\pm$ .95. The best fit power law spectrum is given by

$$\frac{dN}{dE} = 6942 \; E^{-3.79 \pm 0.95} \text{ photons cm}^{-2} \text{ sec}^{-1} \text{ keV}^{-1}$$

However, the power law provides a very poor fit to the flux distribution as is evident by the large error ($\sim$ 1.00) in spectral index. Exponential also gives an equally bad fit to the data. It is interesting to note that during this part of observation of Cyg X-1, flux in the highest energy channel i.e. 106.0-121.0 keV, has decreased below detectable level and this point has not been plotted in the Fig. 5.11.

It is clear from the observations that the source Cyg X-1 has shown considerable spectral changes in its

emission at energies $>$ 29 keV over 20 - 25 minute time intervals during this flight. This provides, for what is probably for the first time at high energies, an evidence for the existence of spectral variations over short period durations. Spectral variations could be investigated in finer detail in this observation of Cyg X-1, than had been possible before, probably because of better exposure efficiency on the source and lower background conditions in this flight.

5.5:3 Average Time Integrated Spectrum

The time averaged spectrum for Cyg X-1 for the entire duration of observation is shown in Fig. 5.12 and can be fitted best to a power law spectral function of the type:

$$\frac{dN}{dE} = 32.5 \quad E^{-2.37 \pm 0.08} \text{ photons cm}^{-2} \text{ sec}^{-1} \text{ keV}^{-1}$$

This power law spectrum provides a very good fit to data in this case. The exponential spectrum was also fitted to the observed flux distribution in this case but it did not fit to the data at all.

This time averaged spectral distribution is different from the normally observed spectrum for this source ($\alpha \sim 1.9$). The average integrated intensity of Cyg X-1 in the energy range 20-150 keV during this flight is $\sim 2.43 \cdot 10^{-8}$ ergs cm^{-2} sec^{-1}.

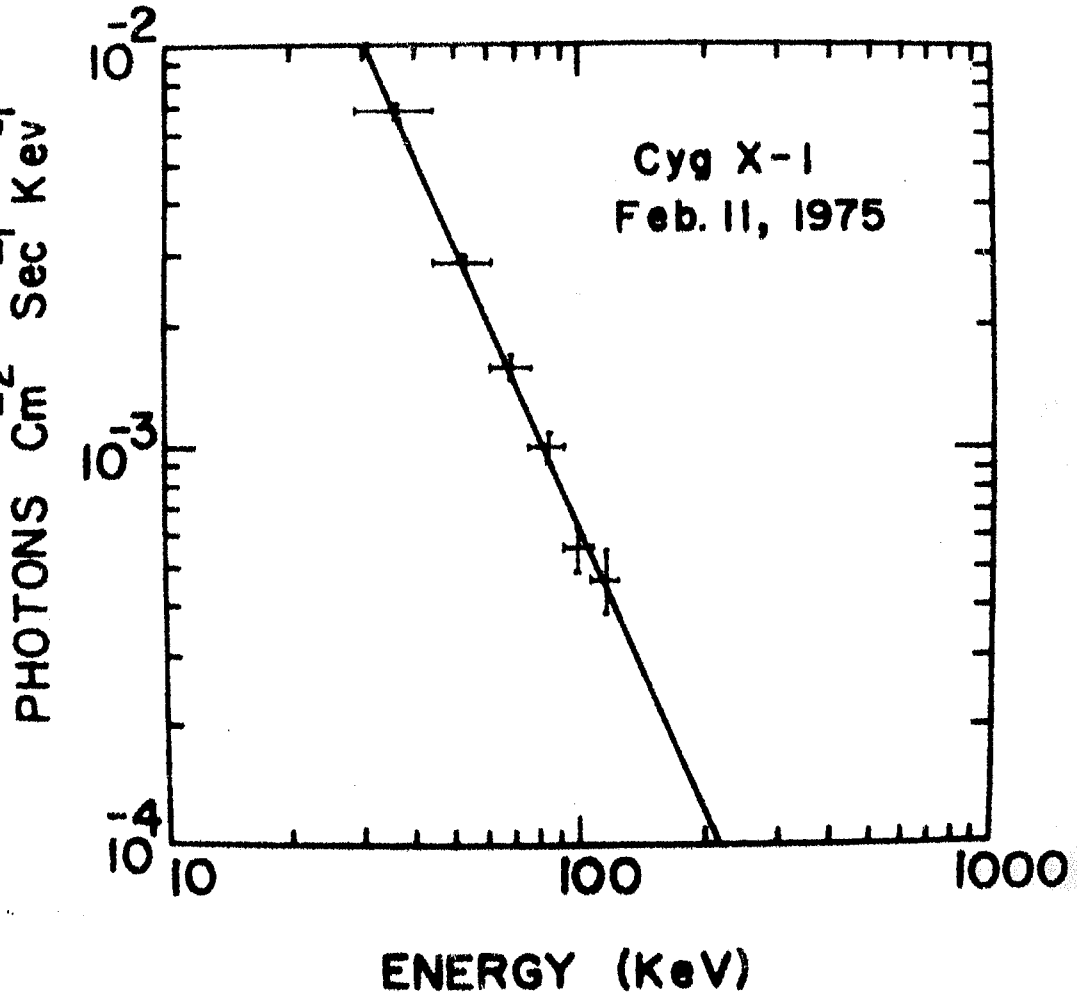

Fig. 5.12 : Time averaged spectrum of Cyg X-1 for entire duration of February 11, 1975 observation.

CHAPTER VI

X-RAY EMISSION CHARACTERISTICS AND MODELS FOR CYG X-1 : DISCUSSION AND CONCLUSIONS

In this chapter we discuss the implications of the results presented earlier in relation to the X-ray emission characteristics and models of Cyg X-1. Our results will be first discussed and compared with other observations at different energies in an attempt to understand the short and long term X-ray emission characteristics of the source. Subsequently, various models for Cyg X-1, which have been proposed to explain its X-ray emission, will be described and examined in the light of totality of observations made on this source.

6.1 INTENSITY AND ENERGY SPECTRUM OF CYG X-1

Fig. 6.1 shows the representative observations of Cyg X-1 made over a wide energy range with good accuracy, reported till 1971, as compiled by Agrawal et al. (1972b). The observations plotted in this figure are for normal state of Cyg X-1 at energies > 20 keV when the source did not exhibit any unusual behaviour in its emission. Most of the observations shown in the figure can be represented

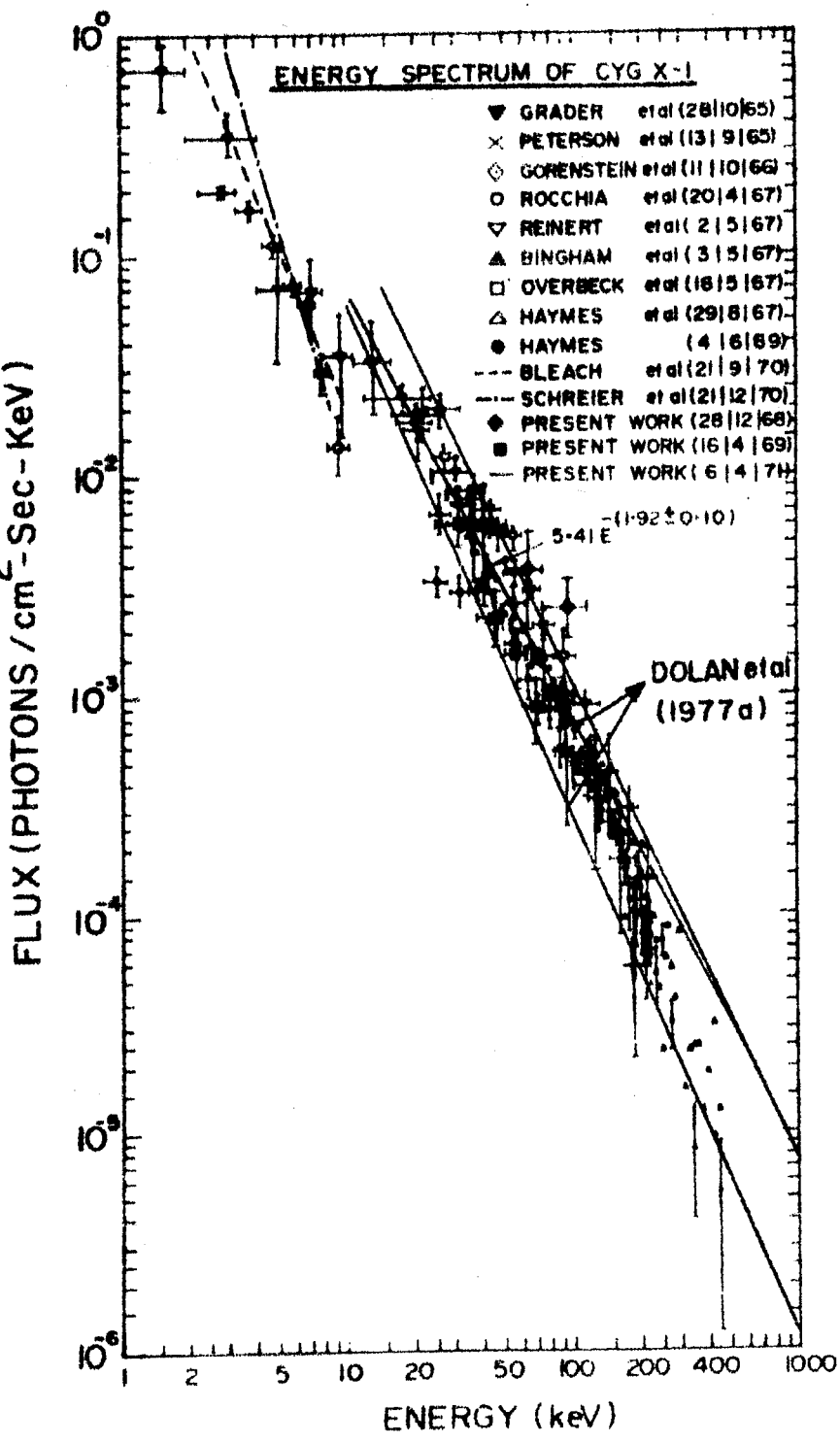

Fig. 6.1 : Representative observations of energy spectrum of Cyg X-1 as compiled by Agrawal et al.(1972b). Also plotted are typical best fit spectra at energies > 20 keV reported by Dolan et al.(1977a) during periods when source was in low and high states respectively, as defined at low energies (< 10 keV).

by a power law spectrum with spectral index α lying between 1.8 and 2.0. Our measured values of α = 1.90 and 1.95 for quiet state in March 29, 1972 and January 18, 1973 flights respectively, are in good agreement with these and confirm that the average spectrum of the source in the quiet state is best represented by $\sim E^{-1.9}$ to $E^{-2.0}$. However, it should be noted that some observers (e.g. Bingham and Clark 1969; Reinert 1969; Riegler 1969 and Haymes et al. 1968) have found that an exponential spectrum also gives an adequately good fit to their measurements. Haymes et al. (1968) found that a single exponential spectrum with kT $\sim$ 94 keV fits their data over the entire energy range of 35-453 keV, while Reinert (1969) fitted a value of kT $\sim$ 78 keV for his data in the 20-200 keV range. Although our observation of January 18, 1973 could also be fitted to an exponential spectrum with kT $\sim$ 29 keV, the poor statistics of the data does not add weight to the above conclusion.

Fig. 6.1 also shows a large scatter between various intensity measurements at different energies. As pointed out in Section 1.7:2, Dolan et al. (1977a) have reported observation of an anticorrelated transition at energies above 20 keV, coincident with low energy transition from low to high state in November 1975. The ratio of intensity of these two states at high energies is $\sim$2 to 3. They have given typical best fit spectra taken

during periods of high and low intensity, which are plotted in Fig. 6.1. This figure clearly shows that almost all the observations above 20 keV reported till 1971, as shown in Fig. 6.1, are contained between these two spectral states of Cyg X-1 and the two best fit spectral representations provide lower and upper bounds to intensity measurements at high energies made upto 1971.

To further investigate the intensity and energy spectrum of the source at energies $>$ 20 keV, we have plotted in Fig. 6.2 some of the recently reported observations. The figure shows the observations of Matteson et al. (1976) on July 17, 1969 and September 9, 1970 when an anomalously low intensity was observed from Cyg X-1 in 20-200 keV energy range, the three reported observations of anticorrelated transition of Cyg X-1 at high energies by Coe et al. (1976), Sommer et al. (1976), and Dolan et al. (1977a) and two observation points of Baker et al. (1973) in MeV energy range. The observations of Dolan et al. (1977a) have been plotted as typical best fit straight lines in two states derived by them, as in Fig. 6.1, and of Sommer et al. (1976) in low energy high state and of Coe. et al. (1976) in both low and high states have been shown as flux points at different energies as derived by them. Also shown, as flux points, in the figure are our observations of normal spectrum on March 29, 1972 and

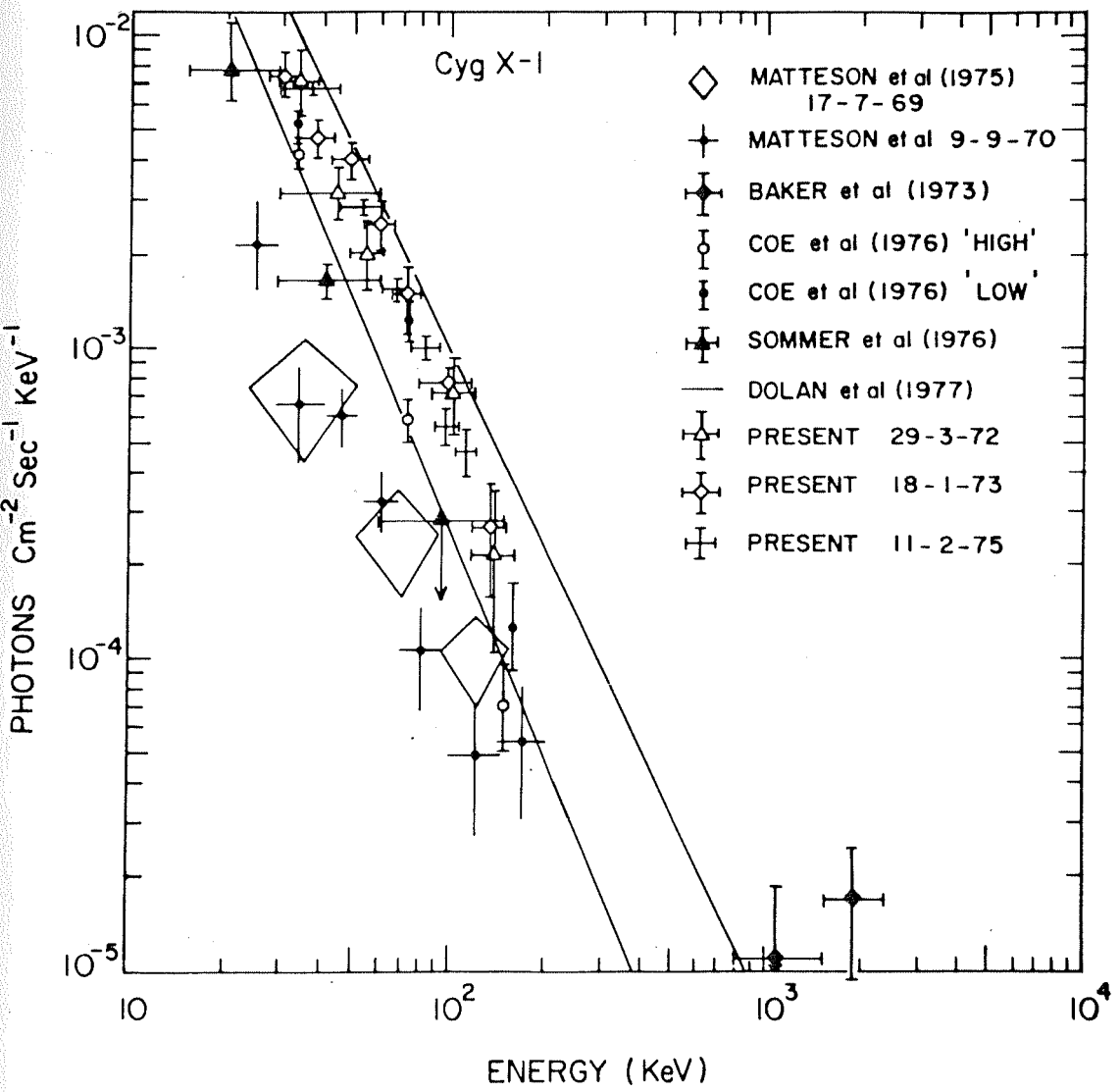

Fig. 6.2 : Some of the recently reported observations of energy spectrum of Cyg X-1 at energies > 20 keV, reported after those plotted in Fig. ϕ.1 (see text for details).

January 18, 1973 and of total time averaged spectrum of February 11, 1975. It is seen from this figure that the high energy observations of Coe et al. (1976) and Sommer et al. (1976) performed during the low energy high state are in fact closer to the lower bound of the spectral representation at high energies corresponding to high state given by Dolan et al. (1977a) and are almost the lowest intensity measurements at these energies reported so far (except for the two anomalously low intensity observations by Matteson et al. 1976). The high energy observation points of Coe et al. (1976) corresponding to the low state of the source, as defined from low energy measurements, are significantly higher than the high energy observations taken during the high state of the source. However, their observations are still lower than the upper spectral representative line suggested by Dolan et al. (1977a) for low state. Our own observational points for three flights also do not lie on any of the two spectral lines of Dolan et al. (1977a) for low and high states, indicating that the variations in intensity of Cyg X-1 at these energies are more complex than can be represented by the two spectra of Dolan et al. (1977a) for these two states.

Further, Coe et al. (1976) and Dolan et al. (1977a) have fitted their data at energies > 20 keV corresponding to the low state with a power law spectrum with spectral

index α of $\sim$ 1.8 and 2.05 $\pm$ 0.03 respectively, whereas the data corresponding to the high state has α = 2.39 $\pm$ 0.04 (Dolan et al. 1977a). In other words, the spectral index at high energies does not show significant departure from the normal α (lying between 1.8 and 2.0) during the low state and it is only during the high state, the high energy spectrum shows considerable steepening. This behaviour is similar to the behaviour of the source at low energies. where α, which is normally about 1.6, increases to $\sim$ 3 to 5 for high state. Thus, the data clearly indicate that the normal behaviour of the Cyg X-1 X-ray source is characterised by the low intensity state at low energies (high intensity at energies $>$ 20 keV) with essentially a spectral index of about 1.7 $\pm$ .2 upto $\sim$150 keV.

Another feature which is conspicuous in Fig. 6.2 is the presence of an anomalously low intensity observed by Matteson et al. (1976) on two occasions, about 14 months apart. The observed intensity during these two periods is about a factor of three lower than the lowest intensity observed by Coe et al. (1976), Sommer et al. (1976) and Dolan et al. (1977a). Since there are no observations of Cyg X-1 above 20 keV between July 17, 1969 to September 9, 1970 time interval, it is not possible to confirm or deny the continued existence of an anomalously low intensity for the entire duration of 14 months. On the basis of

these observations. Matteson et al. (1976) have concluded that there is yet another stable state of Cyg X-1 X-ray emission at high energies. In our opinion, the observed anomalously low intensity at high energies of Matteson et al. (1976), if genuine, probably represents unstable configuration of the source and not a phenomena representing a quasi-stable state.

The available few observations at energies >150 keV show considerable inconsistency. Whereas the observations of Haymes et al. (1968) and Haymes and Harnden (1970) show a softening of the spectrum above 150 keV, the observation of Baker et al. (1973), taken at a different epoch, indicate a hardening of the spectrum in MeV energy range. These observations are generally consistent with the extrapolated behaviour of the source at lower energies where it exhibits extreme variability. However, the large statistical errors in the data in this energy range do not permit us to draw definite conclusions.

In summary, the salient features of the source are:

a) At low energies (<20 keV), Cyg X-1 remains in one of the two states of emission differing in intensity by a factor of ~ 4 to 5; the high state occurring for $\sim 10\%$ of the time.

b) At energies $>$20 keV, Cyg X-1 probably switches between two states of X-ray emission differing in intensity by a factor of $\sim$2 to 3 in anticorrelation with the observed behaviour at lower energies, the low intensity state at high energy corresponding to the high state at low energies.

c) The normal state of emission at energies $>$ 20 keV has a power law spectral index lying between 1.8 to 2.0 and corresponds to the low state at low energies. The spectral index seems to steepen when the high energy intensity shows a radical decrease.

d) Change or otherwise of spectral slope in MeV energy range of Cyg X-1 X-ray emission needs further experimental observations.

6.2 SHORT PERIOD TIME VARIATIONS IN CYG X-1

6.2:1 Flare Phenomena

Flare-like enhancement of flux observed in the March 29, 1972 flight is undoubtedly an unusual phenomenon observed in the emission of Cyg X-1 at hard X-ray energies. At low energies, millisecond bursts have been observed where the increase in flux is by several factors over the average intensity. Also, Canizares and Oda (1977) observed the source at low energies (2-20 keV) from SAS-3 on five occasions in 1975 and 1976 and reported that on one

occasion, in October 1976, the source exhibited an unusual degree of activity, including large number of rapid flares with time scales of 1-10 sec and intensity enhancements by a factor of $\sim$2 to 4, the like of which was not observed in the earlier SAS-3 observations. The source was in its low state of emission at the time of this observation.

Flare-like enhancements for Cyg X-1 at energies $>$20 keV, where intensity increases by a factor of $\sim$2 to 3, have been reported on three occasions (Agrawal et al. 1971, 72a; Fuligni and Frontera 1973 and Nakagawa et al. 1973). However, Matteson et al. (1976) have reported that they observed no such flare activity in five balloon observations of Cyg X-1 with total flight duration of $\sim$6 hours, which indicates that these are indeed uncommon events. Table 6.1 gives a summary of all the observational results on the previously reported flares and on the flare observed by us. The table also indicates the phase of optical binary at the time of observation. On the basis of existing data a sporadic "flare-like" activity seems to be an important, though rare, characteristic of Cyg X-1 hard X-ray emission. Examination of results presented in Table 6.1 indicates that there is no consistent picture with regard to spectral variability during flares. The observations of Frontera and Fuligni (1975a)

TABLE 6.1

SUMMARY OF FLARE OBSERVATIONS AT HIGH ENERGIES

ate & time f obser- ation	Flight duration	Detector field of view (FWHM) and Cyg X-3 contribution	Observation	Spectrum	Phase of binary at time of obser- vation	Referen- ces
1	2	3	4	5	6	7
pril 6, 971 058 UT	Source tracked for ~3 hrs with average efficiency of ~50% by employing two detectors.	18.6° Cyg X-3/Cyg X-1 contribution ~20% at the time of flare, otherwise around 30%.	In the 22.5 - 88 kev range intensity shot up by a factor of ~2.3 for 3 min. Rise and fall lasted for ~ 9 min. Indication of depression in intensity after the flare but its statistical significance is not very high. Similar increase was seen at high energies also.	No change in spectrum was observed. Flare (~3 min) and quiet non-flaring (~4 min) power spectral indices are ~1.77 + 0.25 and ~1.74 + 0.2 respectively.	0.32	Agrawal et al. (1971, 72a)
uly 1, 972 045 UT	Cyg X-1 tracked for ~1 hr 30 min with ~85% exposure efficiency.	13° Cyg X-3/Cyg X-1 contribution ~25%.	In 40 - 100 keV energy range intensity went up by a factor of ~1.8 in ~2 min. Total duration of event ~3 min.	Spectrum softened during the flare with a power law index of ~2.7 + 0.1 compared to quiet non-flaring value of ~1.84 + 0.5.	0.02	Fuligni & Frontera (1973); Frontera & Fuligni (1975a).

TABLE 6.1 (contd.)

1	2	3	4	5	6	7
			Simultaneously a lower state of flux was found in 100-200 keV range lasting for about 20 min.			
October 7, 1972 1010 UT	The source transited across detector field of view and was seen for ~3 hrs with varying exposure efficiency.	$4^{\circ} \times 20^{\circ}$ Cyg X-3 contribution not given in the paper.	Intensity in the 30 - 70 keV range increased by a factor of ~4. The flare had a rise time of ~15 min and decay time ~10 min with total duration of ~25 min.	Spectrum softened during the flare with a power law index of ~2.9 compared to quiet state value of ~1.7.	0.59	Nakagawa et al. (1973)
March 29, 1972 0510 UT	Source tracked for ~1 hr 15 min with ~90% exposure efficiency.	18.8° Cyg X-3/Cyg X-1 contribution ~30 to 40%.	The characteristics of the flare were different in 29.0 - 60.0 keV and 87.5 - 160.0 keV energy channels. In 29.0 - 60.0 keV range intensity went up by a factor of ~2 and flare lasted ~ 12 min, whereas in 87.5 - 160.0 keV range intensity	The spectrum was found to harden during the flare with a power law index of ~1.00 compared to quiet state value of ~1.9.	0.27	Present

TABLE - 6.1 (contd.)

1	2	3	4	5	6	7
			went up by a factor of ~5 but flare lasted ~6 min only. Basically a hard X-ray flare. Also the peak rise in intensity in 29.0 - 60.0 keV was 6 min later than in ~ 87.5 - 160.0 keV range.			

and Nakagawa et al. (1973) indicate that the spectrum softens during the flare whereas that of Agrawal et al. (1971, 72a) leads to the conclusion that there is no change in the spectrum. Our observation, on the other hand, indicates that spectral hardening occurs during the flare. Similar discrepancies in the behaviour of spectral index have been noted by Canizares and Oda (1977) at low energies also. Attempts to relate the flare occurrence with the phase of binary system indicate that flaring activity is independent of the phase. The picture with regard to the flaring phenomenon, thus, appears to be quite complex.

Table 6.1 also shows that in the 20-100 keV energy range all the earlier flare observations exhibit an increase in intensity by a factor of $\sim$2 to 3 and that at energies $>$ 100 keV the relative increase in intensity is much smaller. However, in the flare observed by us, as against a two fold increase in the 20$\sim$90 keV energy range, the increase in the 90-160 keV energy range is larger and more spectacular, being almost by a factor of 5. Further, the peak rise in intensity occurs over a much shorter time interval of $\sim$ 1 minute, one minute being the minimum time resolution of our experiment. This indicates that the flare observed by us is basically a hard X-ray flare, confined mainly to energies $>$ 90 keV. This flare is thus different from the ones reported by other experimenters and is more

like a γ-ray burst of smaller size (compared to those observed by Vela satellites). It should be noted here that Vela detectors are relatively insensitive to the events having a duration of $\sim$1 minute, and that some of the high energy γ-ray bursts reported by other workers (Kane and Share 1977) have typical time scales of 1-100 sec.

As pointed out in Section 1.7:4, there is strong evidence suggesting a connection between γ-ray bursts and Cyg X-1 and that some of the reported γ-ray bursts have originated from a region containing Cyg X-1, within the observational uncertainties. Further, as pointed out by Ruderman (1975) and Strong and Klebesadel (1976), the temporal variations and spectra of some of the γ-ray bursts (e.g. April 27, 1972) closely resemble the hard X-ray emission from Cyg X-1. Considering the energetics and spectral characteristics, the flare which has been observed by us has a considerable resemblance to some of the γ-ray bursts, thus further supporting the above hypothesis.

Earlier spectral measurements of γ-ray bursts from IMP-6 and IMP-7 satellites at energies above 100 keV showed (Cline and Desai 1975) that the time-integrated spectra of all the events are similar; they can be fitted by an exponential $\left(\frac{dN}{dE} \propto \exp\left[\frac{-E_\gamma}{150\ \text{keV}}\right]\right)$ for $E_\gamma < 400$ keV

and by a power law ($\frac{dN}{dE} \propto E_\gamma^{-\alpha}$) with $\alpha \sim 2.5$ at higher energies. These spectral measurements led various authors to characterise the bursts only by their high energy emission ($E_\gamma > 200$ keV). However, recently Kane and Share (1977) have demonstrated that hard X-ray radiation (20-150 keV) represents a significant fraction ($\sim$ 20-60%) of the energy emitted during the bursts, with most of these exhibiting a power law spectrum with spectral index $\alpha \sim 1.0$ to 1.4 in this energy range (Kane and Share 1977; Wheaton et al. 1973; Metzger et al. 1974; Imhof et al. 1974). The observed spectral index of ~ 1.0 for the present flare is thus consistent with the observed characteristics of many γ -ray bursts. Also, in 20-130 keV energy range the bursts have typical time integrated energies of $\sim 10^{-5}$ ergs cm^{-2}; ranging between 8×10^{-6} to 1×10^{-4} ergs cm^{-2} (Kane and Share 1977). In the present case, the excess flux during the flare in 20-150 keV energy range being $\sim 3 \times 10^{-8}$ ergs sec^{-1} cm^{-2}, averaged over a period of 10 minutes, the total time integrated energy for the event works out to $\sim 1.8 \times 10^{-5}$ ergs cm^{-2}, which is of the same order as reported by Kane and Share (1977). The burst observed on October 7, 1972, for which source location is well known, had a duration of $\sim$104 sec, time integrated total energy in 20-130 keV range of $\sim 8 \times 10^{-5}$ ergs cm^{-2} and a power law spectral index of ~ 1.2 (Kane and Share 1977) and is

quite similar to the event observed by us.

A peculiar feature of the event reported here is the strong indication of a time delay of almost 5 minutes in the enhancement of intensity at low energy channels as compared to that in the high energy channels. We believe that the early enhancement in X-ray flux at high energy is an important feature of the source itself which must have its origin in the very mechanism of the emission, and which must be considered before evolving a realistic model for the source.

6.2:2 Short Term Fluctuations in Intensity

Besides measuring a steady-state spectrum with spectral exponent typically between 1.8 and 2.0 and flare-like enhancements, some of the balloon observations of Cyg X-1 have also revealed the existence of intensity fluctuations over intervals of a few minutes (Matteson et al. 1976; Agrawal et al. 1971; Fuligni and Frontera 1973). Our observation on February 11, 1975, however, provides first definitive indication of fluctuations in intensity on a minute to minute basis at these energies. It is not clear whether such fast fluctuations could be detected in this observation because of better exposure efficiency on the source and lower background conditions, or the source was in an unusually active state at the time of

this observation. The time averaged spectrum for this observation of the source is a power law with a spectral index of $\sim$ 2.37, which is different from the normal spectrum for the source. Of the many observations, Matteson et al. (1976) found similar large scale fluctuations in intensity over periods of $\sim$ 10 minutes on one occasion (in June 1972). None of the previous observations, however, had good enough statistics to detect fast intensity fluctuations at one minute level. At low energies, the source is known to exhibit fluctuations down to seconds and subseconds level, the fluctuation characteristics varying with time. For example, in October 1976 the characteristic time scales of fluctuations were $\sim$ 1 to 10 sec, about 2-4 times longer than that observed in October 1975 (see Canizares and Oda 1977). The time scales for short term variability at higher energies ($\sim$ minute) seem to be order of magnitude higher than at low energies (second and subsecond). Due to the poor statistics of data obtained so far, extensive observations at higher energies are required to elaborate detailed temporal chracteristics of these fluctuations. In the light of the current understanding of this source where hard X-rays originate in the inner region of accretion disk (Thorne and Price 1975; Shapiro et al. 1976 etc.), such fluctuations cannot be explained in terms of free fall (which is of the

order of 6 x 10^{-4} sec) and require mechanisms such as gas drifts along the inner unstable region of the accretion disk (Novikov and Thorne 1973) to explain the long time scales.

The intensity fluctuations on minute to minute basis in February 11, 1975 observation seemto be superimposed on long duration aperiodic changes in the level of intensity (Section 5.10). As pointed out in Section 5.5:1, these variations over $\sim$ 20-30 minutes seem to be correlated for first three energy channels i.e. upto 76.0 keV, and the corresponding fluctuations in source intensity above $\sim$ 76.0 keV are less conspicuous. This can also be seen from Fig. 5.9 where the average intensities for these time intervals for the first three and last three energy channels are separately plotted. In the 76.0-121.0 keV range the intensity shows an abrupt increase during 1015-1115 hours IST and then reverts to almost a constant lower level, within statistics, during the rest of the observation time. On the other hand, the intensity in the 29-76 keV energy range fluctuates between high and low intensity levels with a duration of $\sim$ 20-30 minutes for almost the entire duration of flight. This type of fluctuations in intensity over a few tens of minutes have not been reported earlier. "Absorption dips" lasting few tens of minutes have been

observed in Cyg X-1 X-ray emission at low energies by Copernicus (Mason et al. 1974), OSO-7 (Li and Clark 1974) and ANS (Parsignault et al. 1976) near orbital phase 0.0 of the binary system. A typical absorption event seen by ANS is shown in Fig. 1.6. These cause $\sim$50% reduction in the flux at a few keV with negligible effect at higher energies, and are presumably due to the absorption of soft X-rays by gas streaming onto the X-ray source. The cause of changes in intensity over the time scales reported here is not apparent.

If the low flux values seen on two occasions in this observation for $\sim$20 to 30 minutes is a common feature caused by attenuation due to Compton scattering, then the derived minimum column density along the line of sight should cause dramatic changes at low energies when high and low energy X-ray emission have a common origin. Such a phenomenon has not been reported so far. Further, the phase of the binary system at the time of our observation being 0.6, it is unlikely that the decrease in intensity is caused due to the attenuation in the intervening stream of matter. Possibly, the decreases in intensity reported here have their origin in changes in the source emission spectral characteristics itself.

6.2:3 Short Period Variations in Spectrum

The photon spectra calculated for the above mentioned periods of low and high intensity in source emission show a complex variability. Even though a power law spectrum can be fitted to most of the observations, the value of spectral index α shows large fluctuations, varying between $\sim$ 1.90 to 3.80. For the intensity during the time interval of 1115-1135 hours IST, however, an exponential spectrum with kT$\sim$33 keV also provides equally good alternate fit to the observations instead of a power law with α = 3.24. The presence of fast intensity fluctuations and complex spectral variability in X-ray emission of the source indicates that the accretion disk around the compact object was in a highly turbulent and disturbed state at the time of this observation. The time averaged spectrum for this observation ($\alpha \sim 2.37$) is also different from the normally observed power law spectrum ($\alpha \sim 1.8$) at these energies. Further, at the time of this observation, the source was probably undergoing transition from one state to another (Section 6.3). It is quite probable that fast intensity fluctuations and complex spectral variability occur only during such transitions. However, we cannot confirm or deny this at present, because for two of the three other observations when source was in intermediate state of

emission (Section 6.3; Clark et al. 1968; Agrawal et al. 1972b, April 16, 1969) no intensity and spectral fluctuations have been reported, probably because of poor statistics of data obtained, and for third occasion (April 6, 1971) Agrawal et al. (1972b) have reported some evidence for intensity fluctuations and indication of spectral variability. On the other hand, in the observation of Matteson et al. (1976) in June 1972 when intensity and spectral fluctuations were reported, no time averaged spectrum for the entire duration of observation has been given and, hence, we cannot evaluate the average intensity of the source at 30 keV for this observation. Thus we cannot ascertain the state of emission of the source (as defined in Section 6.3) from Fig. 6.6.

An interesting aspect of the complex spectral time variability of the source emission reported here is the existence of an apparent correlation between K and α for a spectrum of the form

$$\frac{dN(E)}{dE} = KE^{-\alpha} \qquad (6.1)$$

This is shown in Fig. 6.3 where we have plotted log K vs power law spectral index α for different time intervals and also for the total time averaged spectrum. In spite of the large error bars, the figure does indicate the presence of

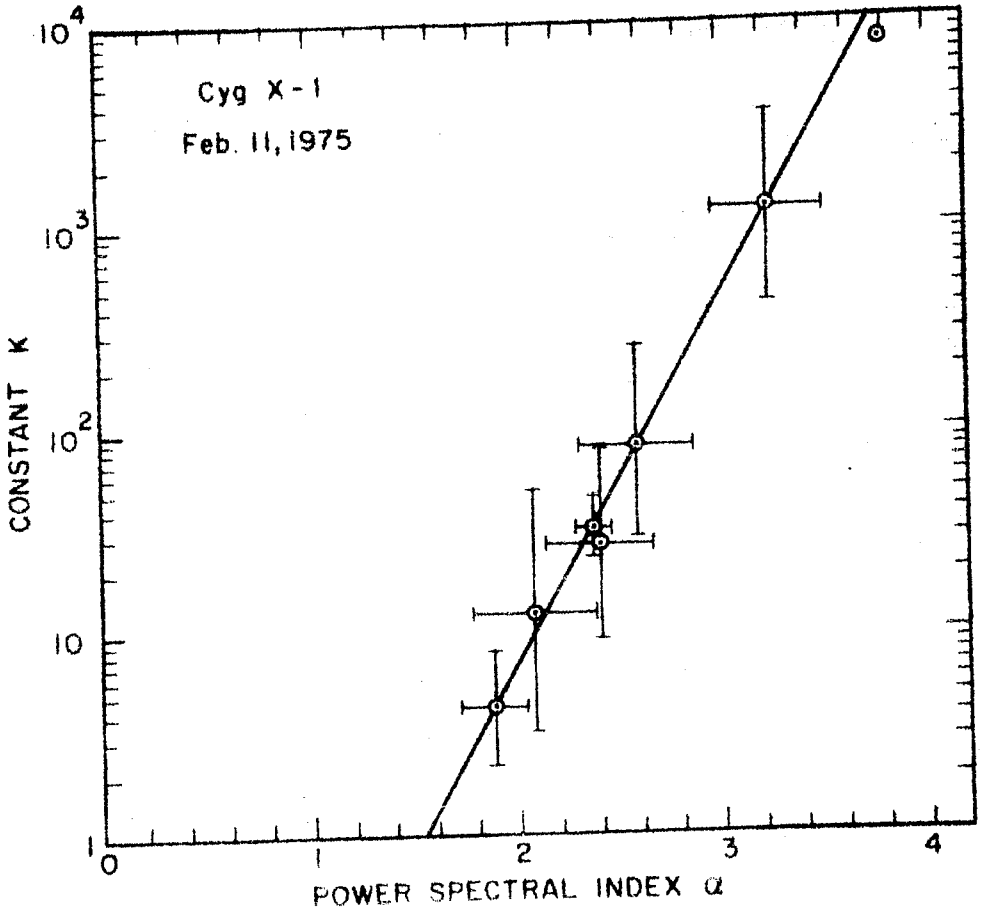

Fig. 6.3 : Constant K vs power spectral index α for best fit power law spectra for time intervals shown in Fig. 5.10 and also for total time averaged spectrum for February 11, 1975 observation of Cyg X-1, plotted on log-linear scale.

a linear relation between log K and α. This type of behaviour is expected for spectra displaying anticorrelated variability about a pivotal energy E_p. Comparing the typical spectra for the above case, represented by the equation

$$\frac{dN(E)}{dE} = K' \left(\frac{E}{E_p}\right)^{-\alpha} \qquad (6.2)$$

where K' is a constant, with equation 6.1 it is clear that

$$\log K = \log K' + \alpha \log E_p \qquad (6.3)$$

In other words a plot of spectral observations on a (α, log k) plane should indicate the presence of a linear correlation between α and log K about a pivotal energy E_p, provided the source exhibits anticorrelated spectral variability. The slope of the best fit line to the points in the figure is $\sim$1.82 implying $E_p \sim 66$ keV. This indicates that flux enhancements at energies less than $\sim$66 keV tend to be accompanied by a decline at higher energies and vice versa. This conclusion about source emission is also supported by Fig. 6.4 where we have plotted power law best fit spectra for three time intervals (A, C and D; see Fig. 5.11) and for total time averaged spectrum (Fig. 5.12), for which the points in (α, log K) plot in Fig. 6.3 are lying exactly on

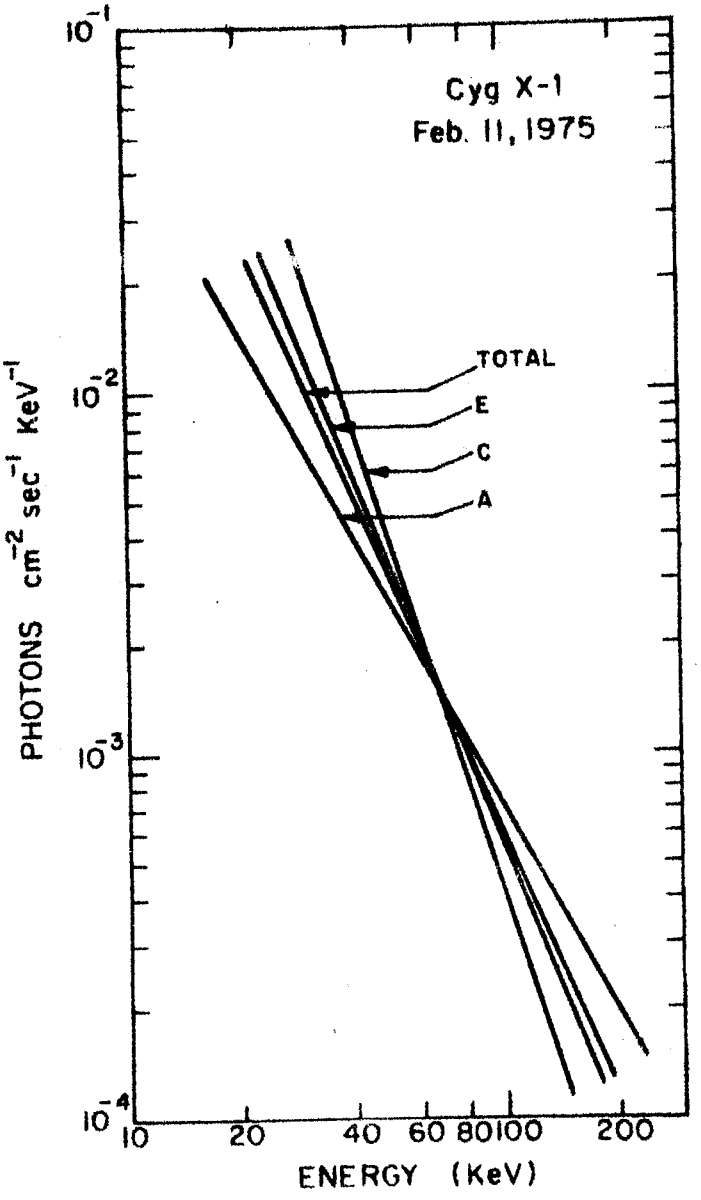

Fig. 6.4 : Power law best fit spectra for three time intervals (A, C, and D; Section 5.5:2) and for total duration of February 11, 1975 observation of Cyg X-1 showing anticorrelated spectral variability around 70 keV. (see text for details).

the best fit line. This figure also indicates that source exhibits anticorrelated spectral variability around $\sim$70 keV for the complex spectral variations observed over a period of $\sim$ 20 to 30 minutes.

6.3 LONG TERM VARIATIONS OF FLUX FROM CYG X-1 : SEARCH FOR SYSTEMATIC VARIABILITIES

In order to study the long term ($\sim$days, months and years) characteristics of Cyg X-1 X-ray emission at high energies we have made a critical study of all the available observations of Cyg X-1 at energies $\geq$ 20 keV, most of which have been made from balloon-borne experiments with observation times of the order of $\sim$ 1 hour. Relevant information concerning these observations, like date of observation, energy range of measurement and the reported spectral characteristics etc., is listed in Table 6.2. The normalised flux at 30 keV is also given in the same table. The flux values and spectral indices are for normal and time averaged state of Cyg X-1. The values of flux where not directly available, have been obtained from the best fit spectra reported by the investigators. The flux values at 30 keV and power law spectral index α have been plotted as a function of date of observation in Fig. 6.5, which includes all reported measurements at energies $\geq$ 20 keV made between 1971-78. The figure indicates that, in addition to the

TABLE 6.2

SUMMARY OF OBSERVATIONS OF CYG X-1 AT ENERGIES >20 keV

Date of observation	Experimenter	Phase of binary (±0.03)	Energy range (keV)	FWHM	Energy spectrum Power law K	Energy spectrum Power law ∝	Flux at 30keV Photons $cm^{-2} sec^{-1} keV^{-1}$	Symbol used in Fig.6.6
1	2	3	4	5	6	7	8	9
April 2, 1965 0300-0600 UT	McCracken (1966)	.453	20-58	19°	-	1.7	$(7.5\pm1.0)\times10^{-3}$	
April 13, 1965 0850-0943 UT	Brini et al. (1965)	.45	20-200	32°	-	2.0	5.0×10^{-3}	a
Oct. 28, 1965 1805 UT	Grader et al. (1966)	.87	1-40 Rocket obs.	$60^{\circ}\times14^{\circ}$	-	(1.5±.2)	$(7.4\pm2.8)\times10^{-3}$	b
Jan. 13, 1966 1858 UT	Boldt et al. (1966)	.624	20-100	20°	-	-	$(7.2\pm2.0)\times10^{-3}$	
April 5, 1966 0810-0850 UT	Bleeker et al. (1967)	.184	20-130	18°	16 Also exp. $\bar{k}T$=35keV	(2.2±.8)	$(9\pm1.8)\times10^{-3}$	
April 27, 1966 1230 UT	Riegler (1969)	.143	20-60	27.6°	7.47 Also exp. $\bar{K}$=0.53 $KT=34.2^{+12.4}_{-7.2}$keV	(20±.3)	$(8.2\pm1.8)\times10^{-3}$	
July 19, 1966 0810 UT.	Clark et al. (1968)	.93	20-100	12°	- Also exp. $\bar{k}T=60\pm20$keV	(1.6±.2)	$(5.9\pm1.0)\times10^{-3}$	

TABLE 6.2 (contd.)

1	2	3	4	5	6	7	8	9
ept.14, 1966 0331-0427 UT	Peterson et al. (1968)	.08	20-200	8.4^{o}	3.58	$(1.93\pm.2)$	$(4.8\pm.8)\times10^{-3}$	
ept.19, 1966	Overbeck et al. (1967)	.143	23-97	8.4^{o}	4	2	$(5.1\pm0.8)\times10^{-3}$	
eb.13, 1967 2124 UT	Lewin et al. (1968)	.344	20-100	7.1^{o}	-	1.6	$(7.3\pm1.8)\times10^{-3}$	
pril 20, 1967 0545-0615 UT	Rocchia et al. (1969)	.012	18-130	$30^{o}\times4.5^{o}$	3.05	$(1.83\pm.15)$	$(6.5\pm1.1)\times10^{-3}$	
pril 29, 1967 1200-1500 UT	Chodil et al. (1968a)	.674	23-80	20^{o}	-	1.5	$(1.05\pm0.2)\times10^{-2}$	
ay 3, 1967 0930-1115 UT	Bingham and Clark (1969)	.365	20-130	24^{o}	60.0 ± 4.4 Also exp. $K=0.99\pm.07$ $kT=30^{+18.0}_{-8.7}$ keV	$(2.5^{+.6}_{-.5})$	$(1.1\pm.2)\times10^{-2}$	
ay 3, 1967 1000-1220 UT	Reinert (1969)	.37	20-100	22^{o}	3.45 Also exp. $K=.46$ $kT=78\pm10$ keV	$(1.7\pm.1)$	$(1.0\pm.12)\times10^{-2}$	
			100-200		9.50	$(3.1^{+1.5}_{-0.6})$		
ay 16, 1967 1341-1421 UT	Overbeck & Tananbaum (1968a, b)	.713	23-101	8.4^{o}	-	1.7	$(9.8\pm1.5)\times10^{-3}$	

TABLE 6.2 (contd.)

1	2	3	4	5	6	7	8	9
May 25, 1967 1144-1344 UT	Overbeck & Tananbaum (1968a, b)	.311	23-101	8.4°	-	1.7	$(1.0\pm.1)\times10^{-2}$	
June 27, 1967	Overbeck & Tananbaum (1968a, b)	.187	23-101	8.4°	-	1.7	$(5.0\pm0.6)\times10^{-3}$	
Aug. 29, 1967	Haymes et al. (1968)	.565	35-123	24°	(3.42 ± 0.58)	$(1.80\pm.04)$	$(7.5\pm.6)\times10^{-3}$	
				Also exp. K=0.24±.003 kT=(94.4±0.8)keV				
			152-453		(390±340)	(2.80±.16)		
Oct. 21, 1967 0300-0500 UT	Glass (1969)	.457	20-70	19°	3.36	1.78	$(8.1\pm0.8)\times10^{-3}$	
				Also exp. K=0.3 kT=75 keV				
Jan. 15, 1968 1915-2005 UT	Metzger & Dolan (1968)	.32	20-70	12°	-	-	$(1.0\pm0.4)\times10^{-2}$	b
Oct. 25, 1968 2055 UT	McClintock et al. (1969)	.034	15-65	13°	(10.5 ± 1.2)	$(2.0\pm.3)$	$(1.17\pm.13)\times10^{-2}$	c
Dec. 22, 1968 0500-0535 UT	Agrawal (1972)	.274	30-119	18.6°	-	-	$(6.0\pm3.2)\times10^{-3}$	b
April 16, 1969 2212-2315 UT	Agrawal et al. (1972b)	.93	25-150	18.6°	3.54	$(1.89\pm.22)$	$(5.9\pm0.9)\times10^{-3}$	
				Also exp. K=0.46 kT=(32.9±6.3)keV				

TABLE 6.2 (contd.)

1	2	3	4	5	6	7	8	9
ay 11, 1969 500 UT	Webber & Reinert (1970)	.296	25-150	5.5^{o}x20^{o}	-	2	$(4.0\pm1.1)\times10^{-3}$	
une 5, 1969	Haymes & Harnden (1970)	.77	34-124 154-449	12^{o}	(4.57 ± 0.61) (1403 ± 1371)	$(1.91\pm.03)$ (3.1 ± 0.2)	$(6.6\pm.8)\times10^{-3}$	
une 10, 1969 900-1000 UT	Matteson et al. (1976)	.656	17-203	5.9^{o}	-	$(1.88\pm.07)$	$(6.5\pm.7)\times10^{-3}$	
uly 17, 1969 400-1000 UT	Matteson et al. (1976)	.244	24-159	5.9^{o}	-	$(1.6\pm.5)$	$(1.0\pm.4)\times10^{-3}$	
ept.9, 1970 445-0545 UT	Matteson et al. (1976)	.037	20-200	5.9^{o}	-	$(2.31\pm.23)$	$(1.2\pm0.4)\times10^{-3}$	
pril 6, 1971 346-0315 UT	Agrawal et al. (1972b)	.323	22-154	18.6^{o}	5.41 Also exp. K=0.41 kT=(49.8 ± 4.6)keV	$(1.92\pm.1)$	$(8\pm.5)\times10^{-3}$	
)ec. 17-24, 1971	Baity et al. (1973)	-	7-32 32-250	6.5^{o}	0.23 3.1×10^{-3}	$(1.04\pm.17)$ $(2.28\pm.36)$	$(7\pm.2)\times10^{-3}$	d
lar. 29, 1972)500-0600 UT	Present	.271	29-160	18.9^{o}	3.6	$(1.90\pm.1)$	$(5.9\pm1.2)\times10^{-3}$	
une 11, 1972)930-1000 UT	Matteson et al. (1976)	.517	20-200	5.9^{o}	-	2.1	No spectrum given, Therefore, flux at 30 keV can not be obtained.	

TABLE 6.2 (contd.)

1	2	3	4	5	6	7	8	9
une 20, 1972 300 UT	Brisken (1973)	.111	15-80		.169±.01	$(1.15^{+.18}_{-.16})$	$(3.6\pm0.8)\times10^{-3}$	
une 23, 1972 516-0616 UT 318-0918 UT	Matteson et al. (1976)	.64	20-200	5.9°		Varying between (1.2 to 2.5)	Spectrum variable and no time averaged spectrum has been given.	
une 19.5- uly 5.4, 1972	Ulmer (1975)	-	7-38 38-320	6.5°	0.26	(1.1±.3) (2.6±.7)	Reported flux values averaged over ~10 days.	
uly 1, 1972 035-0200 UT	Fuligni & Frontera (1973) Frontera & Fuligni (1975a)	.022	20-200	13°	4.4±1.0	(1.8±.05)	$(7.4\pm0.4)\times10^{-3}$	
ct. 7, 1972	Nakagawa et al. (1973)	.588	20-100	-	-	1.7	Spectrum not given	
an. 18, 1973 630 UT	Present	.951	20-160	13.5°	6.6 Also exp. kT=29.4keV	(1.95±.1)	$(7.8\pm1.4)\times10^{-3}$	
eb. 2.5-5.7, 973	Ulmer (1975)	-	7-22 22-300	6.5°	0.34 10	(1.0±.2) (2.0±.2)	Reported flux values averaged over ~4 days.	

TABLE 6.2(contd.)

1	2	3	4	5	6	7	8	9
11, 1975 5-0715 UT	Present	.564	29-121	13.5°	32.5	$(2.37\pm.08)$	$(1.0\pm.04)\times10^{-2}$	
4-10, 5	Coe et al. (1976)	-	26-1200	3°	-	-	$(5.0\pm.6)\times10^{-3}$	d
11-15, 5	Coe et al. (1976)	-	26-1200	3°	3.3	1.81	$(5.8\pm.8)\times10^{-3}$	d
4, 1975 5-2330 UT	Sommer et al. (1976)	.185	25-150	$4^{\circ}\times22^{\circ}$	-	-	$(4.0\pm1.4)\times10^{-3}$	
17, 1975	Dolan et al. (1977a)	.35-.45	20-3000	5°	-	(2.4 ± 0.4)	$(5\pm1.1)\times10^{-3}$	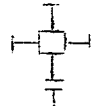
10, 1976	Dolan et al. (1977a)	.45-.55	20-3000	5°	-	(2.1 ± 0.1)	$(1.18\pm.14)\times10^{-2}$	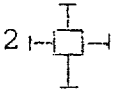

a-- Observation not used in Fig.6.6 as no error bar has been given.

b-- Observation not used in Fig.6.6 as statistical significance of data is less than 3σ.

c-- Observation not used in Fig.6.6 as Cyg X-1 was observed for only 5 min.

d-- Observation not used in Fig.6.6 as reported flux values have been averaged over $\sim$6 days.

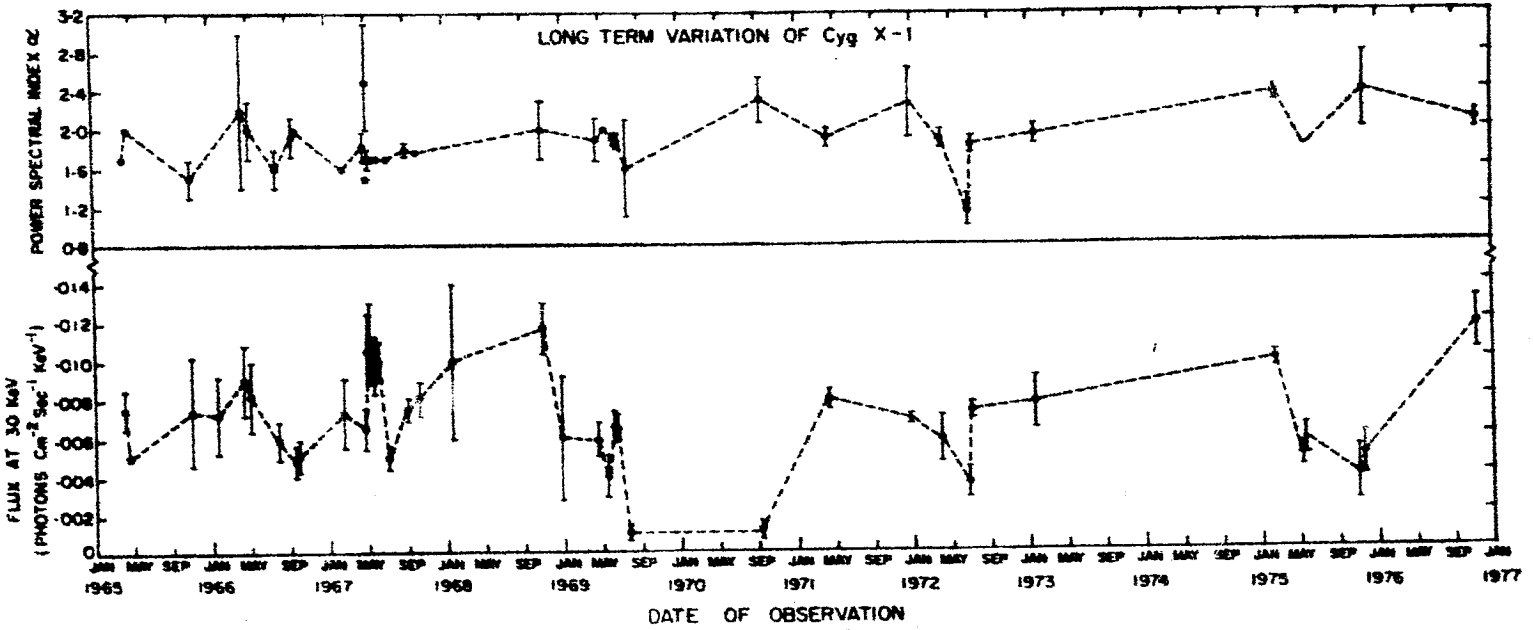

Fig. 6.5 : Photon flux of Cyg X-1 at 30 keV and best fit power spectral indexα measured by various experimenters plotted as a function of the date of observation. (see text and Table 6.2 for references and other details of various observations).

short period fluctuations in intensity described earlier, the X-ray flux even during normal 'quiet' condition shows significant variations from epoch to epoch, intensity varying by a factor of two or more. Likewise, the power spectral index α also shows variations, α varying between 1 to 2.4, the most probable value being $\sim 1.9 \pm 0.1$.

To investigate systematic long term changes, if any, in the variability of Cyg X-1 intensity, we have looked for the existence or otherwise of variations in intensity at 30 keV with phase of the Cyg X-1 binary system. The phase of the binary for various observations is given in Table 6.2. To avoid any bias in the selection of data we have included almost all the observations given in Table 6.2 for this analysis for which intensity at 30 keV and phase of the binary at the time of observation is available, neglecting only those with very poor statistics (less than 3σ confidence level).

Fig. 6.6 shows intensity of Cyg X-1 at 30 keV for these observations as a function of phase of the binary system at the time of observations (phase $0.0 \sim$ phase of closest approach of optical star to us). Different symbols shown in the figure refer to the source (s) from which most of the information concerning the observation has been derived. The horizontal bars for the two observations of

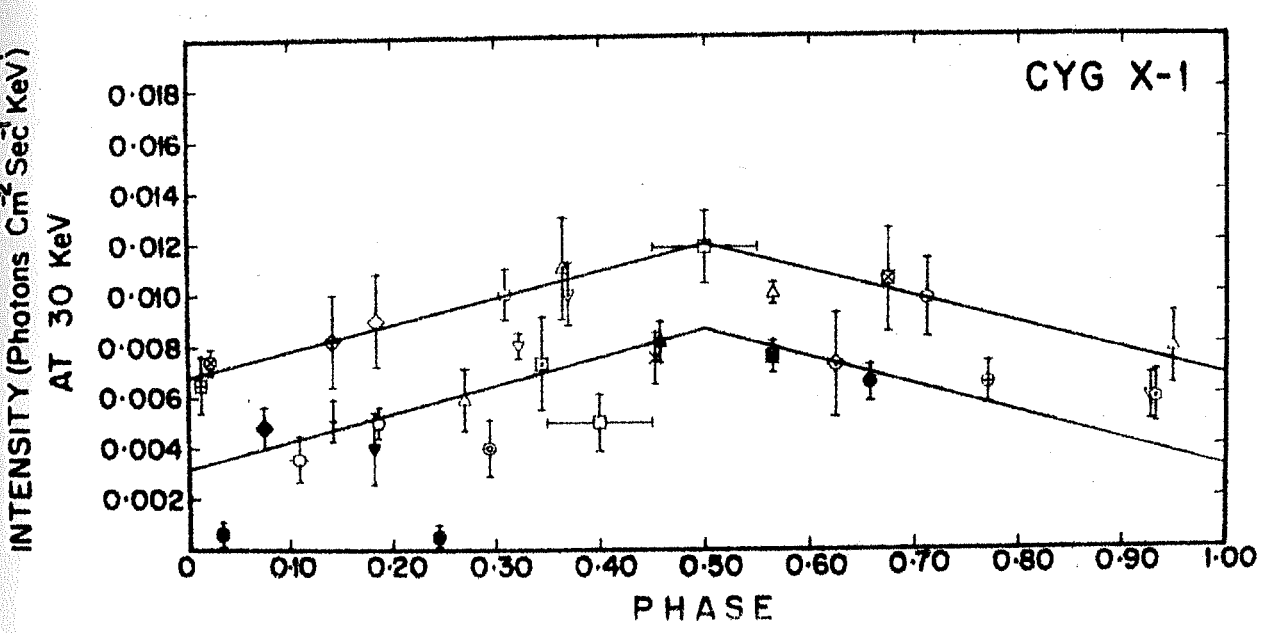

Fig. 6.6 : X-ray intensity at 30 keV plotted as a function of the phase of Cyg X-1 binary system for all the observations made on the source. For an explanation of different symbols used, see text and Table 6.2.

Dolan et al. (1977a) show the longer time period ($\sim$ 1 day) over which their two observations were averaged. The figure clearly shows a definite correlation between intensity at 30 keV and phase of the binary, exhibiting a linear variation of intensity with phase, intensity being maximum at phase 0.5. However, we find that a single line fit to all the data provides a very poor fit to all the data points, χ^2 for such a fit being $\sim$ 5 per degree of freedom. Upon careful examination of data, however, we find a striking feature, that most of the data points tend to cluster around two straight lines running parallel to each other. We have separated the observation points into two sets and have then fitted best fit lines to these two sets of points. These best fit lines are shown in the figure. Only two observational points of Matteson et al. (1976), when the source showed an anomalously low intensity, lie significantly below the best fit lines. The observations of Webber and Reinert (1970) and of Dolan et al. (1977a) for 'high state' of low energy, lie just above one standard deviation away from lower best fit line; the rest being well within one standard deviation of the two best fit lines. The correlation coefficient for a single line fit to all the data points is $\sim$ 0.43 whereas two line fit gives a correlation coefficient of $\sim$ 0.93 for both the lines. Similarly,

χ^2 for a single line fit is $\sim$ 5 per degree of freedom whereas it is only $\sim$ 0.4 per degree of freedom for two line fit. This points to the fact that the source normally remains in one of the two distinct states of emission. Observations of Agrawal et al. (1972b), Clark et al. (1968) and our observation of February 11, 1975 which lie between the two lines were most probably taken when source was undergoing transition from one state to another.

Following points emerge from this analysis:

1. There is clear evidence for the presence of two distinct, high and low, states of emission for Cyg X-1 at energies $\sim$ 30 keV, the intensity in two states differing by a factor of $\sim$ 2.

2. Distinct phase variability of intensity at these energies is seen for both the states, intensity at phase 0.5 being greater by a factor of nearly $\sim$ 2 compared to that at phase 0.0.

3. Variation of intensity with phase is similar for both low and high states and it is, thus, independent of state of emission of the source. Therefore, the intrinsic source intensity is modulated by purely orbital motion. The variation of intensity

with phase for two states is given by

$I = (0.0109 \pm 0.0015)P + (0.0032 \pm 0.0006)$ low state

$I = (0.0103 \pm 0.0013)P + (0.0068 \pm 0.0005)$ high state

where I is the source intensity (photons cm^{-2} sec^{-1} keV^{-1})at 30 keV and P is the phase of the Cyg X-1 binary system.

4. The source spends almost equal time in the two states at these energies, which indicates that none of the states is a stable one.

5. From the figure we find that the source can be in any state at a given phase, which points to the fact that there is no preferential tendency for any state to occur for a given phase and that switch over from one state to other may be fast, independent of the phase of the binary system.

It should be noted here that the deductions regarding the existence of two states is not an artifact of the analytical or experimental procedures adopted by different experimenters. Nor is it due to the presence or absence of Cyg X-3 in the detector field of view for the following reasons:

a) Such an hypothesis would require Cyg X-3 to have a constant intensity at this level, which it

obviously does not have, being invisible relative to Cyg X-1 above 20 keV most of the time.

b) The intensity of Cyg X-1 should show a correlation between detector collimation and derived intensity, Cyg X-3 being only $\sim 7^{\circ}$ away from Cyg X-1. However, we find that collimation of less than 7° FWHM have seen Cyg X-1 in a state of high intensity and collimation of more than 9° FWHM have ascribed to it a state of low intensity.

c) Overbeck et al. (1967, 68a) observed Cyg X-1 on four separate times with the same equipment, experimental technique and data reduction method. Cyg X-3 was not in the field of view. We find the source to be in low state for two of their observations and in high state for the remaining two. Similarly, the source is in low state in one of our observation in March 29, 1972 and in high state in the other observation on January 18, 1973.

As mentioned earlier, the source exhibits anticorrelated spectral variability at a pivot energy around $\sim$7 keV so that flux enhancements at low energies ($E < 10$ keV) are accompanied by a reduction at high energies and vice versa (Coe et al. 1976; Sommer et al. 1976; Dolan et al. 1977a). We have, therefore, tried to investigate whether

the source behaviour presented here at energies $\sim$30 keV is present also at low energies ($E < 20$ keV), by attempting a similar analysis of low energy data. Unfortunately, most of the available satellite observations in this energy range have been reported as intensity and spectrum averaged over a day or two and therefore it is not possible to assign a unique phase to these data. We could get only six observations having good statistics for which phase and intensity at $\sim$3 keV could be obtained. This number is not statistically significant enough to enable us to draw any meaningful conclusions.

The low and high states at hard X-ray energies reported here do not seem to be same as the ones observed at low energies, because at low energies, according to current understanding, the source spends only 10% of time in high state whereas we find that at high energies it spends almost equal time in the two states. Also, there are two reported observations of low energy high state at hard X-rays shown in Fig. 6.6, by Sommer et al. (1976) and Dolan et al. (1977a), both of which lie below the low state line drawn in the figure. This indicates that the transitions reported at low energies may be the ones involving intensity changes on a bigger scale than reported here and which occur less frequently, compared to the ones we are reporting.

This will then indicate that the high energy variations of Cyg X-1 may involve an additional third state; the source being in one of the two states described above and going over to a third very low level intensity state when it transits into the high intensity state at low energies.

The power law spectral index α for both the states reported here does not show any correlation for the two states and is almost the same ($\alpha \sim 1.8$ to 2.0). This further strengthens our view that the two states reported by us for high energy X-ray emission from the source most probably correspond to sub-states of the normally observed low state reported at low energies.

The phase variability we are reporting here shows a linear dependence of intensity on phase, unlike the one reported by All Sky Monitor (ASM) on board Ariel V satellite (Holt et al. 1976a, b), where they only observed a minimum in intensity in phase with superior conjunction of the binary system. The variation of intensity with phase reported here is much more prominent compared to that reported by ASM at lower energies. The behaviour reported here is very unusual and is quite unlike the eclipsing type of pattern normally expected for a binary system and is more likely to have its origin in a phenomenon related to the orbital motion of the system.

In the light of our current understanding of the Cyg X-1 source, we suggest that the characteristic fundamental property of this source is the two state emission at high energies emanating from the inner region of the accretion disk, the two states having equal probability of occurrence. The normal state at low energies, emitted from the outer disk, is the one corresponding to the low state in intensity for about 90% of the time. On rare occasions when the low energy emission flips to high state, the high energy X-ray component shows a further decrease, which could be interpreted as the third state of emission at high energies.

6.4 MODELS FOR CYG X-1

Based on the preceding discussion, we list the following prominent features of Cyg X-1 X-ray source which should be explained by an acceptable theoretical model for this source:

1. The X-ray spectrum of the source extends upto few hundreds of keV.
2. The source exhibits large irregular fluctuations in its emission on time scales ranging from a few milliseconds to days.

3. The source, on occasions, exhibits flare like enhancements. Some of the flare events at high energies (>20 keV) show a remarkable resemblance to typical γ-ray bursts.

4. The normal state of the source is characterised by a low intensity state at low energies in which the source spends almost 90% of its time. For this state, the source spectrum can be fitted to a single power law over 1-100 keV energy range with a spectral index of $\simeq 1.7 \pm 0.2$.

5. When the source occasionally transits to high state, persisting for about weeks to months, the total luminosity at ~ 1 keV increasesby factor of ~ 5 and spectrum over 1-10 keV energy range steepens with $\alpha \sim 3$ to 5.

6. At high energies the source exhibits an anticorrelated spectral variability. The intensity above ~ 7 keV shows a drastic reduction when the low energy intensity is in the high state.

7. In addition, the present study indicates that at energies $\sim$ 30 keV the source goes on regularly switching between two states differing in intensity by a factor of ~ 2, which most probably are sub-states of the low energy low state. In

both these states the intensity at 30 keV exhibits a linear variation with the phase of Cyg X-1 binary system.

As discussed in Chapter I, the optical and X-ray observations of Cyg X-1 suggest that it is a compact object and has a mass larger than what is normally assigned to a neutron star, thus indicating it to be a black hole. Even the presence of millisecond bursts, however, cannot provide an unambiguous proof for the black hole. In order to be consistent with black hole dimensions, one would really require microsecond pulsations to be present which, with the present state of art in X-ray astronomy, is difficult to establish.

Assuming the presence of a black hole in X-ray emitting object of Cyg X-1, X-rays could be produced as the black hole accretes mass from its companion. However, theories of X-ray emission from matter accreting around black holes are still in a hazy state, mainly because of considerable uncertainties still existing regarding various parameters of local physics of accretion disks around black holes. For this reason, such models have only been able to qualitatively account for some of the features of X-ray emission and cannot explain all the features in a sufficiently quantitative manner.

Triple star systems in which an X-ray emitting neutron star orbits one (close triple) or both (distant triple) members of a massive binary system of normal stars have also been proposed as alternate models (Bahcall et al. 1974; Fabian et al. 1974). Such models, however, require the neutron star to be non-magnetic (or magnetic field over the time to have decayed to a very low value) because of the absence of regular X-ray pulsations. Alternately, the rotational axis and magnetic axis of the star will have to be aligned with each other, which is less probable. Simple stability calculations (Shipman 1975) for such systems over a time scale $\gtrsim 10^6$ years indicate that triple star system would have become unbound when the neutron-star progenitor exploded. For distant triple star model the system would have acquired a very high space velocity due to the explosion, which is incompatible with observations. A fairly comprehensive search carried out for the third low mass star by Abt et al. (1977) has yielded no positive results. Even though the triple star model cannot be ruled out, the available model is not worked out in sufficient detail and hence does not lend itself to a rigorous examination. We have, therefore, primarily concentrated on accretion disk black hole models, which have been elaborated in greater detail, for further discussions.

6.4:1 Mode of Mass Transfer and Formation of a Disk

It becomes imperative to consider the details of the geometry of accretion flow, that is, whether the mass transfer is through stellar wind or from Roche lobe overflow and whether an accretion disk around the black hole is formed or matter accretes spherically. As pointed out in Sections 1.6:2 and 1.9:1, optical and X-ray absorption data for this binary system appear to present evidence for the existence of gas streams from the primary which fill the Roche lobe and overflow through Lagrangian point L_1. However, for 15-30 $M_\odot$ supergiant the accretion rates resulting from Roche lobe overflow are so large ($\dot{M} \sim 10^{-3}$ $M_\odot$ yr^{-1}; van den Heuvel 1975; Lamers et al. 1976) that X-ray emission from the compact companion would be quickly extinguished. A BO star of 15-30 $M_\odot$, on the other hand, is most likely to lose mass at a significant rate by means of stellar wind without filling and overflowing the Roche lobe. However, a firm spectroscopic evidence for a spherical stellar wind accretion strong enough to power the observed X-ray source, $\dot{M}_w \sim 10^{-5} - 10^{-6} M_\odot$ yr^{-1} (cf Davidson and Ostriker 1973), is lacking. The mode of mass transfer in this system is probably intermediate between the two extreme cases of Roche lobe overflow and a strong stellar wind.

It is not yet established whether or not the accreted gas from the wind flows spherically onto the X-ray source or forms an accretion disk. Earlier studies of spherically symmetric laminar flow seemed to indicate that for the mass transfer rates required to give the observed luminosities of 10^{37} -10^{38} erg sec^{-1}, cooling time of the gas would be so short compared to the free-fall time that the gas would arrive essentially cold at the Schwarzschild radius. There being no solid surface to convert kinetic energy into thermal energy, very little of this would be radiated away (Shvartsman 1971; Shapiro 1973). This indicated that the gas accreting onto the black hole should form an accretion disk around the compact object and cannot accrete spherically. However, it has been shown (Meszaros 1975) that turbulent accretion (Shvartsman 1971; Illarionov and Sunayaev 1975) with magnetic reconnection provides a viscous dissipation mechanism which ensures that gravitational energy is converted into heat at all radii down to Schwarzchild radius, without needing to invoke a solid surface to stop the flow, and may thus generate the required spectrum via Comptonization at $T_e \sim 10^{9}$ °K. However, detailed calculations on the efficiency of the mechanism and spectrum of X-rays which such a mechanism can provide, are yet to be worked out.

In contrast, an accretion disk model for black hole is better understood and is able to explain, at least qualitatively, a number of observed features of the spectrum of Cyg X-1 (Eardley et al. 1975; Ichimaru 1977). The disk is formed when accreting matter has specific angular momentum with respect to the black hole. In case of Roche lobe overflow the gas can easily form an accretion disk due to the angular momentum carried by the gas with respect to the secondary (Prendergast and Taam 1974) but for a smooth stellar wind such a disk formation is difficult. However, theoretical fits to the optical light curves (Avni and Bahcall 1975; Bochkarev et al. 1975) show that for Cyg X-1 system the companion nearly fills its Roche lobe (filling factor $\gtrsim$ 95%), so that wind may strongly be enhanced by the low surface gravity of the primary below Lagrangian point L_1 and may possess significant angular momentum as it flows through a broad nozzle towards the compact star (Basko and Sunyaev 1973). Calculations of the angular momentum transported in the accreted gas from a spherical wind (Illarionov and Sunyaev 1975; Shapiro and Lightman 1976) indicate the existence of a small amount of net angular momentum about the black hole for wind accretion, which is much smaller than that resulting from Roche lobe overflow by three to four orders of magnitude, but which can still lead to the

formation of a marginal disk (Shapiro and Lightman 1976). Taking these factors into account, the existence of a small hot X-ray emitting disk in the system seems to be a likely mechanism. The result of a phase modulation of intensity at 30 keV presented in this thesis, which seems to be coupled with orbital motion of binary, introduces further complications in the nature of orbital configuration, geometry of accretion flow and the existence of a simple disk.

6.4:2 Accretion Disk Models

In these models a Keplerian motion of accreting matter from the main star is assumed which forms an orbiting disk around the black hole, its inward drift being due to the radial motion which is caused by the outward transport of the angular momentum. The outward transport of angular momentum is due to viscous stresses removing the angular momentum. The standard time averaged accretion disk models are essentially based on two sets of physical laws i) Conservation laws for radial transport of mass, energy and angular momentum in the disk and ii) 'Local' physical laws (equation of state, vertical pressure balance, viscous heating, radiative transfer). The equations used to describe conservation laws are rather reliable, but equations of 'local' physics are very shaky, especially in their description of viscosity. This lack of appropriate description of viscosity leads to various uncertainties about the

disk structure and its stability, and thus has given rise to a number of models for the structure of the accretion disk and emission mechanism of X-rays, depending on the approximations made regarding 'local' physics of the disk.

The first model of "standard" Newtonian accretion disk developed by Pringle and Rees (1972) and Shakura and Sunyaev (1973) assumed that the viscous shear stress $t_{\phi r}$ induced by magnetic turbulence is constant throughout the disk and is given by $t_{\phi r} = \alpha P$, where P is the pressure in the gas and α is a constant number believed to lie between 1 and 10^{-3}. These models can explain the observed complex short time variability of X-ray emission of the source. For example, the orbital period of a 'hot spot' around the black hole will produce fluctuations in X-ray emission at 1-10 millisecond level, the presence of many such hot spots can give rise to the complex short time fluctuations. Fluctuations on time scales from several milliseconds to a few tenths of a millisecond will also arise because of magnetohydrodynamic turbulence in the inner region of the disk.

These models, however, cannot explain the emission of hard X-rays upto a few hundred keV requiring temperatures of $\sim 10^{9^{o}}$ K. The maximum temperature which the gas can achieve in these models is $\sim 10^{8^{o}}$K, thus making them

capable of emitting only very soft X-rays at luminosities of about 10^{37} erg sec^{-1}. Further, there is no mechanism in these models which can explain the observed long term transitions from one state to another. Also, an instability (called L-E instability; Lightman and Eardley 1974) arises in the inner zone where radiation pressure dominates gas pressure ($P_R > P_G$) rendering the thin disk models secularly unstable in the inner zone.

In order to overcome these difficulties, following two major modifications have been proposed :

1. 'Modified' accretion disk model proposed by Thorne and Price (1975) and developed in detail by Shapiro et al. (1976) and Ichimaru (1977).

2. Accretion disk corona model proposed by Liang and Price (1977) and Bisnovatyi-Kogan and Blinnikov (1977).

In the modified accretion disk model first proposed by Thorne and Price (1975) purely on phenomenological grounds, hard X-ray spectrum (extending upto few hundred keV) is emitted from a hot ($\sim 10^{9}$ K), optically thin ($\tau \sim 1$) but geometrically thick inner zone which is surrounded by a cooler, optically thick outer region. Soft X-rays result from the thermal emission from the outer, optically thick,

cool region at a distance of $\sim$ 100 km from the black hole. Hard X-rays, which are emitted from the optically thin inner region where radiative cooling can balance viscous heating at temperatures of the order of $10^{9^{o}}$K, get their energy from repeated inverse Compton scattering of soft photons by high energy thermal electrons (Comptonization). When an instability in the outer region (Lightman and Eardley 1974) developes, the inner region swells, the boundary moves outwards and soft X-rays are suppressed (low state). When the L-E instability is not operative, soft X-rays from outer region are predominant (high state). It must be pointed out that the model does not bring out clearly the fact that the normal behaviour of the X-ray source corresponds to the low state at low energies, and the high state at low energies really is the excited state. Further, our finding regarding the two states of intensity level at high energies, even during normal state of the source, requires to be explained.

In accretion disk corona models it is assumed that the disk is optically thick all the way upto the innermost stable orbit. Such a disk, analogous to solar photosphere, is likely to form a corona depending upon the disk accretion parameters, somewhat similar to the solar corona at high electron ion temperatures. In this connection

Liang and Price (1977) have argued that an accretion disk pumps energy into an outer tenuous layer of its atmosphere to form a high temperature corona. Convection is the main energy transfer mechanism along Z-coordinates in the central part of the disk. Convection generates an acoustic flux which dissipates in the upper, optically thin layers of the disk and heats them. The origin of the hard X-ray radiation in such a model may again be due to Comptonization of soft X-rays, produced in the lower disk layers, in the high temperatures corona ($T_e \sim 10^{9^o}$ K). In such a model where convection plays an important role in the transfer of energy out of the disk into the corona, any decrease in the convective energy transport would make the disk hotter and cool the corona, resulting in a transition of soft X-ray component to increased level. Such a transition could be due to a change in the accretion rate. Standard model calculations for an accretion disk (Shakura and Sunyaev 1973; Pringle and Rees 1972; Novikov & Thorne 1973) show that vertical temperature gradient $\frac{dT}{dZ}$ in the disk decreases with increased mass-accretion rate. Since the strength of the convective instability depends on $\frac{dT}{dZ}$ (Spiegel 1971), an increase in accretion rate could trigger the transition from low to high state. However, the various uncertainties and simplified assumptions made,

difficulty in constructing a predictive, mathematical model of the corona, and the very qualitative nature of the model as a whole do not permit a critical evaluation of this model.

6.4:3 Modified Accretion Disk Models

The modified accretion disk model, developed by Shapiro et al. (1976) and Ichimaru (1977), is essentially based on the phenomenological model proposed by Thorne and Price (1975). Shapiro et al. (1976) have shown that the cool disk model is not unique and a second 'hot disk' solution for the equations of disk structure exists, subject to the same boundary conditions. Their solution gives a hot, two temperature, gas-pressure dominated disk with electron temperature close to 10^{9}°K (which is nearly independent of the radius) and a much higher ion temperature, because the electrons lose energy in X-ray emission through Comptonization and ion-electron coupling time scale (= ion-viscous heating time scale in steady state) is longer than the electron cooling time scale. This model qualitatively fits the observed spectrum of Cyg X-1 from 8 to 500 keV, which is produced in the hot inner two temperature region of the accretion disk by Comptonization of soft photons. However, it is not clear how the intensity transitions occur in such a model. Eardley (1976) and

Eardley and Lightman (1976) have suggested, on an adhoc basis, that a plausible candidate for the soft photon source in high state is a cool, optically thick accretion disk within the thin scattering cloud, which varies in intensity. Spectral time variations, then, may be caused by a varying intensity of inner photon source embedded inside the stable hot cloud (Eardley 1976). However, according to this view the whole spectrum below $\sim$ 100 keV is an accurate power law at any one instant; while Tananbaum et al. (1972), Heise et al. (1975) and Sanford et al. (1975) report an excess at E $\sim$ 10 keV in the high state over the extrapolation of the steep log-E power law.

A major drawback of the calculations of Shapiro et al. (1976) is their assumption that viscous shear stress $t_{\phi r}$ induced by magnetic turbulence is constant throughout the disk. This has been taken care of in another version of modified accretion disk solution obtained by Ichimaru (1977). This model is based on an explicit formulation of viscous stresses arising from turbulent magnetic fields, instead of assuming, as in earlier models, constant ratio α of the viscous stress to the pressure, $t_{\phi r} = \alpha P$. Ichimaru finds that two physically distinct states exist in the middle part of the accretion disk, depending on the physical condition of the accreting gas

near the outer boundary, corresponding to high and low states of Cyg X-1. The accreting gas may evolve into either an optically thick (geometrically thin) disk or an optically thin (geometrically thick) disk in the middle region, depending on the accretion rate and temperature at the outer boundary of the disk. The optically thick middle disk emits the enhanced soft X-rays observed in the high state. Ichimaru also finds that for the inner region his solution of disk structure gives existence of a single (optically thin, geometrically thick) region which is similar to the hot disk solution of Shapiro et al. (1976), and most of the parameters obtained by Ichimaru (geometrical dimensions, temperatures etc.) for inner region are essentially the same as of Shapiro et al. (1976).

An attractive feature of Ichimaru model is its ability to explain high-low transitions without invoking an adhoc mechanism. This model can explain the bimodal transitions by assuming that the average accretion rate falls in the vicinity of critical condition and fluctuations in the accretion rate can produce the bimodal transitions. Further, the fluctuations of the accretion rate without crossing the Ichimaru threshold for the high-low transitions will cause long term intensity and spectral variations. The observed anticorrelated spectral

variability can be explained as due to the additional supply of soft photons from the middle, cold disk which leads to the decrease in the electron temperature in the inner disk, lowering the hard X-ray intensity as the soft X-ray intensity increases. Whereas the approach of this model is encouraging, quantitative evaluation of various effects, particularly the significant properties brought out in the body of this thesis, is necessary before drawing conclusions on the validity of the model. Studies along these lines are under progress and these will be published in due course.

In all the accretion disk models proposed so far, X-rays from a few to a few hundred keV are emitted because of the unsaturated Comptonization of soft photons. It has been shown by calculations of Comptonization that the mechanism of repeated inverse Compton scattering of initially soft photons in a finite, optically thin plasma cloud containing a thermal distribution of electrons at either a non-relativistic, semi-relativistic or relativistic electron temperature results in a power law spectrum (Pozdnyakov et al. 1976; Shapiro et al. 1976; Katz 1976 and Eardley 1976). In all these cases it is found that an upper cut-off at $h\nu = (2-3)\ kT_e$ arises in the spectrum, and that above $E \gtrsim kT_e$ inverse Compton spectrum steepens roughly

exponentially. The value of T_e, electron temperature of the hot cloud, in Cyg X-1 is a very important parameter which can be determined by observations through identification of the upper cut-off. As pointed out in Section 6.1, there is some observational data to suggest the existence of a knee in the Cyg X-1 spectrum at $\sim$ 150 keV, and others suggest that the knee may be at still higher energies (Baker et al. 1973). Observations are difficult near and above $\sim$ 150 keV and the presence of a knee at $\sim$ 150 keV itself is yet to be established firmly. It is also possible, as indicated in Section 6.1, that spectrum in this energy range shows some variability, which will indicate a change in the electron temperature of the cloud. If the knee at 150 keV is real, then the average value of T_e in the hot plasma must be near $5 \times 10^{8^o}$ K. On the other hand, if power law spectrum extends to E $\gtrsim$ 500 keV, as is suggested by other observations, then T_e will be correspondingly higher. According to the disk models of Shapiro et al. (1976) and Ichimaru (1977), we should have $T_e \sim 5 \times 10^{8} \sim 2 \times 10^{9^o}$ K, which is consistent with observations.

From the above discussion it is clear that theories of accretion disk around black hole are still in a preliminary state, mainly because of considerable uncertainties

in parameters determining local physics. The exact mechanism of viscosity and radiation transfer in the disk around black hole, which plays a crucial role in the energy dissipation and subsequent removal of energy by radiation processess, is not clear as yet. Theoretical predictions at present are not of the type which can be tested by rigorous observations and thus make it difficult to really discriminate between various models. Even though the modified accretion disk model (Shapiro et al. 1976; Ichimaru 1977), with its capability to offer semi-qualitative explanation of the observed features of Cyg X-1 emission, appears to be moderately successful and thus more promising; in the framework of our present understanding of this model it is not possible to explain the existence of two regularly switching states and binary phase modulation of intensity at $\sim$30 keV reported here. Thus far, sufficient consideration to general relativistic effects (red shift, gravitational focussing and black hole radiation recapture effects) has not been given in these models.

The author is engaged in these studies and the results of the same will be published in due course.

6.5 SUMMARY

Cyg X-1 is clearly one of the most interesting and puzzling objects in the sky, noted for its peculiar features

in several respects. In this thesis we have presented results on short as well as long term X-ray emission characteristics of this source at high energies (>20 keV). Several interesting and new results have emerged from from the present studies, which are summarised below:

1. Examination of all the observations made on the source so far at energies $>$ 20 keV indicates that during low state quiet condition the spectrum of the source can be best fitted to a power law with an index of $\sim$1.8, upto $\sim$ 150 keV. The high energy spectrum steepens when the source switches to high state at low energies.

2. The observations indicate that on rare occasions the source exhibits a 'flare-like' activity at high energies. In the event observed by us, intensity in 29.0-76.0 keV energy range went up by a factor of $\sim$ 2, whereas in 87.5-160.0 keV range it went up by a factor of $\sim$ 5. Moreover, there is strong indication of a time delay of $\sim$ 5 minutes in the enhancement of intensity in 29.0-76.0 keV energy channels as compared to that in the high energy channels. The spectrum of the source during the flare hardened considerably and was consistent with a power law having an index

of $\sim$ 1.0. Based on considerations of energetics and spectral characteristics, this flare has close resemblance to some of the γ -ray bursts, thus lending weight to the view that Cyg X-1 is a potential source of γ -ray bursts.

3. The observations also indicate that on occasions this source exhibits large random fluctuations in intensity by a factor of $\sim$3 to 4 at high energies on time scales of $\sim$1 minute, which are mainly confined to energies $\lesssim$ 76.0 keV. In addition, the source also exhibits periods of high and low intensity for durations of $\sim$20 to 30 minutes which are accompanied by complex spectral variability, the spectral index of the best fit power law spectrum varying over a wide range from $\sim$1.9 to 3.80. The source exhibits anticorrelated spectral variability around $\sim$70 keV for these complex spectral variations.

4. A major result which emerges from our study is that the source has two distinct levels of hard X-ray emission, differing in intensity by a factor of $\sim$ 2. In addition, it exhibits a linear variability of intensity with the 5.6 day binary

period at these energies. Variations of intensity with phase of the binary system is same for both the states and source spends almost equal time in these two states. In the light of our current understanding of Cyg X-1, we suggest that the characteristic fundamental property of this source is the two state emission at high energies emanating from the inner region of the accretion disk, both the states having equal probability of occurrence. The normal state at low energies, of emission from the outer region of the disk, is the one corresponding to the low state in intensity for about 90% of the time. On rare occasions when the low energy intensity emission flips to high state, the high energy X-ray component seems to show a further decrease which could be interpreted as the third state of emission at high energies.

Various theories of X-ray emission of Cyg X-1 are in a hazy state at present and theoretical predictions are not amenable to direct comparison with experimental observations. At present, the modified accretion disk model (Shapiro et al. 1976; Ichimaru 1977) appears to be moderately successful in explaining some of the observed

features of Cyg X-1 emission, and thus more acceptable. Further integrated development of theoretical and experimental studies is necessary to achieve deeper understanding of this fascinating and important object.

IONIZATION EFFECTS OF THE CELESTIAL X-RAY SOURCES IN LOWER ATMOSPHERE

CHAPTER - VII

IONIZATION EFFECTS OF CELESTIAL X-RAY SOURCES IN THE LOWER ATMOSPHERE

7.1 INTRODUCTION

The possible significance of X-radiation in the formation of D-region ionosphere was suggested many years ago by Muller (1935) and again by Rawer (1952) and more recently by Chamberlain (1961). Using the data obtained during solar maxima, Poppoff and Whitten (1962) demonstrated that the solar X-radiation plays a significant role in the formation of lower D-region of ionosphere. In the investigation of VLF field strength variations associated with the changes in the solar X-ray emission, Ananthakrishnan (1969) was able to clearly demonstrate that in addition to the effect of solar X-rays on the ionization at D-region altitudes during the day, a clearly observable ionization at these altitudes caused by non-solar X-ray sources exists during the night time when the effect of solar X-rays is virtually absent. The resultant electron density changes as revealed by the study of VLF propagation characteristics that include field strength and phase variations can thus be exploited to detect the X-ray sources.

However, opinions published in the literature regarding the importance of strong non-solar X-ray sources like Sco X-1 on the nocturnal D-region ionization have been conflicting. While the ground based experimental observations of Ananthakrishnan and Ramanathan (1969), Edwards et al. (1969) and Kaufman et al. (1970) on Sco X-1 and other X-ray sources such as Cen X-2 and Cen X-4 using VLF propagation techniques indicated that the effect of X-ray sources on the night-time ionosphere is an observable phenomenon, those of Burgess and Jones (1969) corresponding to their data of Omega Navigational system suggested otherwise. Other techniques that depend upon the flourescence effects of the atmospheric constituents in ultraviolet, visible and infrared due to excitation by X-rays also support the detection of such phenomena (Charman et al. 1970; O'Mongain and Weekes 1974; Elliot 1972; Fazio 1974 and Weekes 1976). Theoretically, comparing the relative contribution from ambient ionizing agents like Lyman-α radiation and galactic cosmic rays to the electron production rate in the night-time D-region with that expected from Sco X-1, Poppoff and Whitten (1969) concluded that the effects of X-ray sources should not be discernible in producing significant electron density perturbation over the ambient

condition. These authors also objected to the interpretation by Ananthakrishnan and Ramanathan (1969) on the basis of the observed time profile. From a similar but more detailed analysis, Francey (1970) questioned the analysis done by Poppoff and Whitten and showed that the relative importance of contribution from discrete cosmic X-ray sources to the electron production rates in the night time D-region critically depends on the assumed concentration of NO (which is ionized by Lyman-α) in the 80-90 km region. That is, the observability of the effect due to strong celestial X-ray sources like Sco X-1 depends on the magnitude of their ionization effect in relation to that from all other causes, and in particular to magnitude of ionization due to Lyman-α.

Since the cosmic X-ray sources are primarily investigated using rocket, balloon or satellite borne instrumentation, which by their very nature can only be epochal, the possibility of continuous long term monitoring of at least strong sources through their ionization effects on the D-region ionosphere assumes a great significance. With above considerations in mind, we have critically evaluated the effects of strong celestial sources like Sco X-1, Tau X-1 and galactic centre group of X-ray sources; strong transient X-ray sources like A0535+26 and A0620-00 and also

the integrated effect of several cosmic X-ray sources studied by a number of satellites that include Uhuru, ANS, Ariel V and SAS-3, on the lower atmosphere.

7.2 RESPONSE OF IONOSPHERE TO X-RAYS

It has been shown by a number of authors (Whitten et al. 1965; Swider 1969; Francey 1970) that the X-rays in the energy range 1-10 keV impinging on the top of atmosphere produce ionization mainly in 80-90 km height interval. At lower altitudes, the effect of X-rays becomes relatively unimportant due to exponential absorption they undergo in the 80-90 km height interval. Also, for normal power law spectrum of the type E^{-2} X-ray flux above 10 keV is very low so that it contributes very little to ionization. Therefore, we will consider the effect of X-rays in 1-10 keV energy range only in the subsequent discussion. The energy absorption per unit volume from a monoenergetic beam of X-rays of intensity I (keV cm^{-2} sec^{-1}) passing through an absorber of thickness dx (cm) is given by

$$\frac{dI}{dx} = \rho . \mu(E) . I \qquad \text{keV } cm^{-3} \text{ sec}^{-1} \qquad (7.1)$$

where ρ is the density of the absorber in g cm^{-3} and $\mu(E)$ is mass absorption coefficient of X-rays of energy E in cm^2 g^{-1}. The electron production rate q(h) in a volume

element of atmosphere at altitude h km will be thus given by

$$q(h) = \frac{\mu(E).\rho(h).I(h)}{Q} \text{ electrons } cm^{-3} \text{ sec}^{-1} \qquad (7.2)$$

where $Q \approx 0.035$ keV is the average energy for the production of an ion pair in air, $\rho(h)$ is density of air (g cm^{-3}) at height h and I(h) is the intensity of the X-ray source in keV cm^{-2} sec^{-1} at height h and is related to primary intensity I_o by

$$I(h) = I_o \exp\left[-\mu(E)\int_h^{\infty} \rho(H) \text{ Sec } Z \, dH\right] \qquad (7.3)$$

where Z is the 'local' zenith angle of the source at height h which is given by

$$\text{Cos } Z = \left[1-\left\{\frac{R\bullet h}{R+H} \cdot \text{Sin } z\right\}^2\right]^{-\frac{1}{2}} \quad R\text{-earth's radius} \qquad (7.4)$$

for a reasonable approximation for the curved atmosphere (for $H \gg h$ and actual zenith angle $z < 90^o$).

Thus the electron production rate due to X-rays in the energy range E_1 to E_2 at height h of atmosphere and local zenith angle Z can be calculated from

$$q(h) = \frac{\rho(h)}{Q}\int_{E_1}^{E_2} \mu(E)\ f(E)\ dE\ \exp\left[-\mu(E)\int_h^{\infty}\rho(H)\ \mathrm{Sec}\ Z\ dH\right]$$

$$= \frac{\rho(h)}{Q}\int_{E_1}^{E_2} \exp\left[-\mu(E)\ \mathrm{Sec}\ Z\int_h^{\infty}\rho(H)\ dH\right]\mu(E)\ f(E)dE \quad \ldots (7.5)$$

where Z is given by equation 7.4 and $f(E) = \left(\frac{dN}{dE}\right) \cdot dE$ is the source X-ray intensity in keV cm^{-2} sec^{-1}.

Similarly, electron production rate due to diffuse cosmic X-ray background is obtained by integrating the contribution over all energy elements for the solid angle $d\Omega$ over the zenith angle Z and azimuth from 0 to 2π. Since

$$d\Omega = \mathrm{Sin}\ z.\ d\theta.\ dz$$

we have $$q(h) = \frac{2\pi\ \rho(h)}{Q}\int_{E_1}^{E_2} \mu(E)\ f(E)\int_0^{89}\mathrm{Sin}\ Z\ \exp\left\{-\mu(E)\int_h^{\infty}\rho(H)\ \mathrm{Sec}\ Z\ dH\right\} dZ\ dE \quad \text{electrons } cm^{-3}\ sec^{-1} \quad (7.6)$$

It is clear from equation 7.5 that changes in the source spectrum should be reflected in q(h). Fig. 7.1 shows the results of computations of the electron production

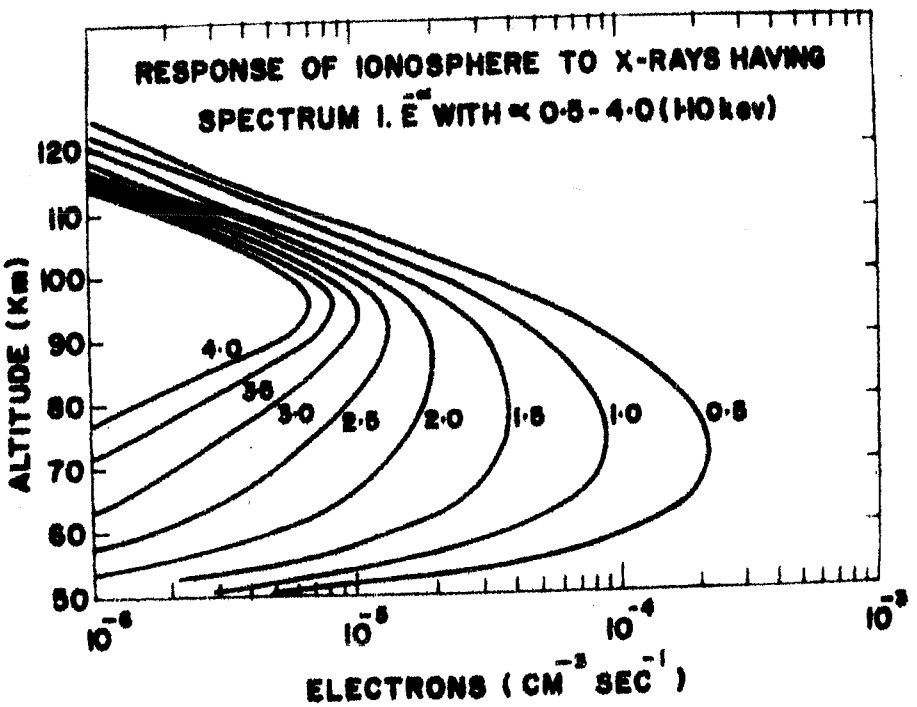

Fig. 7.1 : Altitude profile of ionization produced in the D-region of ionosphere due to X-rays of 1-10 keV having a spectral shape of the form $\frac{dN}{dE} = E^{-\alpha}$ photons cm^{-2} sec^{-1} keV^{-1} with values of α ranging between 0.5 to 4.0.

rate as a function of altitude for an assumed spectrum of the type

$$\frac{dN}{dE} = 1.E^{-\alpha} \text{ photons cm}^{-2} \text{ sec}^{-1} \text{ keV}^{-1}$$

for different values of α ranging between 0.5 to 4.0. Profiles shown in the figure correspond to zenith angle $\chi = 0^{o}$ for photons in the 1-10 keV range. It is obvious that as the spectrum softens the peak of production rate moves up from about 70 to 95 km, considering that photons above 10 keV contribute little to the electron production at altitudes below 70 km due to their lower flux and also because of large recombination effects.

7.3 AMBIENT SOURCES OF IONIZATION IN THE NIGHT-TIME D-REGION

The feasibility of observing the effect due to the passage of celestial sources depends critically upon the relative magnitude of this effect compared with the ionization due to other background sources in the night time ionosphere. Therefore, in this section, we first attempt to make reliable estimates of the electron production rates due to various ambient ionization agencies responsible for the production of electrons in the nocturnal D-region.

These agencies are identified to be

i) Diffuse cosmic X-rays

ii) Galactic cosmic radiation

iii) Lyman-α radiation and

iv) Meteors

Unlike the first three agencies, the ionization effect from meteors is sporadic and uncertain. However, it is believed that the effect should be much less than 10^{-3} cm^{-2} sec^{-1} (Thomas 1971). Owing to the highly infrequent nature of this source, it has not been considered here.

The D-region ionization due to diffuse cosmic X-rays has been evaluated using equation 7.6 and assuming a spectral function of the type

$$\frac{dN}{dE} = 13.6\ E^{-1.7} \text{ photons cm}^{-2} \text{ sec}^{-1} \text{ sr}^{-1} \text{ keV}^{-1}$$

in the 1-10 keV energy range (Prakasarao et al. 1971). Since the effect due to the difference between different atmospheric models is completely negligible below $\sim$ 100 km in these computations (Francey 1970), we have used the CIRA 1972 model for the atmospheric densities.

The galactic cosmic ray effect is determined for $\lambda_m = 23^\circ$ and is based on the calculations of Velinov (1968).

The extent of variation in the production rates resulting from solar modulation of the cosmic radiation and the seasonal variation of the atmospheric densities has also been estimated.

One important and crucial source of night time D-region ionization, on which considerable uncertainties still exist, is the ionization due to Lyman-α radiation. The Lyman-α radiation produces ionization at around 85 km in the atmosphere through photoionization of nitric oxide (Nicolet and Aikin 1960). Ionization rate due to Lyman-α of intensity I (photons cm^{-2} s^{-1} sr^{-1}) has been calculated using the relation

$$q(h) = 2\pi\, n_1(h)\, I\, \sigma_i \int \exp\left[-\sigma_a \sec\chi \int n_2(h)\, dh\right] \sin\chi\, d\chi$$

where $n_1(h)$ and $n_2(h)$ are the number densities of NO and O_2 respectively at height h, χ is the zenith angle, $\sigma_a = 10^{-20}$ cm^2 is the absorption cross section of O_2 for Lyman-α (Watanabe 1958) and $\sigma_i = 2 \times 10^{-18}$ cm^2 is photoionization cross section of NO at the same wave length (Watanabe 1958). A free space intensity of $\sim 2 \times 10^{-3}$ ergs cm^{-2} s^{-1} sr^{-1} is assumed for the night time Lyman-α at the top of the atmosphere and is representative of average conditions (Meier 1970; Hinteregger 1965). The height profile of

Lyman-α in the 70-90 km altitude range is derived by assuming the O_2 distribution predicted by CIRA 1972, since below 120 km altitude, where most of the Lyman-α absorption takes place, all the atmospheric models essentially predict the same value.

The principal difficulty in the estimation of the Lyman-α ionization stems from the uncertainties in our knowledge of the nitric oxide density profile. In the present study a profile similar to that observed by Meira (1971) has been used, but with the value of NO density normalized to 2×10^6 cm^{-3} at 75 km, at which altitude the agreement between independent observational and analytical results is good (Mitra 1969; Nicolet 1965; Wagner 1966; Pearce 1969). The resulting profile of NO further yields densities at other altitudes which are in reasonable agreement with the corresponding values obtained by the independent means cited above. Fig. 7.2 summarizes the experimental status of NO concentration in the mesosphere.

Besides this, the Lyman-β component could also cause some degree of ionization. But the high absorption cross section of O_2 ($\sim 1.5 \times 10^{-18}$ cm^2) for this radiation (Young et al. 1968) results in the flux of Lyman-β at depths below 90 km to be too negligible to become a signi-

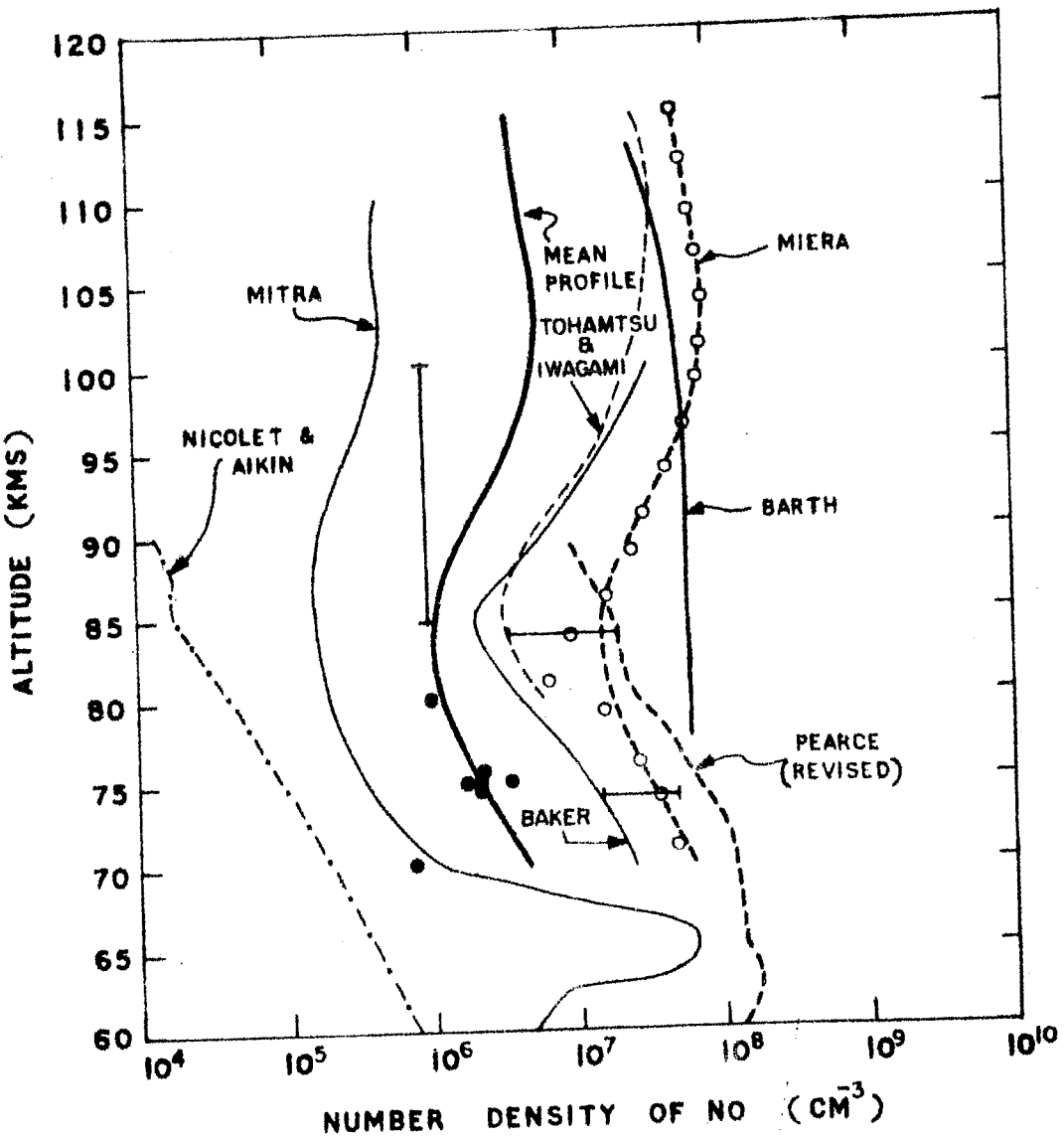

Fig. 7.2 : Some of the available experimental and theoretical results on the vertical distribution of NO density. The mean profile used in the present work is also shown.

ficant source of ionization.

The best estimates of electron production rates in the night time ionosphere due to different ionizing agents, computed as outlined above, are shown in Fig. 7.3. The total ambient effect from all the background agencies is shown by dotted curve.

7.4 IONIZATION DUE TO COSMIC X-RAY SOURCES

In this section we present the results of calculations of the electron density perturbations in the ionospheric D-region for strong steady X-ray sources Sco X-1, Tau X-1 and galactic centre group and transient X-ray sources A 1118-61, A 0535+26 and A 0620-00; which will be followed by a critical examination of their detectability in relation to the above ambient ionization agents. In the end we will examine the integrated effects of many of the known X-ray sources discovered by Uhuru, ANS, Ariel V and SAS-3 satellites, in order to understand the totality of their effects.

7.4:1 Ionization due to Sco X-1, Tau X-1 and Galactic Centre

Electron production rates for X-rays from Sco X-1 and Tau X-1 as well as from galactic centre have been calculated using equation 7.4. The calculations have been made for zenith angles $\chi = 0^{\circ}$ and for 45°, 60° and 10° for

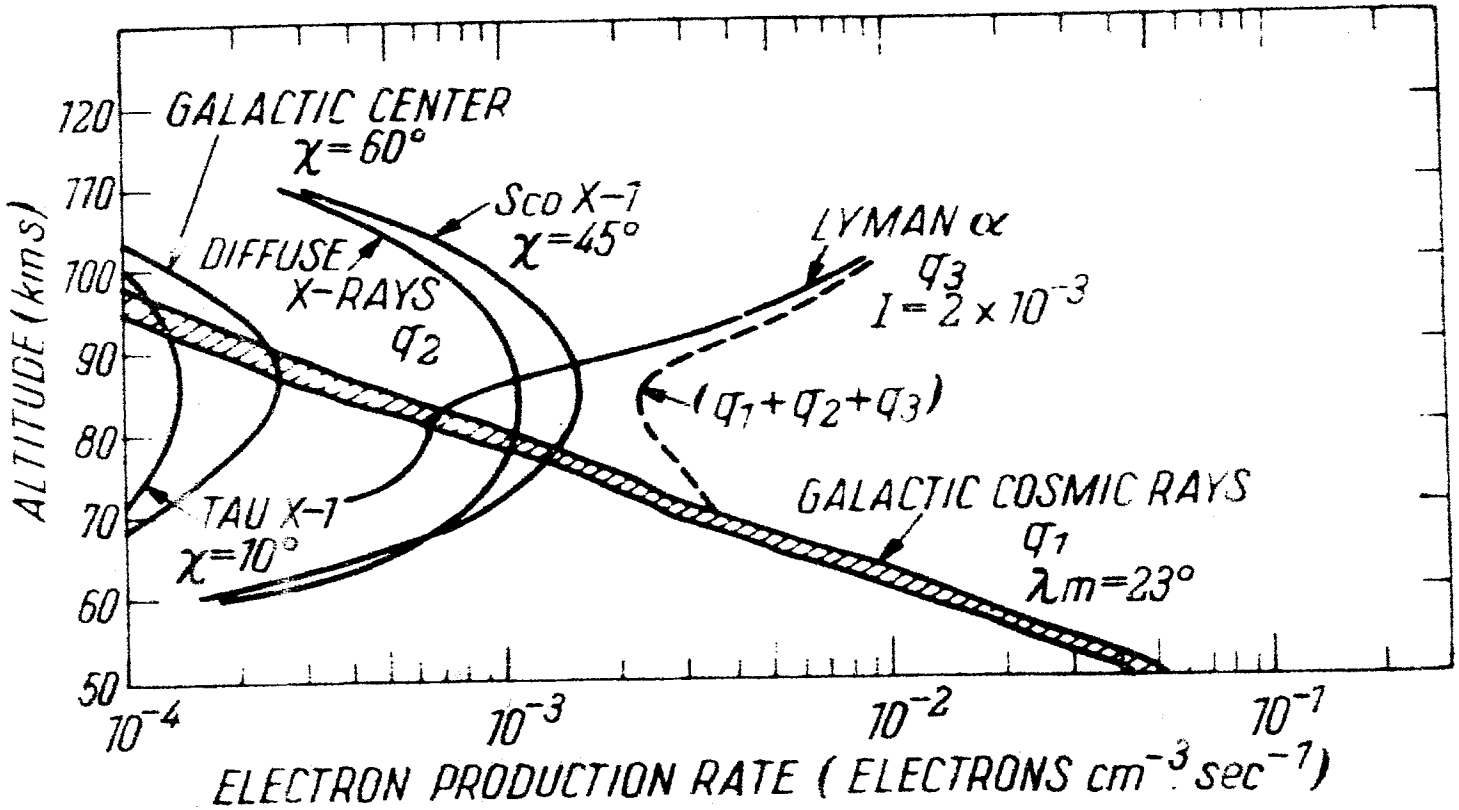

Fig. 7.3 : The altitude profile of the electron production rates due to stable background agencies viz. galactic cosmic rays, diffuse cosmic X-ray background and Lyman-α. Also shown are the transient effects arising from the passage of Sco X-1, galactic centre sources and Tau X-1. The total ambient effect from all the background agencies is shown by the dotted curve.

Sco X-1, the galactic centre and Tau X-1 respectively, corresponding to the meridian transit of these sources over geographic latitude 32°N (Geomagnetic latitude $\lambda_m = 23^{\circ}$), and are shown in Fig. 7.4. The values of the relevant parameters of these sources used in the calculations have been taken from the measurements of Gorenstein et al. (1969), Chodil et al. (1968b) and Riegler et al. (1968). These effects of Sco X-1, galactic centre, and Tau X-1 for $\chi = 45^{\circ}$, 60° and 10° respectively have also been plotted in Fig. 7.3 along with electron production rates due to other ambient ionizing agencies. It is seen from Fig. 7.3 that below about 70 km altitude, the most important ionizing agent is galactic cosmic radiation and above about 90 km Lyman-α dominates the ionization. But in the height range 70-90 km strong celestial X-ray sources like Sco X-1 can contribute very significantly to the ionization in the night time ionosphere.

As a next step, we have attempted to estimate the resultant increase in the electron density due to passage of these X-ray sources. The calculation of electron density N_e from electron production rates q_j is carried out using the well-known formula for equilibrium condition

$$\frac{\sum q_j}{N_e^2} = \psi$$

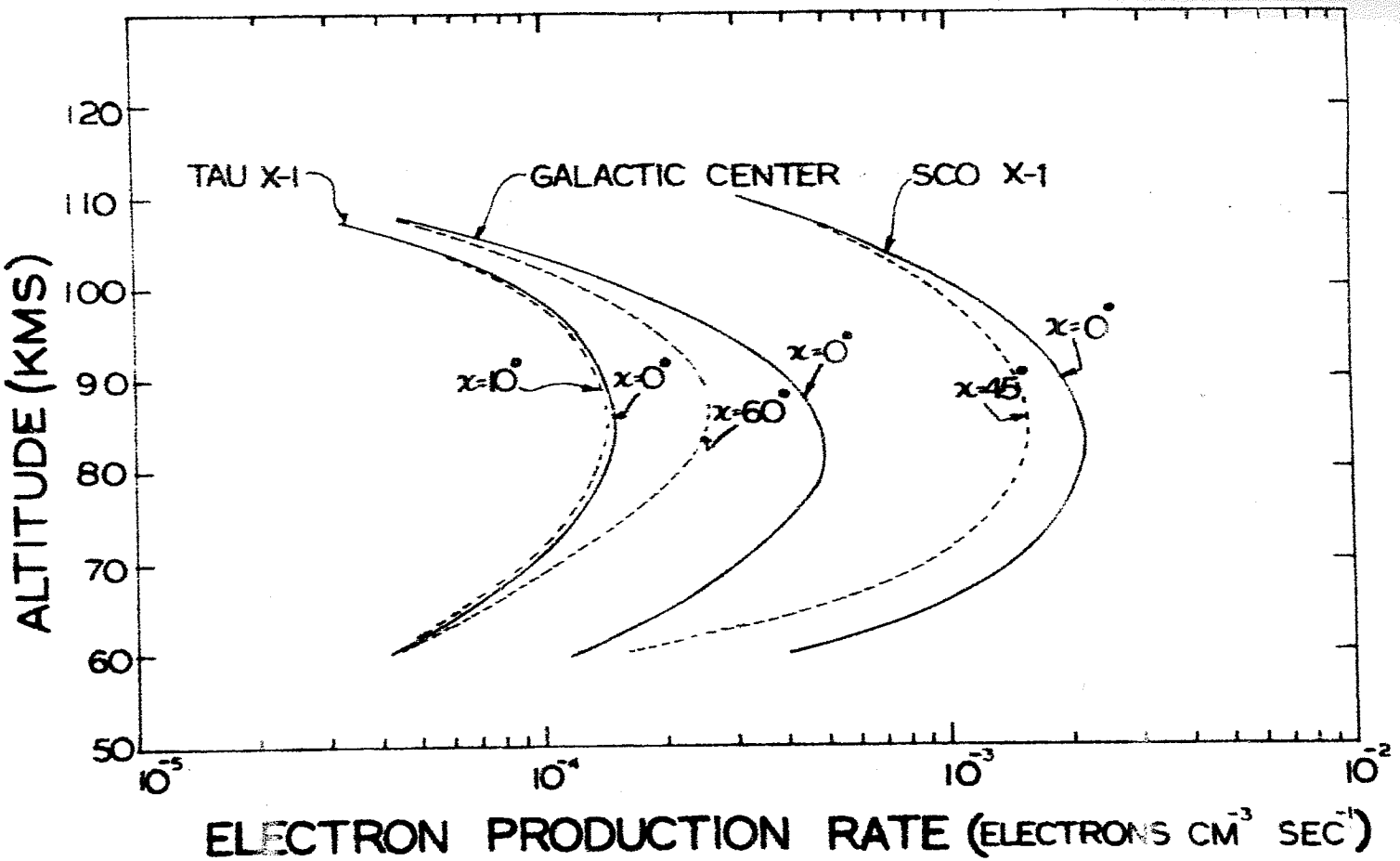

Fig. 7.4 : The altitude profile of electron production rates due to Sco X-1, galactic centre and Tau X-1. The production rates are given for the zenith angle $\chi = 0^{\circ}$ and that corresponding to the meridinal transit of these sources over geographic latitude 32° N.

where ψ is the effective recombination coefficient. Owing to the inadequate information on the values of ψ for the nocturnal D-region, the electron density perturbation due to discrete X-ray sources has been evaluated by comparing the directly measured night time electron density profiles (Deeks 1966; Mechtly and Smith 1968; Subbaraya et al. 1971) with the calculated electron production rates. With these observed values of N_e and the computed values of q_j corresponding to the ambient ionization agents, the values of recombination coefficient ψ as a function of altitude have been calculated, which are shown in Fig. 7.5. We have also examined the available data on the electron loss rate coefficient ψ for night time due to different authors (Bailey 1968; Mitra 1968; Potemra et al. 1969; O'Mongain and Baird 1976) which are summarized in Fig. 7.5. Comparison of different data shows that there is a fairly good agreement between various values of electron loss coefficient as deduced by Bailey (1968), Mitra (1968), Potemra et al. (1969) and present values in $\sim$ 80 km height. The electron density enhancements due to X-rays from Sco X-1, galactic centre and Tau X-1 sources at 45°, 60°, and 10° zenith angles respectively, corresponding to meridian transit of these over 32°N latitude, have been computed using the values of ψ at different altitudes derived as above. These

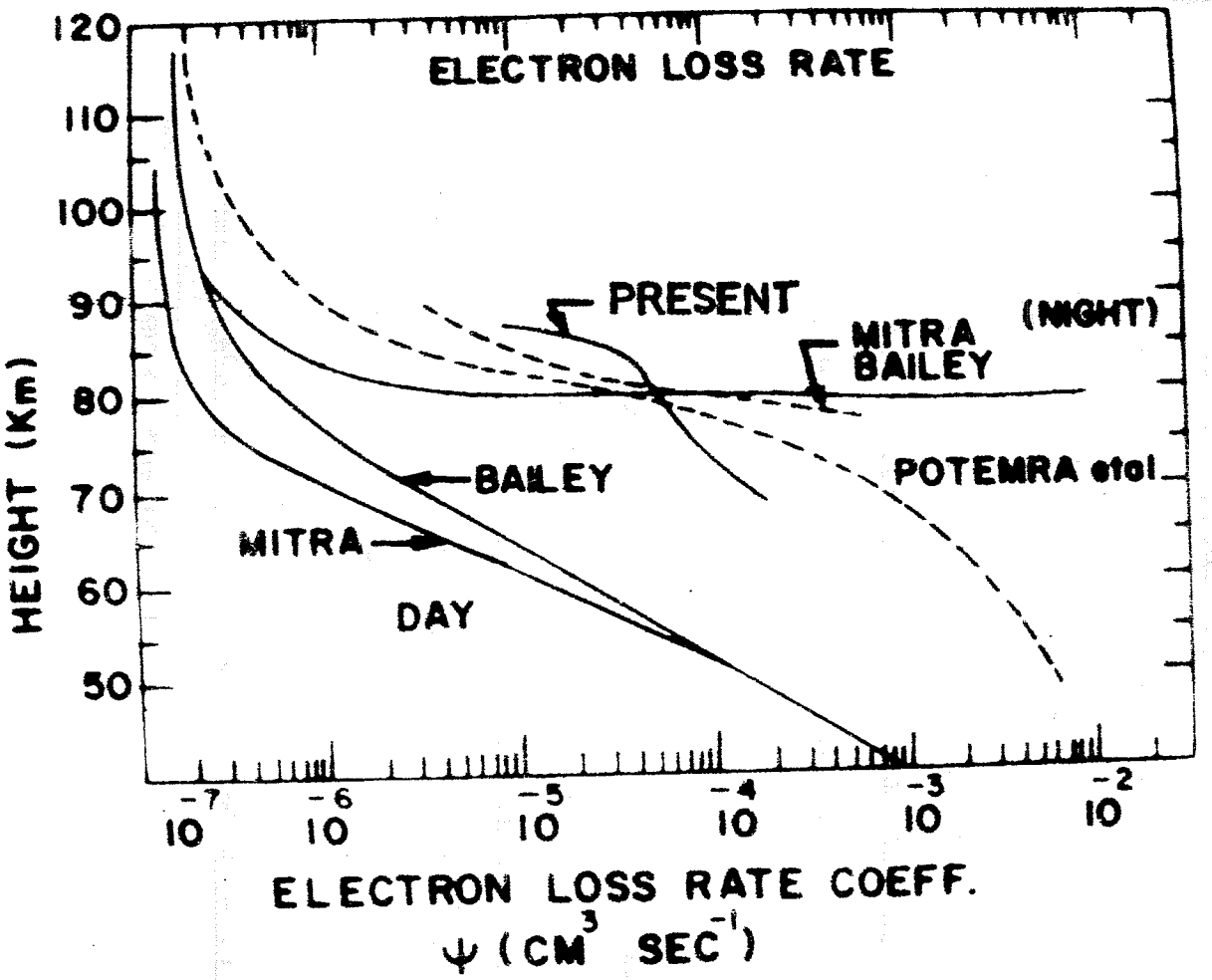

Fig. 7.5 : Data on the electron loss rate coefficient at different heights in the D-region of ionosphere.

electron density enhancements at different altitudes are summarized in Table 7.1. It is seen from this table that electron density increase due to Sco X-1 is quite significant at $\sim$ 85 km and should be definitely observable. However, results for galactic centre sources and Tau X-1 are less striking. In Fig. 7.6 we have shown electron density increase over the ambient values at 85 km height as a function of time, both before and after the meridian transit of these sources. From this figure it is clear that effect due to X-ray source Sco X-1 should be observable for about 2-3 hours on either side of the meridian transit of this source. In addition, owing to the fact that galactic centre meridian transit takes place only 1 hr 25 min after the transit of Sco X-1, the effect from these two sources will be seen as a composite one which will result in a shift in the time of peak electron density enhancement by about 20-30 minutes. Further, the expected duration of the effect for Tau X-1 should be longer compared to that for Sco X-1.

7.4:2 Ionization due to Transient X-ray Sources

In view of the possibility of detecting and monitoring transient X-ray sources through their ionospheric effects, we have made calculations of electron density perturbation in the ionospheric D-region for some of the more prominent sources of this class in this section. Thereafter,

TABLE 7.1

ight km)	Ambient production rate $(q_1+q_2+q_3)$ $(cm^{-3}sec^{-1})$	Electron density increase due to Sco X-1 and galactic centre (G.C.)					Electron density increase due to Tau X-1		
		Ambient electron density N_e (cm^{-3}) Summer[a]	q(h) Sco X-1 $(cm^{-3}sec^{-1})$	q(h) G.C. $(cm^{-3}sec^{-1})$	ΔN Sco X-1 (cm^{-3})	ΔN G.C. (cm^{-3})	Ambient electron density N_e (cm^{-3}) Winter[b]	q(h) Tau X-1 $(cm^{-3}sec^{-1})$	ΔN Tau X-1 (cm^{-3})
.0	2.996×10^{-3}	6.4	1.210×10^{-3}	1.65×10^{-4}	1.184	0.175	7.0	1.15×10^{-4}	0.133
.5	2.675×10^{-3}	7.0	1.365×10^{-3}	1.95×10^{-4}	1.603	0.251	9.6	1.25×10^{-4}	0.223
.0	2.413×10^{-3}	7.0	1.500×10^{-3}	2.20×10^{-4}	1.915	0.313	9.4	1.36×10^{-4}	0.263
.5	2.287×10^{-3}	7.0	1.565×10^{-3}	2.42×10^{-4}	2.085	0.361	15.0	1.43×10^{-4}	0.470
.0	2.284×10^{-3}	10.0	1.600×10^{-3}	2.55×10^{-4}	3.040	0.540	600.0	1.42×10^{-4}	18.300
.5	2.674×10^{-3}	2.0×10^{3}	1.580×10^{-3}	2.60×10^{-4}	523.0	95.0	700.0	1.40×10^{-4}	18.100
.0	3.458×10^{-3}	8.0×10^{3}	1.480×10^{-3}	2.45×10^{-4}	1560.0	278.0	500.0	1.35×10^{-4}	9.700

- N_e taken from Subbaraya et al. (1971) and Deeks (1966)

- N_e taken from Deeks (1966).

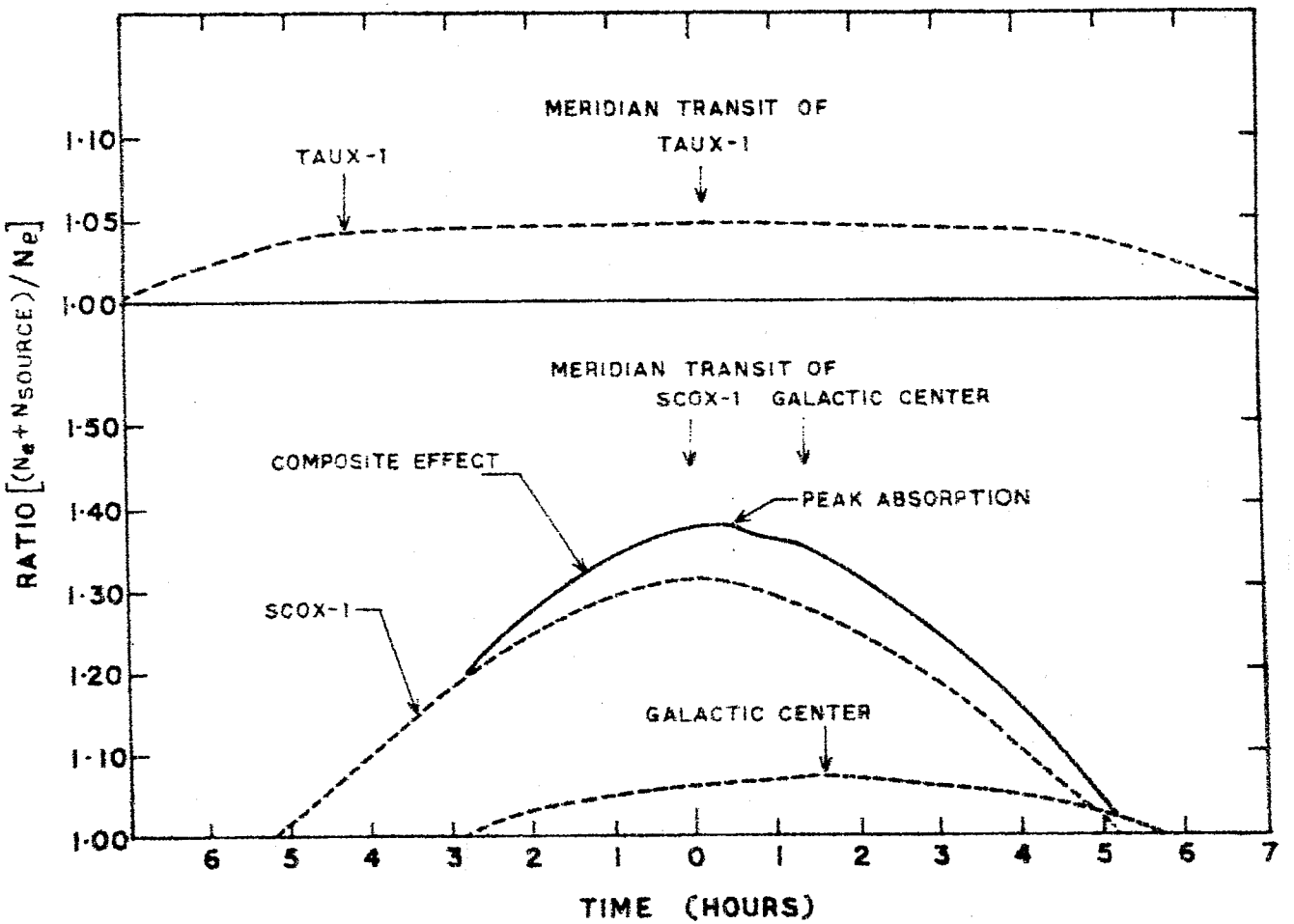

Fig. 7.6 : Time profile of excess ionization shown as the ratio of the total electron density, including the contribution from discrete sources, to the ambient value. The values correspond to 85 km altitude. The composite effect expected from Sco X-1 and galactic centre is also shown.

a critical comparison between the expected effects for such sources and that from Sco X-1 has been made to ascertain the detectability of the transient sources.

i) Source A 1118-61

This source made its appearance in X-ray sky (R.A. = 11 hr 18 min and Declination = -61^{o}) on December 18, 1974 (Ives et al. 1975) and by December 27, 1974 the intensity rose to a maximum level of $\sim$ 1.3. 10^{-9} ergs cm^{-2} sec^{-1} in the 2 to 6 keV band, which subsequently reduced in about 8 days time below the detectable level. The spectral distribution around the period of peak emission for this source seems to be governed by a power law with a spectral exponent value of $\sim$ 0.91. Fig. 7.7 shows the electron production rate profile for A 1118-61 computed for measured intensity of X-ray emission on December 26, 1975 using equation 7.4 for zenith angle $\chi = 0^{o}$. For comparison the corresponding profile for Sco X-1 is also shown in the figure. It is clear that the expected electron production rate at the peak period for this source is at least an order of magnitude lower than that for Sco X-1. Besides, the altitude of maximum production for this source is around 70 km in contrast to about 85 km for Sco X-1. Due to much higher recombination rates (at least an order of magnitude higher) at altitudes of 70 km compared to that at 85 km, the expected equilibrium electron densities are

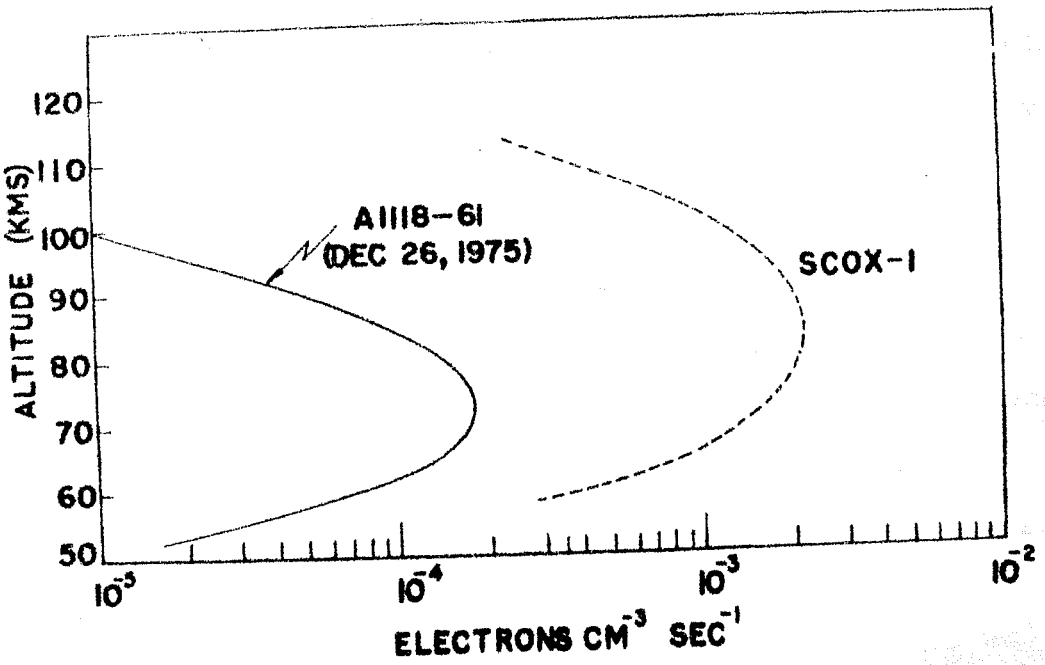

Fig. 7.7 : The altitude profile of electron production rates due to A 1118-61 at its maximum on December 26, 1975. For comparison the corresponding profile for Sco X-1 is also shown in the figure.

also much lower. Therefore, the chance of detecting this source through its ionospheric effect is low because of its weak ionizing effect at D-region altitudes and the prevailing high recombination rates at these altitudes.

ii) Source A 0535+26

This source was discovered by modulation collimator experiment on board Ariel V on April 13, 1975. The intensity level on the first day of observation was about 4.4×10^{-9} ergs cm^{-2} sec^{-1} in the 2 to 5 keV band. A rapid increase in its emission flux started occurring around April 20, 1975, reaching a maximum level of 2.2×10^{-8} ergs cm^{-2} sec^{-1} by April 30, 1975. The source decayed below the level of detectability by June 9, 1975 (Ricketts et al. 1975a; Rosenberg et al. 1975). The spectrum observed in early May 1975 showed that it is extremely hard ($\sim E^{-0.8}$), with an evidence for softening towards the final phase ($E^{-1.1}$ around June 1, 1975). Fig. 7.8 shows electron production rate profiles for May 19, 1975 and June 1, 1975. As in the case of A 1118-61, the electron production rate for this source also is about an order of magnitude lower than that for Sco X-1 and the chance of detecting this source through its ionospheric effect is also not high.

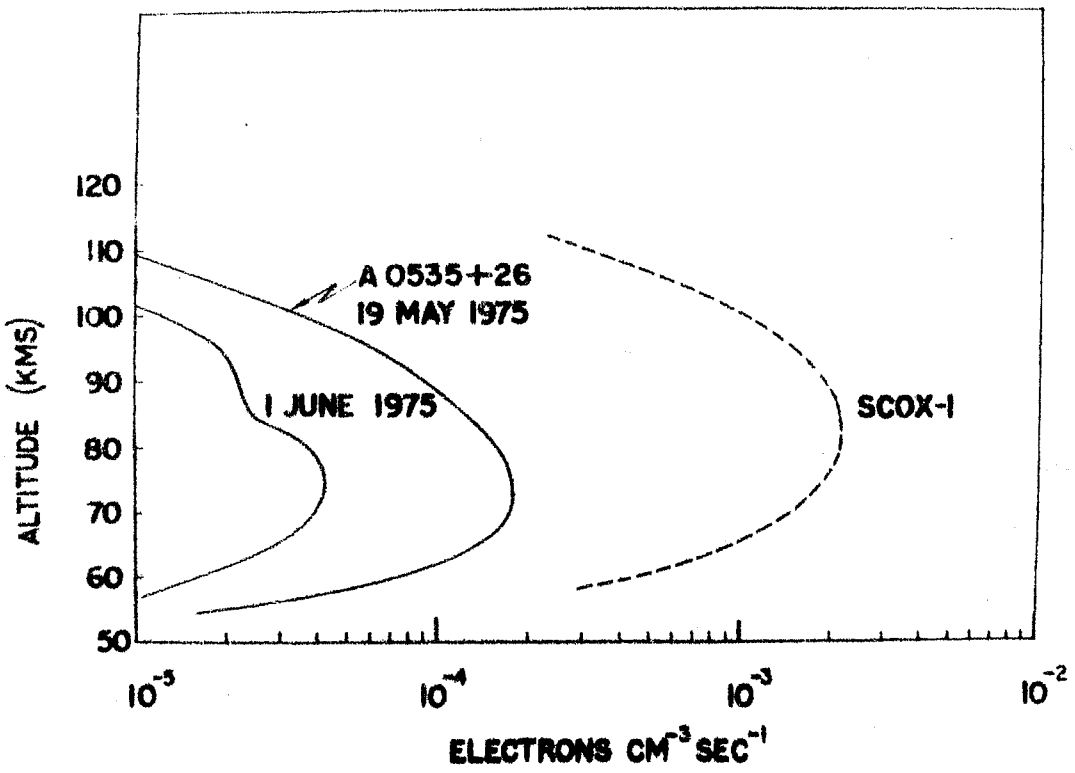

Fig. 7.8 : The altitude profile of electron production rates due to A 0535+26. The rates are shown for two epochs of its life. The maximum intensity occured around June 1, 1975.

iii) Source A 0620-00

A 0620-00, one of the strongest transient X-ray source, was discovered by Ariel V on August 3, 1975 (Elvis et al. 1975). At the peak of its active phase (August 11-16, 1975) the X-ray flux emitted by this source was almost four times that of Sco X-1, the strongest of the steady sources known so far. This transient source also exhibited remarkable spectral variabilities during its rise and decay phases. In fact, the spectral exponent varied from 0.7 to 5.7 over a period of about 15 days of its rising phase (Ricketts et al. 1975b). From the available data (Ricketts et al. 1975b) on the intensity and spectrum, the ionization production rates have been computed as a function of altitude over 0^{o} latitude. The results are presented in Fig. 7.9 for a number of values of the spectral exponent corresponding to the different epochs of the source. As is clear from Fig. 7.9, the peak of the production rate shifts from around 75 km to 90 km as the intensity and spectral features change. Whereas a general shifting of the peak of electron production rate to higher altitudes is observed as the spectrum softens up to $\alpha = 4.75$ and $E_a = 1.9$ (Curves A to F), further softening results again in the lowering of the altitude of peak production rate due to the increase of the low energy cut off value of the X-ray flux (G and H). Further, it is observed that the electron production rate for several days

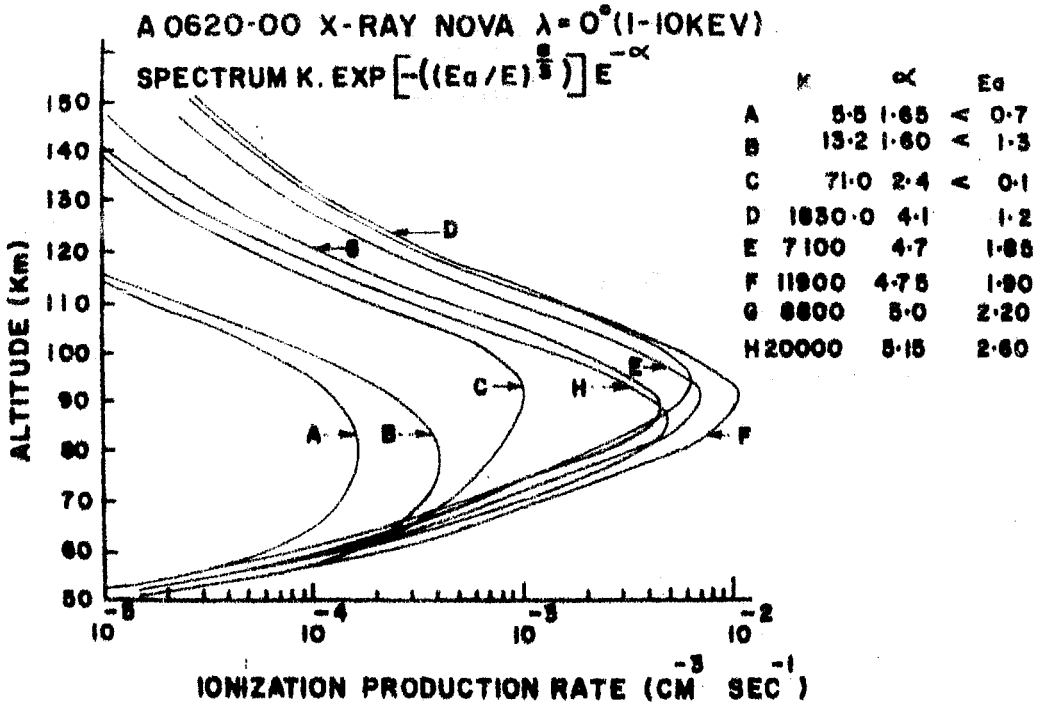

Fig. 7.9 : The altitude profile of electron production rates due to A 0620-00 over 0° latitude at various epochs of its life. The alphabets refer to the spectrum observed at these epochs corresponding to which spectral parameters are given.

for this source is comparable to or higher than that from Sco X-1, and around the intensity maximum is as high as 10 times that from Sco X-1. The effect of the transient X-ray source A 0620-00 should, therefore, be significant for the period August 3-18, 1975 and there is distinct possibility of detecting this transient source in the available VLF data for this period.

7.4:3 Integrated Effects of Cosmic X-ray Sources

In this section we examine the integrated effect of several cosmic X-ray sources studied by a number of satellites, in order to understand the totality of their effects on the nocturnal D-region of ionosphere. These studies have been made for different times of the year for two different latitudes (0^{o} and $+38^{o}$) under midnight conditions.

The X-ray sources identified for the present investigation correspond to third Uhuru catalog (Giacconi et al. 1974) supplemented with data reported from ANS, Ariel V and SAS-3 observations. As a first step towards the evaluation of the integrated ionospheric effect of cosmic X-ray sources, the contribution due to the galactic centre group of X-ray sources has been estimated. The results of the calculation (from individual sources and sum total) carried out for 0^{o} geographic latitude

corresponding to the meridinal transit of this group of sources at local midnight on May 25 are presented in Fig. 7.10 along with the estimated contribution from Cygnus group of sources. The details of the sources considered are given in Table 7.2. Only those sources that contribute more than 5% of the total production rate are shown in the figure. The combined effect of all the known steady X-ray sources on the D-region of the ionosphere is also computed corresponding to a height of 80 km for the geographic latitudes $\lambda = 0^{\circ}$ and $\lambda = 38^{\circ}N$. The calculations have been made for the following two conditions:

i) The first day of each month for the whole year, corresponding to midnight and for sources with zenith angles of 70° or less.

ii) Effects of transient sources have not been included.

The results for electron production rate at 80 km so obtained are presented in Fig. 7.11. Also, the number of sources considered for the calculation is indicated on a monthwise basis in the same figure. It is seen from this figure that the production rate has a broad maximum around July for both the latitudes with minimum occurring around March-April. Further, the ratio of the maximum to minimum production rate is found to be about 10.

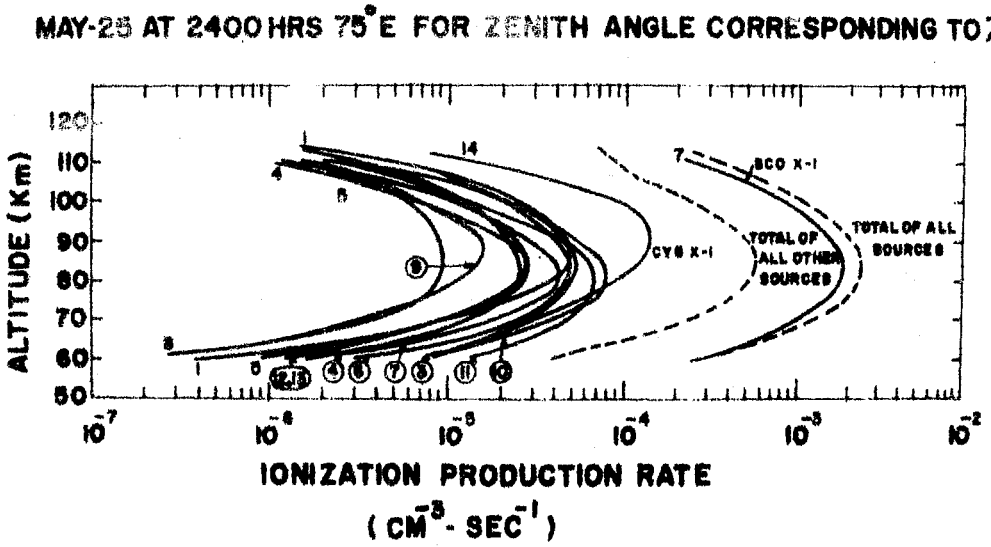

Fig. 7.10 : The altitude profile of electron production rates due to the strong galactic centre X-ray sources. The calculations correspond to the meridinal transit of galactic centre on May 25 at midnight and latitude 0^{o} (see Table 7.2 for details).

TABLE 7.2

DETAILS OF THE X-RAY SOURCES USED FOR FIG. 7.11

L. No.	Source	Position (deg.) R.A.	Decln.	Spectral parameters*		Reference
1	2	3	4	5		6
.	3U1516-56 (Cir X-1)	229.18	-56.98	C = 2.33 kT = 0.95 N_H = 0.79 x 10^{22}	(BB)	Cruddace et al. (1972)
.	Sco X-1 3U1617-15	244.28	-15.54	-	(E)	Jayanthi (1973)
.	3U1538-52 (GX327+2.5)	234.56	-52.18	C = 21 kT = 6.13 N_H = 0.79 x 10^{22}	(E)	Cruddace et al. (1972)
.	3U1642-45 (GX340+0)	250.53	-45.53	C = 0.45 kT = 1.34 N_H = 1.2 x 10^{22}	(BB)	-do-
.	3U1630-47 (GX337+0)	247.54	-47.27	C = 14 kT = 3.06 N_H = 7.1 x 10^{22}	(E)	-do-
.	3U1702-36 (GX349+2)	255.58	-36.36	C = 7.34 kT = 8.63 N_H = 1.1 x 10^{22}	(E)	-do-
.	3U1705-44	256.35	-44.05	-		Jones (1977)

TABLE 7.2 (contd.)

1	2	3	4	5		6
8.	3U1727-33 (GX340+0)	261.84	-33.70	C = 0.45 kT = 1.337 N_H = 1.2 x 10^{22}	(BB)	Margon et al. (1971) Jones (1977)
9.	3U1744-26 (GX3+1)	266.19	-26.56	C = 1.11 kT = 0.863 N_H = 0.79 x 10^{22}	(BB)	Cruddace et al.(1972)
10.	3U1758-20 (GX9+1)	269.64	-20.54	C = 1.0 kT = 1.08 N_H = 0.25 x 10^{22}	(BB)	-do-
11.	3U1813-14 (GX17+2)	273.29	-14.06	C = 3.94 kT = 0.82 N_H = 1.6 x 10^{22}	(BB)	-do-
12.	GX357+2.5	268.89	-33.80	C = 1.33 kT = 4.83 N_H = 0.35 x 10^{22}	(E)	-do-
13.	Ser X-1 (3U1837+04)	279.33	4.99	C = 0.85 kT = 4.2 N_H = 0.56 x 10^{22}	(E)	Hill et al. (1975)
14.	Cyg X-1 (3U1956+35)	299.09	35.06	C = 10 kT = 2.6 ± 0.2 N_H = 17 x 10^{22}	(P)	Heise et al. (1975)

* (BB) = Black Body - $dN/dE = C.\exp(-N_H\sigma).E^2 (\exp(E/kT)-1)^{-1}$

(E) = Exponential - $dN/dE = C.\exp(-N_H\sigma).\exp^{(-E/kT)}$.

(P) = Power - $dN/dE = C.\exp(-N_H\sigma) E^{-\alpha}$

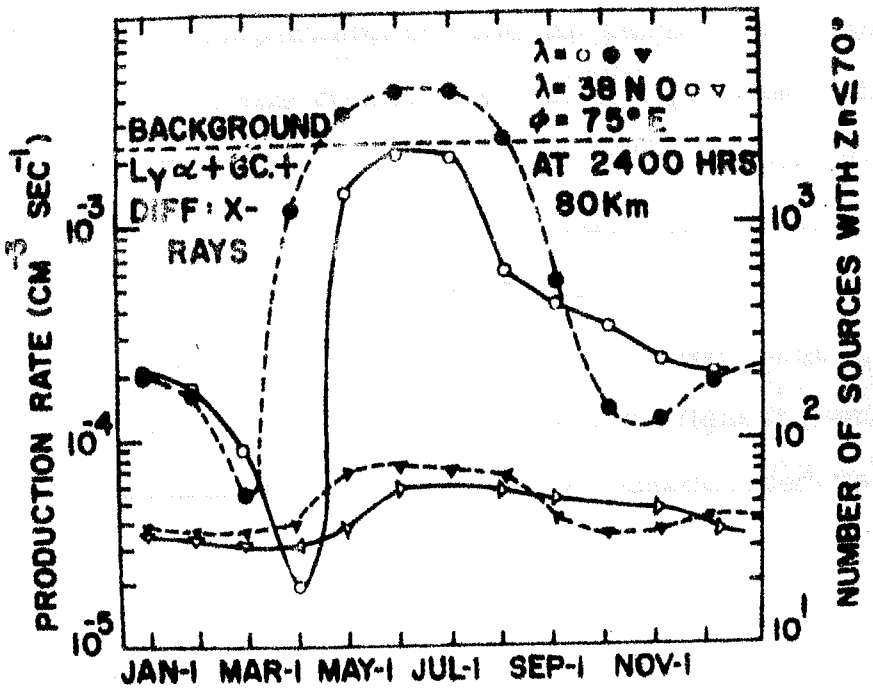

Fig. 7.11 : Electron production rates at 80 km due to all the Uhuru sources calculated at different times of the year. Solid points are for 0^{o} latitude and open points for 38^{o}N. Lower two curves denote the number of sources contributing to the production rate and the scale for this is on the right hand side of the figure.

Next, we have attempted to estimate the resultant increase in the electron density at 80 km for different months. Since a comparison of the different data for ψ, the electron loss rate coefficient for night time, from Fig. 7.5 shows that there is fairly good agreement between various values of the electron loss rate coefficient as deduced by Bailey (1968), Mitra (1968), Potemra et al. (1969) and present values for 80 km height; we have used a value of 3.5×10^{-5} cm^3 sec^{-1} for ψ. The electron density enhancement due to X-ray source (N_{source}) has been calculated using the formula

$$\psi = \frac{Q_{amb} + Q_{source}}{\left[N_{amb} + N_{source}\right]^2}$$

where Q_{amb} is the ambient electron production rate due to agencies such as Lyman-α, cosmic background X-rays and galactic cosmic rays (Section 7.3), Q_{source} is the electron production rate due to X-ray sources as shown in Fig. 7.11, and N_{amb} is the electron density prevailing under stable conditions. The calculation of ambient electron production is for solar minimum conditions. The values of N_{amb} and Q_{amb} have been adopted from Poppoff et al. (1975) and from Section 7.3 respectively. The results of the calculations are shown in Fig. 7.12. It can be seen that for $\lambda = 0^o$, about 8 electrons cm^{-3} are produced corresponding to the

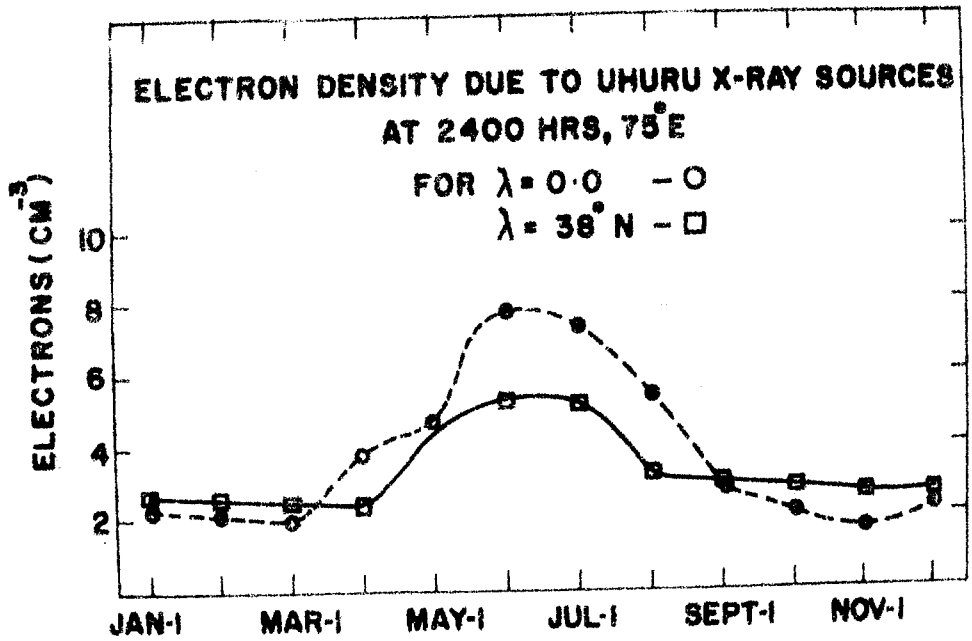

Fig. 7.12 : Electron density increases at 80 km at different times of the year due to all the Uhuru sources, corresponding to electron production rates shown in Fig. 7.11.

disposition of sources on the first day of June over the corresponding background level of six electrons cm^{-3}. The resultant electron density is thus found to be more than a factor of two of the ambient value due to the influence of the X-ray sources. In this connection, it may be mentioned that the use of more complete equation

$$\frac{dN}{dt} = Q(t) - \gamma N^2$$

for the present case of near midnight conditions and determining $Q(t)$ with and without the X-ray sources leads to the electron density values which are within 10-15% of those reported here using the simpler equation for equilibrium conditions.

The present study, thus, indicates that the integrated effect from most of the known X-ray sources results in an electron density perturbation in the night time D-region of the ionosphere at a level roughly equal to the ambient value, for midnight conditions, and during the period around the minimum of solar activity. This, in turn, should lead to a significant variation of the electron density on an annual basis. The effect is comparable in magnitude to that of Sco X-1 and should be detectable by the conventional VLF propagation techniques. By continuous monitoring of the VLF field strength or phase variation

around local midnight over a year, the integrated effect from cosmic X-ray sources should be discernible during the months of May - August.

7.5 Summary

The main points emerging from present study are the following:

1) There is a strong evidence for the detection of ionospheric effects due to strong celestial X-ray sources like Sco X-1, especially at low latitudes. Presently available evidence shows that the contributions to night-time ionization of equatorial D-region ionosphere from cosmic X-rays, cosmic rays and Lyman-α are comparable with each other.

2) The effect of these sources persists for about 2-3 hours on either side of the time corresponding to the peak effect, the extent of spread depending on the declination of the source as well as on the nature of its energy spectrum. The ionosphere behaves as an X-ray telescope with a large opening angle so far as the transit of celestial sources is concerned.

3) On an average basis, it should be possible to study systematic long-term variations of the intensity of strong X-ray sources in the time scales of a few months to a few years using the data on VLF propagation.

4) The ionospheric effects due to weak transient sources like A 1118-61 and A 0535+26 are not observable, the electron production rates for these sources being an order of magnitude lower than that due to Sco X-1. However, the effect of A 0620-00 is very significant, being comparable to that due to Sco X-1, and search of the available VLF data for the period August 3-18, 1975 should prove rewarding to identify and possibly quantify the effect of this source on the lower ionosphere. Further, distinct changes in electron production rate profile are expected due to the spectral variability of this source.

5) Study of the integrated effect of cosmic X-ray sources leads to the conclusion that the effect is roughly equal to the ambient value of electron density perturbation in night time D-region and

there should be detectable annual variation of the electron density, with the maximum effect being observed around May-August.

APPENDIX I

ENERGY RESOLUTION IN A SCINTILLATION SPECTROMETER

The processes leading to output pulse at anode of the photomultiplier tube, starting from energy deposition in the crystal are:

a) Conversion of energy deposited in the crystal into visible photons with an efficiency C_p.

b) Escape of these photons from scintillator with a probability T_p, determined by transparency of the scintillator.

c) Light collection at photocathode of photomultiplier with an efficiency G_p for that crystal-PM assembly.

d) Production of electrons by photocathode with an efficiency Q, defined as quantum efficiency of photocathode.

e) Collection of these photoelectrons at first dynode of P M tube with an efficiency F_c.

f) Multiplication in photomultiplier dynode structure with an overall gain M.

All these processes have normal statistical fluctuations as well as some effects which are non-statistical

in nature. Breitenberger (1955) has studied the detailed statistical theory of variance of output pulse amplitude distribution in terms of variance in individual processes leading to this pulse. He has shown that probabilities T_p, G_p, Q and F_c are all instrumental constants of given scintillation spectrometer and are also mutually interdependent and therefore can not be treated independently. These four probabilities can be defined by a single probability $P = T_p\ G_p\ Q\ F_c$ which is the probability that an optical photon produces a photoelectron which reaches the first dynode. P is called transfer efficiency of the spectrometer.

Thus, the mean number of electrons arriving at the anode of photomultiplier following total absorption of each photon is given by

$$\bar{N} = \bar{n} \cdot \bar{p} \cdot \bar{M}$$

where $\bar{n}$ is average number of optical photons produced by the incident photon

$\bar{p}$ is mean transfer efficiency as defined above and

$\bar{M}$ is mean overall gain of photomultiplier.

If $V(n)$, $V(p)$ and $V(M)$ are the fractional variances [defined as $\frac{(\text{standard deviation})^2}{(\text{average})^2}$ or $V(n) = \frac{\sigma_n^2}{\bar{n}^2}$] in number of photons emitted, photon transfer efficiency and electron multiplication respectively, then fractional variance in pulse height, $V(N)$, is given by (Breitenberger 1955)

$$V(N) = V(p) + \left[1+V(p)\right]\left[V(n) - \frac{1}{\bar{n}}\right] + \frac{1+V(M)}{\bar{n}\,\bar{p}} \qquad \text{(AI:1)}$$

$$\text{and } V(M) = V_1(R) + V(R)\,\frac{\bar{R}}{\bar{R}_1\,(\bar{R}-1)} \qquad \text{(AI:2)}$$

where $\bar{R}_1$ and $\bar{R}$ are mean gains of first dynode and subsequent dynodes respectively and $V_1(R)$ and $V(R)$ are their variances.

Shape of final pulse height distribution is determined by superposition of probability distribution of above parameters. Final pulse height distribution will have a Gaussian shape if parameter distribution itself is a narrow Gaussian. It can be shown that when average number of photons $\bar{n}$ emitted per scintillation is large, the shape of pulse height distribution for totally absorbed monoenergetic incident photons can be closely approximated by a Gaussian distribution. In this case, probability of obtaining a pulse height corresponding to energy E', when energy loss in crystal is E, is given by

$$P(E,E') = \frac{1}{\sqrt{2\pi}\,\sigma(E)} \exp\left[\frac{-(E-E')^2}{2\,\sigma^2\,(E)}\right]$$

The width of any distribution is usually defined in terms of the full width of pulse height distribution at half maximum of the pulse height (FWHM). For a Gaussian pulse height distribution FWHM is related to standard deviation σ by the relation

$$FWHM = 2\sqrt{2\ln 2}\,\sigma(E) = 2.354\,\sigma(E)$$

A useful figure of merit for a photon spectrometer is the ratio of the full width of the pulse height distribution at half maximum of pulse height to the pulse height at the maximum of distribution. This quantity, commonly known as resolution, can be written in terms of fractional variance as

$$\eta^2 = \frac{(FWHM)^2}{(\bar{N})^2} = 5.56\,\frac{\sigma^2}{(\bar{N})^2} = 5.56\,V(N)$$

$$\text{or } \eta = 2.354\sqrt{V(N)}$$

For getting best resolution (i.e. smallest practicable value of η) even in presence of $V(p)$ and nonstatistical variance in $V(n)$, we see from equations AI:1 and AI:2 that

i) $\bar{n}$ should be large i.e. the scintillator must have a high scintillation efficiency.

ii) Photon transfer efficiency $\bar{p}$ must be made as high as possible by increasing the light collection, through use of suitable optical coupling between the phosphor and photomultiplier to minimise the loss due to total internal reflection at the phosphor - photomultiplier interface; by the use of photomultiplier with high quantum efficiency in the wave length region in which phosphor emits; and by choice of photomultiplier which collects a large fraction of photoelectrons emitted by the photocathode at the first dynode. Also, the electrons emitted by photocathode should be shielded from magnetic fields, including earth's magnetic field, to prevent them being deflected away from the dynode, which can be achieved by enclosing the photomultiplier tube within a magnetic shield.

iii) R_1 should be large, i.e. first dynode gain should be high, so that V(M) is small. This can be done by keeping the voltage between cathode and first dynode as high as the tube will permit without increasing the tube noise.

The non-statistical terms in variance of n, p and M are due to:

i) Local variations in the luminescence efficiency of phosphor, produced by inhomogeneities in the activator concentration, lattice effect etc.

ii) Differing photon collection efficiency of photocathode from event to event for scintillations occuring at different points in the phosphor, because of variations in optical geometry and presence of optical flaws in crystal. Also, photocathode conversion efficiency differs from one point to another. This effect can be minimised by choosing phosphors free from optical flaws (so that it has same transparency at every point) and by the use of a short light pipe between crystal and photomultiplier, which distributes light over a larger area of photocathode to reduce the effect of non-uniformity in response of photocathode.

iii) Variation in fraction of electrons collected by dynodes, especially the first, because of poor focussing and inhomogeneous dynode surfaces. This can be minimised through choice of a good photomultiplier tube and by enclosing it in a magnetic shield.

In the ideal case when non-statistical fluctuations in $\bar{n}$ and M are negligible and only normal Poisson fluctuations occur in the production of photons in the scintillator ($\sigma = \sqrt{\bar{n}}$; $V(n) = \frac{1}{\bar{n}}$), in the multiplication process in photomultiplier tube ($\sigma_R = \sqrt{\bar{R}}$; $V(R) = \frac{1}{\bar{R}}$) and photon transfer efficiency remains constant [$V(p) = 0$], fractional variance in final pulse height will be given by

$$V(N) = \frac{1+V(M)}{\bar{n}\,\bar{p}} \qquad \text{(AI:3)}$$

where

$$V(M) = V_1(R) + V(R)\frac{\bar{R}}{R_1(\bar{R}-1)} \qquad \text{(AI:4)}$$

$$= V(R)\frac{\bar{R}}{\bar{R}-1} \quad \text{assuming same average gain for each dynode; } R_1 = R$$

$$= \frac{1}{\bar{R}}\,\frac{\bar{R}}{\bar{R}-1} = \frac{1}{\bar{R}-1} \qquad \text{(AI:5)}$$

A NaI (Tl) scintillator has a scintillation efficiency of $\sim$ 13%. The fluorescent photons are emitted at wavelength close to 4200 $\mathring{A}$ ($h\nu$ = 3 e V). Thus we require $(3.0/_{0.13})$ e V or 23 e V per fluorescent photon.

Thus, average number of optical photons for an incident X-ray photon of energy E keV will be

$$\bar{n} = \frac{E}{.023}$$

Also, light collection to photocathode is rarely better than 60% and photocathode efficiency of an S-11 cathode (like say in RCA 8055 PM tube used in present experiment) is about 20%.

Therefore, $\bar{p} = .6 \times .2 = .12$, assuming 100% transparency of crystal to its own radiation and collection of all photoelectrons at first dynode.

Total gain of a typical photomultiplier tube is $\sim 10^6$, which gives $\bar{R} \approx 4$ for a 10 dynode stage photomultiplier tube.

$$\text{Therefore, } V(M) = \frac{1}{4-1} = .33$$

Substituting above values in equation AI:3 we get fractional variance in pulse height as

$$V(N) = \frac{1.33}{.12 \times \bar{n}} = \frac{11}{\bar{n}} = \frac{11 \times .023}{E} = \frac{.25}{E}$$

and resolution η is

$$\eta = 2.35\sqrt{V(N)} = \frac{2.35 \times \sqrt{.25}}{\sqrt{E}} = \frac{2.35 \times .5}{\sqrt{E}}$$

$$\text{or } \eta \approx 1.2\ E^{-0.5}$$

and

$$\sigma = \sqrt{V(N) \cdot E^2} = \sqrt{\frac{.25}{E} \cdot E^2} = \sqrt{.25E}$$

$$\text{or } \sigma \approx .5\sqrt{E}$$

Thus, in ideal case σ varies as $.5E^{-\frac{1}{2}}$. But in practice such small value of σ is rarely achieved, because in

practical spectrometers V(p), V(n) and V(M) have both non-statistical as well as statistical terms. The values of these terms are different for different scintillator - photomultiplier tube assemblies, and can not be completely determined theoretically. In addition to the theoretical estimates, the shape and width of pulse height distribution for X-ray telescopes used in present experiments were also evaluated using radioactive sources, as described in Chapter II.

REFERENCES

Abt, H.A., Hintzen, P., and Levy, S.G.	1977	Astrophys. J., 213, 815.
Agrawal, P.C., Gokhale, G.S., Iyengar, V.S., Kunte, P.K., Manchanda, R.K., and Sreekantan, B.V.	1971	Nature, 232, 38.
Agrawal, P.C.	1972	Ph.D. Thesis, Univ. Bombay.
Agrawal, P.C., Gokhale, G.S., Iyengar, V.S., Kunte, P.K., Manchanda, R.K., and Sreekantan, B.V.	1972a	Nature, 238, 22.
Agrawal, P.C., Gokhale, G.S., Iyengar, V.S., Kunte, P.K., Manchanda, R.K., and Sreekantan, B.V.	1972b	Astrophys. Space Sci., 18, 408.
Ananthakrishnan, S.	1969	Ph.D. Thesis, Univ. Gujarat.
Ananthakrishnan, S., and Ramanathan, K.R.	1969	Nature, 223, 488.
Auriemma, G., Cardini, D., Costa, E., Giovannelli, F., Orciuolo, M., and Ranieri, M.	1976	Nature, 259, 27.
Avni, Y., and Bahcall, J.N.	1975	Astrophys. J., 197, 675.
Bahcall, J.N., Dyson, F.J., Katz, J.I., and Paczynski, B.	1974	Astrophys. J., Lett., 189, L17.
Bahcall, J.N.	1975	Lectures at Enrico Fermi Summer School, Varenna, on the Phys. and Astrophys. of Neut. Stars and Black Holes, N. Holl. Pub. Co., Amster.
Bahcall, J.N., and Ostriker, J.P.	1975	Nature, 256, 23.

Bailey, D.K.	1968	Rev. Geophys., 6, 289.
Baity, W.A., Ulmer, M.P., Wheaton, W.A., and Peterson, L.E.	1973	Nature Phys. Sci., 245, 90.
Baker, K.D., Nagy, A.F., Olsen, R.O., Oran, E.S., Randhawa, J., Strobel, D.F., and Tohmatsu, T.	1977	J. Geophys. Res., 82, 3281.
Baker, R.E., Lovett, R.R., Orford, K.J., and Ramsden, D.	1973	Nature Phys. Sci., 245, 18.
Barth, C.A.	1966	Ann. Geophys., 22, 198.
Basko, M.M., and Sunyaev, R.A.	1973	Astrophys. Space Sci., 23, 117.
Bingham, R.G., and Clark, C.D.	1969	Astrophys. J., 158, 207.
Bisnovatyi-Kogan, G.S., and Blinnikov, S.I.	1977	Astron. Astrophys., 59, 111.
Bleeker, J.A.M., Burger, J.J., Deerenberg, A.J.M., Scheepmaker, A., Swanenburg, B.N., and Tanaka, Y.	1967	Astrophys. J., 147, 391.
Bochkarev, N.G., Karitskaya, E.A., and Shakura, N.I.	1975	Sov. Astron. Lett., 1, 118.
Boldt, E., McDonald, F.B., Riegler, G., and Serlemitsos, P.	1966	Phys. Rev. Lett., 17, 447.
Boldt, E., Holt, S., Rothschild, R. and Serlemitsos, P.	1975	Proc. Intl. Conf. X-rays in Space, ed. D. Venkatesan, U.of Calgary Press, pp 69.
Bolton, C.T.	1972a	Nature, 235, 271.
Bolton, C.T.	1972b	Nature Phys. Sci., 240, 124.
Bolton, C.T.	1975	Astrophys. J., 200, 269.
Bowyer, S., Byram, E.T., Chubb, T.A., and Friedman, H.	1965	Science, 147, 394.
Braes, L.L.E., and Miley, G.K.	1971	Nature, 232, 246.
Braes, L.L.E., and Miley, G.K.	1972	Nature Phys.Sci., 235, 147.

Brecher, K., and Caporaso, G.	1976	Nature, 259, 377.
Bregman, J., Butler, D., Kemper, E., Koski, A., Kraft, R.P., and Stone, R.P.S.	1973	Astrophys. J., Lett., 185, L 117.
Breitenberger, E.	1955	"Scintillation Spectrometer Statistics" in Progress in Nuclear Physics, ed. O.R. Frisch, Vol. 4, pp 56, Pergamon Press (N.Y.).
Brini, D., Cattani, D., Ciriegi, U., Fuligni, F., Galli, M., Gandolfi, A., Moretti, E., and Sacchi, C.	1965	Ann. Astrophys., 28, 1034.
Brinkman, A.C., Parsignault, D.R., Schreier, E., Gursky, H., Kellogg, E.M., Tananbaum, H., and Giacconi, R.	1974	Astrophys. J., 188, 603.
Brisken, A.F.	1973	Ph.D. Thesis, Univ. Maryland, GSFC X-660-73-245.
Brown, R.L., and Gould, R.J.	1970	Phys. Rev. D., 1, 2252.
Brucato, R., and Kristian, J.	1973	Astrophys. J., Lett., 179, L 129.
Burgess, B., and Jones, T.B.	1969	Nature, 224, 680.
Byram, E.T., Chubb, T.A., and Friedman, H.	1966	Science, 152, 66.
Canizares, C.R.	1976	Astrophys. J., Lett., 207, L 101.
Canizares, C.R., and Oda, M.	1977	Astrophys. J., Lett., 214, L 119.
Carpenter, G.F., Eyles, C.J., Skinner, G.K., Wilson, A.M., and Willmore, A.P.	1977	Mon. Not. R. Astr. Soc., 179, 27 P.
Chamberlain, J.W.	1961	Physics of the Aurora and Airglow, Academic Press.

Charman, W.N., Drever, R.W.P., Fruin, J.H., Jelley, J.V., Elliot, J.L., Fazio, G.G., Hearn, D.R., Helmken, H.F., Rieke, G.H., and Weekes, T.C.	1970	I.A.U. Symp. No.37 on Non-Solar X- and Gamma-Ray Astronomy (Ed. Gratton, L.), D.Reidel, pp 41.
Chodil, G., Mark, H., Rodrigues, R., and Swift, C.D.	1968a	Astrophys. J., Lett., 151, L 1.
Chodil, G., Mark, H., Rodrigues, R., Seward, F.D., Swift, C.D., Turiel, I., Hiltner, W.A., Wallerstein, G., and Mannery, E.J.	1968b	Astrophys. J., 154, 645.
C.I.R.A.	1972	COSPAR International Reference Atmosphere, Akademie-Verlag, Berlin.
Clark, G.W.	1965	Phys. Rev. Lett., 14, 91.
Clark, G.W., Lewin, W.H.G., and Smith, W.B.	1968	Astrophys. J., 151, 21.
Cline, T.L., and Desai, U.D.	1975	Astrophys. J., Lett., 196, L 43.
Coe, M.J., Engel, A.R., and Quenby, J.J.	1976	Nature, 259, 544.
Cooke, B.A., Ricketts, M.J., Maccacaro, T., Pye, J.P., Elvis, M., Watson, M.G., Griffiths, R.E., Pounds, K.A., McHardy, I., Maccagni, D., Seward, F.D., Page, C.G., and Turner, M.J.L.	1978	Mon. Not. R.Astr. Soc., 182, 489.
Coyne, G.V., Gehrels, T., and Serkowski, K.	1974	Astron. J., 79, 581.
Cruddace, R., Bowyer, S., Lampton, M., Mack, J., and Margon, B.	1972	Astrophys. J., 174, 529.
Davidson, K., and Ostriker, J.P.	1973	Astrophys. J., 179, 585.
Deeks, D.G.	1966	Proc. R.Soc. London, Ser. A., 291, 413.
Dolan, J.F.	1970	Space Sci. Rev., 10, 830.

Dolan, J.F., Crannell, C.J., Dennis, B.R., Frost, K.J., and Orwig, L.E.	1977a	Nature, 267, 813.
Dolan, J.F., Dennis, B.R., Crannell, C.J., Frost, K.J., and Orwig, L.E.	1977b	Highlights of Astronomy, ed.E.A. Müller, Vol.4, pp 99.
Downes, D.	1970	Ph.D. Thesis, Univ. Harvard.
Eardley, D.M., Lightman, A.P., and Shapiro, S.L.	1975	Astrophys. J., Lett., 199, L 153.
Eardley, D.M.	1976	Symp. on X-ray Binaries, ed. Y. Kondo and E. Boldt, (NASA SP-389, Greenbelt, MD), pp 379.
Eardley, D.M., and Lightman, A.P.	1976	Nature, 262, 196.
Edwards, P.J., Burtt, G.J., and Knox, F.	1969	Nature, 222, 1053.
Elliot, J.L.	1972	Smithsonian Astrophys. Obs., Spec. Rep. 341.
Elvis, M., Page, C.G., Pounds, K.A., Ricketts, M.J., and Turner, M.J.L.	1975	Nature, 257, 656.
Evans, R.D.	1955	Atomic Nucleus Mc Graw Hill.
Evseyev, O.A., Mansurov, V.N., Pavlova, V.S., Pustilnik, L.A., Shvartsman, V.F., Tsarevsky, G.S., and Yakushev, A.K.	1974	I.A.U. Symposium No.67. on Variable Stars and Stellar Evolution, ed. V.E.Sherwood and L. Plaut, pp 477.
Fabian, A.C., Pringle, J.E., and Whelan, J.A.J.	1974	Nature, 247, 351.
Fazio, G.G.	1974	Methods of Exp. Phys., (Ed. Marton, L.), Vol. 12, 315, Academic Press.
Forman, W., Jones, C., and Tananbaum, H.	1976	Astrophys. J., 208, 849.

Forman, W., Jones, C., Cominsky, L., Julien, P., Murray, S., Peters, G., Tananbaum, H., and Giacconi, R.	1978	Astrophys. J., Suppl. Ser. No.4, 38, 357.
Francey, R.J.	1970	J. Geophys. Res., 75, 4849.
Fritz, G., Henry, R.C., Meekins, J.F., Chubb, T.A., and Friedman, H.	1969	Science, 164, 709.
Frontera, F., and Fuligni, F.	1975a	Astrophys. J., 196, 597.
Frontera, F., and Fuligni, F.	1975b	Astrophys. J., Lett., 198, L 105.
Frontera, F., and Fuligni, F.	1976	Astrophys. Space Sci., 42, 185.
Fuligni, F., and Frontera, F.	1973	Astron. Astrophys., 28, 373.
Gehrels, T.	1972	Astrophys. J., Lett., 173, L 23.
Giacconi, R., Gursky, H., Paolini, F.R., and Rossi, B.B.	1962	Phys. Rev. Lett., 9, 439.
Giacconi, R., Murray, S., Gursky, H., Kellogg, E., Schreir, E., Matilsky, T., Koch, D., and Tananbaum, H.	1974	Astrophys. J., Suppl. Ser. No.237, 27, 37.
Glass, I.S.	1969	Astrophys. J., 157, 215.
Gorenstein, P., Kellogg, E.M., and Gursky, H.	1969	Astrophys. J., 156, 315.
Gorenstein, P., and Tucker, W.H.	1976	Annu. Rev. Astron. Astrophys., 14, 373.
Grader, R.J., Hill, R.W., Seward, F.D., and Toor, A.	1966	Science, 152, 1499.
Gursky, H., Giacconi, R., Gorenstein, P., Waters, J.R., Oda, M., Bradt, H., Garmire, G., and Sreekantan, B.V.	1966	Astrophys. J., 146, 310.

Gursky, H., Gorenstein, P., Kerr, F.J., and Grayzeck, E.J.	1971	Astrophys. J., Lett., 167, L 15.
Haymes, R.C., Ellis, D.V., Fishman, G.J., Glenn, S.W., and Kurfess, J.D.	1968	Astrophys. J., Lett., 151, L 125.
Haymes, R.C., and Harnden, F.R., Jr.	1970	Astrophys. J., 159, 1111.
Heise, J., Brinkman, A.C., Schrijver, J., Mewe, R., den Boggende, A., Gronenschild, E., Parsignault, E., Grindlay, J., Schnopper, H., Schreier, E., and Gursky, H.	1975	Nature, 256, 107.
Hilditch, R.W., and Hill, G.	1974	Mon. Not. R. Astr. Soc., 168, 543.
Hill, R.W., Burginyon, G.A., and Seward, F.D.	1975	Astrophys. J., 200, 709.
Hiltner, W.A.	1956	Astrophys. J. Suppl. Ser., 2, 389.
Hinteregger, H.E.	1965	Space Sci. Rev., 4, 461.
Hjellming, R.M., and Wade, C.M.	1971	Astrophys. J., Lett., 168, L 21.
Hjellming, R.M.	1973	Astrophys. J., Lett., 182, L 29.
Hjellming, R.M., Gibson, D.M., and Owen, F.N.	1975	Nature, 256, 111.
Hjellming, R.M.	1976	Symp. on X-ray Binaries, ed. Y.Kondo and E. Boldt, (NASA SP-389, Greenbelt, MD), pp 495.
Holt, S.S., Boldt, E.A., Schwartz, D.A., Serlemitsos, P.J., and Bleach, R.D.	1971	Astrophys. J., Lett., 166, L 65.
Holt, S.S., Boldt, E.A., Kaluzienski, L.J., and Serlemitsos, P.J.	1975	Nature, 256, 108.

Holt, S.S., Boldt, E.A., Serlemitsos, P.J., and Kaluzienski, L.J.	1976a	Astrophys. J., Lett., 203, L 63.
Holt, S.S., Kaluzienski, L.J., Boldt, E.A., and Serlemitsos, P.J.	1976b	Nature, 261, 213.
Hutchings, J.B., Crampton, D., Glospey, J., and Walker, G.A.H.	1973	Astrophys. J., 182, 549.
Ichimaru, S.	1977	Astrophys. J., 214, 840.
Illarionov, A.F., and Sunyaev, R.A.	1975	Astron. Astrophys., 39, 185.
Imhof, W.L., Nakano, G.H., Johnson, R.G., Kilner, J.R., Reagan, J.B., Klebesadel, R.W., and Strong, R.B.	1974	Astrophys. J., Lett., 191, L 7.
Ives, J.C., Sanford, P.W., and Bell-Burnell, S.J.	1975	Nature, 254, 578.
Jayanthi, U.B.	1973	Ph.D. Thesis, Univ. Gujarat.
Jones, C.	1977	Astrophys. J., 214, 856.
Kane, S.R., and Share, G.H.	1977	Astrophys. J., 217, 549.
Katz, J.I.	1976	Astrophys. J., 206, 910.
Kaufmann, P., Paes de Barros, M.H., and Nepomuceno Vianna, E.	1970	Nature, 228, 1080.
Kellogg, E.M.	1975	Astrophys. J., 197, 689.
Kemp, J.C., Herman, L.C., Rudy, R.J., and Barbour, M.S.	1977	Nature, 270, 227.
Kemp, J.C., Barbour, M.S., Herman, L.C., and Rudy, R.J.	1978	Astrophys. J., Lett., 220, L 123.
Lamb, F.K., Pethick, C.J., and Pines, D.	1973	Astrophys. J., 184, 271.

Lamers, H.J.G.L.M., van den Heuvel, E.P.J., and Petterson, J.A.	1976	Astron. Astrophys., 49, 327.
Landau, L.D., and Lifshitz, E.M.	1959	Fluid Mechanics, Pergamon Press.
Lanning, H.H.	1975	Mon. Not. R. Astr. Soc., 173, 15 P.
Lester, D.F., Nolt, I.G., and Radostitz, J.V.	1973	Nature Phys. Sci., 241, 125.
Lester, D.F., Nolt, I.G., Stearns, S.A., Straton, P., and Radostitz, J.V.	1976	Astrophys. J., 205, 855.
Lewin, W.H.G., Clark, G.W., and Smith, W.B.	1968	Canadian J. Phys., 46, S 409.
Lewin, W.H.G.	1977	Mon.Not.R.Astr.Soc., 179, 43.
Li, F.K., and Clark, G.W.	1974	Astrophys. J., Lett., 191, L 27.
Liang, E.P.T., and Price, R.H.	1977	Astrophys. J., 218, 247.
Liden, K., and Starfelt, N.	1954	Arkiv Fur Fysik, 7, 427.
Lightman, A.P., and Eardley, D.M.	1974	Astrophys. J., Lett., 187, L 1.
Lyutyi, V.M., Syunyaev, R.A., and Cherepaschuk, A.M.	1973	Sov. Astron. -A.J., 17, 1.
Manchanda, R.K., Iyengar, V.S., Agrawal, P.C., Gokhale, G.S., Kunte, P.K., and Sreekantan, B.V.	1971	Nature Phys. Sci., 232, 190.
Margon, B., Bowyer, S., Lampton, M., and Cruddace, R.	1971	Astrophys. J., Lett., 169, L 45.
Margon, B., Bowyer, S., and Stone, R.P.S.	1973	Astrophys. J., Lett., 185, L 113.
Markert, T.H., Bradt, H.V., Clark, G.W., Lewin, W.H.G., Li, F.K., Schnopper, H.W., Sprott, G.F., and Wargo, G.F.	1975	I.A.U. Circ. No.2765.

Markert, T.H., Canizares, C.R., Clark, G.W., Li, F.K., Northridge, P.L., Sprott, G.F., and Wargo, G.F.	1976	Astrophys. J., 206, 265.
Markert, T.H., Canizares, C.R., Clark, G.W., Hearn, D.R., Li, F.K., Sprott, G.F., and Winkler, P.F.	1977	Astrophys. J., 218, 801.
Mason, K.O., Hawkins, F.J., Sanford, P.W., Murdin, P., and Savage, A.	1974	Astrophys. J., Lett., 192, L 65.
Matsuoka, M.	1970	Institute of Space and Aeronautical Science, University of Tokyo, Report No.445.
Matteson J.L.	1971	Ph.D. Thesis, Univ. California, San Diego, La Jolla.
Matteson, J.L., Mushotzky, R.F., Paciesas, W.S., and Laros, J.G.	1976	Symp. on X-Ray Binaries, ed.Y.Kondo and E. Boldt, (NASA SP-389, Greenbelt, MD), pp 407.
McClintock, J.E., Lewin, W.H.G., Sullivan, R.J., and Clark, G.W.	1969	Nature, 223, 162.
McCracken, K.G.	1966	Science, 154, 1000.
Mechtly, E.A., and Smith, L.G.	1968	J. Atmos. Terr. Phys., 30, 363.
Meier, R.R.	1970	Space Res. X, 572.
Meira, L.G., Jr.	1971	J. Geophys. Res., 76, 202.
Meszaros, P.	1975	Nature, 258, 583.
Metzger, A.E., and Dolan, J.F.	1968	Astron. J., 73, S 107.
Metzger, A.E., Parker, R.H., Gilman, D., Peterson, L.E., and Trombka, J.I.	1974	Astrophys. J., Lett., 194, L 19.
Michalsky, J.J., Swedlund, J.B., and Avery, R.W.	1975a	Nature, 254, 39.

Michalsky, J.J., Swedlund, J.B., and Stokes, R.A.	1975b	Astrophys. J., Lett., 198, L 101.
Michalsky, J.J., and Swedlund, J.B.	1977	Astrophys. J., 212, 221.
Milgrom, M., and Shaham, J.	1977	Nature, 270, 228.
Mitra, A.P.	1966	J. Atmos. Terr. Phys., 28, 945.
Mitra, A.P.	1968	J. Atmos. Terr. Phys., 30, 1065.
Mitra, A.P.	1969	Space Res. IX, 418.
Miyamoto, S., Fujii, M., Matsuoka, M., Nishimura, J., Oda, M., Ogawara, Y., Ohta, S., and Wada, M.	1971	Astrophys. J., Lett., 168, L 11.
Mohanty, D.K., Balasubramanian, V., and Swarup, G.	1971	Nature Phys. Sci., 232, 191.
Muller, E.	1935	Z. Astrophys., 10, 52.
Nakagawa, M., Sakurai, H., and Kitamura, T.	1973	Proc. 13th International Cosmic Ray Conference, Vol.1, pp 73.
Nicolet, M., and Aikin, A.C.	1960	J. Geophys. Res., 65, 1469.
Nicolet, M.	1965	J. Geophys. Res., 70, 679 and 691.
Nishimura, J., Fujii, M., Tawara, Y., Oda, M., Ogawara, Y., Yamagami, T., Miyamoto, S., Kajiwara, M., Murakami, H., Yoshimori, M., Nakagawa, M., and Sakurai, T.	1978	Nature, 272, 337.
Nolt, I.G., Kemp, J.C., Rudy, R.J., Southwick, R.G., Radostitz, J.V., and Caroff, L.J.	1975	Astrophys. J., Lett., 199, L 27.
Novikov, I.D., and Thorne, K.S.	1973	Black Holes, ed.C. DeWitt and B.S. DeWitt, Gordon and Breach (N.Y.)

Oda, M., Clark, G., Garmire, G., Wada, M., Giacconi, R., Gursky, H., and Waters, J.	1965	Nature, 205, 554.
Oda, M., Gorenstein, P., Gursky, H., Kellogg, E., Schreier, E., Tananbaum, H., and Giacconi, R.	1971	Astrophys. J., Lett., 166, L 1.
Oda, M., Wada, M., Matsuoka, M., Miyamoto, S., Muranaka, N., and Ogawara, Y.	1972	Astrophys. J., Lett., 172, L 13.
Oda, M., Takagishi, K., Matsuoka, M., Miyamoto, S., and Ogawara, Y.	1974	Publ. Astron. Soc. Japan, 26, 303.
Oda, M., Doi, K., Ogawara, Y., Takagishi, K., and Wada, M.	1976	Astrophys. Sp. Sci., 42, 223.
Oda, M.	1977	Space Sci. Rev., 20, 757.
Ogawara, Y., Matsuoka, M., Miyamoto, S., Muranaka, N., Nishimura, J., and Oda, M.	1976	Astrophys. Sp. Sci., 42, 211.
Ogawara, Y., Doi, K., Matsuoka, M., Miyamoto, S., and Oda, M.	1977	Nature, 270, 154.
O'Mongain, E., and Weekes, T.C.	1974	Publ. Astron. Soc. Pacific., 86, 470.
O'Mongain, E., and Baird, G.A.	1976	Astrophys. Sp. Sci., 42, 63.
Overbeck, J.W., Womack, E.A., and Tananbaum, H.D.	1967	Astrophys. J., 150, 47.
Overbeck, J.W.	1968	NASA Contract. Rep., NASA CR-1045.
Overbeck, J.W., and Tananbaum, H.D.	1968a	Astrophys. J., 153, 899.
Overbeck, J.W., and Tananbaum, H.D.	1968b	Phys. Rev. Lett., 20, 24.
Parsignault, D.R., Epstein, A., Grindlay, J., Schreier, E., Schnopper, H., Gursky, H., Tanaka, Y., Brinkman, A.C., Heise, J., Schrijver, J., Mewe, R., Gronenschild, E., and den Boggende, A.	1976	Astrophys. Sp. Sci., 42, 175.

Pearce, J.B.	1969	J. Geophys. Res., 74, 853.
Peterson, L.E., Jacobson, A.S., Pelling, R.M., and Schwartz, D.A.	1968	Canadian J. Phys., 46, S 437.
Peterson, L.E.	1970	Non-Solar X - and Gamma-Ray Astronomy, I.A.U. Symp.No.37, ed.L.Gratton, D. Reidel.
Pietsch, W., Kendziorra, E., Staubert, R., and Trümper, J.	1976	Astrophys. J., Lett., 203, L 67.
Poppoff, I.G., and Whitten, R.C.	1962	J. Geophys. Res., 67, 2986.
Poppoff, I.G., and Whitten, R.C.	1969	Nature, 224, 1187.
Poppoff, I.G., Whitten, R.C., and Willoughby, D.S.	1975	J. Atmos. Terr. Phys., 37, 835.
Potemra, T.A., Zmuda, A.J., Haave, C.R., and Shaw, B.W.	1969	J. Geophys. Res., 74, 6444.
Pounds, K.A.	1976	Comments Astrophys., 6, 145.
Pozdnyakov, L.A., Sobol', I.M., and Sunyaev, R.A.	1976	Sov. Astron. Lett., 2, 55.
Prakasarao, A.S., Sharma, D.P., Jayanthi, U.B., and Rao, U.R.	1971	Astrophys. Space Sci., 10, 150.
Prendergast, K.H., and Taam, R.E.	1974	Astrophys. J., 189, 125.
Price, W.J.	1964	Nuclear Radiation Detection, McGraw Hill.
Pringle, J.E., and Rees, M.J.	1972	Astron. Astrophys., 21, 1.
Pringle, J.E., Rees, M.J., and Pacholczyk, A.G.	1973	Astron. Astrophys., 29, 179.
Rao, U.R., Kasturirangan, K., Sharma, D.P., and Radha, M.S.	1976	Nature, 260, 307.
Rappaport, S., Zaumen, W., and Doxsey, R.	1971a	Astrophys. J., Lett., 168, L 17.

Rappaport, S., Doxsey, R., and Zaumen, W.	1971b	Astrophys. J., Lett., 168, L 43.
Rawer, K.	1952	The Ionosphere, Frederick Ungar Publishing Co. (N.Y.).
Reinert, C.P.	1969	Ph.D. Thesis, Univ. Minnesota Tech. Rep. CR-132.
Rhoades, C.E., Jr., and Ruffini, R.	1974	Phys. Rev. Lett., 32, 324.
Ricketts, M.J., Turner, M.J.L., Page, C.G., and Pounds, K.A.	1975a	Nature, 256, 631.
Ricketts, M.J., Pounds, K.A., and Turner, M.J.L.	1975b	Nature, 257, 657.
Riegler, G.R., Boldt, E., and Serlemitsos, P.	1968	Astrophys. J., Lett., 153, L 95.
Riegler, G.R.	1969	Ph.D. Thesis, Univ. Maryland, NASA Report X-611-69-1.
Robinson, E.L., Nather, R.E., Africano, J., and Smith, B.	1978	Nature, 271, 40.
Rocchia, R., Rothenflug, R., Boclet, D., and Durouchoux, Ph.	1969	Astron. Astrophys., 1, 48.
Rosenberg, F.D., Eyles, C.J., Skinner, G.K., and Willmore, A.P.	1975	Nature, 256, 628.
Rothschild, R.E., Boldt, E.A., Holt S.S., and Serlemitsos, P.J.	1974	Astrophys. J., Lett., 189, L 13.
Rothschild, R.E., Boldt, E.A., Holt, S.S., and Serlemitsos, P.J.	1977	Astrophys. J., 213, 818.
Ruderman, M.	1975	Ann. N Y Acad. Sci., 262, 164.
Sandage, A.R., Osmer, P., Giacconi, R., Gorenstein, P., Gursky, H., Waters, J., Bradt, H., Garmire, G., Sreekantan, B.V., Oda, M., Osawa, K., and Jugaku, J.	1966	Astrophys. J., 146, 316.

Sanford, P.W., Ives, J.C., Bell-Burnell, S.J., Mason, K.O., and Murdin, P.	1975	Nature, 256, 109.
Schreier, E., Gursky, H., Kellogg, E., Tananbaum, H., and Giacconi, R.	1971	Astrophys. J., Lett., 170, L 21.
Seward, F.D.	1970	An illustrated catalog of cosmic X-ray sources, LLL Report UCID-15622.
Seward, F.D., Page, C.G., Turner, M.J.L., and Pounds, K.A.	1976a	Mon. Not. R. Astr. Soc., 175, 39P.
Seward, F.D., Page, C.G., Turner, M.J.L., and Pounds, K.A.	1976b	Mon. Not. R. Astr. Soc., 177, 13P.
Shakura, N.I., and Sunyaev, R.A.	1973	Astron. Astrophys., 24, 337.
Shakura, N.I., and Sunyaev, R.A.	1976	Mon. Not. R. Astr. Soc., 175, 613.
Shapiro, S.L.	1973	Astrophys. J., 185, 69.
Shapiro, S.L., and Lightman, A.P.	1976	Astrophys. J., 204, 555.
Shapiro, S.L., Lightman, A.P., and Eardley, D.M.	1976	Astrophys. J., 204, 187.
Sharma, D.P., Jain, A.K., Kasturirangan, K., Jayanthi, U.B., and Rao, U.R.	1973	Nature Phys. Sci., 246, 107.
Shibazaki, N., and Hoshi, R.	1975	Progr. Theor.Phys., 54, 706.
Shields, G.A., and Wheeler, J.C.	1976	Astrophys. Lett., 17, 69.
Shipman, H.L.	1975	Astrophys. Lett., 16, 9.
Shulman, S., Fritz, G., Meekins, J.F., Friedman, H., and Meidav, M.	1971	Astrophys. J., Lett., 168, L 49.
Shvartsman, V.F.	1971	Sov. Astron-AJ, 15, 377.

Silk, J., and Arons, J.	1975	Astrophys. J., Lett., 200, L 131.
Smith, H.E., Margon, B., and Conti, P.S.	1973	Astrophys. J., Lett., 179, L 125.
Sommer, M., Maurus, H., and Urbach, R.	1976	Nature, 263, 752.
Spiegel, E.A.	1971	Annu. Rev. Astron. Astrophys., 9, 323.
Stein, J.A., and Lewin, W.H.G.	1967	J.Geophys. Res., 72, 383.
Stevens, J.C., Garmire, G.P., and Riegler, G.R.	1972	Astrophys. J., Lett., 175, L 73.
Strong, I.B.	1975	Proc. 14th International Cosmic Ray Conference, Vol.1, pp 237.
Strong, I.B., Klebesadel, R.W., and Evans, W.D.	1975	Ann. NY Acad. Sci., 262, 145.
Strong, I.B., and Klebesadel, R.W.	Oct., 1976	Sci. American, 235, 66.
Subbaraya, B.H., Prakash, S., and Gupta, S.P.	1971	Indian J. Pure Appl. Phys., 9, 626.
Sutherland, P.G., Weisskopf, M.C., and Kahn, S.M.	1978	Astrophys. J., 219, 1029.
Swider, W., Jr.	1969	Rev.Geophys., 7, 573.
Tananbaum, H., Kellogg, E., Gursky, H., Murray, S., Schreier, E., and Giacconi, R.	1971	Astrophys. J., Lett., 165, L 37.
Tananbaum, H., Gursky, H., Kellogg, E., Giacconi, R., and Jones, C.	1972	Astrophys. J., Lett., 177, L 5.
Taylor, J.H., Hugu enin, G.R., and Hirsch, R.M.	1972	Astrophys. J., Lett., 172, L 17.
Terrell, N.J., Jr.	1972	Astrophys. J., Lett., 174, L 35.
Thomas, L.	1971	J.Atmos. Terr. Phys., 33, 157.

Thorne, K.S., and Price, R.H.	1975	Astrophys. J., Lett., 195, L 101.
Tohmatsu, T., and Iwagami, N.	1975	Space Res. XV, 241.
Trimble, V., Rose, W.K., and Weber, J.	1973	Mon. Not. R. Astr. Soc., 162, 1 P.
Ulmer, M.P., Baity, W.A., Wheaton, Wm. A., and Peterson, L.E.	1974	Astrophys. J., 192, 691.
Ulmer, M.P.	1975	Astrophys. J., 196, 827.
van den Heuvel, E.P.J.	1975	Astrophys. J., Lett., 198, L 109.
Velinov, P.	1968	J. Atmos. Terr. Phys., 30, 1891.
Villa, G., Page, C.G., Turner, M.J.L., Cooke, B.A., Ricketts, M.J., Pounds, K.A., and Adams, D.J.	1976	Mon. Not. R. Astr. Soc., 176, 609.
Wade, C.M., and Hjellming, R.M.	1972	Nature, 235, 271.
Wagner, Ch.U.	1966	J. Atmos. Terr. Phys., 28, 607.
Walborn, N.R.	1973	Astrophys. J., Lett., 179, L 123.
Walker, E.N.	1972	Mon. Not. R. Astr. Soc., 160, 9 P.
Walker, E.N., and Rolland Quintanilla, A.	1974	Mon. Not. R. Astr. Soc., 169, 247.
Walker, E.N., Watson, M.G., and Holt, S.S.	1977	Nature, 270, 230.
Walker, E.N., and Rolland Quintanilla, A.	1978	Mon. Not. R. Astr. Soc., 182, 315.
Watanabe, K.	1958	Advances in Geophysics, Vol.5, 153, Academic Press (N.Y.).
Webber, W.R., and Reinert, C.P.	1970	Astrophys. J., 162, 883.

Webster, B.L., and Murdin, P.	1972	Nature, 235, 37.
Weekes, T.C.	1976	J. Atmos. Terr. Phys., 38, 1021.
Weisskopf, M.C., Kahn, S.M., and Sutherland, P.G.	1975	Astrophys. J., Lett., 199, L 147.
Weisskopf, M.C., Silver, E.H., Kestenbaum, H.L., Long, K.S., Novick, R., and Wolff, R.S.	1977	Astrophys. J., Lett., 215, L 65.
Weisskopf, M.C., and Sutherland, P.G.	1978	Astrophys. J., 221, 228.
Wheaton, W.A., Ulmer, M.P., Baity, W.A., Datlowe, D.W., Elcan, M.J., Peterson, L.E., Klebesadel, R.W., Strong, I.B., Cline, T.L., and Desai, U.D.	1973	Astrophys. J., Lett., 185, L 57.
Wheeler, J.C.	1977	Astrophys. J., 214, 560.
Whitten, R.C., Poppoff, I.G., Edmonds, R.S., and Berning, W.W.	1965	J.Geophys. Res., 70, 1737.
Young, J.M., Carruthers, G.R., Holmes, J.C., Johnson, C.Y., and Patterson, N.P.	1968	Science, 160, 990.